



September 24-25-26, 2018

Grenoble



# 15<sup>th</sup> International Workshop on 1&2 Dimensional Magnetic Measurement and Testing

Program and book of abstracts



## Local Organization



Grenoble Electrical Engineering Laboratory  
Grenoble Alpes University  
[www.g2elab.grenoble-inp.fr](http://www.g2elab.grenoble-inp.fr)

## Partners



[www.communaute-univ-grenoble-alpes.fr](http://www.communaute-univ-grenoble-alpes.fr)



[www.univ-grenoble-alpes.fr](http://www.univ-grenoble-alpes.fr)



[www.cnrs.fr](http://www.cnrs.fr)



[www.grenoble-inp.fr](http://www.grenoble-inp.fr)



[www.grenoble-lanef.fr](http://www.grenoble-lanef.fr)



[www.energiesdufutur.fr](http://www.energiesdufutur.fr)



## Sponsors



[www.megger.com](http://www.megger.com)



[www.brockhaus.com/measurements](http://www.brockhaus.com/measurements)



[www.irt-saintexupery.com](http://www.irt-saintexupery.com)



[www.supergrid-institute.com](http://www.supergrid-institute.com)



## Welcome to Grenoble

For this 15th edition of the International Workshop on 1&2 Dimensional Magnetic Measurement and Testing, 2DM 2018, we are pleased to welcome you to Grenoble on 24, 25 and 26 September at the new GreEn-ER site of the Grenoble Alpes University community.

Since its first edition in 1991, in Braunschweig - Germany, this international Workshop has been dedicated to the methods of characterization of magnetic materials in their theoretical and experimental aspects as well as their application advances.

This Workshop brings together academic and industrial specialists in order to promote and strengthen the links between fundamental and applied research in the field of magnetic measurements and tests. This biennial event is not intended to compete with major international conferences; it is above all a place for human-sized meetings and friendly exchanges between participants. It allows the dissemination of research and development work, with about 60 contributions presented in the form of oral and poster sessions, five keynotes and one plenary session, arranged in the traditional single plenary session.

We would like to thank the members of the 2DM Steering Committee who provided the scientific preparation for this event.

Finally, we would like to thank the members of the local organizing committee and the administrative and technical staff of the G2Elab laboratory and the GreEn-ER site for their investment in the organization of this event.

We wish you a Workshop rich in scientific and technical exchanges as well as a very pleasant stay in Grenoble.

Afef KEDOUS-LEBOUC and Nicolas GALOPIN  
2DM 2018 Co-Chairs

## Organising Committee

The workshop is organized by the MADEA team (Materials, Machines and Advanced Electromagnetic Devices) of the Electrical Engineering Laboratory of Grenoble (G2Elab - Grenoble Alpes University - CNRS - Grenoble INP).

- Afef KEDOUS LEBOUC (co-chair)
- Nicolas GALOPIN (co-chair)
- Hervé CHAZAL
- Olivier GEOFFROY

With the support of the administrative pole of G2Elab

- Catherine VALENTIN
- Lalasoa RAYNAUD

### Professional Congress Organiser

- Insight-Outside - [www.insight-outside.fr](http://www.insight-outside.fr)

## Honorary Chairman

- Dr. Johannes SIEVERT, Germany

## International Steering Committee

- Dr. Carlo RAGUSA (chair), Italy
- Dr. Johannes SIEVERT (honorary chair), Germany
- Dr. Carlo APPINO, Italy
- Prof. Luc DUPRE, Belgium
- Prof. Masato ENOKIZONO, Japan
- Dr. Fausto FIORILLO, Italy
- Dr Afef KEDOUS-LEBOUC, France
- Prof. Yongjian LI, China
- Prof. Anthony MOSES, UK
- Prof. Helmut PFUETZNER, Austria
- Mr. Stefan SIEBERT, Germany
- Prof. Marian SOINSKI, Poland
- Prof. Derac SON, Korea
- Dr. Kiyoshi WAJIMA, Japan
- Dr. Xing ZHOU, China
- Prof. Jian Guo ZHU, Australia

## Editorial Board

- Dr. Hervé CHAZAL, France
- Dr. Nicolas GALOPIN, France
- Dr. Olivier GEOFFROY, France
- Dr. Afef KEDOUS-LEBOUC, France
- Dr. Carlo RAGUSA, Italy
- Dr. Georgi SHILYASHKI, Austria
- Dr. Johannes SIEVERT, Germany

## Scope of the Workshop

This Workshop aims at promoting and strengthening the links between the fundamental and industrial research on magnetic measurement, testing and modelling. The topics of the Workshop concern:

- fundamental problems, magnetisation processes and domains,
- measurement and modelling of magnetic properties of soft magnetic materials, relevance of microstructures,
- high frequency magnetic measurements,
- characterisation of permanent magnets and their measurements,
- industrial magnetic measurements and testing, measurement standards,
- non-destructive magnetic testing and bio-electromagnetic testing,
- magnetic sensors,
- two dimensional magnetic metrology,
- magnetostriction, magnetocaloric and anisotropy measurement,
- modelling of magnetic material behaviours (characteristics under scalar and/or vectorial magnetic excitations including harmonics and DC offset, hysteresis and power losses, coupled phenomena, etc...),
- relevance to applications in electromagnetic devices (transformers, motors, etc...),
- other relevant topics.

## General Informations

### Registration and secretariat

The registration desk and the secretariat are located on the ground floor of the GreEn-ER building from Monday until the last day of the workshop.

### Welcome cocktail

A welcome refreshment will be offered at GreEn-ER building on 24 September 2018 during the reception and registration time (17:30 - 19:30).

### Conference dinner

The gala dinner will be held at the restaurant Téléférique. Located in the top of the Bastille, in the heart of old Grenoble, the panoramic restaurant at 476 meters of altitude offers an exceptional view overlooking Grenoble and its surroundings.

Appointment is given to all participants at 7:00 pm at the cableway station. Do not forget the dinner coupon, which will be exchanged for a ticket to access the cableway (round trip) and the restaurant.

The cableway station is located in the heart of the historic Grenoble, on the Stéphane Jay quay, on the left bank of the Isère river, at the entrance to the Jardin de Ville. Accessible by bus and tramway (lines A, B, C1, C3, C4, 17, 40) Victor Hugo station, then simply cross the Jardin de Ville.

Téléférique Grenoble-Bastille  
Quai Stéphane Jay  
38000 Grenoble

GPS coordinates:  
45°11' 35" N, 5°43' 34" E



## Instructions for presentations

To check the type of your presentation, the title of your session, and the schedule, see the following pages of this technical program (also available on the workshop website <https://2dm2018.sciencesconf.org>).

To be eligible for journal publication, each paper must be presented by one of the authors. No-show paper will not be eligible for submission to the Journal of Applied Electromagnetics and Mechanics (IJAEM) for publication. The authors are expected to revise and submit their full papers by 15 October 2018 for peer review.

### Oral presentations

Each presentation is scheduled for a duration of :

- Regular: 15 minutes + 5 minutes for exchanges and questions.
- Keynote : 25 + 10 minutes for exchanges and questions.
- Plenary : 35 + 10 minutes for exchanges and questions.

Thank you in advance to keep the presentation time in order to allow questions and discussions.

The lecture room is equipped with a computer and a video projector.

All presentations must be loaded on the computer of the room before the beginning of the session and at least 5 minutes before.

It is important to pay attention to the compatibility of the files (ppt, pptx and odp). These formats (ppt, pptx and odp) are naturally accepted, but require a previous check for their correct operation. A PDF format is preferred and recommended.

### Poster presentations

The poster format is in A0 (84.1 cm x 118.9 cm) in portrait mode. No specific template is imposed. Poster presentations simply consisting of a hard copy of the paper is inappropriate and will be marked as a No-show paper.

The duration of the poster sessions is 01:30. These sessions are sandwiched between lunch and a coffee break, which leaves more time for exchanges.

All the materials for the poster sessions will be provided at the reception desk.

Participants are encouraged to install their poster in the morning and remove it at the end of the day.

## Practical Informations

Grenoble, capital of the French Alps surrounded by a spectacular natural landscape, is the second France's most important centre of scientific research and high-tech industry after Paris. University town with several large institutions and research facilities, Grenoble is also known for its outstanding quality of life, its museums and gastronomy. Host of the 1968 Winter Olympics, the city center is the focal point for a metropolitan area of over 450,000 inhabitants, including 60,000 students. Surrounded by the mountain ranges of Chartreuse, Vercors and Belledonne, the city lies on the bank of the river Isère. In Grenoble, you can love city life and wildlife at the same time, enjoy winter and summer altogether, mountain hikes and contemporary art exhibitions on a same day, you may strongly support sustainable development and be keen on archaeology, too.

The venue of the event, at GreEn-ER research center on electrical energy and renewable resources, is expected to perfectly serve the organization of an enjoyable and fruitful 2DM 2018.

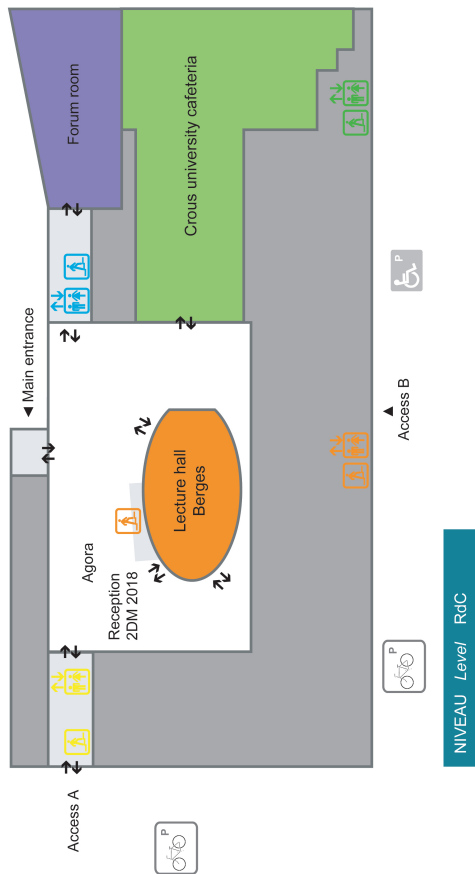
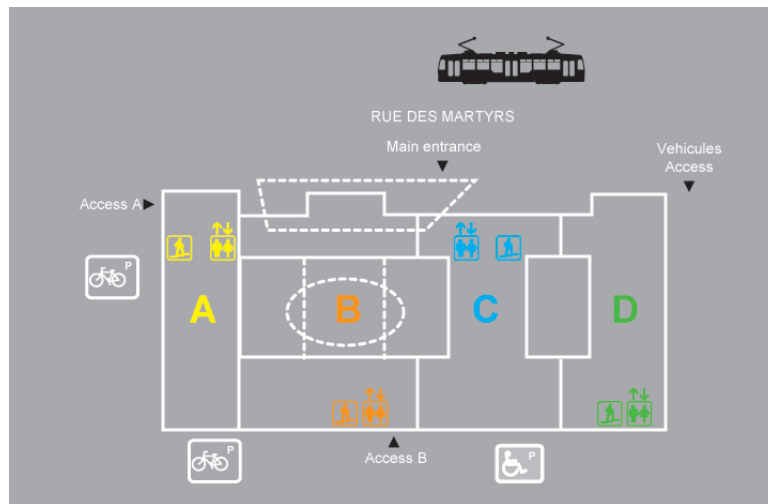


Grenoble Electrical Engineering  
Laboratory  
GreEn-ER Building  
21 avenue des Martyrs  
38000 Grenoble  
[www.g2elab.grenoble-inp.fr](http://www.g2elab.grenoble-inp.fr)  
[2dm2018@sciencesconf.org](mailto:2dm2018@sciencesconf.org)

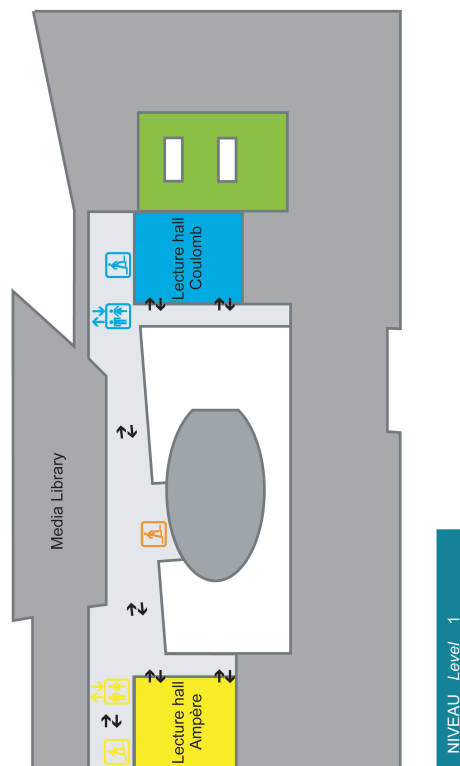
The GreEn-ER building is easily accessible from tram line B. It is located opposite the CEA-Cambridge station on the Grenoble Scientific Polygon (presqu'île scientifique).



# GreEn-ER building plan



Ground floor



First floor



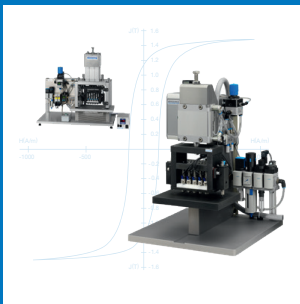
## Industrial and Laboratory Measuring Technology for Soft Magnetic Materials



### Measuring Unit MPG 200 D

- Core loss tester
- Determination of all magnetic properties
- According to IEC 60404-ff

**NEW: FT 600 with  
pneumatic drive**



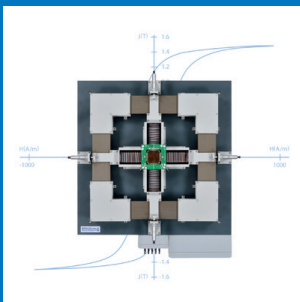
### Franklin Tester FT 600

- Determination of surface resistance
- Quality control of insulation coating
- According to IEC 60404-11 & ASTM A717-01



### EBA Inline Measuring System

- Continuous inline quality control
- Measurement of specific hysteresis loss and peak induction
- Monitoring and documentation



### Rotational Powerloss Tester RPT

- Rotational and ellipsoidal magnetisation
- Axial measurements at various angles to the rolling direction
- H-coils and B-coils (optional pocket) measurement method

### Measuring Technology for Hard and Soft Magnetic Materials

Dr. Brockhaus Messtechnik GmbH & Co. KG

Gustav-Adolf-Str 4 · D-58507 Lüdenscheid · Germany

Phone: +49 (0) 2351 3644-0 · Fax: +49 (0) 2351 3644-44  
measurements@brockhaus.com

[WWW.BROCKHAUS.COM](http://WWW.BROCKHAUS.COM)



# Test instruments for the maintenance of electrical power systems

Megger manufacture safe and powerful electrical test equipment for the most demanding environments to keep the world moving and the Power on:

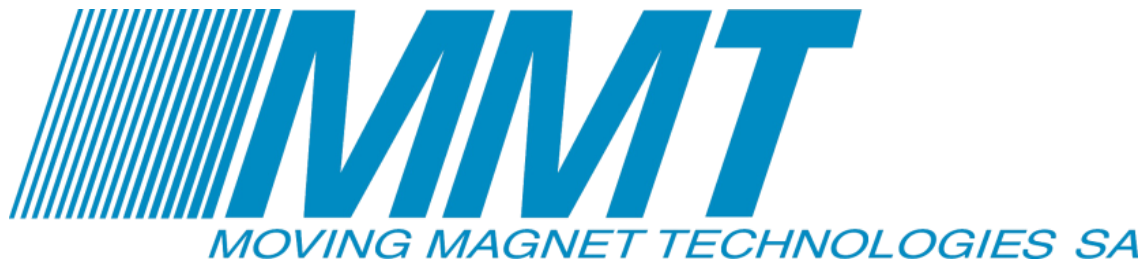
- **High-voltage insulation resistance testing**
- **Effective and simple relay testing**
- **The most experienced in circuit breaker testing**
- **Worldwide leader in cable diagnostics and cable fault solutions**
- **Widest range of transformer testing products**
- **Providing quality test solutions for low voltage installations**



Scan the QR code  
to find out more.

**Megger**<sup>®</sup>  
Power on





## MOVING MAGNET TECHNOLOGIES

**Mechatronic & electromagnetic systems engineering services**

### **MMT, Mechatronics Innovation supplier**

MMT's aim is to provide our customers with the most efficient and reliable contactless solutions for motion control and drive systems. Our team of experts is developing innovative solutions for electromagnetic position sensors, electric motors and direct drive actuators. These solutions are industrialized by our customers under a license agreement with the help of MMT's technical support.

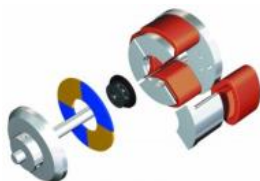
### **Expertise & Innovation in Electromagnetic Systems**

MMT's expertise in electromagnetism can also be utilized as engineering services. We can offer various services ranging from simulation, calculation, sizing studies to complete mechanical design, prototyping and testing of electromagnetic systems based on our patents but also on public domain structures or on customer specific solutions.

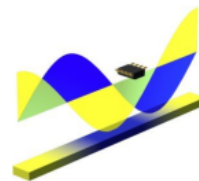
### **Technologies**



Brushless DC  
motors and stepper  
motors

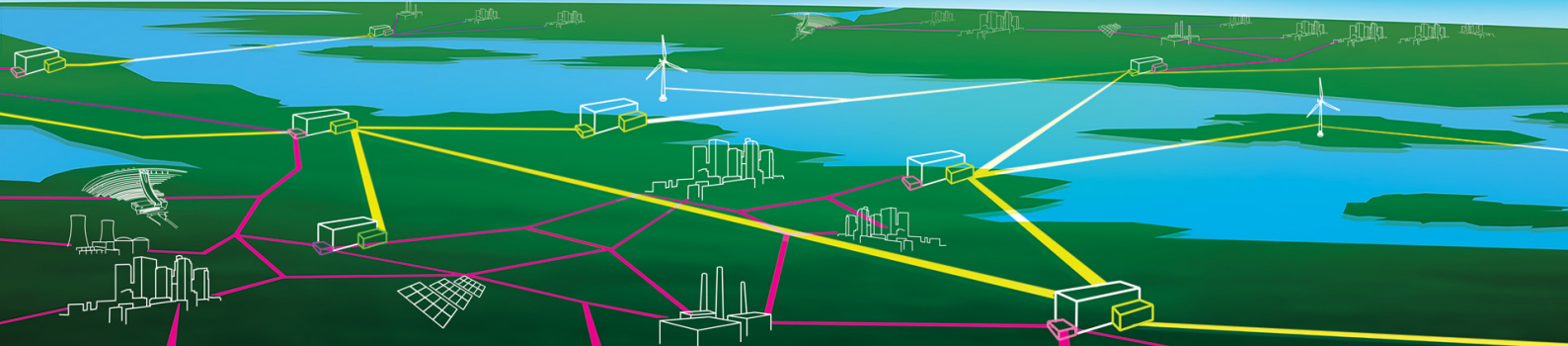


Direct Drive  
Actuators



Magnetic position  
sensors

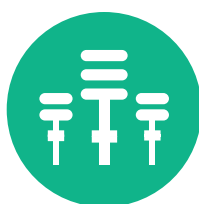




## SuperGrid Institute offers a complete range of services to meet your needs



5 R&D programs



Research & Innovation test platforms



Added value Services & Expertise



Learning & Training facilities



Innovations & Technology transfer

SuperGrid Institute is a research and innovation center, federating academic and industrial players.

We are experts in High Voltage DC interconnected with AC networks, energy conversion, systems and equipment.

We develop technologies for the future power transmission networks. We offer high value added technologies and services to support our clients' business.



Shaping power transmission  
SuperGrid Institute SAS - 23 Rue Cyprian, BP 1321 - 69611 Villeurbanne CEDEX, France  
+33 4 28 01 23 23 - [accueil@supergrid-institute.com](mailto:accueil@supergrid-institute.com) - [www.supergrid-institute.com](http://www.supergrid-institute.com)



## 2DM 2018 Program Overview

MONDAY 24 SEPTEMBER

REGISTRATION  
and  
WELCOME COCKTAIL

17:30 - 19:00

TUESDAY 25 SEPTEMBER

8:00 - 9:00	WELCOME
9:00 - 9:15	OPENING SESSION
9:15 - 10:00	PLENARY
10:00 - 11:00	OS1-A
11:00 - 11:25	COFFEE BREAK
11:25 - 13:00	OS2
13:00 - 14:00	LUNCH
14:00 - 15:30	POSTER SESSION 1
15:30 - 16:00	COFFEE BREAK
16:00 - 18:00	OS3

CONFERENCE DINNER  
Restaurant "le Téléferique"

19:00 - 23:00

WEDNESDAY 26 SEPTEMBER

8:00 - 9:00	WELCOME
9:00 - 10:35	OS1-B
10:35 - 11:00	COFFEE BREAK
11:00 - 13:00	OS4
13:00 - 14:00	LUNCH
14:00 - 15:30	POSTER SESSION 2
15:30 - 16:00	COFFEE BREAK
16:00 - 17:15	OS5
17:15 - 17:45	REPORT & CLOSURE

OS1-A

OS2

OS3

OS1-B

OS4

OS5

1D Measurement and Non-Conventional Characterisation

2D Characterisation and Modeling

Magnetic Modelling

1D Measurement and Non-Conventional Characterisation

Multiphysics Coupling

Applications, Sensors, NDT



# Table of contents

<b>Plenary Lecture</b>	<b>3</b>
Measurements and magnets are everywhere: advanced magnetic testing methods as requisites for physical understanding, progress in standards and materials, and improved applications , Fausto Fiorillo . . . . .	5
<b>OS1-A: 1D Measurement and Non-Conventional Characterization</b>	<b>9</b>
Measurement accuracy using tangential search coils with round rotational loss testers, Kitzberger Martin [et al.] . . . . .	11
Investigation on Conductivity and AC Magnetic Loss of Nd-Fe-B Sintered Magnet., Shutta Yusaku [et al.] . . . . .	13
Computer-controlled electromagnetic control and image capture system for alignment of magnetic graphene nanofillers in epoxy composites, Hall Jeremy [et al.] .	15
<b>OS2: 2D Characterization and Modeling</b>	<b>17</b>
Optimum magnetising apparatus for standardised measurements of rotational power loss, Zurek Stan . . . . .	19
Comprehensive Magnetic Properties Measurement of the Laminated Silicon Steel by a Novel High Frequency 2-D Magnetization Structure, Zhang Kai [et al.] . . .	22
Vector Magnetic Hysteresis Characteristics, Enokizono Masato [et al.] . . . . .	24
Energy loss along different directions in GO steel sheets, Appino Carlo [et al.] . .	26
<b>PS1: Poster Session</b>	<b>29</b>
PS1-1: Analysis of High Frequency Effects of Excitation Winding in High Frequency Rotating Tester with Nanocrystalline material, Dou Yu [et al.] . . . . .	31
PS1-2: Characterization of NdFeB Bonded Magnets for Halbach Magnets in Electric Vehicles Motors, Jha Amit [et al.] . . . . .	33
PS1-3: Design of a Single Sheet tester coils' windings for the magnetic, electric and mechanical measurements of magnetized electrical steels and soft magnetic materials, Maloberti Olivier [et al.] . . . . .	35
PS1-4: Electrical and magnetic characterization of parallelepipedic sample extracted from massive claw poles alternator, Jamil Meryeme [et al.] . . . . .	37
PS1-5: Frequency dependence of anisotropy of specific total loss in Goss textured electrical steel, Pluta Wojciech . . . . .	39
PS1-6: From magnetic spectroscopy and fractional Cole-Cole model to high amplitude dynamic scalar hysteresis cycles, Ducharne Benjamin . . . . .	41
PS1-7: Hybrid computing based on measured vector magnetic properties of electrical steel sheets for high performance electromagnetic devices, Tsuchida Yuji [et al.] . . . . .	43
PS1-8: Influence of Distortion Factor of Induced Voltage of B-coil on Magnetic Property Measured with a Single Sheet Tester, Shibataki Takuya [et al.] . . . . .	45
PS1-9: Investigating a zero-field energy minimization principle to control the domains size by lines scribed with a laser on surface oriented magnetic structures., Maloberti Olivier [et al.] . . . . .	47
PS1-10: Investigation on Deterioration of Magnetic Properties of Laminated Iron Core Due to Different Welding Conditions, Mitani Ryo [et al.] . . . . .	49

PS1-11: Modelling of Hysteresis Phenomenon Based on the Elemental Operator and Wind-rose Method, Duan Nana [et al.] . . . . .	51
PS1-12: Multi-directional Non-linear FEM Modelling of Magnetic Flux in Transformer Cores with Consideration of Overlaps, Shilyashki Georgi [et al.] . . . . .	53
PS1-13: Nondestructive Testing of Ferromagnetic Tubes using a Bobbin-type Intergrated Hall Sensor Array, Park Juhyeon [et al.] . . . . .	55
PS1-14: Optimisation of laser domain refinement of grain-oriented silicon steel for low loss and magnetostriction, Davies Ryan [et al.] . . . . .	57
PS1-15: Optimization of a single strip tester to measure magnetic properties of electrical sheet steel at medium frequencies, Owzareck Michael [et al.] . . . . .	59
PS1-16: Research of Harmonic Effects on Core Loss in Soft Magnetic Composite Materials, Yu Xinran [et al.] . . . . .	62
PS1-17: Sensitivity analysis of iron loss and hysteresis models' parameters to the sheets thickness and magnetic polarisation according to the quality of GO SiFe, Maloberti Olivier [et al.] . . . . .	64
PS1-18: The Role of the Critical Induction for Off-plane Flux in Transformer Cores, Shilyashki Georgi [et al.] . . . . .	66
PS1-19: Two-dimensional magnetical characterization of soft magnetic material under arbitrary mechanical stress, Thul Andreas [et al.] . . . . .	68
PS1-20: Verification of the Magnetic Path Length of Epstein Frame and Single Sheet Tester by H-coil Technique, Zhou Xing . . . . .	70
<b>OS3: Magnetic Modeling</b>	<b>73</b>
Broadband magnetic losses in soft magnets: experimental and theoretical analysis, Dobák Samuel [et al.] . . . . .	75
Testing the sheet thickness independence of a new dynamic magnetization property based on domains and walls within the diffusion-like equation for GO SiFe, Maloberti Olivier [et al.] . . . . .	78
Phenomenological modeling of hysteresis curves near transition temperature in La(Fe,Si)13-based alloys, Gozdur Roman [et al.] . . . . .	80
Phenomenologic model for incremental permeability micro-magnetic non destructive testing technique, Ducharne Benjamin [et al.] . . . . .	82
Efficient and novel simulation method for the effective permeability of randomly ordered structures, Woeckinger Daniel [et al.] . . . . .	84
<b>OS1-B: 1D Measurement and Non-Conventional Characterization</b>	<b>87</b>
Thermographic Measurement of Losses Due to Inter-laminar Contacts in Electrical Sheets, Belhacen Anouar [et al.] . . . . .	89
Universal modular high power wide frequency range controlled system for magnetic measurements, Rygał Roman [et al.] . . . . .	92
Novel model-based digital controller for facilitating soft magnetic material measurement under controlled magnetizing conditions, Vo Anh Tuan [et al.] . . . . .	94
Temperature dependence of magnetic losses in Co-doped Mn-Zn ferrites, Beatrice Cinzia [et al.] . . . . .	96
<b>OS4: Multiphysics Coupling</b>	<b>99</b>
Relevance of multiscale approach for the modeling of various magneto-mechanical problems, Hubert Olivier . . . . .	101
On the correlation of crystallographic macro texture and magnetic magnetization anisotropy in non-oriented electrical steel, Leuning Nora [et al.] . . . . .	104
Influence of Laminating Process on Magnetic Property of Permendur or High Power Density of Motors, Ako Yuya [et al.] . . . . .	106
The effet of punching on electrical machine, El Youssef Mohamad [et al.] . . . . .	108
Frequency dependence and vector magnetic properties of non-oriented electrical steel sheet under arbitrary stress conditions, Kai Yuichiro [et al.] . . . . .	110

<b>PS2: Poster Session</b>	<b>113</b>
PS2-1: A measuring system for the magnetic properties of amorphous strip under high-frequency PWM excitation, Zhang Xiwei [et al.] . . . . .	115
PS2-2: A Multiphysics-dependent hysteresis model with experiment validation, Xu Weijie [et al.] . . . . .	117
PS2-3: Advanced iron-loss estimation for arbitrary magnetization loci in non-oriented electrical steel considering anisotropic effects, Schauerte Benedikt [et al.]	119
PS2-4: Application of orientation distribution functions' theory in the case of grain-oriented steels cut through non-conventional technologies, Manescu Paltanea Veronica [et al.] . . . . .	121
PS2-5: Assessment of Static B-H Relationship for Soft Magnetic Alloys Using a Novel Equipment, Manescu (paltanea) Veronica [et al.] . . . . .	123
PS2-6: Development of Measurement Method for Magnetostriction of Electrical Steel Sheets Using an Open-type Single Sheet Tester., Matsubara Ryo [et al.] . .	125
PS2-7: Eddy-Current Loss Measurement of Permanent Magnet Material at different frequency, Li Yongjian [et al.] . . . . .	127
PS2-8: Galvanically separated voltage sensor used in industrial magnetic core measurements, Rygał Roman [et al.] . . . . .	129
PS2-9: Improved High-Frequency Rotating Magnetic Properties Tester for Ultrathin Silicon Steel Material Considering Stress Effects, Zhang Changgeng [et al.] .	131
PS2-10: Improved nondestructive testing of condenser tubes using a cylinder-type integrated hall sensor array, Kim Sejin [et al.] . . . . .	133
PS2-11: Influences of Machining and Acid Etching on Magnetic Properties of Soft Magnetic Composites, Higashigawa Yuto [et al.] . . . . .	135
PS2-12: Iron Loss Estimation Method of PWM Inverter-Fed AC Filter Reactor, Kubo Toshihiro [et al.] . . . . .	137
PS2-13: Loss model for transformer core under non-sinusoidal excitation, Zhao Zhigang [et al.] . . . . .	139
PS2-14: Magnetic Properties Measurement of Nanocrystalline Under DC Bias, Sun He [et al.] . . . . .	141
PS2-15: Measurement and Loss Estimation of Nanocrystalline Cores With Non-sinusoidal Excitations, Yue Shuaichao [et al.] . . . . .	143
PS2-16: Methods of improving magnetic properties for powder cores made of nanocrystalline flakes, Grybos Dominik [et al.] . . . . .	145
PS2-17: Modeling of DC-biased hysteresis loops with the GRUCAD description, Jastrzebski Radoslaw [et al.] . . . . .	147
PS2-18: Modeling of magnetic component behaviors under distorted excitations based on an integrated magnetic measure-bench, Liu Tao [et al.] . . . . .	149
PS2-19: Novel H-coil design with improved off-axis immunity, Zurek Stan . . . .	151
PS2-20: Research of the influence of DC component to stray-field loss under AC-DC hybrid excitation, Zhao Zhigang [et al.] . . . . .	153
PS2-21: Research on the improved loss model of electrical steel sheets under non-sinusoidal excitation, Zhigang Zhao [et al.] . . . . .	155
 <b>OS5: Applications, Sensors, NDT</b>	 <b>157</b>
Inline integration of electromagnetic NDT methods using 3MA, Gabi Yasmine [et al.] . . . . .	159
A Novel Family of Magnetic Detector Bands of Minimum Effective Thickness, Pfützner Helmut [et al.] . . . . .	162
Nondestructive testing and evaluation of high pressure feed water heat exchanger tubes using differential-type bobbin probes and solid-state integrated GMR sensor arrays, Sim Sunbo [et al.] . . . . .	164



# Plenary Lecture



## Plenary Lecture

*”Measurements and magnets are everywhere: advanced magnetic testing methods as requisites for physical understanding, progress in standards and materials, and improved applications”*



**Dr. Fausto Fiorillo**

*Istituto Nazionale di Ricerca Metrologica-INRIM, Torino, Italy*

**Dr. Fausto Fiorillo** is a physicist. He earned his degree from the University of Torino in 1972. He worked since 1973 as a scientist and since 1995 as Research Director at the Istituto Elettrotecnico Nazionale Galileo Ferraris, now Istituto Nazionale di Ricerca Metrologica (INRIM), in Torino. He officially retired on January 1, 2012 and is now serving as an associate scientist at INRIM. His scientific work and interests have been mainly devoted to the properties of magnetic materials and their measurement, with special focus on magnetization process and losses. He authored/co-authored some 210 peer-reviewed publications in international scientific journals, review monographs, and chapters on international series on magnetic materials. He is the author of the comprehensive treatise “Measurement and Characterization of Magnetic Materials” (10 Chapters, 647 pages), published by Academic Press-Elsevier, December 2004.

# Measurements and magnets are everywhere: advanced magnetic testing methods as requisites for physical understanding, progress in standards and materials, and improved applications

Fausto Fiorillo

*Istituto Nazionale di Ricerca Metrologica-INRIM, 10135, Torino, Italy*  
[f.fiorillo@inrim.it](mailto:f.fiorillo@inrim.it)

Measurements mean knowledge. No scientific and technological activity can be rationally pursued without resorting to some kind of well-defined and reproducible measurement. This is especially true for magnetic materials, where advances in the physical understanding of their properties and in the variety and efficiency of their applications hang on the development of solid and innovative measurement techniques. These must relate, in any case, to the rigorous framework provided by the coherent SI system of units, to which they can be traced through an unbroken chain of calibrations, ultimately linked to the activity of the National Metrological Institutes. The appearance of novel physical phenomena and new or improved materials, and the development of increasingly fast digital methods in measurement control and data acquisition and handling have brought about new challenges and opportunities in magnetic measurements. Enhanced measurement methodologies, developed either for basic investigations or for keeping abreast of new advances in materials and applications, eventually call for an evolution of the Standards, the tool by which the novel achievements in measuring methods are transferred to industry, in order to cover, under strict reproducibility requisites, the broadening demands of the market.

In this communication we shall highlight the physical principles underlying the modern methodologies employed in the characterization of hard and soft magnetic materials, by considering both standard measuring approaches to materials of present-day industrial interest and some recent developments and results ensuing from novel and improved techniques, namely concerning the investigation of the magnetization process and the magnetocaloric effect.

The talk will develop, in particular, around the following main topics:

- The landscape of present-day IEC standards in magnetic measurements.
- Epstein versus Single Sheet Tester method: the results of a recent IEC-TC68 broad intercomparison.
- Two-dimensional measurements in magnetic sheets up to saturation. Fieldmetric versus thermometric measurements.

- Measurements of permanent magnets: the VSM and the Pulsed Field Magnetometer methods versus the closed-circuit hysteresisgraph method.
- Measurement of magnetic losses in soft magnetic materials from DC to the GHz range. Fast stroboscopic techniques elucidate the evolution of the domain wall dynamics versus frequency.
- Calorimetric techniques for the characterization of the magnetocaloric effect on low Curie temperature materials, for perspective use in magnetic refrigeration.

We shall look, in particular, at the physical insight gained by the application of these techniques, besides highlighting their technical features and perspectives. While not pretending to provide a description of the present state of the art in magnetic measurements, the selected examples are chosen to convey trends and ideas lying behind advances in experimental methods, an indispensable step on the road to improved materials and applications.



# **OS1-A: 1D Measurement and Non-Conventional Characterization**

Session Chairman

**Yongjian LI**

Hebei University Of Technology - China



## Measurement accuracy using tangential search coils with round rotational loss testers

M. Kitzberger<sup>1</sup>, G. Bramerdorfer<sup>1</sup>, M. Cossale<sup>1</sup>, W. Amrhein<sup>1</sup>

<sup>1</sup>*Johannes Kepler University Linz, Institute for Electric Drives and Power Electronics, Altenbergerstr. 69, 4040 Linz, Austria*

*E-mail: martin.kitzberger-1@jku.at ; gerd.bramerdorfer@jku.at ; m.cossale@gmail.com*

*Keywords:* fieldmetric method, tangential search coils, extrapolation method, round rotational loss tester.

Iron losses in ferromagnetic materials under circular or arbitrary two dimensional magnetization show a different propagation with regard to the flux density magnitude when compared to iron losses arising for uniaxial alternating magnetization. Hence, characterisation of iron losses under two dimensional magnetization, has become an important topic in electrical machine design due to complex two dimensional flux density loci forming in some parts of rotor and stator laminations. Most commonly, for iron loss determination under two dimensional magnetization either square shaped single sheet testers (SST) or round rotational single sheet testers (RRSST) are utilized where, due to its versatility and speed, the field metric method is frequently applied. With the field metric method, specific iron losses  $P_{Fe}$  in W/kg are directly calculated from measured loci of field intensity  $H_x(t)$ ,  $H_y(t)$  and flux density  $B_x(t)$ ,  $B_y(t)$  over time, as well as single sheet specimen mass density  $\rho$  and magnetization period  $T$ . Hence, reasonable accuracy of two dimensional field intensity and flux density measurement is vital for a precise determination of indeed arising iron losses. This is particularly important, as for rotational loss measurements, contrary to measurements under alternating magnetization, there is currently no standard defined, making comparison of results obtained by different laboratories using numerous setups a challenging goal.

The main scope of this paper is the experimental and numerical investigation of achievable measurement accuracy with tangential field intensity search coils (H-coils), using the RRSST setup presented in Figure 1. Special emphasis is taken on the practical suitability of the H-field extrapolation method proposed in [1] and [2] for local two dimensional field intensity measurement inside the single sheet. The presented RRSST-setup incorporates four flat tangential field intensity search coils with their axes oriented along the  $x$ - and  $y$ -direction illustrated at the top of Figure 2. H-coils are mounted on an  $xyz$ -moveable positioning table with 1  $\mu$ m resolution below the single sheet specimen. This allows for a variation of distance  $z_1$  and  $z_2$  of the search coils as well as the investigation of tangential field intensity propagation  $H_{x,y}(x, y, z)$  at arbitrary positions below the sheet. A direct comparison of measured two dimensional tangential field intensity obtained by conventional flat H-coils and the extrapolation method can therefore be made. To further investigate the influence of yoke height  $h_s$  and singlesheet diameter  $d_s$  on measurement accuracy while using H-coils with or without extrapolation, a magnetostatic 2d- and 3d-finite element simulation (FEM) of the test setup was performed. Subsequently, for verification of the numerically obtained results, a regular grid of test points below the single sheet surface was defined where field intensity along the  $x$ - and  $z$ -direction was measured locally using a precision flux meter with coil probes. As an example, at the bottom of Figure 2 vertical field intensity component with varying distance from the single sheet center is shown for a flux density of 1 T and different sheet diameters  $d_s$ . Measured and simulated

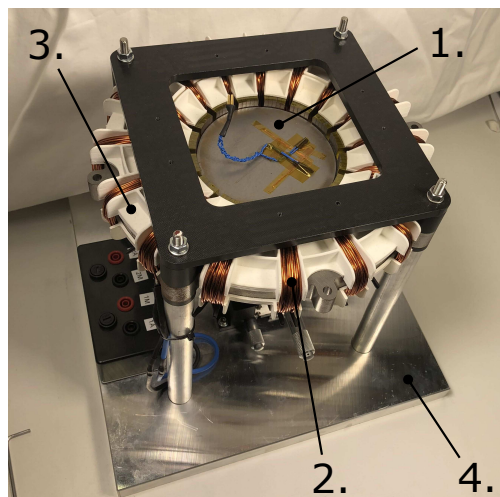


Figure 1: RSSST Setup. (1) Single sheet specimen with B-coils wound through holes (2) Toroidal two phase winding (3) Magnetizing stator with insulation (4) Base plate with xyz-moveable table.

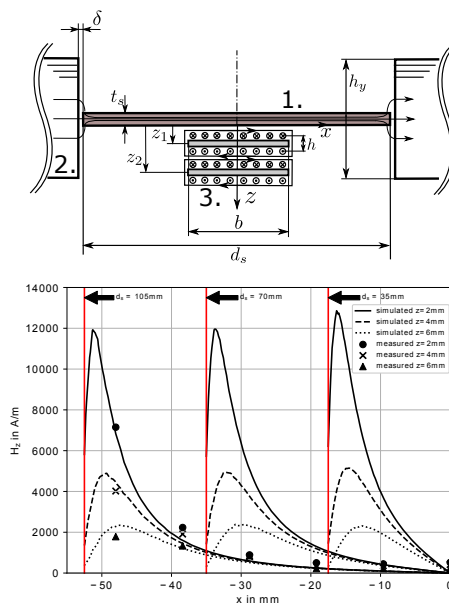


Figure 2: Top: Coil Arrangement. (1) Single sheet specimen, (2) Magnetizing yoke, (3) H-field search coils mounted on a xyz-moveable table. Bottom: Propagation of unwanted vertical field intensity component  $H_z$ .

results for vertical as well as horizontal field intensity component reveal that practical suitability of the extrapolation method is highly dependent on the diameter  $d_s$  of the used test specimen as well as outline of the yoke. Therefore, care has to be taken to not introduce systematic errors when using the extrapolation method.

The final paper will give a detailed analysis of the obtained experimental and numerical results and will further discuss their implications on usability of the extrapolation method. Furthermore, the impact on obtained rotational losses values will be discussed mathematically supported by measurements using the test setup.

#### Acknowledgements

This work has been supported by the COMET-K2 Center for Symbiotic Mechatronics of the Linz Center of Mechatronics (LCM) funded by the Austrian federal government and the federal state of Upper Austria.

#### References

- [1] Y.Kawase T. Nakata and M. Nakano. Improvement of measuring accuracy of magnetic field strength in single sheet testers by using two h coils. *IEEE Transactions on Magnetics*, Vol.64, 1987.
- [2] S. Tumanski. A multi-coil sensor for tangential magnetic field investigations. *Journal of Magnetism and Magnetic Materials Volumes 242245, Part 2, Pages 1153-1156*, 2002.

# Investigation on Conductivity and AC Magnetic Loss of Nd-Fe-B Sintered Magnet.

Yusaku Shutta<sup>1</sup>, Yuya Ako<sup>1</sup>, Yasuhito Takahashi<sup>1</sup>, Koji Fujiwara<sup>1</sup>,  
Junji Kitao<sup>2</sup>, and Masaki Yamada<sup>2</sup>

<sup>1</sup> *Doshisha University, Kyoto, Japan*

*E-mail: {ctwb0348@mail4; ctwb0301@mail4; ytakahashi@mail;  
koji.fujiwara@mail} .doshisha.ac.jp*

<sup>2</sup> *Mitsubishi Electric Corporation, Hyogo, Japan*

*E-mail: {Kitao.Junji@df; Yamada.Masaki@bp}.MitsubishiElectric.co.jp*

**Keywords:** Nd-Fe-B sintered magnet, conductivity, anisotropy, AC magnetic loss, motor

Nd-Fe-B sintered magnets are one of the essential constituent elements of motors. Lowering of remanence due to the temperature rise (thermal demagnetization) is a significant issue in designing high-efficiency motors with high power-weight ratio. To reduce eddy-current loss and suppress thermal demagnetization, a magnet is commonly divided to small segments. Therefore, it is indispensable to accurately grasp AC loss property and conductivity of the permanent magnet for the appropriate magnet segmentation [1]. In this study, three kinds of permanent magnets with different remanence  $B_r$  and coercivity  $H_c$  are selected for investigation. For each magnet, two specimens with alignment directions are prepared. AC loss and conductivity of them are measured. Furthermore, the influence of magnetization on AC loss and conductivity is examined.

Table 1 shows the dimensions of specimens used. No. means the grade of the prepared permanent magnet. L and C indicate that the alignment direction is parallel and vertical to the longitudinal direction of the specimen, respectively. The conductivity of each specimen was measured by the four-terminal method. Furthermore, to investigate the influence of magnetization on conductivity, unmagnetized specimens are also measured. To confirm the reproducibility, three measurements were performed for the same specimen. Fig. 1 shows the measurement results of the conductivity  $\sigma$  for Nos. 1L and 1C, and the error  $\varepsilon$ , which is the relative difference with respect to the averaged value of measurement results. It seems that the magnetization does not affect the conductivity. Because the variation in three measurements is within  $\pm 0.6\%$ , this measurement has sufficient accuracy. Fig. 2 compares the conductivities of three kinds of permanent magnets with different specifications. The difference in conductivities between them is very small.

AC loss was measured. Size of specimen is  $20\text{ mm} \times 20\text{ mm} \times 50\text{ mm}$ . Exciting direction is the longitudinal direction of the specimen. Maximum flux density was controlled at 0.01 T and the frequency was changed from 50 Hz to 10 kHz. Fig. 3 shows the frequency dependence of AC loss  $W$  for Nos. 1L and 1C. The alignment direction gives the influence to AC loss. Fig. 4 shows the results of iron loss separation for No. 1L. It is performed by using the results at 50, 100, and 200 Hz. It is confirmed that the hysteresis loss  $W_h$  is extremely smaller than the eddy current loss  $W_e$  for magnetized No. 1L. However,  $W_h$  for unmagnetized No. 1L is not negligibly small.

Although the conductivity of permanent magnet has the anisotropy, it does not depend on the magnetization. From the fact that unmagnetized permanent magnets have a small  $W_h$ ,  $W_h$  may significantly affect loss property for a small-sized permanent magnet having a low magnetization rate because  $W_e$  decreases when the specimen size decreases.

Table 1. Specifications of specimens.

No.	Grade	Alignment direction	Size [mm]	Density [kg/m <sup>3</sup> ]
1L	Low $B_r$ · High $H_c$	longitudinal	5 × 5 × 50	7600
1C		crosswise		
2L	Middle $B_r$ · Middle $H_c$	longitudinal		
2C		crosswise		
3L	High $B_r$ · Low $H_c$	longitudinal		
3C		crosswise		

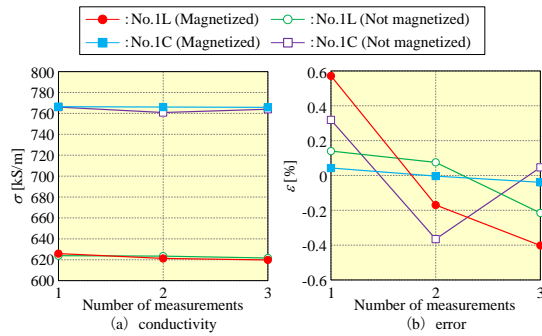


Fig. 1. Measurement results of the conductivity.

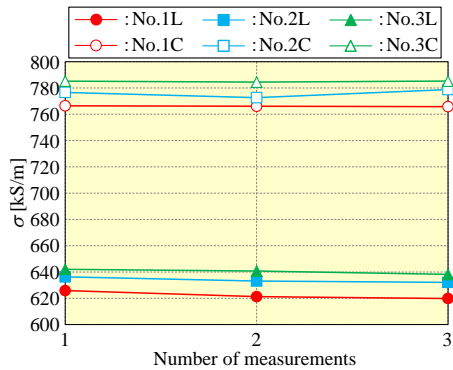


Fig. 2. Comparison of conductivity.

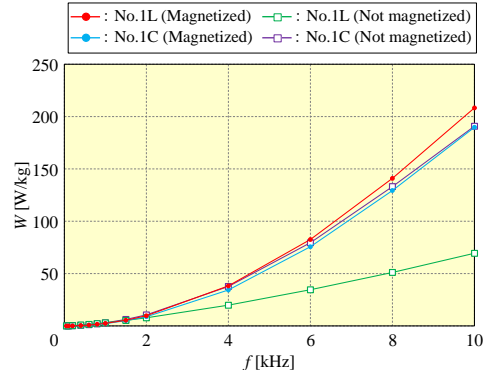
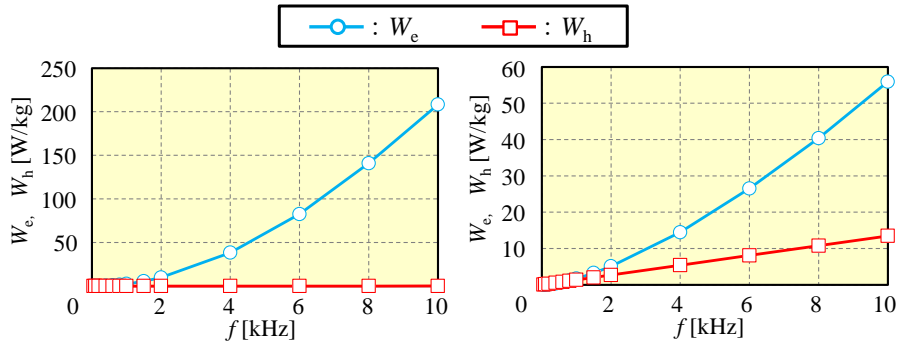


Fig. 3. AC loss property.



(a) Magnetized No. 1L (b) Unmagnetized No. 1L

Fig. 4. Iron loss separation.

Reference

[1] K. Yamazaki and Y. Fukushima, “Effect of Eddy-current Loss Reduction by Magnet Segmentation in Synchronous Motors with Concentrated Windings,” *IEEE Trans. Industry Applications*, vol. 47, no. 2, pp. 779-788 (2011).

# Computer-controlled electromagnetic control and image capture system for alignment of magnetic graphene nanofillers in epoxy composites.

Christopher Dyer<sup>1</sup>, Kyriaki Gkaliou<sup>1</sup>, Philip Anderson<sup>1</sup>, Christopher Harrison<sup>1</sup>, Mark Eaton<sup>1</sup> and Jeremy Hall<sup>1</sup>

<sup>1</sup> Cardiff School of Engineering, Cardiff University, Cardiff, CF24 3AA, UK  
E-mail: halljp@cardiff.ac.uk

*Keywords: electromagnet system, magnetic alignment, optical microscope, LabVIEW, automation*

Polymer nanocomposites have attracted much attention due to their outstanding properties and significant potential application in many fields. However, bulk application is limited due to poor manufacturing scalability while maintaining organized microstructures [1]. Active assembly of nanoparticles using magnetic fields is a promising nano-manufacturing method, as it allows control of alignment direction, is inexpensive, non-damaging, scalable and allows organization of fillers by inter-particle motions [2]. The formation of magnetic chains into the polymer matrices has previously been achieved [3] by applying a magnetic field in the range of a few tens to hundreds of mT. A static magnetic field strength in the range of 80 – 100 mT has been found to be effective in producing the required alignment of the ferrite decorated graphene nano-particles (GNPs) used in this research.

This paper describes the development of an automated image capture and magnetic control system shown in Fig. 1a to study the alignment of coated GNPs in an epoxy matrix. Over the full curing period, this system can continuously observe using an optical microscope the alignment process in an applied magnetic field, providing more accurate information about the behavior of the magnetic nanoparticles in the epoxy matrix compared to a manual method that only allowed observation of the sample after the experiment had been conducted.

LabVIEW was used to develop a Virtual Instrument (VI) simultaneous user interface and program. LabVIEW Vision Acquisition Software (VAS) contains a variety of sub VIs which can implement the control of any supported camera and Digital to Analog Converter (DAC).

The uncured epoxy was applied to a glass microscope slide. This was held in position between the magnetic poles on a 3D printed plastic former designed to locate both the electromagnet and the slide, shown as a schematic drawing in Fig. 1b. A steel C-core with an air gap of 30 mm between faces of 30 x 30 mm was used to set up the magnetic field across the uncured specimen with a uniformity sufficient for alignment of the nano-filler clusters [4]. The electromagnet was energized by a software-controlled power supply unit which allows the user to define the required magnetic field strength through the LabVIEW VI.

Due to automation of the image capture during the curing process, a large number of curing conditions could be analysed and examined at any point during the process. Examples of specimens cured without and with the presence of the applied magnetic field are shown in Fig. 2a and Fig. 2b, respectively. Further studies are planned to examine the GNP loading, field strength and time with the aim to identify the optimum conditions for alignment of GNP clusters in the cured material.

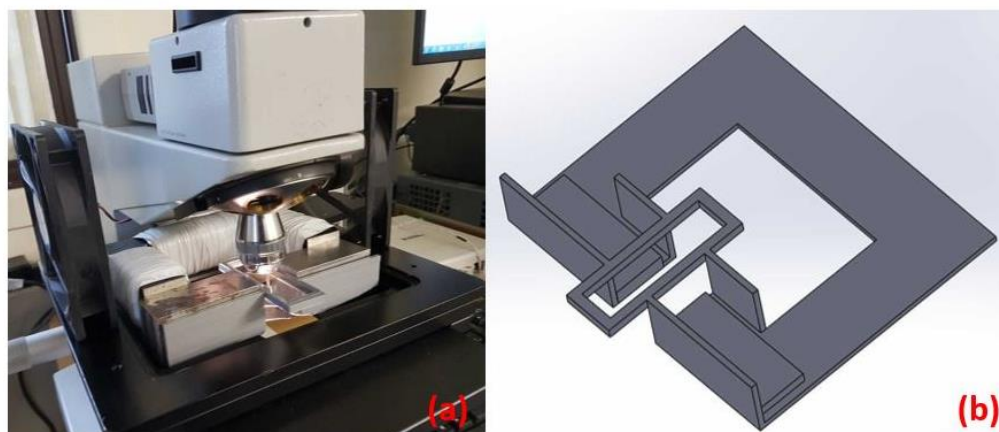


Figure 1a) Photograph of the magnetization system comprising the plastic former, electromagnet and specimen slide holder located beneath the microscope objective and b) the schematic drawing of the 3D model of the former, approximate dimensions 165 x 142 x 32 mm.

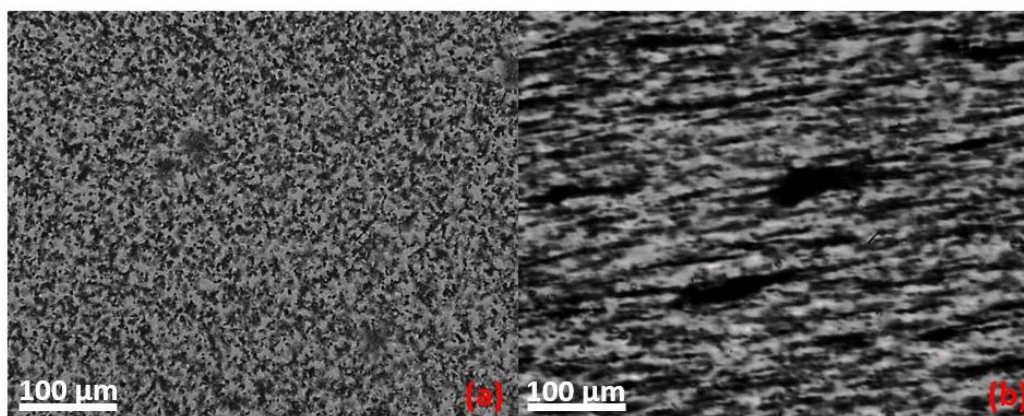


Figure 2a) Image of specimen with a GNP concentration of 0.5% cured without applied field showing a random dispersion of nanofillers. b) Specimen cured sample in a magnetic field showing alignment of ferrite coated GNPs aligned parallel to direction of the applied field.

#### References

- [1] "Nanoparticle alignment using oscillating magnetic fields for scalable nanocomposite manufacturing." Spencer M.P and Yamamoto N., 57th AIAA/ASCE/AHS/ASC Structures, Structural Dynamics, and Materials Conference. 2016.
- [2] "Composites science and technology", Haibat J. et al., 152, 2017
- [3] "Formation of magnetically anisotropic composite films at low magnetic fields", Zahedi, M.G. et al., Smart Materials and Structures 26.4, 2017
- [4] "Magnetic-responsive hybrids of Fe<sub>3</sub>O<sub>4</sub> nanoparticles with  $\beta$ -lactoglobulin amyloid fibrils and nanoclusters", Bolisetty, S. et al., Acs Nano 7.7, 6146-6155, 2013

# OS2: 2D Characterization and Modeling

Session Chairman

**Stefan SIEBERT**

Brockhaus Measurements - Germany



## Keynote Lecture

*"Optimum magnetizing apparatus for standardized measurements"*



**Dr. Stan Zurek**

*Megger Instruments Ltd, Kent, United Kingdom*

**Stan Zurek** graduated as MSc at Czestochowa University of Technology, Poland in 2000. He completed his PhD degree at Wolfson Centre for Magnetics, Cardiff University, UK in 2005, where he continued to work as a Research Associate. In 2008 he joined Megger Instruments Ltd where he currently holds the position of Manager of Magnetic Development in R& D department, being responsible for all aspects of electromagnetic technologies. He was elevated to IEEE Senior Member in 2010. He has authored and co-authored over 80 scientific papers and is a co-inventor on 11 patent applications. Recently he published a comprehensive book on measurements of rotational power loss: "Characterisation of Soft Magnetic Materials Under Rotational Magnetisation".

# Optimum magnetising apparatus for standardised measurements of rotational power loss

Stan Zurek

*Megger Instruments Ltd, Archcliffe Road, Dover, CT17 9EN, Kent, United Kingdom*

*E-mail: stan.zurek@ieee.org*

*Keywords:* Rotational power loss, magnetising yoke, magnetising apparatus.

Several international research laboratories attempted the round robin measurements of rotational power loss  $P_{rot}$ , with the aim of possible standardisation of the measurement method [1,2]. Majority of the laboratories employed the fieldmetric method, some used the thermometric technique. The comparison showed discrepancies at the level of tens of percents and thus at the time the results were deemed to be too unreliable for a standardisation procedure.

High levels of magnetisation could not be achieved with the magnetising yokes used for those measurements and the scattering of the measurements was not very well understood at the time.

Over the past two decades the computer technology progressed significantly. The data acquisition devices became less expensive, but also much more sophisticated offering simultaneous sampling, faster sampling rates and higher resolution. Hence, any inaccuracies resulting from the data acquisition (and generation) were appreciably reduced [3].

Digital technology also facilitated improvements in digital feedback algorithms, which can attain better stability and accuracy, as well as speed of control. However, excessive acceleration should be avoided [4]

The clockwise-anticlockwise (CW-ACW) differences in measured  $P_{rot}$  are now much better understood. Obviously, the results should be averaged from the two directions of rotations [1, 2]. The large CW-ACW differences at high amplitudes of magnetisation were shown to be attributed to the small angular misalignment between the sensors of flux density  $B$  and magnetic field strength  $H$  [5].

Recently, also an explanation for the CW-ACW differences persisting at lower excitation was also proposed [6]. Such differences can arise because of the non-ideal immunity of H-coils to the off-axis vector components of  $H$  [7]. Some improvements to magnetic shielding offering possibility of more efficient and more uniform magnetisation were proposed as well [8].

Analysis of all these improvements allows performing an analysis of the likely "optimum" design for the rotational magnetisation apparatus [4]. A synthesis of such a hypothetical optimum apparatus is presented in this paper.

It should be noted that most of the concepts referred to in this paper are supported by results already reported in the literature, with larger samples used in some systems, by using two-phase round yokes, larger B-coils and larger H-coils [4]. Just five ideas would require further experimental validation: maximum practical sample size, type of yoke winding (simple or "sinusoidal"), circular sample positioning (notches/edges), vertical shielding and rigorous testing of PCB-based H-coils.

The sample has 20 cm diameter and has trimmed straight edges for precise linear and angular positioning. The yoke is made similar to a stator of an induction rotor, with two-phase windings, with quasi-sinusoidal turn distribution. The B-coils can be as large as 150 mm, and their wires can be accommodated in a groove underneath the PCB-based equally large H-coils. The "vertical"

shielding can be added around the sample if it was found to be beneficial through experiments (Fig. 3b).

Hence the hypothetical "optimum" magnetising setup could look as shown in Fig. 1.

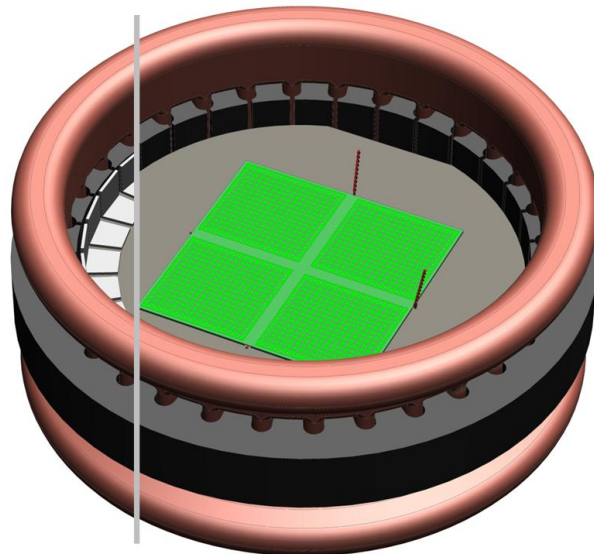


Figure 1: Overview of a magnetising apparatus without shielding and with visible straight edges of the sample (and an optional "vertical" shield).

### References

- [1] Sievert J., et al., "Intercomparison of measurements of magnetic losses in electrical sheet steel under rotation flux conditions", Commission of the European Communities, Report EUR 16255 EN, EC Brussels, Luxembourg, 1995
- [2] Sievert J., et al., "European intercomparison of measurements of rotational power loss in electrical sheet steel", *Journal of Magnetism and Magnetic Materials*, Vol. 160 (1996), 1996, p. 115
- [3] Zurek S., et al., "Errors in the power loss measured in clockwise and anticlockwise rotational magnetisation. Part 2: Physical phenomena", *IEE Proceedings, Science, Measurement and Technology*, Vol. 153 (4), 2006(b), p. 152
- [4] Zurek S., "Characterisation of Soft Magnetic Materials Under Rotational Magnetisation", CRC / Taylor & Francis, 2017, ISBN 978-1-138-30436-9
- [5] Zurek S., et al., "Errors in the power loss measured in clockwise and anticlockwise rotational magnetisation. Part 1: Mathematical study", *IEE Proceedings, Science, Measurement and Technology*, Vol. 153 (4), 2006(a), p. 147
- [6] Zurek S., "Effect of off-axis H-coil sensitivity on clockwise-anticlockwise differences of rotational power loss in isotropic samples", *IET Science, Measurement & Technology*, accepted for publication, Mar 2018.
- [7] Zurek S., "Sensitivity to off-axis vector components of typical wire wound flat H-coil configurations", *IEEE Sensors Journal*, Vol. 17 (13), 2017, p. 4021.

# Comprehensive Magnetic Properties Measurement of the Laminated Silicon Steel by a Novel High Frequency 2-D Magnetization Structure

Yongjian Li<sup>1</sup>, Kai Zhang<sup>1</sup>, Changgeng Zhang<sup>1</sup>, Shuaichao Yue<sup>1</sup> and Qingxin Yang<sup>1,2</sup>

<sup>1</sup> State Key Laboratory of Reliability and Intelligence of Electrical Equipment Hebei University of Technology, 300130, Tianjin, China

<sup>2</sup>Tianjin Key Laboratory of ATEEE, Tianjin Polytechnic University, Tianjin, 300387, China  
(liyongjian@hebut.edu.cn)

**Keywords:** Ultra-thin silicon steel, 2-D magnetic properties, high frequency, composite magnetic sensor

## 1. Introduction

The measurement of high frequency magnetic properties is important in design and performance optimization of the electrical apparatus, not only in the application of traditional motors and transformers, but also in emerging power electronics and special motors [1]. With the improvement of the processing technology of silicon steel materials, the thickness of ultra-thin silicon steel gradually approaches that of nanocrystalline, making the high-frequency performance of electrical steel sheets greatly improved, and gradually applied to the field of high-frequency transformers [2, 3]. The optimal design of these electromagnetic devices is inseparable from the accurate magnetic properties measurement [4]. Therefore, it is necessary to study the high-frequency rotating magnetic properties of magnetic materials [5]. Ultra-thin silicon steel is selected as the material of the magnetizing circuit instead of the nanocrystalline for ultra-thin silicon steel is easier to be processed into the desired core shape [6, 7].

## 2. Methods and Results

The novel 2-D magnetic tester consists of four orthogonal laminated cores, four multilayer excitation windings, which are wound around the four pairs of orthogonal core-poles. In order to concentrate magnetic flux density and enhance the excitation field, core poles are shaped into frustum of a square pyramid, as shown in Fig. 1. To acquire a uniform field, two guarding pieces, which are of the same material and grain oriented direction as the specimen, are attached on each surface of the specimen. The magnetic material specimen with  $B-H$  sensing structure is placed in the center of the tester, as shown in Fig. 1.

The comprehensive magnetic properties of the specimen are measured in different excitation models, with feedback control, harmonics compensation, and automated data processing, as shown in Fig. 2. More detailed magnetic properties in different frequencies and corresponding core loss features of the specimen will be presented in the full paper.

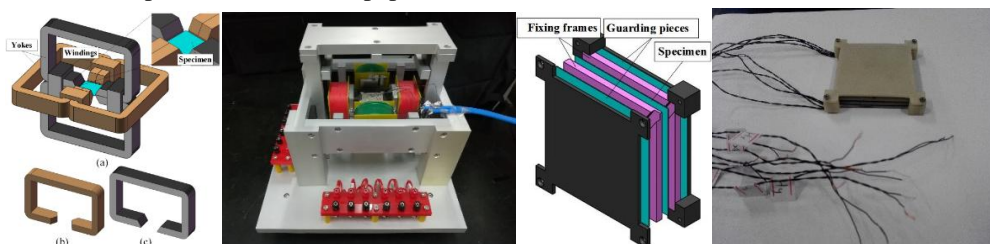


Fig. 1. The Novel 2-D high frequency magnetization structure. (a) 2-D magnetic properties magnetization structure. (b) and (c) are two types of laminated “C-type” core, B-H sensing structure

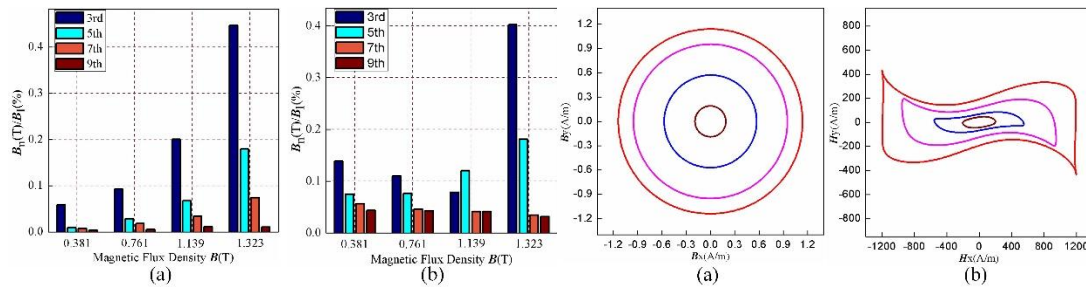


Fig.2. Ratio of harmonics to fundamental components under rotating magnetic measurement in rolling direction and tangential direction. (a) rolling direction (b) tangential direction, the rotating magnetic properties measurement with harmonics compensation method. (a)  $B$  loci and (b)  $H$  loci.

### 3. Conclusions

By using the newly designed 2-D magnetic properties tester with feedback control, harmonics compensation, and automated data processing, comprehensive magnetic properties of the magnetic material specimen are measured and analyzed. The magnetic properties for the magnetic material specimen in different directions are obtained, which is rarely studied but important to practical application.

#### References

- [1] T. Filchev, F. Carastro, P. Wheeler, and J. Clare, “High voltage high frequency power transformer for pulsed power application,” in *Proc. 14th Int. Power Electron. Motion Control Conf. (EPE/PEMC)*, Sep. 2010, pp. T6-165–T6-170.
- [2] Derebasi N, Rygal R, Moses A J, et al. A novel system for rapid measurement of high-frequency magnetic properties of toroidal cores of different sizes[J]. *Journal of Magnetism & Magnetic Materials*, 2000, 215(1):684-686.
- [3] Watakabe R, Tanaka M, Takahashi Y, et al. Study on Standard Measurement Method of Magnetic Property of Fe-based Amorphous Strip -round robin test results[J]. *IEEE Transactions on Magnetics*, 2016, 52(5):1-1.
- [4] Y Li, Q Zhao, L Wang, and C Zhang, “Improved High-Frequency Rotating Magnetic Properties Tester for Nanocrystalline Soft Magnetic Material,” *IEEE Trans Magn.* pp.99(2017):1-1.
- [5] Pftzner H, Mulasalihovic E, Yamaguchi H, et al. Rotational Magnetization in Transformer Cores—A Review[J]. *IEEE Transactions on Magnetics Mag*, 2011, 47(11): 4523-4533.
- [6] C Zhang, Y Li, J Li, Q Yang, and J Zhu, “Measurement of Three-Dimensional Magnetic Properties With Feedback Control and Harmonic Compensation,” *IEEE Trans. Ind. Electron* 64.3(2017):2476-2485.
- [7] Shen W, Wang F, Boroyevich D, et al. Loss characterization and calculation of nanocrystalline cores for high-frequency magnetics applications[J]. *IEEE Transactions on Power Electronics*, 2008, 23(1): 475-484.

# Vector Magnetic Hysteresis Characteristics

Masato Enokizono<sup>1,2</sup>, Daisuke Wakabaysh<sup>2</sup>

<sup>1</sup>Vector Magnetic Characteristic Technical Laboratory, Japan  
E-mail: enoki@oita-u.ac.jp

<sup>2</sup>Nippon Bunri University, Japan  
E-mail: wakabayshids@nbu.ac.jp

**Keywords:** Vector magnetic characteristics, vector hysteresis loop, electrical steel sheet

The magnetic characteristics of magnetic materials has vector relation on constitute equation generally. However conventional hysteresis characteristic is only rolling direction of steel sheet and is not general characteristics. It is due to orientation, rolling anisotropy, and crystal anisotropy. Therefore magnetoc flux density vector  $\mathbf{B}$  is not parallell to magnetic field strength vector  $\mathbf{H}$  and difference phase angle between vect  $\mathbf{B}$  and vector  $\mathbf{H}$ , wkich can be definded specific phase angle  $\theta_{BH}$ . In this paper the magnetic characteristic from the viewpoint of the vector relation is reviewed.

Figures 1(a) and (b) show the  $|\mathbf{B}|_{\max}-|\mathbf{H}|_{\max}-\theta_{BH}$  curve insted of conventional B-H curve about non-oriented electrical stel sheet and grain-oriented electrical steel sheet, respectively. This is possible to know the essence of the magnetic characteristic by showing vector hysteresis property by the 3D scatter diagram. Especially, handling of  $\theta_{BH}$  is necessary. By being dependent on time-related phase angle and spatial phase angle, the hysteresis property changes.

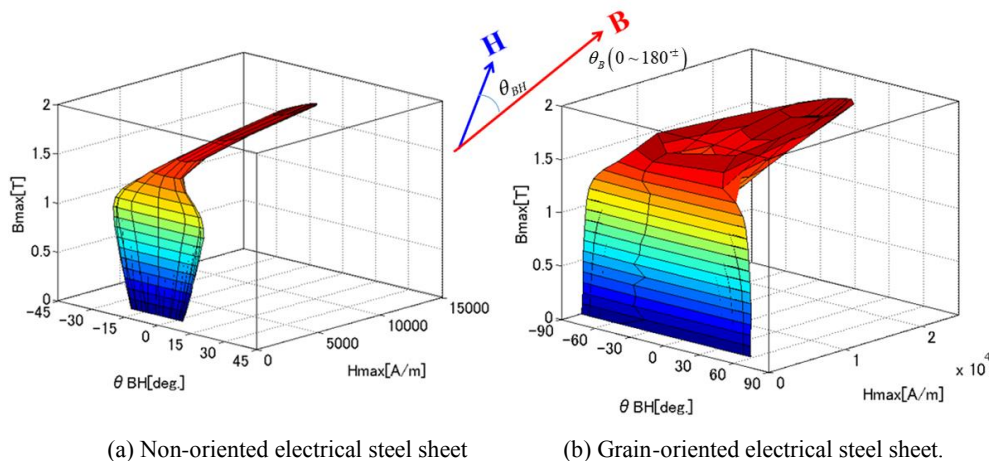
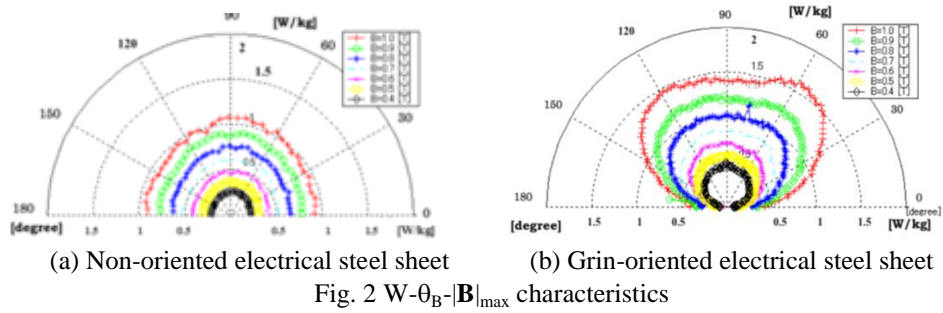


Fig. 1 Vector magnetic charcteristics,  $|\mathbf{B}|_{\max}-|\mathbf{H}|_{\max}-\theta_{BH}$  curve

Figure 2 shows the magnetic power loss characteristics as  $W-\theta_B-|\mathbf{B}|_{\max}$  distribution. The arbitrary directional dependence of magnetic power loss gives the knowledge which is important for the design of electrical machinery and apparatus.



In this workshop, we discuss the point to be watched carefully with the establishment of the concept of the vector magnetic characteristic.

### References

- [1] M. Enokizono, "Vector Magnetic Characteristic Technology and Design Method", Kagakujyoho shuppan Co., Ltd., ISBN: 978-4-904774-36-6 (2015.4) 262 Japanese Book.
- [2] URL <http://www.vector-mgttec.jp/>

# Energy loss along different directions in GO steel sheets

Carlo Appino<sup>1</sup>, Enzo Ferrara<sup>1</sup>, Carlo Ragusa<sup>2</sup>, Olivier de la Barrière<sup>3</sup>,  
Fausto Fiorillo<sup>1</sup>

<sup>1</sup>*Nanoscience and Materials Division, Istituto Nazionale di Ricerca Metrologica Torino, Italy*  
*c.appino@inrim.it; e.ferrara@inrim.it; f.fiorillo@inrim.it*

<sup>2</sup>*Energy Department, Politecnico di Torino, Torino, Italy, carlo.ragusa@polito.it*

<sup>3</sup>*Laboratoire SATIE, CNRS-ENS Cachan, France; barriere@satie.ens-cachan.fr*

*Keywords:* Grain-oriented Fe-Si, Magnetic losses, Magnetization process.

Grain-oriented (GO) Fe-Si sheets are often used in high-power rotating machines and in electrical motors having specific requirements, like synchronous reluctance motors with reduced torque ripple [1], where the material response along directions different from the rolling direction (RD) matters, both in terms of magnetization curve and of energy losses. Such response should also be known for transformers, where the flux deviates from RD in T-joints and corners, besides forming two-dimensional patterns [2]. But the experiments show that the DC magnetization curves and hysteresis loops depend in a complex fashion on the angle  $\theta$  made by the applied field with respect to RD in the lamination plane [3]. This effect can be quantitatively interpreted in terms of evolution of the domain wall processes, passing from the regular displacements of  $180^\circ$  domain walls for RD-directed field to the unfolding and combination of  $90^\circ$  and  $180^\circ$  domain wall displacements upon increasing  $\theta$  [4]. It has been actually shown that, by relying on Néel magnetic phase theory and pre-emptive knowledge of the material behavior along TD and RD, one can predict the normal magnetization curve, hysteresis loop shape, and the quasi-static loss dependence on the angle  $\theta$  in high-permeability GO sheets [4]. It is remarked, however, that, with the sole exception of RD and TD, the magnetic behavior of the GO alloys not only depends on  $\theta$ , but it is also strongly affected by the sample geometry. It is the very same limitation occurring in the classical measurement of the magnetization curve in cubic single crystals, where defined crystallographic cutting planes must be identified for the test sample, in order to obtain a fully flux-closed magnetic circuit [5]. In the present experiments, two sample geometries have been chosen: 1) Classical 30 mm wide Epstein strips, where the macroscopic magnetization is always directed with the field, whatever the  $\theta$  value, as imposed by a high transverse demagnetizing field; 2) X-stacked 120 mm wide sheets, where the transverse field is negligible and a two-dimensional macroscopic magnetization process takes place. The strong evolution of the measured DC magnetic properties with  $\theta$  and sample shape have an obvious counterpart in the dynamic properties, where both classical and excess loss depend on the sheet cutting angle according to whether Epstein or X-stack configurations are considered [5]. To such evolution, only phenomenological descriptions have been given so far in the literature [6]. In this work we have thus investigated the magnetic energy loss versus frequency ( $1 \text{ Hz} \leq f \leq 800 \text{ Hz}$ ) and peak polarization ( $0.15 \text{ T} \leq J_p \leq 1.4 \text{ T}$ ) in high-permeability 0.29 mm thick GO sheets, where the field is applied along angles  $\theta$  to RD ranging with  $15^\circ$  steps between  $0^\circ$  and  $90^\circ$ . Experiments have been performed by means of a calibrated hysteresisgraph-wattmeter, with digitally controlled sinusoidal induction waveform. The sheet/strip sample is inserted in the 240 mm long gap of a laminated

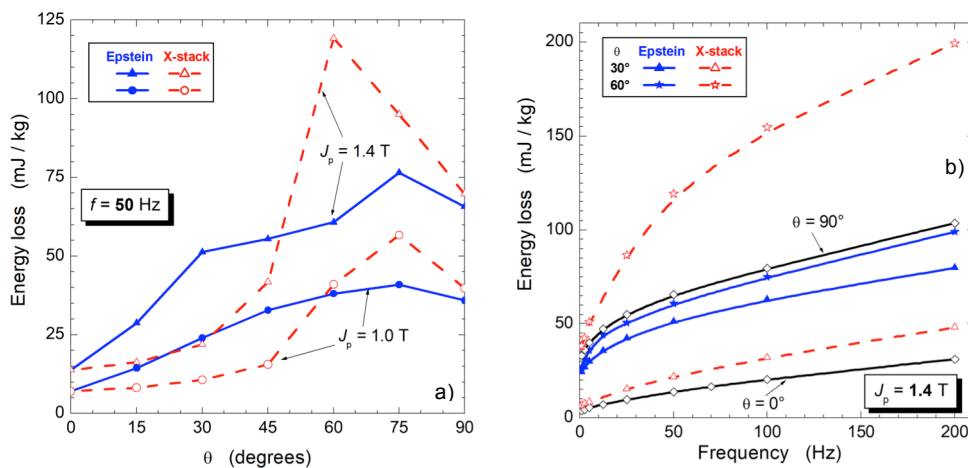


Figure 1: High-permeability GO Fe-Si sheets. a) Energy loss measured at 50 Hz versus cutting angle  $\theta$  at two  $J_p$  values in single Epstein strips (solid lines) and X-stacked sheets (dashed lines). b) Frequency dependence of the energy loss at  $J_p = 1.4$  T for  $\theta = 0^\circ, 30^\circ, 60^\circ,$  and  $90^\circ$ . The loss figure along RD and TD is independent of the sample arrangement (single strip/X-stack).

double-C vertical yoke, endowed with 125 mm  $\times$  30 mm pole faces and air-flux compensated windings. The results shown in Fig. 1, comparing the 50 Hz energy loss vs.  $\theta$  at two peak polarization values and the loss vs. frequency  $W(f)$  curves at  $J_p = 1.4$  T, provide significant examples of the large differences arising in the obtained loss figure with the single Epstein strip and the X-stack configurations for  $\theta$  different from  $0^\circ$  and  $90^\circ$ . In the single Epstein strips, the applied field  $H_a$  and the transverse demagnetizing field  $H_d$ , resulting from a high demagnetizing factor, compound to activate the  $180^\circ$  and  $90^\circ$  domain wall processes in such a way that the transverse macroscopic magnetization is negligible and  $J$  is always directed along the strip length. With the X-stacked configuration,  $H_d \cong 0$  and the magnetization process has a two-dimensional character. This is reflected in a very different evolution of the magnetic loss  $W$  vs.  $f$  in these two cases and calls for a suitable generalization of the loss decomposition procedure, according to the Statistical Theory of Losses. In the present work, such a general approach to the dynamic losses is worked out and a prediction for the loss components for single strips and X-stacked GO sheets as a function of the angle  $\theta$ , up to the frequency engendering incipient skin effect, is made.

### References

- [1] Taghavi, S., Pillay, P., *IEEE Trans. Ind. Appl.*, **52** (2016), 3729 - 3738.3
- [2] Pfützner, H., Mulasalihovic, E., Yamaguchi, H., Sabic, D., Shilyashki, G., Hofbauer, F., *IEEE Trans. Magn.* **47** (2011) 4523-4533.
- [3] Baghel, A.P.S., Ram Sai, B., Chwastek, K., Daniel, L., Kulkarni, S.V., *J. Magn. Magn. Mater.* **418** (2016), 14-20.
- [4] Fiorillo, F., Dupré, L.R., Appino, C., Rietto, A.M., *IEEE Trans. Magn.* **38** (2002), 1467-1476.
- [5] Dupré, L. R., Fiorillo, F., Melkebeek, J., Rietto, A. M., Appino, C., *J. Magn. Magn. Mater.* **215-216**, (2000), 112-114.
- [6] Pluta, W.A. *IEEE Trans. Magn.* **52** (2016), 6300912.



# **PS1: Poster Session**

Session Chairs

**Masato ENOKIZONO**

Oita University, Electrical And Electronic Eng. - Japan

**Carlo APPINO**

Inrim National Institute Of Metrological Research - Italy



# Analysis of High Frequency Effects of Excitation Winding in High Frequency Rotating Tester with Nanocrystalline material

Yu Dou<sup>1</sup>, Yongjian Li<sup>1</sup>, Changgeng Zhang<sup>1</sup>, Angxuan Li<sup>1</sup>, and Jianguo Zhu<sup>2</sup>

<sup>1</sup> State Key Laboratory of Reliability and Intelligence of Electrical Equipment, Hebei University of Technology, Tianjin, China

<sup>2</sup> School of Electrical, Mechanical and Mechatronic Systems, University of Technology, Sydney, NSW 2007, Australia

E-mail: liyongjian@hebut.edu.cn

**Keywords:** the skin effect, the proximity effect, distribution capacitance, segmented winding with copper foil.

In multi-phase power transformers and rotating electrical machines, the rotating magnetic flux may cause the increase of core losses, leading to local overheating and damage of the equipment. Nevertheless, the traditional measurement method of magnetic properties for nanocrystalline is ring specimen method, which is difficult to accurately describe high frequency rotating magnetic properties of nanocrystalline in engineering practice. The main difficulty to test the magnetic properties for nanocrystalline at high-frequency is that the core losses of magnetic circuit increase acutely with the increasing frequency and the influence of high frequency effects [1] [2].

This paper presents a segmented winding with copper foil, which can reduce the influence of high frequency and distribution capacitance. An equivalent model for the AC resistance of the foil winding is established, which determines the optimum thickness of copper foil under different excitation frequency. The method of installing annular ferromagnetic plate to restrain the proximity effect is proposed, which plays a key role in the establishment of high frequency rotating magnetic field.

## II. DESIGN OF THE SEGMENTED COPPER WINDING

The 2D magnetic tester with foil winding has several advantages. However, the distributed capacitance in foil winding has increased compared with copper wire windings. (Although the 2D magnetic tester with foil winding has several advantages, the distributed capacitance in foil winding will increase compared with copper wire windings.) Different connection ways between the winding layers lead to different potential, and then form the different equivalent capacitance [3]. Fig. 1 depicts the simplified mathematical models of (a) single segmented winding and (b) multi-segmented winding. The analytic expression of equivalent distribution capacitance of single segmented winding is(takes a form):

$$C_{\text{single}} = \frac{(n-1)C_1}{n^2} = \frac{(n-1)\varepsilon S}{n^2 d}$$

the distribution capacitance of segmented winding is analytical calculated as:

$$C_{\text{multi}} = \frac{(n-1)C_1}{n^2 q^2} = \frac{(n-1)\varepsilon S}{n^2 q^2 d}$$

where  $\varepsilon$  is the dielectric constant of the winding interlayer insulation medium,  $S$  is the average area of the winding,  $d$  is the winding layer spacing, and  $C_1$  is the static capacitance of the two layer

winding with an equivalent area of  $S$ . It can be seen that the distribution capacitance of the copper foil winding can be reduced by increasing the number of winding layers and the number of segments.

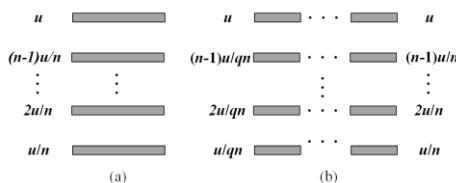


Fig.1 Mathematical model of copper foil winding with two different winding modes.

With the increase of frequency, the influence on the current distribution in copper foil produced by the magnetic field is more and more apparent. Mathematical model of magnetic field intensity of copper foil winding is shown in Fig.2. (a). Combined the Bessel equation of internal magnetic field strength  $H$  and the boundary conditions, the approximate relation between the AC resistance and the DC resistance under the influence of skin effect and proximity effect is:

$$\frac{R_{ac}}{R_{dc}} = \Re \left[ md \left[ \coth(md) + \frac{2(p^2 - 1)}{3} \tanh\left(\frac{md}{2}\right) \right] \right] = \beta \left[ \frac{\sinh 2\beta + \sin 2\beta}{\cosh 2\beta - \cos 2\beta} + \frac{2(p^2 - 1)}{3} \frac{\sinh \beta - \sin \beta}{\cosh \beta + \cos \beta} \right]$$

The proximity effect is caused by leakage at the end of copper foil winding. Therefore, how to control the leakage magnetic field distribution along the axial direction of the winding and reduce the radial component of the leakage flux at the end of winding is the key to restrain the proximity effect. In this paper, the method of installing annular ferromagnetic plate at the end of segmented copper foil winding and between two segments winding to restrain the proximity effect is proposed. The comparison of the current distribution in segmented winding is shown in Fig. 2 (c), in which the black portion is the ferromagnetic material. It can be seen that the radial component of the leakage magnetic field is effectively controlled when the annular ferromagnetic plate is arranged, and the current distribution in the copper foil winding is more uniform. In conclusion, a segmented winding with copper foil is designed based on the excitation structure as shown in Fig2. (d).

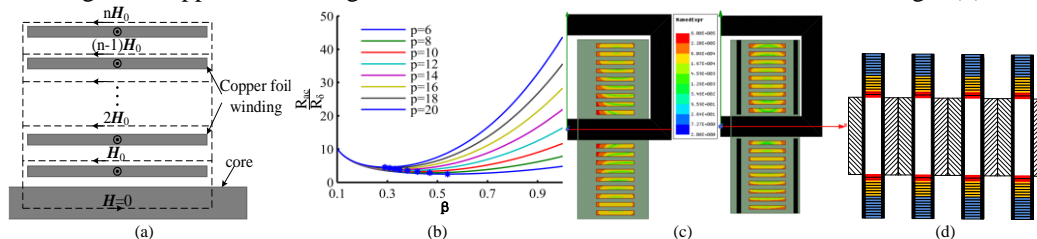


Fig.2 (a) Mathematical model of magnetic field intensity of copper foil winding. (b) Optimization curve of winding thickness. (c) The comparison of the current distribution in segmented winding without and with annular ferromagnetic plate. (d) Diagram of segmented winding with copper foil.

## References

- [1] M. Birkfeld and K.A. Hempel, "A device for measuring the magnetic properties of ring specimens at high frequencies." J. Magn. Mater, vol. 133, pp.393-395, 1994.
- [2] T. Nakata, N. Takahashi, K. Fujiwara, and M. Nakano, "Measurement of Magnetic Characteristics along Arbitrary Directions of Grain-oriented Silicon Steel up to High Flux Densities," IEEE Trans. Magn., vol. 29, no. 6, pp. 3544-3546, 1993.
- [3] F. Blache, J. Keradec, and B. Cogitore, "Stray capacitance of two winding transformers: Equivalent circuit measurements calculation and lowering," Industry Applications Conference, Soc. Annu. Meeting, Conference Record of the IEEE, vol.2, (1994), pp. 1211-1217.

# Characterization of NdFeB Bonded Magnets for Halbach Magnets in Electric Vehicles Motors

Amit Kumar Jha<sup>1</sup>, Faustin Mandil<sup>2</sup>, Afef Kedous-Lebouc<sup>1</sup>, Lauric Garbuio<sup>1</sup>  
Sophie Rivoirard<sup>2</sup>

<sup>1</sup>Univ. Grenoble Alpes, CNRS, Grenoble INP G2Elab, 38000 Grenoble, France

E-mail: Amit-kumar.jha@g2elab.grenoble-inp.fr ; Afef.Lebouc@g2elab.grenoble-inp.fr

<sup>2</sup>CNRS/ Institut Neel, BP 166; 38042 Grenoble, France

E-mail: faustin.mandil@neel.cnrs.fr; sophie.rivoirard@neel.cnrs.fr

**Keywords:** Bonded NdFeB magnets, Characterisation, Halbach Magnets.

The Halbach magnet has many advantages for high torque density motors [1]. However, the manufacturing of Halbach magnet is complex and very costly which discourages the use of Halbach magnets. Furthermore, the designs presented in literature uses pre-magnetized sintered NdFeB magnets to manufacture Halbach magnet. The use of segments not only makes assembly difficult the airgap flux distribution also deviates significantly from ideal hence, not desirable for the motors. To overcome above mentioned issue the bonded magnets are good choice to produce Halbach magnet. The use of bonded magnets ensures easy manufacturing/assembly ( injection molding) and also realization of ideal airgap flux distribution can be achieved [2].

In this article characterisation of a commercially available anisotropic MF18P bonded NdFeB material from Aichi Steel is presented. The extraction magnetometer was used to measure the magnetic properties of the sample which can apply field up to 7 T and temperature in the range of 300 K to 800 K ( 27 to 527 °C). A cube of 3 mm was made and marked in three directions to perform measurement. More measurement results will be presented in final article.

## 1 Measurement Results

### Anisotropy

Figure 1 shows the demagnetisation of magnet sample in all three direction. It can be seen that the magnet has very high anisotropy. The direction named Prep 1R has high magnetic field compared to other axes and is the easy magnetization axis. The other two hard magnetization axes have very similar magnetic behaviour. The remanence of easy axis is almost 230 % higher than the other two axes. The anisotropic ratio of the magnet was around 0.42.

### Thermal Conductivity

Table 1 presents the thermal measurement performed to find thermal conductivity of the magnet. It can be seen that the specific thermal conductivity value of the magnet is  $1 \text{ W.m}^{-1}.\text{K}^{-1}$  for different temperature range. The slight increase in the conductivity is due to the leakage of heat in the setup.

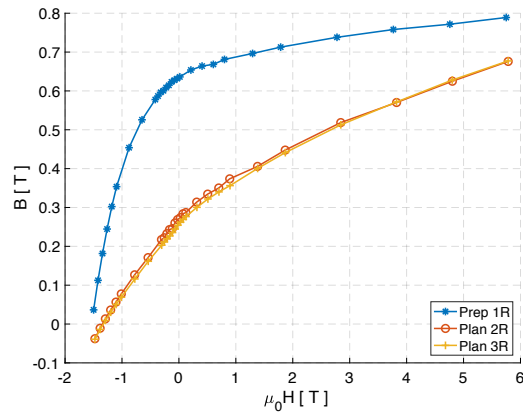


Figure 1: Field density in different direction

Table 1:  $\Delta T$  at different positions on the magnet and the average thermal conductivity of the magnet

$P_{in}$ [ W ]	Pos 1 [ K ]	Pos 2 [ K ]	Pos 3 [ K ]	Pos 4 [ K ]	Average [ K ]	Thermal Conductivity [ $\lambda_{th}$ ]
7.00	5.64	4.43	4.79	5.26	5.02	1.00
9.92	9.24	5.72	5.97	6.92	6.96	1.03
12.94	8.94	7.43	10.4	8.70	8.87	1.05
20.05	13.24	11.33	15.44	12.49	13.12	1.10
24.87	14.91	13.50	18.74	15.14	15.63	1.18

## 2 Conclusion

The characterisation of the magnet shows that magnet can have high remanence value due to high anisotropy. The thermal heat conductivity is also stable for different supplied power. In the final article other measurement results will also be presented.

### Acknowledgements

The research leading to these results has received funding from European Communitys Horizon 2020 Programme ([H2010/2014-2019]) under Grant Agreement no. 674973 (MSCA-ETN DEMETER). This publication reflects only the authors view, exempting the Community from any liability. Project website <http://etn-demeter.eu/>

### References

- [1] Z. Q. Zhu and D. Howe, "Halbach permanent magnet machines and applications: a review," *IEE Proceedings - Electric Power Applications*, vol. 148, no. 4, pp. 299–308, Jul 2001.
- [2] Z. Q. Zhu, Z. P. Xia, K. Atallah, G. W. Jewell, and D. Howe, "Integrated design of magnet powder aligning system and brushless motor using anisotropic halbach cylinders," in *1999. Ninth International Conference on Electrical Machines and Drives (Conf. Publ. No. 468)*, 1999, pp. 123–127.

# Design of a Single Sheet tester coils' windings for the magnetic, electric and mechanical measurements of magnetized electrical steels and soft magnetic materials

O. Maloberti<sup>1,2</sup>, E. Salloum<sup>2</sup>, S. Panier<sup>2</sup>, P. Dassonville<sup>1,3</sup>, J. Stahlschmidt<sup>4</sup>, P. Klimczyk<sup>4</sup>

<sup>1</sup>ESIEE Amiens, 14 quai de la Somme, 80080, Amiens, France

<sup>2</sup>LTI Laboratory, UPJV, Avenue des Facultés - Le Bailly 80 025 Amiens, France

<sup>3</sup>MIS laboratory, 14 Quai de Somme, 80080 Amiens, France

<sup>4</sup>BROCKHAUS, Gustav-Adolf-Str. 4, D-58507 Lüdenscheid, Germany.

*Keywords: magnetic measurements, vibration testing, electrical steels, single-sheet tester.*

Accurate macroscopic measurement of electrical steels requires very specific experimental tools. Magnetic measurements in one direction can be performed with the Ring Core Tester or the Epstein Frame [1], in 2D direction with the Single Sheet Tester [2] and in rotational field with the Rotational Single Sheet Tester [3]. Due to the complexity of the magnetic structure of such materials with domains and walls that change as a function of the working conditions, knowing the electrical conductivity of the material is a pre-requisite to the magnetic measurement. Electrical measurements of the electrical conductivity can be performed with the two or four terminals sensing procedure [4]. Another method consists in using an eddy current probe [5] which is inaccurate for materials with a magnetic structure [6]. Mechanical measurements are of two kinds, the usual non-linear plastic ones such as the tensile strength testing, and the linear elastic ones such as the vibration testing. Most of the time, these measurements are carried out separately without considering the possible couplings between the phenomena. Equipment that make the measurement of the first magneto-electric couplings, including the relationship between the magnetization and the electrical current, already exists but mainly for very thin samples dedicated to the nanotechnologies (see measurements of microscopic magneto-electric effects [7]). In non-linear mechanics, we can easily find apparatuses to measure the impact of a mechanical stress onto the magnetic behavior [8]. We also find apparatuses that aim at measuring the impact of the magnetization onto the strain-stress behavior through the measurements of the magnetostriction effect [9]. Finally, vibrations and noise are most of cases measured directly in a product with accelerometers, vibrometers and microphones.

In this work, we focus on macroscopic samples compatible with classical experimental tools (Epstein, ring core, SST and) and study:

- 1) The impact of the macroscopic magnetization on the macroscopic electrical conductivity,
- 2) The impact of the macroscopic magnetization on the mechanical stress and vibrations.

The aim of this paper is to optimize the design of a specific Single Sheet Tester (SST) dedicated to the magnetic measurements of 150\*150 mm samples with two possible field directions. In parallel, we would like to carry out complementary physical measurements. While measuring an average magnetization within the sample, it should be possible to measure: the surface magnetic field with field sensors, the electrical conductivity with the two or four terminals sensing method and the linear mechanical stresses, vibrations and noise with accelerometers, a laser vibrometer and a microphone. This is not possible in the standard SST. We must adapt the design to have access to the sample, inside the coils' opening, with measuring wires and other thin sensors (field sensors, current sensors, accelerometers, laser spot, ...). The air-gap space between the sample and the coils'

windings is thus increased and divided in several parts separated by small slots. Therefore, we must design the new windings in order to guarantee the following performances:

- 1) a high enough peak magnetic field onto the sample area upon test ( $> 5\,000\text{ A/m}$ ),
- 2) a small enough field gradient and difference on the whole sample area upon test ( $< 0.5\%$ ),
- 3) a high enough fundamental frequency ( $f=1000\text{ Hz}$ ) with a saturation polarization up to  $2\text{ T}$ ,

knowing the limitations of the generator ( $I_{\max} = 26\text{ A}$ ,  $V_{\max} = 100\text{ V}$ ,  $f_{\max} = 20\text{ kHz}$ )

In this paper we suggest using from one to three tools to design the most adapted windings to our needs. We will use a fast-analytical model to find the wires' diameter and the number of layers and turns in both the primary and secondary coils, a 2D numerical model with the Finite Element Method (FEM) to define with accuracy the location of each turn and a 3D model also based on the FEM to have a reference [10]. A discrete optimization procedure onto the number of turns and location of wires will be presented with the fast 2D numerical methods. A sensitivity analysis to some key parameters (magnetic permeability and airgap) will be presented to specify the use limitations. The accuracy and the sensitivity of the magnetic field  $H$  and the induction  $B$  to the electrical current  $I$  and the voltage  $V$  will then be calculated [11]. Finally, Magneto-mechanical simulations will lead to an estimation of the induced stresses (magnetostriction and Maxwell) to guide the experiments.

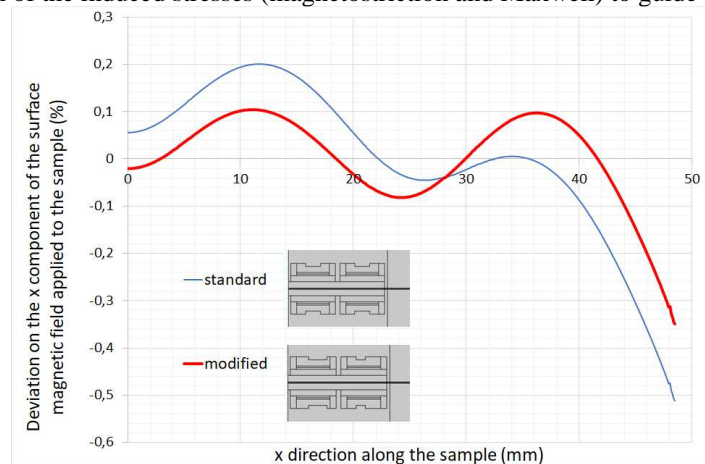


Figure 1: Optimization of primary windings to minimize the field gradient on the sample area upon test.

*Acknowledgements:* The equipment is manufactured by BROKHAUS. This work takes part to a research project that has received funding from the European Research Council under the European Union's H2020-IND-CE-2016-17/H2020-FOF-2017 Program (GA No. 766437).

#### References

- [1] EC 60404-2, Magnetic Materials-Part 2, 3rd ed. Geneva, Switzerland: IEC, 1996
- [2] ASTM A1036 – 04 (2015)
- [3] D. Makaveev et al., *J. Mag. And Magn. Mat.*, 196-197 (1999), pp. 937-939.
- [4] C.L. Petersen et al., *Sensors and Actuators A: Physical*, Vol. 96, no. 1 (2002), pp. 53-58.
- [5] D.Schieber et al., *Journal of the Franklin Institute*, Vol. 310, no. 4–5 (1980), pp. 271-280.
- [6] X. Chen, *NDT & E International*, Vol. 75 (2015), pp. 33-38.
- [7] J.-P. Rivera, Analytical and Applied Chemistry, Sciences II, 1211 Geneva 4, Switzerland.
- [8] M. Rekik et al., *Congrès Français de Mécanique 2013*, Aug 2013.
- [9] T. Nakase et al., *IEEE Transactions on Magnetics*, 35(5) (1999), pp. 3956 – 3958.
- [10] J. V. Leite et al., *COMPEL Int. J. of Computations & Math in Electrical*, 26(4) (2007).
- [11] M. Mikulec, *Journal of Mag. and Mag. Mat.*, Vol. 112, no. 1–3 (1992), pp. 112-114.

# Electrical and magnetic characterization of parallelepipedic sample extracted from massive claw poles alternator

Meryeme Jamil<sup>1,2</sup>, Abdelkader Benabou<sup>1</sup>, Stéphane Clénet<sup>1</sup>, Laure Arbenz<sup>2</sup>, Jean-Claude Mipo<sup>2</sup>

<sup>1</sup>Univ. Lille, Arts et Metiers ParisTech, Centrale Lille, HEI, EA 2697 - L2EP -Laboratoire d'Electrotechnique et d'Electronique de Puissance, F-59000 Lille, France

<sup>2</sup>Valeo/2 rue André Charles Boulle, Créteil, France

E-mail: meryeme.jamil@etudiant.univ-lille1.fr

*Keywords: Electrical conductivity, permeability, correction factor, mini SST, FE simulation.*

## A. INTRODUCTION

Electrical machine performances are strongly related to electromagnetic properties of ferromagnetic materials such as Fe-Si steel. When massive magnetic parts are considered, these properties may be impacted by the manufacturing process, in a heterogeneous way regarding the volume properties. In that case, the electric and magnetic characteristics of the machine components are different from those of the raw material [1]. Extensive researches on the interactions between processes, electromagnetic properties and other material properties have been done, mostly in the case of laminated electrical steel, but rarely in the case of massive forged steel [2]. Moreover, in our experimental investigations on manufactured degraded claw poles steel, the extraction of samples from the magnetic part imposes dimensions that are smaller than the dimensions prescribed in the international standards of magnetic measurements. Thus, the challenge brought by the current study is the development of a specific methodology to characterize the electrical conductivity and the magnetic behavior on the same representative massive parallelepipedic sample extracted from different locations in a claw poles rotor. Additionally, the impact of grain size, mechanical state and forge fiber on electrical conductivity is investigated

## B. METHODOLOGY

The electrical conductivity measurement is based on the four-point method [3]. The four probes are arranged on a straight line with 6mm equidistant spacing, the current is imposed flowing through the outer pair of points and the voltage is measured between the two inner points. To deduce the electrical conductivity, in a general way, a geometrical correction factor  $F$  must be introduced such as:

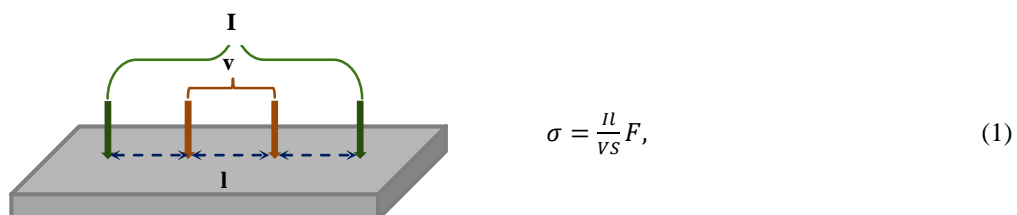


Figure 1 : Four-point method

where  $\sigma$  is the electrical conductivity,  $I$  is current,  $l$  is the distance between the voltage probes,  $V$  is the voltage,  $S$  is the section of the sample and  $F$  is the correction factor. In the literature, this factor  $F$  is calculated analytically for specific geometries of samples and positioning of the point probes regarding the sample edges. Different methods are then proposed, such as the method of images, complex variable theory, the method of Corbino sources, Poisson's equation, Green's functions and conformal mapping [4]. Yet, in our case, the geometrical hypotheses are not verified as the sample dimensions are relatively small regarding its thickness. It is then proposed to determine the correction factor from numerical simulations using 3D electrokinetic field calculation. The model is based on the solution of the electrokinetic problem solved by the finite element method using the scalar potential formulation. For different sample dimensions, the current flowing through the external needles of the sensor is

imposed and the resulting voltage between the internal needles is calculated, so that the correction factor could be deduced from (1).

The magnetic properties can be measured by the use of a miniaturized single sheet tester (SST) as in [5]. Based on the first numerical results of 2D Finite Element (FE) simulations of a miniaturized SST, the magnetic field in the sample will be determined from Hall sensor measurements of the local tangential field that will be extrapolated on the sample surface. Regarding the magnetic flux density, it can be obtained from the voltage measurement on a secondary winding placed around the sample in the region where the magnetic flux is homogeneous. It is planned to perform 3D simulations to validate the sample dimensions verifying all the constraints for accurate determination of electrical and magnetic properties.

### C. RESULTS AND DISCUSSION

As shown in Figure 2 (a), the correction factor  $F$  of the electrical conductivity depends on the sample dimensions. It increases with the increase of the sample width ( $w$ ) and thickness ( $t$ ) and it decreases when the sample length increases. In this work, the choice of the sample dimensions was based on the most constraining part of the forged claw poles. These dimensions are 25mm length, 8 mm width, 8mm thickness, and the calculated correction factor for electrical conductivity is 1,0898. Using this factor, the measurement results of electrical conductivity on samples with variable grain sizes, mechanical states and forge fiber have been obtained from (1). The Figure 2 (b) presents the impact of cold plastic deformation on the electrical conductivity. Given the dispersion and the error related to the measurement system, the three parameters: grain size, plastic deformation and forge fiber do not seem to have any detectable effect on the electrical conductivity, at least with the proposed characterization technique. The results of magnetic measurement will be presented in the full paper.

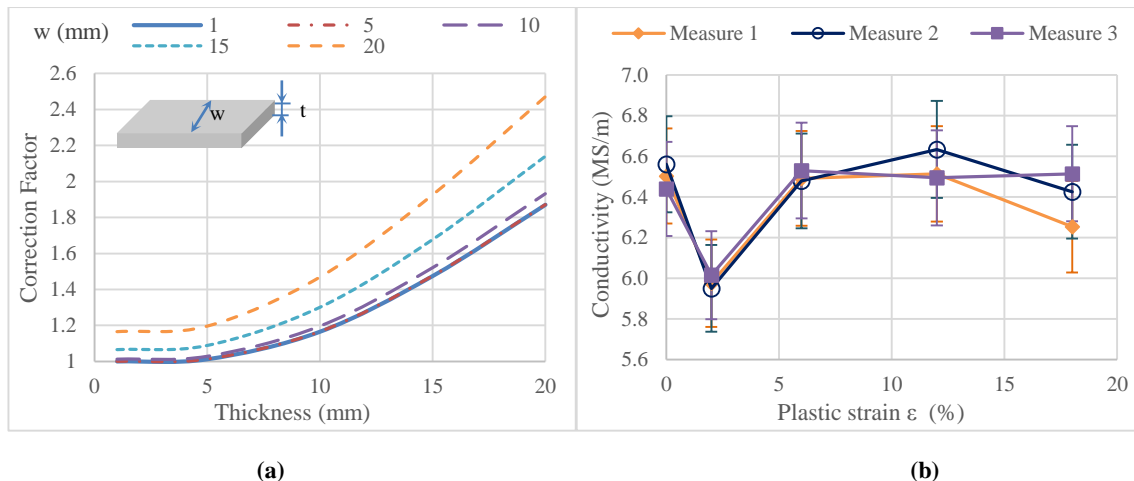


Figure 2 : (a) Simulated correction factor as a function of sample thickness for different widths ( $w$ ) and a fixed length of 25mm. (b) Effect of plastic strain on the electrical conductivity

### References

- [1] Ramarotafika, R., et al., "Experimental characterization of the iron losses variability in stators of electrical machines", *IEEE Trans. Magn.* **48** (2012), 1629–1632.
- [2] Borsenberger, M., et al., "Specific Magnetic Characterization for Massive Magnetic Parts using an Electromagnet Device ". *IGTE*, (2016).
- [3] Arbenz, L., et al., "Characterization of the local electrical properties of electrical machine parts with non-trivial geometry". *Int. J. Appl. Electrom.* **48** (2015), 201-206.
- [4] Schroder, D. K. "Semiconductor material and device characterization", ed John Wiley & Sons, (2006), 8-14.
- [5] De Wulf, M., Makaveev, D., Houbaert, Y., Melkebeek, J., "Design and calibration aspects of small size single sheet testers", *J. Magn. Magn. Mater.*, **254** (2003), 70–72.

# Frequency dependence of anizotropy of specific total loss in Goss textured electrical steel

Wojciech A. Pluta

*Czestochowa University of Technology, Al. Armii Krajowej 17, 42-200 Czestochowa, Poland*

*E-mail: w.pluta@gmail.com*

**Keywords:** directional properties, specific total loss, Goss textures electrical steel.

The production process of electrical steel sheets (ES) can be carried out in such a way that in the final product crystals are ordered in rolling direction (RD). In this direction ES displays most favorable magnetic properties and in directions 55° and 90° appears poor magnetic properties. The amount of crystals oriented along RD in relation to whole amount of crystals decides about directional properties of ES. This is usually described by degree of texture being a measure of amount of crystals oriented along RD in relation to whole amount of crystals. Another way to describe the directional properties is the anisotropy of magnetic properties e.g. flux density or anisotropy of specific total loss. Generally, magnetic anisotropy is determined for a given magnetic parameter at a given value of the abscissa  $y$ . For example, the anisotropy of specific total loss  $\Delta AP_{S,1.5}^{90-0}$  is calculated for the magnetization angles  $x = 90^\circ$  and  $x = 0^\circ$  at the flux density 1.5 T. The anisotropy phenomenon play important role in construction of magnetic circuits.

It is overall accepted that the specific total loss  $P_S$  consist of three components: hysteresis, classical and excess eddy current. The frequency dependence of the three components can be described bertotti model and it can be applied at any angles  $x$  to the RD, is seaparated in the commonly used way as [1]:

$$P_S / f = \underbrace{C_h B_p^\alpha}_{P_h / f} + \underbrace{C_{ce} B_p^2 f}_{P_{ce} / f} + \underbrace{C_{ex} B_p^{3.2} f^{1/2}}_{P_{ex} / f} \quad (1)$$

where:  $C_h$  is the hysteresis loss coefficient,  $\alpha$  is the exponent of flux density,  $C_{ce} = \pi^2 d^2 (6\rho)^{-1}$  is the classical eddy current loss coefficient under sinusoidal magnetization,  $C_{ex}$  is the excess loss coefficient,  $\rho$  is the resistivity and  $d$  is the sheet thickness.

In (1) only classical eddy current specific total loss shows isotropic characters. This is due to the fact it is calculated for perfectly conducting infinite homogenous plate. The hysteresis and excess eddy current loss components display anisotropic character. Additionally, both components show similarity due to their common origin [1, 2]. In Fig.1 are presented experimental data (points) and fitted using (1) energy loss versus frequency for different magnetizing directions obtained for GO steel M150-35S grade at  $B_m = 1.1$  T. In this figure the non-linearity of frequency dependence of anisotropy of specific total loss is visible.

In this paper is presented analysis of frequency and flux density dependence of the anisotropy of specific total loss. The analysis is performed using novel model of directional properties of specific total loss based on loss separation approach [3].

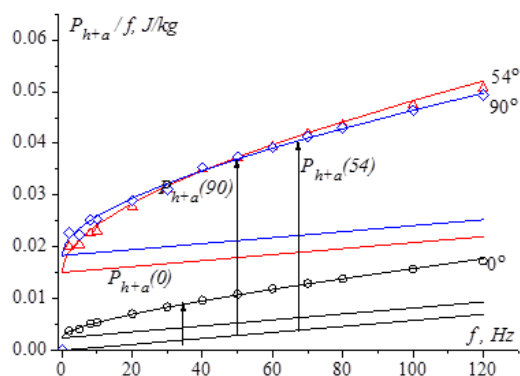


Figure 1: Energy loss per unit mass versus frequency for different magnetizing directions obtained for GO steel M150-35S grade at  $B_m = 1.1$  T.

### References

- [1] Bertotti G., "Hysteresis in magnetism", Academic Press (1998)
- [2] Pluta W.A., Angular properties of specific total loss components under axial magnetization in grain-oriented electrical steel. IEEE Trans. on Magnetics, Vol. 52, nr 4 (2016), 12 stron, s. 6300912.
- [3] Pluta W.A., Calculating power loss in electrical steel taking into account magnetic anisotropy, Przegląd Elektrotechniczny, nr 2 (2018), s. 100-103.

# From magnetic spectroscopy and fractional Cole-Cole model to high amplitude dynamic scalar hysteresis cycles

Benjamin Ducharne<sup>1</sup>, Yves Armand Tene Deffo<sup>2</sup>, Bhaawan Gupta<sup>13</sup>

<sup>1</sup>Laboratoire de Génie Electrique et Ferroélectricité, France  
E-mail: benjamin.ducharne@insa-lyon.fr

<sup>2</sup>Buea University, Cameroun  
E-mail: ytenedeffo@yahoo.com

<sup>3</sup>ElyTMax, Tohoku University, Japan  
E-mail: bhaawan.gupta@insa-lyon.fr

*Keywords:* Magnetic spectroscopy, fractional derivative, dynamic scalar hysteresis.

The development of new electromagnetic designs, such as the improvement of already existing ones require precise simulation and characterization tools. Recent scientific investigations around numerical scheme for ferromagnetic devices mainly focus on coupling Space Discretization Techniques (SDT), Finite Elements Method (FEM), Finite Differences Method (FDM)) to accurate scalar or vector, dynamic or static hysteresis material laws [1][2]. Such simultaneous resolutions lead to accurate results, but require huge memory space and simulation times. In [3]-[5], an original alternative is proposed. In this approach, space discretized technique is replaced by a lump model. Accurate simulation results on a large frequency bandwidth are obtained due to fractional order derivative operators. In such models, a fractional derivative of the induction field  $B$  multiplied to a constant  $\rho$  is considered as an equivalent magnetic excitation field  $H_{equ}$ .

$$\rho \cdot \frac{d^\alpha B(t)}{dt^\alpha} = H_{dyn}(t) - f_{static}^{-1}(B(t)) \quad (1)$$

In ferroelectricity, the dielectric spectroscopy (variation of the dielectric properties of a medium as a function of the frequency) has grown tremendously in stature over the past few years and is now being widely employed in a wide variety of scientific fields such as fuel cell testing, biomolecular interaction and microstructural characterization. The ferroelectric comportment as the frequency is varying known as the dielectric relaxation gives important information about the material constitution and about the physical relations describing the polarization behaviour. Dielectric relaxation is defined as the momentary delay in the dielectric constant of a material. This relaxation is usually described in terms of permittivity as a function of frequency, which can, for ideal systems, be described by the Debye equation [6] which for real material is extended to the fractional Cole-Cole model [7][8].

$$\varepsilon^*(\omega) = \varepsilon'(\omega) - j\varepsilon''(\omega) = \varepsilon_\infty + \frac{\Delta\varepsilon}{1 + (i\omega\tau)^\alpha} \quad (2)$$

Where  $\varepsilon_\infty$  is the modulus of the sample permittivity under high frequency excitation,  $\Delta\varepsilon = \varepsilon_s - \varepsilon_\infty$  where  $\varepsilon_s$  is the quasi-static, low frequency modulus of the permittivity, and  $\tau$  the characteristic relaxation time.  $\alpha$  is linked to the distribution of relaxation time ( $0 < \alpha < 1$ ). Plotting the evolution of the permittivity imaginary part versus its real part leads to the well know semi-circle Cole-Cole

plot characteristic of the material behaviour. By analogy, in [9][10] authors are focusing on magnetic spectroscopy (also called inductance spectroscopy or magneto impedance) and by plotting variation of the permeability imaginary part versus real part of the permeability as the frequency is increasing they obtained semi-circle easy to model with the magnetic equivalent Cole-Cole model.

$$\mu^*(\omega) = \mu'(\omega) - j\mu''(\omega) = \mu_\infty + \frac{\Delta\mu}{1 + (i\omega\tau)^\alpha} \quad (3)$$

By analogy,  $\mu_\infty$  becomes the modulus of the sample permittivity under high frequency excitation,  $\Delta\mu = \mu_s - \mu_\infty$  where  $\mu_s$  is the quasi-static, low frequency modulus of the permeability. In the high amplitude excitation model as in the Cole-Cole model, the dynamic considered from a fractional contribution as  $\alpha$  is non entire. In the final version of this article, we will demonstrate how assuming harmonic evolution of the magnetic induction field, it is very simple to establish the link between both models. In this comparison, for both models  $\alpha$  remains the same and a relation between  $\tau$  and  $\rho$  can be set:

$$\tau^\alpha = \mu_s \cdot \rho \quad (4)$$

First experimental results performed on a typical soft ferromagnetic material ring seems to validate our expectations as relatively correct comparison simulations/measures can be obtained by setting the parameter under weak amplitude Cole-Cole simulations and conserving it for high amplitude dynamic hysteresis model. The issue with the impedance meter characterization rely on the resistive term of the coil which depends on the frequency and which has to be removed for each frequency step of the excitation. A pre-characterisation is done with the wire only and a post processing treatment is performed to precisely return only the evolution of the real and imaginary part of the permeability. The other solution we have is to simulate the whole coil including the frequency dependence of both the electric and magnetic quantities. The first results obtained on a soft ferromagnetic material are very promising, if they are validated on a larger scale, this will confirm that the dynamic behaviour of the magnetization processes in soft ferromagnetic materials that are similar through different scales of amplitude. From a simulation point of view, it also means that the dynamic behaviour of the tested sample can be characterized under weak amplitude excitation with the impedance meter and conserved for the simulation of high amplitude dynamic hysteresis cycles.

### References

- [1] M. Kuczmann, A. Iványi, "The Finite Element Method in Magnetics", Budapest, Academic Press, 2008.
- [2] M. A. Raulet, B. Ducharne, J.P. Masson, and G. Bayada, "The magnetic field diffusion equation including dynamic hysteresis: a linear formulation of the problem", IEEE Trans. on Mag., vol. 40, n° 2, pp. 872 – 875, 2004
- [3] B. Zhang, B. Gupta, B. Ducharne, G. Sebald, T. Uchimoto, "Preisach's model extended with dynamic fractional derivation contribution", IEEE Trans. on Mag., vol. 54 iss. 3, 2017.
- [4] B. Ducharne, G. Sebald, D. Guyomar, G. Litak, "Dynamics of magnetic field penetration into soft ferromagnets", Journal of Applied Physics, pp. 243907, 2015.
- [5] B. Ducharne, G. Sebald, D. Guyomar, G. Litak, "Fractional model of magnetic field penetration into a toroidal soft ferromagnetic sample", International Journal of Dynamics and Control, pp. 1-8, 2017
- [6] Debye, P., "Zur Theorie der anomalen Dispersion im Gebiete der langwelligen elektrischen", Strahlung. Ver. Deut. Phys. Gesell. 15, 777-793, 1913.
- [7] K.S. Cole, R.H. Cole, "Dispersion and Absorption in Dielectrics - I Alternating Current Characteristics", J. Chem. Phys., vol. 9, pp. 341–352, 1941.
- [8] K.S. Cole, R.H. Cole, "Dispersion and Absorption in Dielectrics - II Direct Current Characteristics", J. Chem. Phys., vol. 10, pp. 98–105, 1942.
- [9] R. Valenzuela, H. Montiel, M.P. Gutiérrez, I. Betancourt, "Characterization of soft ferromagnetic materials by inductance spectroscopy and magnetoimpedance, J. Mag. and Mag. Mat., vol. 294, pp. 239-244, 2005.
- [10] R. Valenzuela, "Low-frequency magnetoimpedance: domain wall magnetization process", Physica B., vol. 299, pp. 280-285, 2001.

# Hybrid computing based on measured vector magnetic properties of electrical steel sheets for high performance electromagnetic devices

Yuji Tsuchida<sup>1</sup>, Shohei Ueno<sup>1</sup>, Masato Enokizono<sup>2</sup>, Shinichi Inoue<sup>3</sup>,  
Yoichi Nojima<sup>4</sup>

<sup>1</sup> *Division of Electrical and Electronic Engineering, Oita University, Japan*  
*E-mail: tsuchida@oita-u.ac.jp; ueno-shohei@oita-u.ac.jp*

<sup>2</sup> *Vector Magnetic Characteristic Technical Laboratory, Japan*  
*E-mail: enoki@oita-u.ac.jp*

<sup>3</sup> *Metron Technology Research Co., Ltd., Japan*  
*E-mail: Shinichi.Inoue@metron.co.jp*

<sup>4</sup> *mutec Co. Ltd, Japan*  
*E-mail: nojima@mutec.org*

**Keywords:** Vector magnetic properties, hybrid computing, high performance electromagnetic devices.

In order to development high efficiency electromagnetic devices such as a motor, it is necessary to measure detailed magnetic properties of magnetic materials. Vector magnetic properties are well known as detailed magnetic properties. In the precise measurement of vector magnetic properties [1] - [2], a measurement method combining the search coil method and H coil method is generally used. Therefore, the precise measurement method consumes a lot of time and effort to prepare the measured data. In the search coil method, it is necessary to drill four holes of  $\phi 0.4$  mm in a specimen of 80 mm square and to wind coils through the holes. The H coil method has to use a double H coil. The calibrated double H coil is very expensive and difficult to be handled. Otherwise, a Vector B-H Tester proposed in this paper does not need to wind the search coils and use a double H coil. This paper presents that the Vector B-H Tester can measure vector magnetic properties and evaluate them very easily. So, the measured vector magnetic properties can be applied into the hybrid computing system to develop high performance devices.

Figure 1 shows the measurement system of the Vector B-H Tester. The data collection unit of the Vector B-H Tester consists of two D/A converters, two A/D converters and two power amplifiers for the x- and y- direction. A specimen used in the measurement is an 80 mm  $\times$  80 mm sheet and placed at the centre of the excitation yokes as shown in Figure 1. The x-direction is to be along to the rolling direction. We can generate arbitrary magnetic flux conditions to the steel sheet specimens with the two-directional excitations. The components of the magnetic flux density vector,  $\mathbf{B}$ , in the x- and y-direction are measured by using the B-coil (search coil) directly wound at the excitation yokes. The components of the magnetic field strength vector,  $\mathbf{H}$ , in the x- and y-direction are measured by using magnetizing current method [3]. The excitation currents in the x- and y- direction are measured by using shunt resistances ( $0.5 \Omega$ ) connected with the exciting coils.

Figure 2(a) shows the loci from the measured flux density and field strength vector, and hysteresis loops in the arbitrary directions, respectively. The measured specimen was a non-oriented electrical steel sheet. As shown in this figure, the direction of the flux density vector,  $\mathbf{B}$ , and field strength

vector,  $\mathbf{H}$ , were completely different. Figure 2(b) shows the iron loss distribution in the arbitrary directions. As shown in those figures, the iron loss was the smallest when  $\theta_B = 0^\circ$ , and the iron loss increased as  $\theta_B$  approaching to  $90^\circ$  because the magnetic anisotropy was affected. The Vector B-H Tester can evaluate the magnetic properties such as the magnetic anisotropy very easily.

The detailed discussions about the hybrid computing based on measured vector magnetic properties of electrical steel sheets will be shown in the full paper.

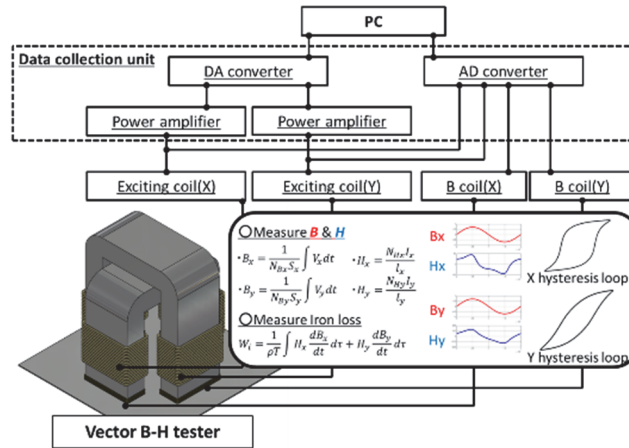
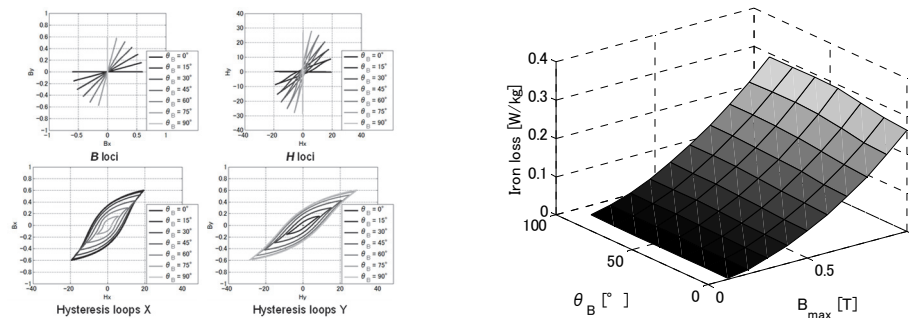


Figure 1: Measurement system.



(a) Measured loci of  $\mathbf{B}$  and  $\mathbf{H}$ , and hysteresis loops (b) Iron loss in each direction  
Figure 2: Measured magnetic properties by V-H Tester.

*Acknowledgements*

Some parts of this work were supported by JSPS KAKENHI Grant Number 17K06465.

*References*

[1] M. Yamagashira, S. Ueno, D. Wakabayashi, M. Enokizono, “Vector magnetic properties and two-dimensional magnetostriction of various soft magnetic materials”, *int. J. Appl. Electromagn. Mech.*, Vol. 44, nos. 3-4, pp. 387-400, 2014.  
 [2] M. Enokizono, “Two-Dimensional Vector Magnetic Property”, *Journal of the Magnetics Society of Japan*, Vol. 27, No.2, pp. 25-30, 2003.  
 [3] S T. Nakata, Y. Ishihara, M. Nakaji, T. Todaka, “Comparison between the H-coil method and the magnetizing current method for the single sheet Tester”, *Journal of Magnetism and Magnetic Materials*, Vol. 215-216, pp. 607-610, 2000.

# Influence of Distortion Factor of Induced Voltage of B-coil on Magnetic Property Measured with a Single Sheet Tester

Takuya Shibataki, Yasuhito Takahashi, and Koji Fujiwara

*Doshisha University, Kyoto, Japan*

*E-mail: {ctwb0347@mail4; ytakahashi@mail; koji.fujiwara@mail}.doshisha.ac.jp*

*Keywords:* Distortion factor, Single sheet tester, Electrical steel sheet, Magnetic properties

It is desirable that the waveform of induced voltage  $v_b$  of the B-coil is substantially sinusoidal when magnetic properties of electrical steel sheets are measured. In order to get the sinusoidal  $v_b$ , the IEC standards specifies that its form factor  $FF$  should be controlled within  $1.11 \pm 0.01$  [1], [2]. However, it is not sufficient because non-sinusoidal waveform can give  $FF = 1.11$ . Ideally, the distortion factor ( $DF$ ) of  $v_b$  should be equal to 0. Therefore, this paper discusses the influence of  $DF_{v_b}$  on measured magnetic properties of electrical steel sheets.

As a specimen, a non-oriented electrical steel sheet M210-35A5 is selected and excited at 1.8 T and 50 Hz. Fig. 1 shows a relationship between the convergence criterion  $DF_{v_b, \text{specified}}$  and the finally obtained  $DF_{v_b}$ . Even when the convergence criterion is satisfied at the termination of a waveform control, the obtained  $DF_{v_b}$  was slightly different from the specified value because the  $v_b$  waveform may change during the averaging process after the termination of waveform control. Fig. 2 shows  $DF_b$  of the flux density  $b$ .  $DF_b$  is essentially smaller than  $DF_{v_b}$  because the influence of higher harmonics in  $b$  can be reduced by integrating  $v_b$ . Fig. 3 shows  $DF_h$  of the magnetic field strength  $h$ .  $DF_h$  is considerably larger than  $DF_b$  due to the strong nonlinearity of magnetization property. Fig. 4 shows a relationship between the maximum magnetic field strength  $H_m$  and  $DF_{v_b, \text{specified}}$ .  $DF_{v_b, \text{specified}}$  may affect the magnetostriction measurement because the change of  $H_m$  is comparatively larger. Figs. 5 and 6 show the differences of the maximum flux density  $B_m$  and  $FF$  between the target waveform and a measured one. If  $\varepsilon_{B_m}$  and  $\varepsilon_{FF}$  are adopted as convergence criteria for the waveform control, their tolerances should be set at less than 0.05 % to realize the sufficient  $DF_{v_b, \text{specified}}$  (for example, 0.2). Figs. 7 and 8 show the relationship between iron loss  $W$  and  $DF_{v_b, \text{specified}}$ , and iron loss corresponding to each component, respectively.  $W_s$  at  $DF_{v_b, \text{specified}} = 0.2$  and 1.0 % is nearly equal to each other (difference < 0.1 %). However, when  $DF_{v_b, \text{specified}}$  is large (1.0 %), an iron loss calculated from the fundamental component increases compared with that at  $DF_{v_b, \text{specified}} = 0.2$  % and those for harmonics become negative.

This paper discusses the influence of the distortion factor of induce voltage of the average flux density in a specimen on various quantities for magnetic measurements. It is demonstrated that a sufficiently small tolerance for the distortion factor is required to get reliable magnetic properties.

## References

- [1] IEC, "Magnetic materials. — Part 3: Methods of Measurement of the Magnetic Properties of Magnetic Sheet and Strip by Means of a Single Sheet Tester," 60404-3 (2010).
- [2] K. Matsubara, et al., "Acceleration Technique of Waveform Control for Single Sheet Tester," *IEEE Trans. Magn.*, vol. 31, no. 6, pp. 3400-3402 (1995).

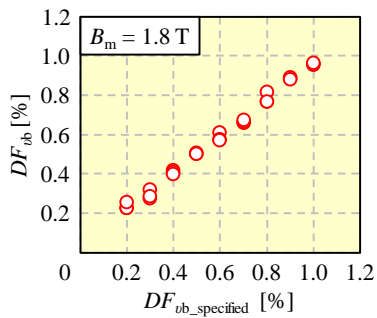


Fig. 1. Relationship between the  $DF_{vb}$  and the  $DF_{vb\_specified}$ .

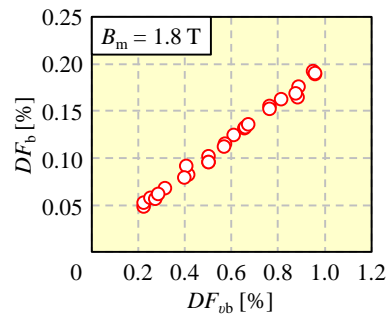


Fig. 2. Relationship between  $DF_b$  and  $DF_{vb}$ .

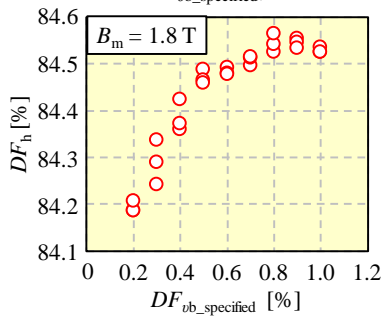


Fig. 3.  $DF_h$  of the magnetic field strength

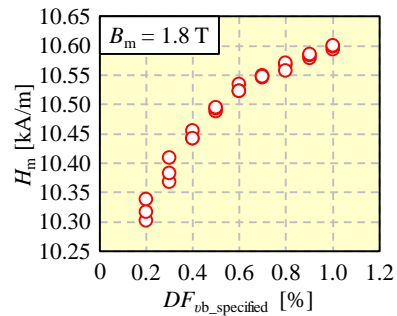


Fig. 4. Maximum magnetic field strength.

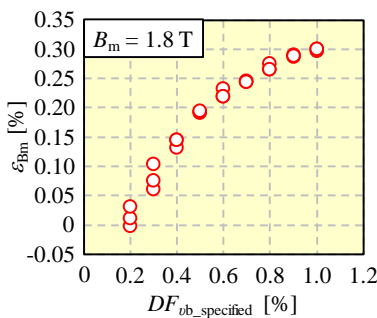


Fig. 5. Difference of  $B_m$  between the target waveform and measured one.

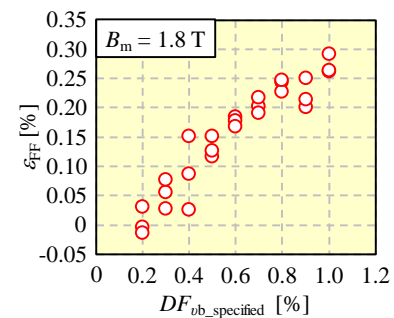


Fig. 6. Difference of  $FF$  between the target waveform and measured one.

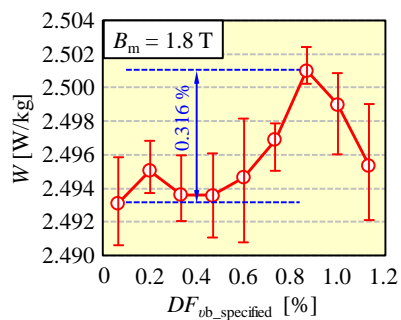


Fig. 7. Iron loss.

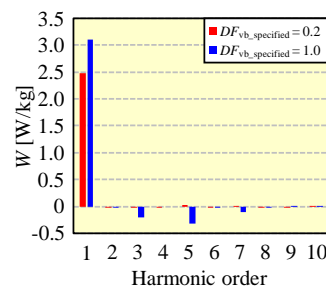


Fig. 8. Iron loss at each harmonic order.

# Investigating a zero-field energy minimization principle to control the domains size by lines scribed with a laser on surface oriented magnetic structures.

O. Maloberti<sup>1,2</sup>, M. Nesser<sup>2</sup>, J. Fortin<sup>2</sup>, P. Dassonville<sup>1,3</sup>, J. Dupuis<sup>4</sup>, Y. Hernandez<sup>4</sup>, C. Pineau<sup>5</sup>, M. Caruso<sup>6</sup>, J-P. Birat<sup>7</sup>, I. Tolleneer<sup>6</sup>, L. Mattei<sup>8</sup>

<sup>1</sup>ESIEE Amiens, 14 quai de la Somme, 80080 Amiens, France.

E-mail: olivie.maloberti@gmail.com; maloberti@esiee-amiens.fr

<sup>2</sup>LTI Laboratory, IUT d'Amiens, Avenue des Facultés - Le Bailly 80 025 Amiens, France.

<sup>3</sup>MIS Laboratory, UPJV, 14 quai de la Somme, 80080 Amiens, France.

<sup>4</sup>MULTITEL, 2 rue Pierre et Marie Curie, 7000 Mons, Belgique.

<sup>5</sup>IRT-M2P, 4 rue Augustin Fresnel, 57070 Metz.

<sup>6</sup>CRM Group Metal Processing, Tech Lane Ghent Science Park / Campus I-Zone A4B, Technologiepark 922A, BE-9052 Zwijnaarde

<sup>7</sup>IF-steelman, 5 rue du gate chaud, 57280 Semecourt, France.

<sup>8</sup>Metafensch, 109 rue de Thionville, 57270 Uckange.

*Keywords: Soft magnetic materials, magnetic structure, laser scribing, demagnetizing energy, anisotropy, magnetic exchange, domains refinement, closure domains, walls energy, walls density.*

It is well known that magnetization curves, hysteresis and iron losses in soft magnetic materials are due to several magnetization reversal processes, such as the magnetic domains walls pinning, displacement, bowing, multiplication, fusion, nucleation and the domains magnetic rotation. Therefore, the shape and size of magnetic domains and the density, area and mobility of domains walls have got a significant impact onto the magnetic behavior, and especially the iron losses [1]. Some dedicated surface treatments have appeared since the end of the 20<sup>th</sup> century to refine the magnetic structure of textured magnetic materials [2, 3]. Several techniques can be considered: the ball scribing [4], the CW or pulsed excimer and CO<sub>2</sub> laser irradiation process [5, 6], the Nd:Yag CW or pulsed laser scribing process [7]. Most of laser patterns investigated correspond to straight lines perpendicular to the rolling direction in GO 3% SiFe alloys. Control of the process requires to first optimize the laser parameters (spot size, peak power, pulse energy, duration and repetition frequency, scanning speed, ...) to get any desired scribing lines [8, 9]. It is then necessary to specify the optimal lines to maximize the dynamic loss reduction due to walls motion and by minimizing the static hysteresis loss increase due to pinning effects [10] but still favoring the walls activation and nucleation [11]. Most studies are essentially practical with magnetic measurements and microscopic observations for various laser parameters [12]. The theory called micro-magnetism [13] can be used to describe the rotation of polarization within a wall, including the calculation of the walls thickness. This method can also be used to describe the domain wall spacing but for very few domains and in a perfect crystal [14] or around small defects [15]. Other authors also experimentally studied the impact of the surface crystallographic texture onto the magnetic structure [16].

In this paper, we focus on a method to help the specification of the best laser patterns to optimize later the magnetic performances (magnetic permeability, coercive force, power losses). To do so, we investigate theoretical tool to estimate statistically the impact of a laser scribing or irradiation pattern onto the main parameters that define a magnetic structure at zero external magnetic field, with magnetic domains and walls, more especially the domains wall spacing.

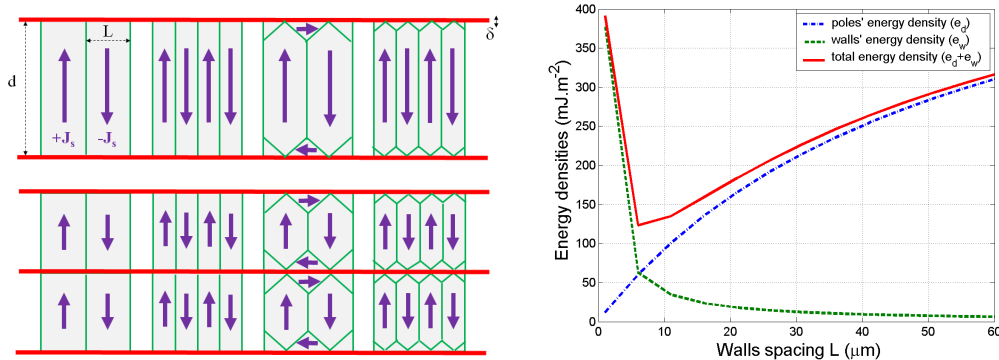


Figure 1a (left): magnetic structures studied and definition of parameters  $d$  (line spacing) and  $L$  (wall spacing) - Figure 1b (right): sensitivity analysis of global energy as a function of the wall spacing.

A test case study will be proposed and is represented in Fig. 1a. We will consider parallel laser lines with a line spacing and a magnetic or/and a heat affected zone (width  $\delta$  and  $\delta'$  and depth  $p$  and  $p'$ ). We make the assumptions that: 1) laser « scribes » modify very locally the magnetic properties such that the polarization is greatly reduced inside the affected zone (induced stress, ablation, damage, ...); 2) laser patterns create located closure domains or magnetic poles that will define one dimension of surface magnetic domains due to an energy minimization principle. The energies that must be considered are the magneto crystalline anisotropy energy in closure domains and walls, the magnetic ordering exchange energy in walls and the demagnetization energy due to magneto-static poles. The calculation of each energy term can be performed as a function of material parameters (magnetic ordering exchange), metallurgical parameters (the texture and magneto crystalline anisotropy) and laser process parameters (line spacing, width and depth). Then a sensitivity analysis (Fig. 1b) can be carried out to analyze the impact of laser parameters (line spacing  $d$ ) and magnetic parameters (domain wall spacing  $L$ ) on the whole surface energy densities. This will help us specify the optimal laser parameters. Finally, additional magnetic observations and measurements will be carried out to correlate the laser scribing process with the magnetic structure and the desired magnetic properties. Magnetic domains observation will be done with the MFM technique and the MOKE imaging technique. The magnetic behavior will be characterized with the SST and the Epstein frames.

**Acknowledgements:** This research has received funding from the European Research Council under the H2020-IND-CE-2016-17/H2020-FOF-2017 Program (Grant Agreement No. 766437).

#### References:

- [1] R.H. Pry, C.P. Bean, *Journal Applied Physics*, vol. 29 (1958), pp. 532 – 533.
- [2] T. Luchi, S. Yamaguchi, and T. Ichiyama, *Journal Applied Physics*, vol. 53 (3), March 1982.
- [3] M. Nakamura et al., *Transactions on Magnetics*, Vol. MAG-23, No. 5, September 1987.
- [4] H. Wang, *Acta Metall. Sin. (Engl. Lett.)*, Vol.26 No. 5, October 2013, pp. 618 – 622.
- [5] S. V. Ponnaluri et al., *Journal of Materials Processing Technology*, vol. 112 (2001), pp. 199 – 204.
- [6] P. Rauscher et al., *Physics Procedia*, vol. 41 (2013), pp. 312 – 318.
- [7] S. Patri et al., *Journal of Material Science*, vol. 31 (1996), pp. 1693 – 1702
- [8] I. Petryshynets et al., *Acta Physica Polonica A*, Vol. 131, No. 4 (2017).
- [9] S. Ahn et al., *Phys. stat. sol. (b)*, vol. 241, No. 7 (2004), pp. 1641 – 1644.
- [10] B. Weidenfeller et al., *Journal of Magnetism and Magnetic Materials*, vol. 133 (1994), pp. 177 – 179
- [11] B. Weidenfeller et al., *Journal of Magnetism and Magnetic Materials*, vol. 160 (1996), pp. 136 – 138.
- [12] V. Puchý et al., *Acta Physica Polonica A*, Vol. 131, No. 6 (2017).
- [13] W.F. Brown, *Journal of Applied Physics*, 49, Issue 3 (1978), p. 1937.
- [14] L. Landau, E. Lifshits, Reprinted from *Phys. Zeitsch. der Sow.*, vol. 8 (1935), pp. 153 – 169.
- [15] M.F. de Campos et al., *Journal of Magnetism and Magnetic Materials*, vol. 301 (2006), pp. 94 – 99.
- [16] M. Bisran, *Journal of magnetism and magnetic materials*, vol. 164 (1996), pp. 300 – 304.

# Investigation on Deterioration of Magnetic Properties of Laminated Iron Core Due to Different Welding Conditions

Ryo Mitani<sup>1</sup>, Kohei Kawaguchi<sup>1</sup>, Yasuhito Takahashi<sup>1</sup>, Koji Fujiwara<sup>1</sup>,  
Makoto Matsushita<sup>2</sup>, Tadashi Tokumasu<sup>3</sup> and Kei Yasumuro<sup>3</sup>

<sup>1</sup>*Doshisha University, Kyoto, Japan*

*E-mail: ctwc0340@mail4.doshisha.ac.jp; duq0321@mail4.doshisha.ac.jp*

*; ytakahashi@mail.doshisha.ac.jp; koji.fujiwara@mail.doshisha.ac.jp*

<sup>2</sup>*Toshiba Corporation, Tokyo, Japan*

*E-mail: makoto.matsushita@toshiba.co.jp*

<sup>3</sup>*Toshiba Infrastructure Systems & Solutions Corporation, Tokyo, Japan*

*E-mail: tadashi2.tokumasu@glb.toshiba.co.jp; kei1.yasumuro@toshiba.co.jp*

**Keywords:** Magnetic property, stator core, punched steel sheet, welding.

In order to improve the efficiency of motors, it is necessary to obtain iron loss property accurately <sup>[1]</sup>. Therefore, it is an important task to understand the degree of deterioration of the magnetic property due to the manufacturing process of the stator core. The authors have been investigating the influence of the number of welding points of the laminated core on the magnetic property, and it is confirmed that the eddy current loss is proportional to the number of welding points and the hysteresis loss is not proportional to it <sup>[2]</sup>. In this paper, the iron losses of stator cores, in which some punched steel sheets are stacked and welded, are measured. These results are compared to evaluate the influence of difference in welding conditions on the deterioration of magnetic properties.

We measured five types of specimens. The stack length of these specimens is 25 mm. The specifications of the specimens and the welding positions are shown in Table 1 and Fig. 1. The number of welding layers, the welding current and the diameter of welding rod were investigated as the welding conditions. The measurements were carried out by an exciting current method at 50 and 100 Hz and the measuring range of magnetic flux density is from 0.05 T to about 1.7 T at intervals of 0.05 T.

Table 1 - Specifications of specimens.

Item	Specimen				
	a	b	c	d	e
Number of welding layers	0	2	1	1	1
Number of welding points	0	8	8	8	8
Welding current [A]	-	200	200	100	100
Diameter of welding rod [mm]	-	4	4	4	2.6

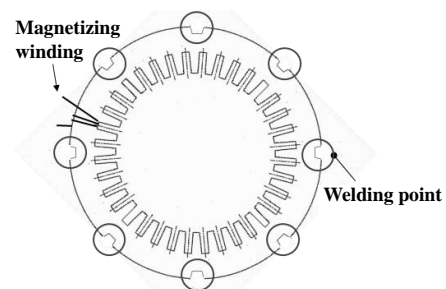


Fig. 1 – Welding points.

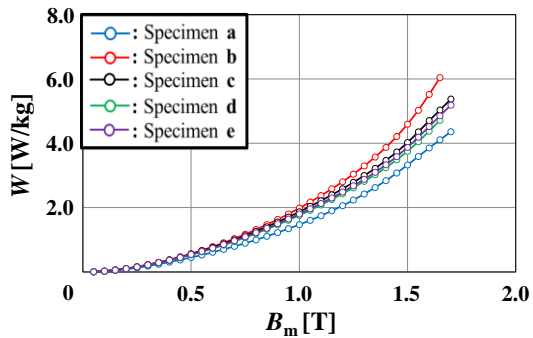


Fig. 2 - Iron loss property (50 Hz).

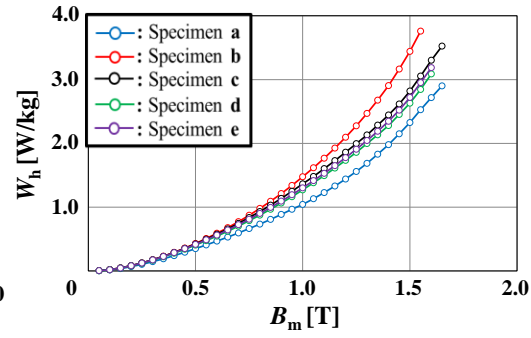


Fig. 3 - Hysteresis loss (50 Hz).

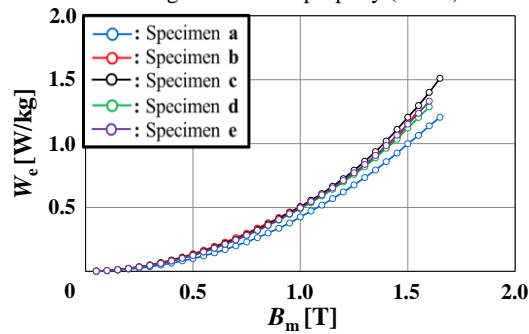


Fig. 4 - Eddy current loss (50 Hz).

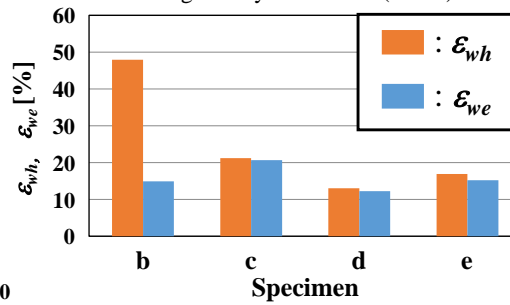


Fig. 5 - Increasing ratio of hysteresis loss and eddy current loss to specimen a (1.5 T).

Fig. 2 shows the measurement results of iron loss. Figs. 3 and 4 show the results of iron loss separation. It can be seen that these characteristics are significantly different depending on the welding conditions. Fig. 5 shows the increase ratio of the hysteresis loss and the eddy current loss with respect to the specimen a.

The deterioration of the magnetic property is dependent on the welding conditions even if the number of the welding points is equal. The maximum difference in hysteresis loss and eddy current loss due to welding conditions is about 0.81 W / kg and about 0.084 W / kg at the magnetic flux density  $B_m = 1.5$  T from Figs. 3 and 4, respectively. Therefore, it is considered that differences in welding conditions have greater effect on hysteresis loss than eddy current loss compared with the number of welding positions. From Fig. 5, it can be confirmed that the influence of the number of welding layers is the largest. In addition, the welding current and the diameter of a welding rod affect the hysteresis loss characteristics. Therefore, it is expected that the hysteresis loss increases due to the thermal stress given to the welding part. Regarding the eddy current loss, a large difference due to welding conditions could not be confirmed compared with the hysteresis loss.

### References

- [1] K. Jeong, Z. Ren, H. Yoon, and C. S. Koh, "Measurement of Stator Core Loss of an Induction Motor at Each Manufacturing Process," *Journal of Electrical Engineering and Technology*, vol. 9, no. 4, pp. 1309-1314 (2014).
- [2] K. Kawaguchi, K. Fujiwara, Y. Takahashi, M. Matsushita, T. Tokumasu, I. Yaguchi, "Deterioration on Magnetic Properties of Laminated Iron Core after Welding Process," *Annual Meeting Record of the institute of Electrical Engineers of Japan*, no. 2-088, pp. 100-101 (2017).

# Modelling of Hysteresis Phenomenon Based on the Elemental Operator and Wind-rose Method

Weijie Xu<sup>1</sup>, Nana Duan<sup>2</sup>, Yongjian Li<sup>3</sup>, Shuhong Wang<sup>2</sup>, Jianguo Zhu<sup>4</sup>

<sup>1</sup> State Grid Shaanxi Electric Power Company Economic Research Institute, China  
E-mail: xuweijie@outlook.com

<sup>2</sup> School of Electrical Engineering, Xi'an Jiaotong University, Xi'an 710049, China  
E-mail: duannana@xjtu.edu.cn; shwang@xjtu.edu.cn

<sup>3</sup> Hebei University of Technology, Tianjin, 300130, China  
E-mail: liyongjian@hebut.edu.cn

<sup>4</sup> University of Technology Sydney, Sydney, NSW 2007, Australia  
E-mail: Jianguo.Zhu@uts.edu.au

**Keywords:** Hysteresis model, wind-rose method, elemental operator.

The Stoner-Wohlfarth (S-W) model is widely used for simulating the magnetic hysteresis phenomenon primarily due to its strong appeal to physical intuition and vectorial nature. Many improvements and extensions have been presented based on the conventional S-W model [1]. The asteroid rule was introduced to directly determine the orientation of magnetization based on the graphical interpretation. However, these phenomena-based methods are lack of physical background and difficult to directly apply in the practical engineering calculation.

Bertotti proposed the original concept of elemental operator with biaxial anisotropy and the corresponding graphical interpretation method, which can be called as wind-rose method [2]. However, similar to the calculation in S-W model, the biaxial operator equilibrium orientation for a given  $\mathbf{H}$  can only be deduced numerically, resulting in an implicit relationship between  $\mathbf{H}$  and  $\mathbf{M}$ , and making the computation of macroscopic hysteresis loop a difficult task.

In the proposed model, it is assumed that the magnetic material is composed of interacting elemental operator which possesses its own biaxial anisotropy and anisotropy coefficient, as illustrated in Figure 1.

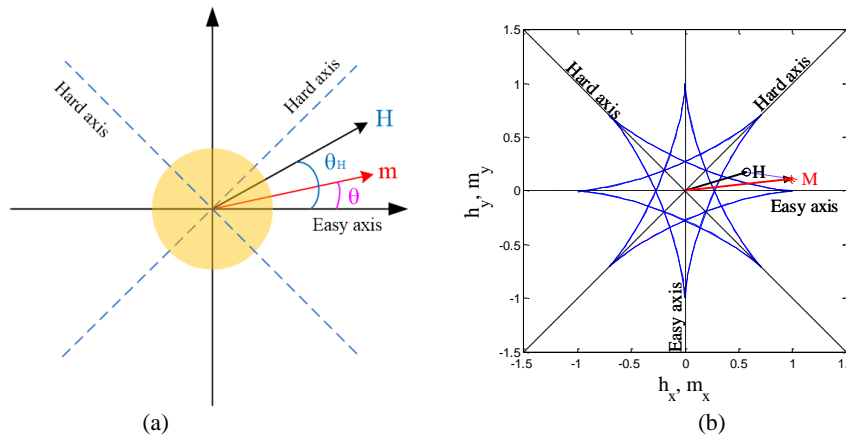


Figure 1: (a) Elemental operator under the magnetic field, and (b) the wind-rose shape of the biaxial elemental operator [2].

Similar to the determination method of S-W particle, the stable orientation of the magnetization vector in the crystal structure can be obtained by minimizing the energy of the elemental operator.

In the rotating magnetization, if the magnetic field with a fixed magnitude but varying rotation angle, is applied on the elemental operator, the corresponding magnetization will follows the rotation but with different rotating angle, as illustrated in Figure 2.

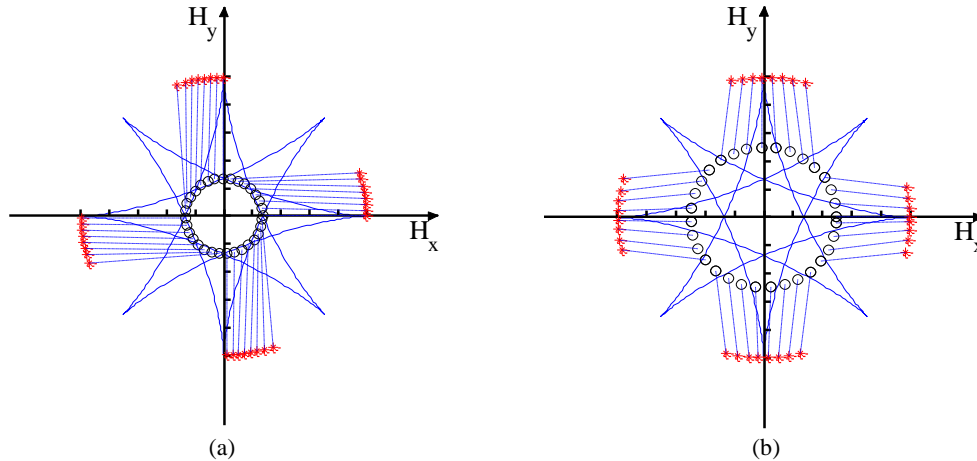


Figure 2: The magnetization orientation of the biaxial operator under different rotational magnetic field when the magnitude of normalized magnetic field is (a)  $h = 0.272$ , (c)  $h = 0.5$ .

To calculate the bulk magnetic hysteresis, a collection of biaxial elemental operators can be considered with different easy axis orientations and weights associated to each operator [3].

$$M(H) = \iiint m(H, \theta) P(h_i, h_k) \cos \theta dh_i dh_k d\theta \quad (1)$$

To simulate the magnetic properties of different materials by this model, the different distribution functions and parameters are needed. Each magnetic material has an optimal distribution function and parameters, which deliver the best results.

#### Acknowledgements

The research leading to these results has received funding from the National Natural Science Foundation of China under Grant 51707142 and in part by the China Postdoctoral Science Foundation under Grant 2016M602818.

#### References

- [1] K.H.J. Buschow, "Handbook of Magnetic Materials", Elsevier (2015), 24, 323-409.
- [2] G. Bertotti, "Hysteresis in magnetism: for physicists, materials scientists, and engineers", New York: Academic (1998), 235-236.
- [3] E Cardelli, "A general hysteresis operator for the modeling of vector fields", *IEEE Trans. Magn.*, 47(2011), 2056-2067.

# Multi-directional Non-linear FEM Modelling of Magnetic Flux in Transformer Cores with Consideration of Overlaps

Georgi Shilyashki<sup>1</sup>, Helmut Pfützner<sup>1</sup>, Fritz Schmöllebeck<sup>2</sup>

<sup>1</sup>*Inst. of Electrodynamics, Microwaves and Circuit Engineering, TU Wien, Austria*  
E-mail: shilyashki@tuwien.ac.at

<sup>2</sup>*Technikum Wien - University of Applied Sciences, Vienna, Austria*

**Keywords:** FEM modelling, transformer cores, flux distribution.

**Abstract** – Recently, most powerful FEM programs were developed that predict distributions of magnetic flux in soft magnetic machine cores with consideration of non-linearity. However, specific problems arise in cores that exhibit singularities like air gaps, small dimensions complicating the meshing. The paper proposes a methodology where gap lengths are enlarged by an extension factor in pre-processing, compensated by an increased gap permeability function in processing. This yields significant decreases of processing time.

## 1. Introduction

Soft magnetic machine cores like that of transformers are built from materials of pronounced non-linearity. For so far numerical modelling by Finite Element Method (FEM), this non-linearity was usually only considered for the rolling direction (RD) of material. But in recent time, most powerful FEM programs were developed, like COMSOL Multiphysics, that offer consideration of multi-directional non-linearity.

In particular in transformer cores, flux distributions are strongly affected by the performance of overlaps (OLs) of corners and T-joints. Their effective permeability shows distinct decreases for instants where the induction  $B_{OL}$  in OLs exceeds the so-called critical induction  $B_{CRIT}$  [1]. So far, this phenomenon was not modelled by means of FEM, due to the a-priori problem that OLs represent singularities as a basic problem of FEM [2-3]. Their interconnection to bulk elements yields strong increases of element numbers, as a reason for long processing times  $T_P$ . For a significant reduction of  $T_P$ , we present here the basic idea of a simple novel methodology.

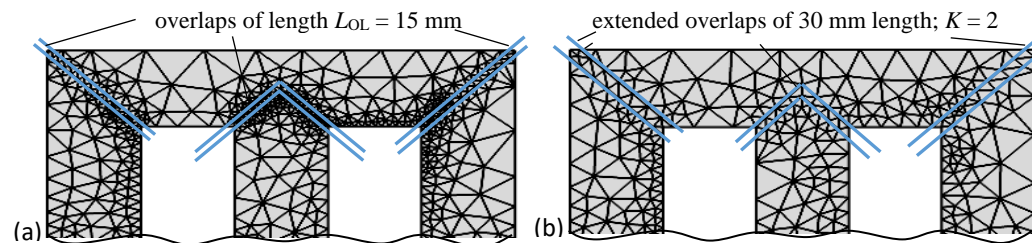


Fig.1. 2D meshing of a three phase, three limb transformer core,  
(a) OLs of 15 mm length, according to practice. (b) Artificially extended length of 30 mm.  
COMSOL Multiphysics 5.2. was used for establishing the meshing as well as for the modelling.

## 2. The Methodology at a Simple Example

The basic idea of method is (i) in pre-processing to increase the length of OLs by an extension factor  $K$ , (ii) in processing to compensate this by a multiplication of the permeability function  $\mu_0(B_{OL})$  by

$K$  and (iii) in post-processing to multiply the field  $H_{OL}$  by  $K$ .

Fig.1. illustrates the strategy for the case of 2D modelling of a 3-phase distribution core, assuming a core length of 1 m and OL-lengths  $L_{OL} = 15$  mm. For the latter value, Fig.1a depicts a mesh as generated for the option "extremely coarse", for a priori reduced  $T_P$ . To interconnect the narrow singularities with the bulk parts of core, a mesh was generated with ca. 3600 elements. Fig.1b shows the case of an extension factor  $K = 2$ , i.e. for doubling the OL-lengths to 30 mm. This favours interconnection, corresponding to a decreased need of the total number of elements, of just 2200.

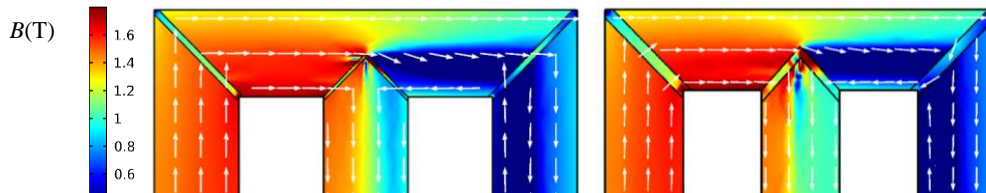


Fig.2. Results of simulation of distribution of induction in the 3-phase transformer core, for the instant of maximum flux in the R-limb which causes distinct circulating magnetization round the right window. (a) For overlap length  $L_{OL} = 15$  mm, as being likely in practice. (b) For a length extension factor  $K = 2$  that reduces processing time, however, reduced resolution leading to a homogenization of the predicted flux distributions. For the simulations, COMSOL Multiphysics 5.2. was used.

Fig.2 shows the resulting distributions of induction for the modulus  $B$  (color-coded) and the corresponding directions of the vector  $\mathbf{B}$  (by arrows). The result concerns a nominal induction of about 1.5 T, considering both non-linear functions  $\mu_{RD}(B_{RD})$  and  $\mu_{TD}(B_{TD})$  (for the transverse direction). The non-linearity  $\mu_{OL}(B_{OLD})$  was considered by RD-values up to  $B_{CRIT}$ , followed by strongly decreased  $\mu_{OL}$ . Results concern the instant of maximum flux in the R-limb. For the practically representative value  $L_{OL} = 15$  mm (Fig.2a), the processing time  $T_P$  proved to be several minutes. With expansion of  $K = 2$  (Fig.2b), it was substantially shortened to ca. 20 s. Such high – but reproducible – differences depend strongly on the assumed constellation of non-linearity. However, the example illustrates the possibility of hyper-proportional consequences of reduced element numbers, interpretations being complicated through the black-box character of the applied FEM program.

With respect to the resulting induction distributions, both results reveal in clear ways distinct circular regional magnetization round the right window, in connection with strongly inhomogeneous induction in the middle S-limb. Compared to Fig.2a without extension of OLs, Fig.2b is characterized by a general tendency of homogenization that can be explained by the lower resolution, as a consequence of OL-expansion. For smaller core sizes, it should be stressed that the expansion yields general modifications of flux distributions in the (size-reduced) bulk parts of core. Further, in general ways, post-processing for presentation of results needs re-dimensioning of OLs. Field intensities  $H_{OL}$  in OLs have to be increased by the applied extension factor  $K$ .

In principle, the here used strategy can be used also for 3D-modelling. However, first 3D tests with consideration of multi-directional non-linearity - including that of overlaps - indicate processing times of more than one day for the here applied processing tool.

*Acknowledgements: We thank for support from the Austrian Science Fund (FWF), Project 28481-N30*

#### References

- [1] Löffler F., Booth T., Pfützner H., Bengtsson C., Gramm K., "Relevance of step-lap joints for magnetic characteristics of transformer cores," IEE Proc.El.Pow.Appl.142 (1995) 371-378.
- [2] Schmöllebeck F., Haas H., "Automatic generation and adaptive refinement of 3D FEM networks (in German)," Proc.7.Winter Meeting TU Karl-Marx-Stadt (1990), 8-23.
- [3] Tang Q. et al. "Magnetic flux distribution in power transformer core with mitred joints," J.Appl.Phys. 117 (2015) 17D522.

# Nondestructive Testing of Ferromagnetic Tubes using a Bobbin-type Intergrated Hall Sensor Array

Juhyeon Park<sup>1</sup>, Jungmin Kim<sup>1</sup>, Hoyong Lee<sup>2</sup>, and Jinyi Lee<sup>1</sup>

<sup>1</sup>Research Center for IT-based Real Time NDT for Nano-Damage Tolerance, Chosun University, Gwangju, 61452, Korea

E-mail: qkrwngus45@daum.net; 79.jmkim@gmail.com; jinyilee@chosun.ac.kr

<sup>2</sup>Department of Defense Science and Technology, Gwangju University, Gwangju, 61743, Korea

E-mail: hylee@gwangju.ac.kr

*Keywords: Ferromagnetic tube, BIHaS, PSECT.*

The eddy current testing (ECT) technique has been developed and applied to monitor the integrity of the tubing system of nuclear power plants. This technique is quite useful to inspect paramagnetic tubes. However, its application has been limited to ferromagnetic tubes due to the short penetration depth of eddy currents in high permeability materials caused by the skin effect [1]. To overcome this problem, remote field eddy current testing (RFECT) and saturation eddy current testing (SECT) were suggested. RFECT has a disadvantage that the inner or outer location of defects cannot be distinguished. Therefore, SECT techniques (full SECT and partial SECT) are suggested alternatively.

This paper proposes a nondestructive testing method based on the partial SECT technique using bobbin-type integrated hall sensor (BIHaS) array. As shown in Fig. 1, the sensor probe consists of permanent magnet and bobbin coil and 15 hall sensors that arranged in the circumferential direction. The permanent magnet magnetizes the specimen in the axial direction and the bobbin coil induces the eddy current in the circumferential direction. By using the permanent magnet, the circumferential directional damage in the ferromagnetic tubes can be inspected easily. Also, the eddy current is maximized when the crack is perpendicular to the direction of induced current. It means that the axial directional damage can be inspected easily by using the bobbin coil. Therefore the partial SECT technique using BIHaS is the most effective NDT method to find damages in ferromagnetic tubes.

For the present, a BIHaS with the partial SECT has been provided by the root-mean-squared (RMS) signals to inspect and evaluate the damages in ferromagnetic tubes [1]. However, it has a limitation to evaluate the damage, that is, the position (inner diameter (ID) or outer diameter (OD)) and the depth. So we propose an improved BIHaS technique which is provided by the impedance and phase images similar with X-probe. Each hall sensor output separates two lines respectively. One line of signals are multiplied with 0° phased square wave and integrated. The others are multiplied with 90° phased square wave and integrated. These processed signals are called as X and Y data in the conventional ECT. The impedance and phase shift images can be calculated by the X and Y data of BIHaS. Fig. 2 shows the MSR tubes for the experiments and the experimental results of the proposed method. Test tube's ID is 14.1mm, outer diameter OD is 19.1mm, and the height of pin is 1.3mm. From the tests, the locations of flat bottom holes (FBH) with 10 ~ 100% W.T were detected without being effected by the tube fins. Also, the quantitative evaluation of the artificial flaws could be possible by calculating impedance (R) and phase angle (Φ). More details will be presented at the conference.

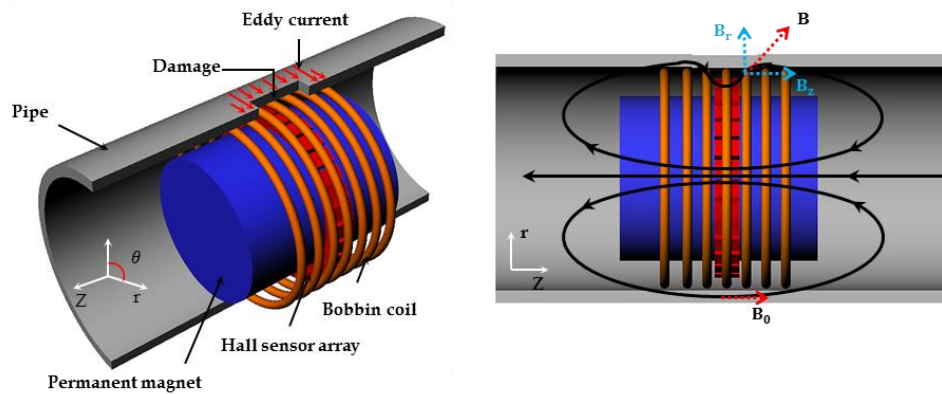


Figure 1: Configuration of BIHaS combined with a permanent magnet

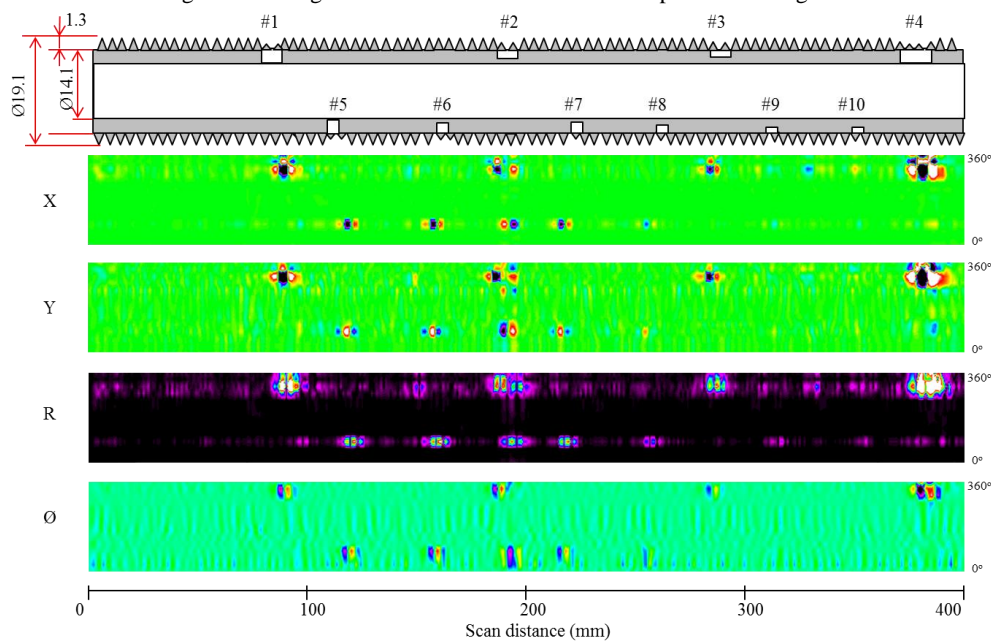


Figure 2: Experimental results of flat bottom holes by using BIHaS

### Acknowledgements

This research was funded by the Korea Institute of Energy Technology Evaluation and Planning (KETEP 20171520101610). We are grateful for the support.

### References

- [1] M. Le, J. Kim, H. Jisoo Kim, Hwa Sik Do and J. Lee, "Nondestructive testing of moisture reheater tubing system using Hall Sensor Array," *Nondestructive Testing and Evaluation*, 33 (2018), 35-44.

# Optimisation of laser domain refinement of grain-oriented silicon steel for low loss and magnetostriction

Ryan Davies<sup>1</sup>, Nicolas Camacho<sup>1</sup>, Philip Anderson<sup>1</sup>, Fiona Robison<sup>2</sup>

<sup>1</sup>Cardiff School of Engineering, United Kingdom

E-mail: [daviesr76@cardiff.ac.uk](mailto:daviesr76@cardiff.ac.uk); [andersonpi1@cardiff.ac.uk](mailto:andersonpi1@cardiff.ac.uk)

<sup>2</sup> Cogent Power Ltd., United Kingdom

E-mail: [fiona.cj.robison@tatasteleurope.com](mailto:fiona.cj.robison@tatasteleurope.com)

**Keywords:** Grain oriented silicon steel; GOES; GOSS; domain refinement; magnetic domains.

Domain refinement of grain oriented electrical steel has become an industry standard practice due to the positive effect that it can have on the overall power loss of GOSS materials showing a decrease in losses of around 10% [1]. Due to the highly anisotropic magnetic behaviour of GOES and the alignment of the ferromagnetic domains in the rolling direction (RD) a laser-irradiated line, scribed transverse to the RD is thought to place artificial grain boundaries across the width of the material and place the regions between the lines under tensile stress [2]. This will lead to a change in wall and magnetostatic energies and the ferromagnetic domains will reform themselves between these new boundaries. At the artificially created boundaries, there will be closure domains that form at 90° to the RD due to energy minimisation requirements that allow a path for the internal domain magnetic flux to pass, meaning that there is no external field and therefore no external storage of energy surrounding the domains. The overall effect that this has on the material if the laser parameters are within certain limits is that the total power loss of the material will decrease with a likely rise in the magnetostriction. If the power density of the laser is too high however, the compressive stress regions imparted by the thermal shock of the laser will become the predominant factor and therefore negatively affect both the overall power loss and the magnetostriction of the sample.

In this work, the industrial DR process was simulated with low power laboratory laser etching equipment in order to study the influence of the DR parameters. In this initial part of the investigation, samples were laser domain refined with line spacing of 20mm, 10mm and 5mm by a Boxford BGL 350 50W laser at 100 mm/s head speed at laser powers of 6.5W through 9.5W in 0.5W steps and at 7W laser power at head speeds of 75mm/s through 225mm/s. The purpose was to ascertain if the individual parameters of the laser had differing impacts on the power loss or if there is a correlation between the total power loss and the total power density of the laser.

Also, a sample of industrially laser domain refined 0.27mm grade GOES material and a sample of 0.27mm grade material domain refined using the laboratory based Boxford BGL 350 laser system were imaged Scanning Electron Microscopy (SEM) imaging in order to compare and contrast the impact that each system had on the surface coating of the material.

The samples were cut from non-domain refined, 500x500mm, 0.27mm thick GOES squares into 500x100mm samples. Using a Bitter technique domain viewer the samples were imaged then tested at 150, 125, 100, 75, 65, 50, 40, 30, 20 and 10Hz at 1.5T flux density in order to ascertain the total power loss before laser domain refinement. This procedure was repeated after each line spacing had been completed. There were also four samples scribed at the aforementioned line spacing at 7W and 100mm/s and tested as mentioned as a control group.

For the SEM imaging a sample of industrial grade 0.27mm GOES with industrial domain refinement and a sample of 0.27mm GOES with domain refinement by the Boxford system were cut to a 40x40mm squares. They were wiped with a cleaning agent to remove any excess Carbon from the surface before being attached to the sample holder by the use of adhesive carbon pads. They were then placed in a Hitachi TM 3030+ table top SEM and imaged using secondary electrons at 15kV.

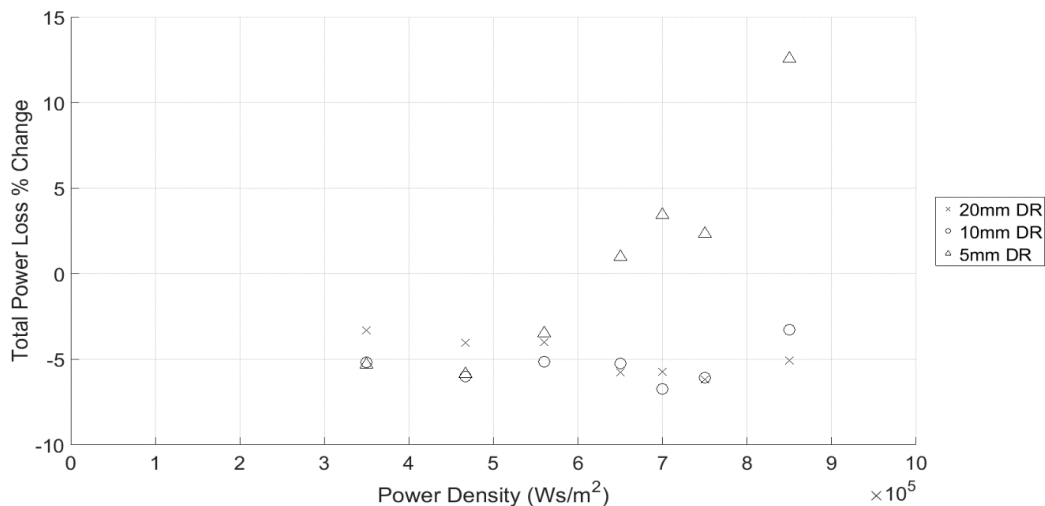


Fig 1. Graph showing percentage change in total power loss for 20mm, 10mm and 5mm laser line spacing as compared to no domain refinement as measured at 1.5T and 50Hz.

The line spacing of the laser domain refinement was shown to be the major influence on the total power loss of the samples tested. However, samples under  $600\text{MWs/m}^2$  laser power density showed little change at 5mm line spacing unlike the samples above  $600\text{MWs/m}^2$ . SEM imaging found that industrial laser domain refinement had much greater uniformity although the width of the affected area of the coating was similar at the widest parts of the Boxford BGL 350 laser lines.

#### Acknowledgements

Cogent Power Ltd. supports this work.

#### References

- [1] Xia, Z., Kang, Y., Wang, Q., 2008. Developments in the production of grain-oriented electrical steel. *Journal of Magnetism and Magnetic Materials*. 320, pp.3229-3233.
- [2] Shilling, J., W., Morris, W., G., Osborn M., L., Rao, P., 1978. Orientation Dependence of Domain Wall Spacing and Losses in 3-Percent Si-Fe Single Crystals. *IEEE Transactions on Magnetics*. Vol. 14 (No. 3), pp. 104-111.

# Optimization of a single strip tester to measure magnetic properties of electrical sheet steel at medium frequencies

Michael Owzareck<sup>1</sup>, Kai Lüning<sup>1</sup>, Nejila Parspour<sup>2</sup>

<sup>1</sup>*BLOCK Transformatoren-Elektronik GmbH, Germany*

*E-mail: michael.owzareck@block.eu, kai.luning@block.eu*

<sup>2</sup>*University of Stuttgart, Institute of Electrical Energy Conversion, Germany*

*E-mail: nejila.parspour@iew.uni-stuttgart.de*

*Keywords:* Single strip tester, electrical sheet steel, medium frequencies.

A reliable simulation and design of inductive components requires knowledge of the core material's magnetic properties [1], [2]. Usually no such data is available for medium frequencies, thus magnetic properties have to be measured. IEC 60404-10 suggests to measure magnetic properties in a frequency range between 400 Hz and 10 kHz by means of an Epstein frame, which however requires high apparent power [3]. Furthermore the mean magnetic path length has to be known to measure the magnetic field strength. Standards such as IEC 60404-10 state a constant length of 940 mm which in reality depends on multiple factors, including frequency and peak flux density. Therefore errors will inevitably be made [4], [5] [6], [7]. Single sheet testers, which are not as popular as Epstein frames, however have some advantages over the Epstein frame [4], [8], [9].

In order to decrease the apparent power demand when measuring Epstein frame sized samples as well as to reduce systematical errors, an optimized single sheet tester, also called single strip tester or SStT, has been developed. A similar design as proposed in [10] has been chosen and optimized for medium frequencies. In this context two yoke materials, ferrite and amorphous alloy, have been compared. Additionally, three possibilities of measuring magnetic field strength have been compared: Measurements by means of flat solenoids, called H-coils, measurements using magneto-resistive sensors [11] as well as the standardized method which utilizes the magnetizing current.

Two prototypes have been designed and built to test and to compare the two different yoke types. Tests with H-coils were promising, thus they are utilized in the developed measurement system. Comprehensive simulations as well as tests were conducted to develop an optimal design and layout of magnetizing and sensing coil as well as the H-coils. The design takes parasitic capacities and resistances, expected voltage and current levels as well as air flux into account. The developed setup is shown in figure 1. Detailed results will be included in the full paper.

A bobbin that is able to accommodate a single Epstein frame sized sample has been developed, figure 1(d-f). The bobbin is manufactured to hold a smaller bobbin for the sense coil, figure 1(d) as well as four H-coils, figure 1(d). This bobbin is mechanically attached to the single strip tester. The developed single strip tester allows measurements of Epstein frame sized samples until their thermal limits are met. Furthermore field strengths and specific losses can be measured without knowing the mean magnetic path length.

Power amplifiers only provide their maximum apparent power at a given output impedance. To transform the single strip tester's impedance close to the amplifier's optimum impedance, transformers with low parasitic capacity and low losses have been developed as described in [12].

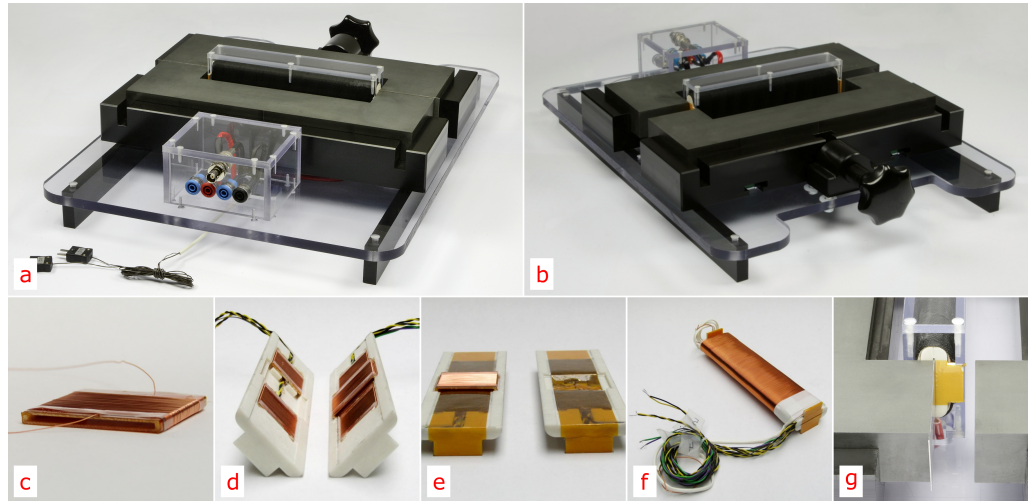


Figure 1: For medium frequencies optimized single strip tester

Summing up, the developed magnetic tester allows Epstein frame sized samples to be measured at frequencies as high as the sample's temperature rise does not exceed the setup's thermal limits. Therefore the maximum frequency is no longer limited by the measuring system but by the sample itself. Now it is possible to measure specific power losses at medium frequencies and also at high flux densities. For example, figure 2 compares measurements of specific losses of M165-35S in a modified 17.5 cm-Epstein frame with measurements in the optimized SSiT.

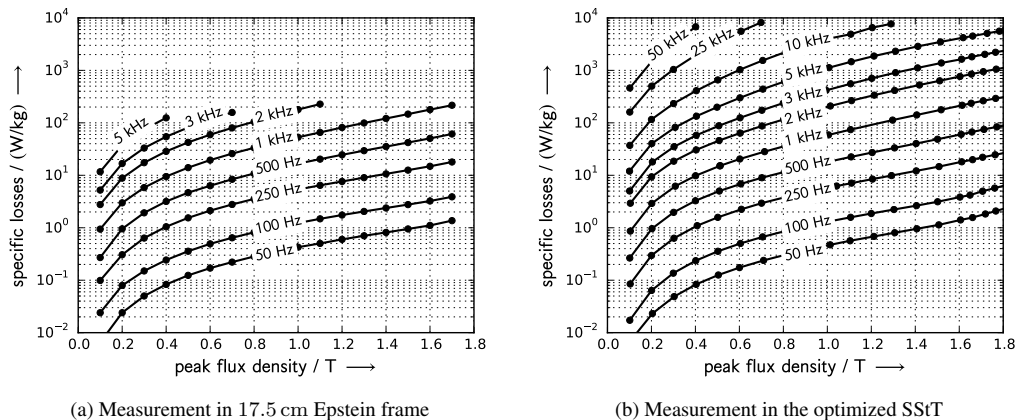


Figure 2: Measurements in an 17.5 cm Epstein frame compared with the optimized single strip tester (SSiT), in both cases M165-35S electrical sheet steel has been measured

As indicated in figure 2, the optimized SSiT allows measurements of M165-35S until approx. 50 kHz, whereas the 17.5 cm Epstein frame only allowed measurements at approx. 5 kHz.

*References*

- [1] Owzareck, M., et al., “Analytical core loss models for electrical steel in power electronic applications”, *13<sup>th</sup> International Conference on Optimization of Electrical and Electronic Equipment*, (2012).
- [2] Owzareck, M., “Calculation method for core losses of electrical steel inductors in power electronic applications”, *PCIM 2015, 19-21 May 2015, Nuremberg, Germany* VDE Verlag.
- [3] IEC 60404-10:2016. *Magnetic materials – Part 10: Methods of measurement of magnetic properties of electrical steel strip and sheet at medium frequencies*.
- [4] Sievert, J., “The measurement of magnetic properties of electrical sheet steel - survey on methods and situation of standards”, *Journal of Magnetism and Magnetic Materials* 215-216, (June 2000), pp. 647-651.
- [5] Hofmann, M., et al. “Numerical Determination of the Effective Magnetic Path Length of a Single-Sheet Tester”, *IEEE Transactions on Magnetics* 50.2, (Feb. 2014).
- [6] Marketos, P, Zurek, S., and Moses, A. J., “A Method for Defining the Mean Path Length of the Epstein Frame”, *IEEE Transactions on Magnetics* Vol. 43, No. 6, (June 2007).
- [7] Marketos, P, Zurek, S. and Moses, A. J., “Calculation of the mean path length of the Epstein frame under non-sinusoidal excitations using the double Epstein method”, *Journal of Magnetism and Magnetic Materials* 320, (2008), pp. 2542-2545.
- [8] Miyagi, D, et al., “Development of Measurement System of Magnetic Properties at High Flux Density Using Novel Single-Sheet Tester”, *IEEE Transactions on Magnetics* 45.10, (Oct. 2009), pp. 3889-3892.
- [9] De Wulf, M, et al., “Design and calibration aspects of small size single sheet testers”, *Journal of Magnetism and Magnetic Materials* Vol. 45, No. 10, (Jan. 2003), pp. 70-72.
- [10] Tumanski, S. and Baranowski, S., “Single strip tester with direct measurement of magnetic field strength”, *Journal of Electrical Engineering* 55.10, (2004), pp. 41-44.
- [11] Tumanski, S. and Baranowski, S., “The Single Strip Tester of Magnetic Materials with AMR Sensors Array”, *Instrumentation and Measurement Technology Conference 2006, Sorrento, Italy*.
- [12] Owzareck, M., “Measurement method for normal magnetization curve of soft magnetic composites with high magnetization currents”, *International Journal of Applied Electromagnetics and Mechanics* Vol. 48, Nos. 2, 3, (2015).

# Research of Harmonic Effects on Core Loss in Soft Magnetic Composite Materials

Yongjian Li<sup>1</sup>, Xinran Yu<sup>1</sup>, Qingxin Yang<sup>2</sup>, Changgeng Zhang<sup>1</sup>, and Shuaichao Yue<sup>1</sup>

<sup>1</sup> State Key Lab of Reliability and Intelligence of Electric Equipment, Hebei University of Technology, Tianjin, China, E-mail: liyongjian@hebut.edu.cn;

<sup>2</sup> Tianjin Key Laboratory of ATEEE, Tianjin Polytechnic University, Tianjin, 300387, China, E-mail: qxyang@tjpu.edu.cn

*Keywords:* soft magnetic composite materials, harmonic, core loss, feedback control method.

## 1. Introduction

Soft magnetic composite material (SMC) are widely employed in electrical machines, especially three dimensional (3-D) magnetic flux machines [1]. The wide application of high voltage direct current transmission (HVDC) and power electronic equipment have introduced a lot of harmonics, which make the operating conditions of electrical machines complicated and diversified. The harmonics will cause core loss increase and local overheating [2]. Therefore, it is necessary to investigate the effects of harmonics on core loss.

In this paper, a magnetic measurement system with frequency domain feedback control method is developed. The system can generate non-sinusoidal waveforms consisting of harmonics with variable orders, contents and phase angles. Core loss measurement of soft magnetic composite materials (SMC) under both sinusoidal and non-sinusoidal excitations is performed. Harmonic effects on core loss are investigated, in terms of the harmonic order, content and phase angle. The frequency domain Bertotti equations are used to predict the core loss and then compared with the measurements. The applicability of this method for non-sinusoidal waveforms is analyzed and discussed in detail.

## 2. Methods and Results

In order to generate an exciting signal with desired harmonic characteristic, a frequency domain feedback control method is designed and applied in the measurement system. The precision and repeatability of the measurement depend strongly on the control method.

In order to validate applicability of the Bertotti frequency-domain equation under non-sinusoidal waveforms, a specific single harmonic is injected to the fundamental waveforms. Initially,  $B$  waveform is controlled to be 1 T at 50 Hz, plus a 0.1 T third harmonic, with the phase angle adjusted from  $0^\circ$  to  $360^\circ$ . The measured loss and calculated values from Bertotti frequency domain equation under different phase angles are shown in Fig. 1(a). It is found that the loss follows the sine trend, running up to maximum at  $0^\circ$  and minimum at  $180^\circ$ . Obviously, the calculated value is constant and independent of phase angle, which indicates the Bertotti frequency domain equation is no longer applicable in this case.

Secondly,  $B$  waveform is controlled to be 1 T at 50 Hz, plus a third harmonic at  $0^\circ$  phase angle, with a variable amplitude from 0 T to 0.5 T. Core loss increases as the harmonic content increases. The measured loss and calculated values under different amplitude are shown in Fig. 1(b). For the case of a specific phase angle, although the variation of calculated values follows the trend of

measured losses, large error still exists and demonstrate a fast rising trend with the harmonic amplitude increasing.

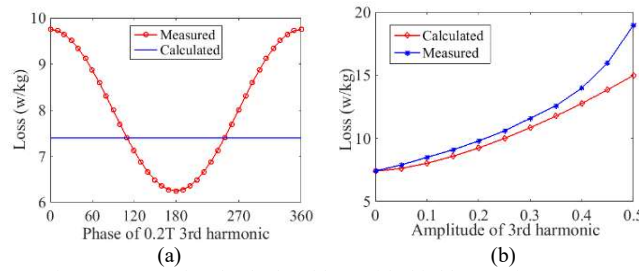


Fig. 1. Measured and calculated loss with third harmonic component

For the 5th harmonic, the effects of harmonic content on core loss is as same as 3rd, while the effects of harmonic phase angle on core loss is opposite. That is, for 3rd harmonic, the maximum loss occurs at  $0^\circ$  and the minimum loss occurs at  $180^\circ$ , while for the fifth harmonic, the maximum loss occurs at  $180^\circ$  and the minimum loss occurs at  $0^\circ$ . Hysteresis loops are shown in Fig. 2.

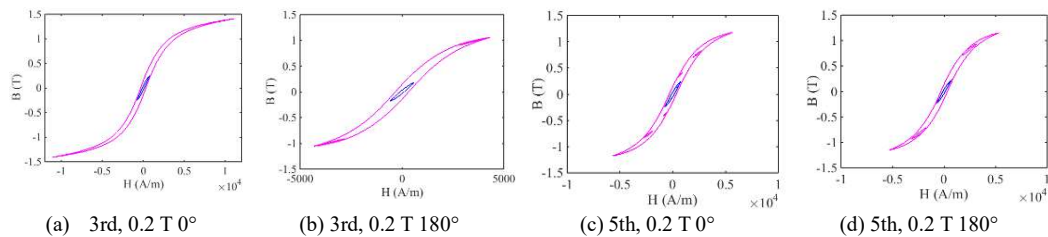


Fig. 2. Hysteresis loops with controlled harmonic order, content and phase angle

#### Acknowledgements

This work was supported in part by the National Natural Science Foundation of China, (No. 51777055, 51690181), the National Key R & D Program of China (2017YFB0903904), and the National Key Basic Research Program of China (973 Project) under Grant 2015CB251000.

#### References

- [1] Cheng Z, Takahashi N, Forghani B, et al. 3-D Finite Element Mod-eling and Validation of Power Frequency Multishielding Effect[J]. IEEE Transactions on Magnetics, 2012, 48(2):243-246.
- [2] Nakamura K, Fujita K, Ichinokura O. Magnetic-Circuit-Based Iron Loss Estimation Under Square Wave Excitation With Various Duty Ratios[J]. IEEE Transactions on Magnetics, 2013, 49(7):3997-4000.
- [3] C. G. Zhang, Y. J. Li, J. S. Li, Q. X. Yang, and J. G. Zhu, "Meas-urement of Three Dimensional Magnetic Properties with Feedback Control and Harmonic Compensation," IEEE Trans. Ind. Electron., vol. PP, no. 99, pp.1-1, 2016.
- [4] Bertotti G. General properties of power losses in soft ferromagnetic materials [J]. IEEE Transactions on Magnetics, 2002, 24(1):621-630.

# Sensitivity analysis of iron loss and hysteresis models' parameters to the sheets thickness and magnetic polarisation according to the quality of GO SiFe

M.L. Ababsa<sup>1,3</sup>, O. Maloberti<sup>1,2</sup>, O. Ninet<sup>3</sup>

<sup>1</sup>ESIEE Amiens, 14 quai de la Somme, 80080 Amiens, France.

E-mail: ababsa.mohamed.lamine@gmail.com, olivie.maloberti@gmail.com

<sup>2</sup>LTI Laboratory, IUT d'Amiens, Avenue des Facultés - Le Bailly 80 025 Amiens, France.

<sup>3</sup>LSEE Laboratory, Technoparc Futura, 62400 Béthune, France.

*Keywords: iron loss, magnetic hysteresis, laminated sheets' thickness, modeling, magnetic domains.*

Iron losses and magnetic hysteresis of soft magnetic materials are mainly due to its microscopic magnetic structures with domains, walls, vortices and other with the microscopic magnetic objects in motion [1, 2, 3]. Behavioral laws have been studied for decades with numerous models, able to reproduce experimental data [4]. The whole model's parameters can be related to crystallographic (easy axis, grains orientation and texture), metallurgical (grains size, boundaries and defects) and magnetic (saturation polarization, domains and walls size and mobility) properties. Materials' parameters should be intrinsic to the material itself so that the local behavioral law associated to the magnetic field diffusion equation are supposed to describe the macroscopic behavior of any sample; whatever its shape and its size [5, 6]. However, research clearly shows that the magnetic domains size depends on the grain and sample shape, dimensions and surface quality [7]. Meanwhile, the walls mobility, bowing, pinning effects and nucleation are greatly influenced by the magnetic walls density and area on one side; and by the grain boundaries, dislocations and other defects, even at the surface, on the other side [8]. It is thus hard to say that the magnetic properties are intrinsic only to the material. We would like to know if the models can describe the impact of these geometry and size effects. We are wondering whether two identical bulk alloys with two different shapes, dimensions or/and surface qualities will require two different sets of parameters. The role played by the sample has been investigated mainly for small particles, single domains and permanent magnets. Some authors have however analyzed the impact of one sample dimension [9] but only on global measurements (loss or hysteresis). The sample is most of cases a thin laminated sheet, it is thus proposed to analyze the impact of a sheet thickness on some models' parameters and to interpret the results for further investigations.

In this paper, we will focus on two usual models, the first for iron losses and the second for hysteresis: the Bertotti loss model and the Jiles Atherton hysteresis model [10, 11]. The method consists in carrying out measurements on samples made with the same GO SiFe alloy but with four different thicknesses (0.23, 0.27, 0.30, 0.35 mm), at several induction magnitudes and frequencies. Models are used to identify the variation of parameters as a function of the thickness from experimental data obtained with the Epstein frame. For each thickness and induction, the whole three loss coefficients can be identified at once with the asymptotic and the ordinary least square method procedure applied on the energy per cycle and per unit mass and squared induction ( $J.kg^{-1}.T^{-2}$ ). The dynamic Jiles Atherton model will be described with an ordinary differential equation involving five parameters that must be identified [12]. The identification procedure is performed using an iterative calculation to fit the differential permeability, the magnetic field or/and the magnetization at specific locations within the cycles measured (coercivity, remanence and saturation).

The present paper highlights critical limitations of the models. First, the loss model coefficients

vary unexpectedly as a function of the induction and the thickness (see Fig. 1). Some recent models solve the first limitation, including a dynamic field varying with the induction and its first derivative [13]. The second limitation would require modelling the relationships between the sample geometry, texture and surface quality with the magnetic structure. Even if the static hysteresis parameters show almost no variation as a function of the thickness, fitting correctly the hysteresis cycles also requires varying some parameters as a function of the induction, as for other similar models [14]. A more critical and general limitation is the dependency of dynamic parameters with the thickness. These variations show discrepancies with the theory, which jeopardize any physical interpretation of identifications. It is nowadays necessary to change the parameters when we change the sample shape or size, even using a simulation software supposed to handle different geometries. We thus discuss investigations on other ways to model soft ferromagnetic materials using a new physical formulation that takes the magnetic structure and its sensitivity to the geometry and surface quality into account at the mesoscopic scale [15], that would complete the theory of micro-magnetism usable only at the microscopic scale [16].

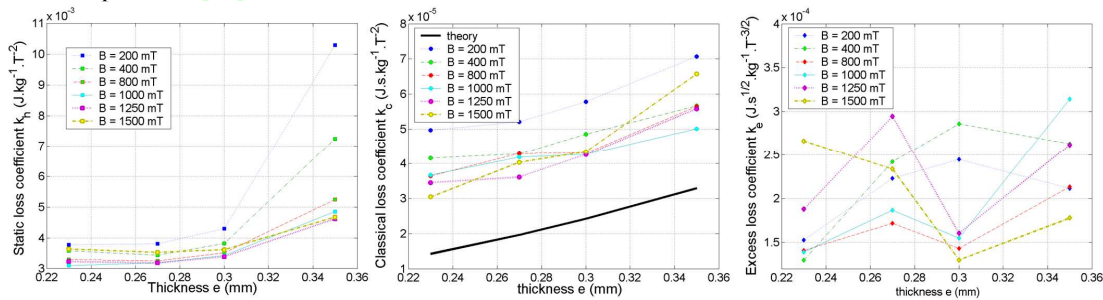


Figure 1: Bertotti loss model parameters vs the magnetic polarization and the thickness.

*Acknowledgements:* The results were obtained using samples with a stress relieving treatment coming from TKES and contributions of the LSEE. Part of the identifications was performed by the ESIEE thanks to the project ESSIAL that received funding from the European Research Council under the European Union's H2020-IND-CE-2016-17/H2020-FOF-2017 Program (Grant Agreement No. 766437).

#### References

- [1] P. Weiss, *J. Phys. Theor. Appl.*, 6 (1) (1907), pp.661-690.
- [2] F.Bitter, *Phys. Rev.*, Vol. 38 (1931), pp. 1903.
- [3] R.H. Pry, C.P. Bean, *J. Appl. Phys.*, vol. 29 (1958), 532-533.
- [4] Olivier Maloberti, PhD thesis en Electrical Engineering, France, 2006.
- [5] M-A. Rault et al., *IEEE Trans. on Magnetics*, 2004, vol. 42, n°2, pp. 872–875.
- [6] V. Basso et al., *J. Appl. Phys.*, 81 (8), 15 April 1997.
- [7] L. Landau, E. Lifshits, Reprinted from *Phys. Zeitsch. der Sow.* 8 (1935), pp. 153–169.
- [8] L. Weil, *Le journal de physique et le radium*, Tome 12 (1931), pp. 437-447.
- [9] J. Schneider, *IEEE Transaction on Magnetics*, Vol. 48, NO. 4, pp 1429-1432, Avril 2012.
- [10] G.Bertotti, *J. of Magnetism and Magnetic Materials*, Vol. 46 (1984), Issues 1–2, Pages 68-80.
- [11] D.C Jiles and D.L Atherton, *J. of Mag. and Mag. Mat.*, Vol. 61 (1986), pp. 48-60.
- [12] D. C. Jiles, *IEEE Transactions On Magnetics*, Vol.30. No.6 (1994).
- [13] T. Chevalier et al., Elsevier Science, *Physica B*, 275 (2000), pp:197-201.
- [14] O. Maloberti et al., *Journal of Mag. and Mag. Mat.*, vol. 304 (2006), pp: 507-509.
- [15] O. Maloberti et al., conference SMM'18 in Cardiff (2007).
- [16] W.F. Brown, *Journal of Applied Physics*, 49, Issue 3 (1978), p. 1937.

# The Role of the Critical Induction for Off-plane Flux in Transformer Cores

Georgi Shilyashki, Helmut Pfützner

*Inst. of Electrodynamics, Microwaves and Circuit Engineering, TU Wien, Austria*

*E-mail: shilyashki@tuwien.ac.at*

**Keywords:** transformer cores, off-plane flux, critical induction

**Abstract** – Corners and T-joints of cores of transformers or shunt reactors contain overlaps of reduced effective cross section of material. Depending on the so-called step number, the “critical induction”  $B_C$  characterizes the flux density beyond that flux is taken up by air gaps. The present study shows that in real cores that consist of several packages,  $B_C$  is linked with a distinct onset of off-plane fluxes, in direction normal to the laminations. This means that core operation above  $B_C$  is characterized by disadvantageous, 3-dimensional flux re-distributions.

## 1. Introduction

Transformer cores tend to be stacked from highly grain oriented SiFe that shows high permeability for the rolling direction. However, corners and T-joints contain air gaps that represent strongest magnetic reluctance. To reduce their impact on the global magnetization, industry assembles the core with overlaps (OLs) of so-called step-lap, where an individual gap is bridged by  $N$  laminations. In [1,2], it was demonstrated that the step number  $N$  corresponds to a well defined “critical induction”  $B_C$  where the bridges are saturated, as a reason for the onset of flux through the gaps. Recently, this was confirmed also by FEM modelling [3]. Fig.1 (from [1]) shows the corresponding increases of OL-excitation for model cores with mitred OLs as being typical for transformers, and for linear OLs as arising in shunt reactors.

Our new study revealed that the induction  $B_{CRIT}$  has an analogous significance for *global* flux distributions in multi-package cores, as used in industry – in particular, for fluxes in normal direction, as reported in the following.

## 2. Experimental

In contrast to earlier measurements on model cores of constant sheet width, this study was made on a more realistic core of three packages with widths of 15 cm, 11 cm and 8 cm, respectively. Assembling was made with  $N = 4$  steps. The tendency of circular limbs in connection with semi-circular yokes was considered by package shifts that cause shifts also of OLs. The core was magnetized with 50 Hz, with nominal induction values  $B_{NOM}$  between 1 T and 1.6 T.

In order to study interactions of the packages, measurements of normal-direction flux density  $B_{ND}$  were made by novel detector band sensors [4, 5]. They consisted of three flat frame-coil windings of 25 mm mean size, print on a 20  $\mu$ m thick plastic substrate, by means of an electrical

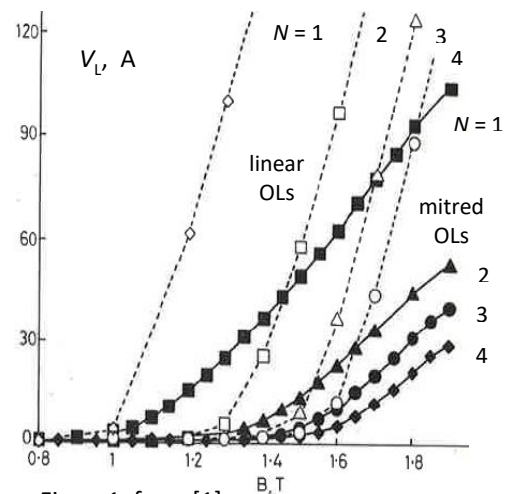


Figure1, from [1].

paint "Bare Conductive" suspension, to prevent substantial inter-laminar air gaps. The focus of measurements was put on border regions between the packages, in particular close to OLs. From the sensor signal, the normal direction induction  $B_{ND}(t)$  was calculated, as an average over the sensor area.

### 3. Results

Fig.2 shows an example of results for a yoke region beside the V-elements of the T-joint, between the packages of 15 cm and 11 cm thickness. We see time courses  $B_{ND}(t)$  for  $B_{NOM}$  of 1 T, 1.3 T, 1.4 T, 1.5 T and 1.6 T.

For low nominal magnetization  $B_{NOM} = 1$ , the induction  $B_{ND}$  remains under the level of 3 mT for the whole period of magnetization. As an interpretation, throughout the core, the OLs do not attain local saturation, according to  $B < B_{CRIT}$ . The packages operate quite independent from each other, their fluxes remaining within each package.

The global flux distribution changes substantially when we increase  $B_{NOM}$  to - and beyond - the critical induction  $B_{CRIT}$  of ca. 1.3 T. In instants of  $B > B_{CRIT}$ , the flux tends to avoid the partly saturated OLs. It bridges the latter by "escaping" to the neighbour package through flux in normal direction. This yields distinct instantaneous increases of  $B_{ND}$  up to the level of 35 mT for  $B_{NOM} = 1,6$  T (Fig.2a).

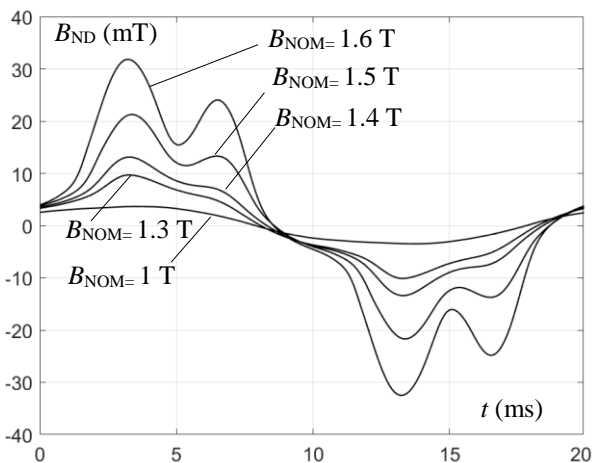


Figure 2

### 4. Conclusions

The study indicates that the practical relevance of the "critical induction"  $B_{CRIT}$  is not restricted to the performance of overlaps, i.e. to their excitation and local losses. Rather,  $B_{CRIT}$  can be assumed to influence the cores global flux distribution in significant ways. For  $B_{NOM} > B_{CRIT}$ , the packages get in distinct inter-connection through off-plane fluxes in normal direction. This means that the core is characterized by complex 3-dimensional flux distributions. As disadvantageous consequences, the levels of flux distortion increase throughout the core, but in particular close to overlaps. This yields an increase of building factor. But even more, it enhances the audible noise of the core, as a parameter of rising relevance.

*Acknowledgements:* We thank for support from the Austrian Science Fund (FWF), Project 28481-N30.

### References

- [1] Löffler F., Booth T., Pfützner H., Bengtsson C., Gramm K., "Relevance of step-lap joints for magnetic characteristics of transformer cores," IEE Proc.El.Pow.Appl.142 (1995) 371-378.
- [2] Ilo A., Pfützner H., Nakata T., „Critical induction, a key quantity for the optimization of transformer core operation," J.Magn.Magn.Mater.215-216 (2000) 637-640.
- [3] Parent G., Penin R., Lecointe J.P., Brudny J.H., Belgrand T., "A new approach to the critical induction in transformer cores," Int.J.Appl.El.Magn.Mech. 50 (2016) 583-592.
- [4] Pfützner H., Shilyashiki G., "A novel family of magnetic detector bands of minimum effective thickness," Submitted for this conference (2018).
- [5] Shilyashki G., Pfützner H., Palkovits M., Windischhofer A., Giefing M., "3D-printed detector band for magnetic off-plane flux measurements in laminated machine cores," Sensors 17/12, 2953, (2017).

# Two-dimensional magnetical characterization of soft magnetic material under arbitrary mechanical stress

Andreas Thul<sup>1</sup>, Piotr Klimczyk<sup>2</sup>, Benedikt Schauerte<sup>1</sup>, Patrick Denke<sup>2</sup> and Kay Hameyer<sup>1</sup>

<sup>1</sup>*Institute of Electrical Machines (IEM), RWTH Aachen University, Germany*  
*E-mail: andreas.thul@iem.rwth-aachen.de*

<sup>2</sup>*Dr. Brockhaus Messtechnik GmbH & Co. KG, Lüdenscheid, Germany*

**Keywords:** rotational magnetization, two-dimensional mechanical stress, magnetic characterization.

The permeability [1] and power loss [2] of soft magnetic materials used in electrical machines can vary considerably when the material is mechanically stressed. Since the active parts of electrical machines are subject to mechanical stress due to various reasons, e.g. rotational forces, housing shrink-fitting, thermal strain or magnetic forces, it is important to examine the influence of mechanical stress under conditions as close as possible to those in the actual applications. In electrical machines, rotating magnetizations occur in parts of the magnetic circuit subjected to various mechanical stresses at different directions within the sheet plane. Therefore, a measurement device, able to generate rotating magnetizations inside a sample, which can be stressed in two directions, has been developed.

Considering possible designs for rotational single sheet testers [3], different numbers of magnetic poles and sample shapes are verified. Here, a four pole design is chosen. The basic setup of the magnetic circuit is shown in Fig. 1. The legs of the cross-shaped sample are clamped to a mechanical load unit to impress a two dimensional stress state inside the sample. The relation of stress and load forces in the tested material will be further discussed in the full paper.

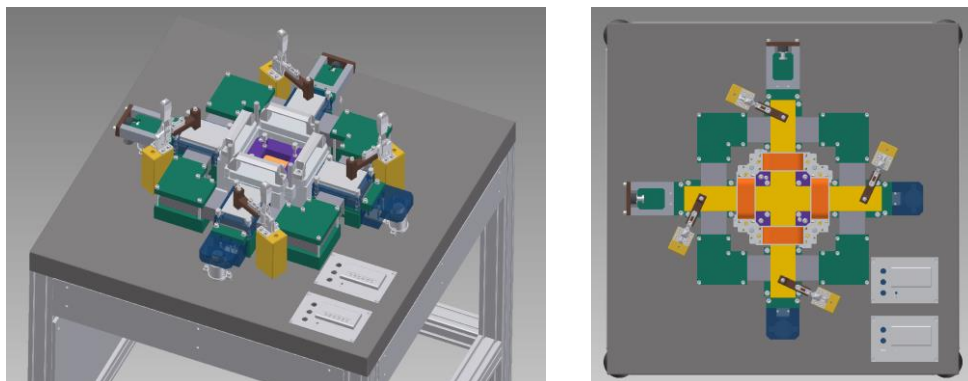


Figure 1: Magnetic circuit of the measurement device. Yellow: sample, orange: magnetizing coils, gray: yokes, blue and green: support structure.

In this set-up the sample is magnetized by four yokes constructed with magnetizing coils. Due to the cross shape, yokes are split into an upper and lower part, with the sample placed in between. The magnetic circuit is closed by four corner yokes. The flux density inside the sample is measured by two perpendicular search coils wound through the holes punched in the sample's center. The field strength is measured by a system of perpendicular tangential field coils below the sample. Fig. 2

shows a photograph of the complete constructed measurement system. For controlling the flux density inside the sample, a period-wise field-oriented control strategy based on [4] is used. Compared to other rotational measurement devices with an air gap between sample and yoke, the nonlinearity of the sample material complicates the control task. The control solution to this problem will be described in detail in the full paper.

In the full paper, measurement results under varying mechanical stress conditions will be presented. Based on those results, models which consider the effect of two dimensional mechanical stress on the magnetic properties may be developed and validated in future works.

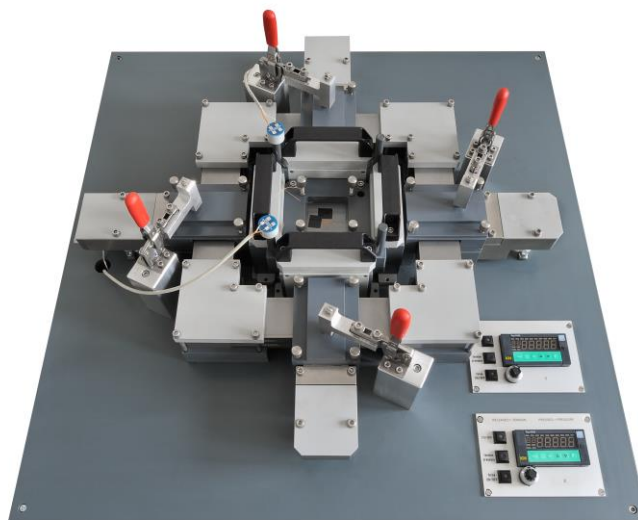


Figure 2: Overview of the complete prototype measurement system.

#### *Acknowledgements*

This work is funded by the German Federal Ministry for Economic Affairs and Energy under the Central Innovation Program for SMEs (ZIM) (FKZ: KF 3464501DF4).

#### *References*

- [1] Leuning, N., Steentjes, S., Schulte, M., Bleck, W., Hameyer, K., Effect of elastic and plastic tensile mechanical loading on the magnetic properties of NGO electrical steel, *Journal of Magnetism and Magnetic Materials*, vol. 417, pp. 42-48 (2016).
- [2] Permiakov, V., Dupré, L., Pulnikov, A., Melkebeek J., Loss separation and parameters for hysteresis modelling under compressive and tensile stresses, *Journal of Magnetism and Magnetic Materials*, vol. 272-276, pp. E553-E554 (2004).
- [3] Sievert, J, "Two-dimensional magnetic measurements - history and achievements of the workshop," *Przegląd Elektrotechniczny* (2011), Nr. R. 87, nr 9b, S. 2–10.
- [4] Thul A., Steentjes S., Schauerte, B., Klimczyk, P., Denke, P., Hameyer, K., "Rotating magnetizations in electrical machines: Measurements and modeling," *AIP Advances*, volume 8, number 5, pages 56815, ISSN 2158-3226, 2018.

# Verification of the Magnetic Path Length of Epstein Frame and Single Sheet Tester by H-coil Technique

Xing ZHOU<sup>1</sup>, Xinhua ZHOU<sup>2</sup>, Ling TANG<sup>1</sup>, Jie SHEN<sup>1</sup>

<sup>1</sup>Test, Inspection and Analysis Centre, Baosteel Co. Ltd., Shanghai, China

E-mail: zhouxing@baosteel.com

<sup>2</sup>Tunkia Co.Ltd., Changsha, China

E-mail: zhouxh@tunkia.com

**Keywords:** Magnetic Path Length, Epstein Frame, SST (Single Sheet Tester), H-coil.

Grain-oriented silicon steel (electrical steel) strip is mainly used for transformer cores to construct AC magnetic path, its magnetic properties are important in design of transformer. To measuring the magnetic properties, such as power loss (specific total loss), magnetic polarization (intrinsic flux density) etc., two IEC standard methods are used in industry, one is Epstein frame [1], another is SST (single sheet tester) [2]. Both the standard methods are using a conventional magnetic path length, which is fixed as 0.94 m for Epstein frame and 0.45 m for standard SST. In literature, studies show it's existed that a deviation of the real magnetic path length from conventional one, for the method of Epstein frame [3] and also for the method of standard SST [4]. For grain-oriented silicon steel, especially high grades of HGO materials with thinner thickness, the deviation of the magnetic path length can cause evident difference in measuring values of magnetic parameters such as power loss and magnetic polarization etc. from the real properties of the materials. This is approved by design engineers of transformer, when they use the measuring values of Epstein frame or standard SST as magnetic properties of electrical steel strips in design of transformer, the performance of final transformer constructed by the electrical steel strips is often better than their expectation.

To investigate on the variation of the real magnetic path length in standard SST and in Epstein frame, in which the magnetic field strength is calculated from magnetizing current (the M.C. method), H-coil technique has been used and designed together with standard methods, then the measuring results can be obtained simultaneously from H-coil and M.C, which gives the information about the real magnetic path length in standard methods comparing with H-coil.

The construction of the tester with both H-coil and M.C is shown as Fig. 1 for SST, a standard tester of the vertical double-yoke type has been used with a specimen size of  $500 \times 500 \text{ mm}^2$  according to the IEC standard [2]. To measure the magnetic field strength with H-coil method, four H-coils connected in series has been mounted in lower yoke and approached 1mm to specimen as shown in Fig. 1. The total turns area of the four H-coils which have been made is about  $0.4 \text{ t}\cdot\text{m}^2$ , then the response of the H-coils is in level of 0.1 mV against 1 A/m of magnetic field strength in 50 Hz.

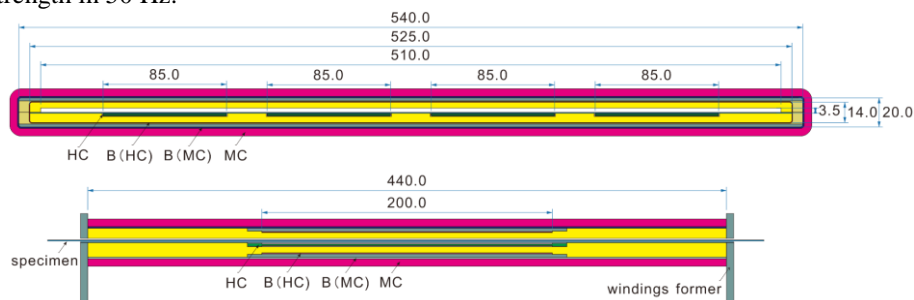


Figure 1: Configuration of the standard SST with H-coil and M.C, in front and side view.

For Epstein frame, assembling with an Epstein frame according to the IEC standard [1], four H-coils have been mounted respectively in four winding formers of the Epstein frame as shown schematically in Fig. 2 for cross-section and side view of one winding former, these four H-coils have been connected in series. The total turns area of the four H-coils which have been made is about  $0.16 \text{ t}\cdot\text{m}^2$ , then the response of the H-coils is in level of several dozens of micro-volt against

1 A/m of magnetic field strength in 50 Hz, a critic technique in signal treatment has been used for this feeble voltage.

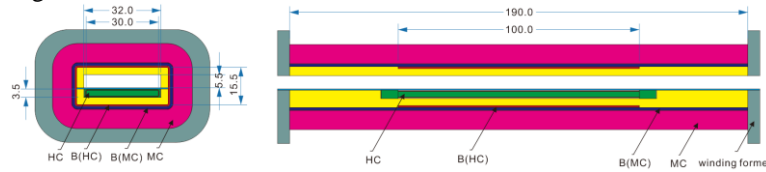


Figure 2: Configuration of the Epstein framework with H-coil and M.C, in cross-section and side view.

Two samples of grade M85-23P5 have been tested and the results obtained with SST are as shown in Table 1. For M.C method, the conventional magnetic path length ( $l_c$ ) has been set from 0.450 m to 0.500 m, comparing with the power loss measured by H-coil, the real magnetic path length ( $l_{real}$ ) of SST used for M.C can be estimated by linear regression of the data of  $l_c$  and power loss or simply by  $l_{real} = l_c \cdot (P_{M.C} / P_{H-coil})$ . Then different  $l_{real}$  has been obtained for different sample and in different level, for example,  $l_{real}$  in 1.7 T is about 0.485 m for sample S1 and is about 0.492 m for sample S2. The values of real magnetic path length ( $l_{real}$ ) of SST used for M.C are not constants either in different magnetic excitation level or for different sample.

Table 1: The results of the standard SST with H-coil and M.C

Sample	Method	$l_c$ (m)	P10 (W/kg)	P13 (W/kg)	P15 (W/kg)	P17 (W/kg)	J8 (T)	J25 (T)
S1	M.C	0.450	0.2700	0.4638	0.6291	0.8933	1.8893	1.9563
		0.460	0.2645	0.4538	0.6154	0.8750	1.8909	1.9571
		0.475	0.2560	0.4394	0.5958	0.8461	1.8932	1.9581
		0.490	0.2482	0.4259	0.5777	0.8202	1.8954	1.9592
		0.500	0.2431	0.4173	0.5659	0.8038	1.8968	1.9599
	H-coil		0.2471	0.4298	0.5822	0.8282	1.8908	1.9539
S2	M.C	0.450	0.2665	0.4568	0.6222	0.8924	1.8779	1.9501
		0.460	0.2609	0.4468	0.6087	0.8731	1.8795	1.9512
		0.475	0.2527	0.4328	0.5896	0.8455	1.8818	1.9525
		0.490	0.2449	0.4195	0.5714	0.8195	1.8840	1.9539
		0.500	0.2398	0.4109	0.5600	0.8031	1.8854	1.9548
	H-coil		0.2409	0.4174	0.5734	0.8159	1.8834	1.9496

The results corresponded to Epstein frame are expected to be obtained and treated in two months before the meeting.

The real magnetic path lengths of SST and Epstein frame used for M.C are not constants, the deviation of the real magnetic path length from conventional one for standard SST and Epstein frame can cause obvious difference of designating properties for the high grades of HGO electrical steel materials. Different effects can influence on this physics parameter [5]-[6], H-coil technique gives a possibility to investigate the problem.

#### References

- [1] IEC 60404-2:2008, *Magnetic materials - Part 2 Methods of measurement of the magnetic properties of electrical steel strip and sheet by means of an Epstein frame.*
- [2] IEC 60404-3:2010, *Magnetic materials - Part 3 Methods of measurement of the magnetic properties of electrical steel strip and sheet by means of a single sheet tester.*
- [3] Philip Marketos, Stan Zurek, Anthony J. Moses, *Calculation of the mean path length of the Epstein frame under non-sinusoidal excitations using the double Epstein method*, Journal of Magnetism and Magnetic Materials, Volume 320, Issue 20, October 2008, Pages 2542-2545.
- [4] Koji Fujiwara, *The measurement of the magnetic properties of soft magnetic materials using field-sensing coils*, Draft Technical Report presented at IEC/TC68/WG2 meeting, 2006, unpublished.
- [5] J. D. Sievert, D. Son, *On the effective magnetic path length used for field strength and loss determination*, Journal of Magnetism and Magnetic Materials, Volume 41, Issues 1-3, February 1984, Pages 235-237.
- [6] T Nakata, Y Ishihara, M Nakaji, T Todaka, *Comparison between the H-coil method and the magnetizing current method for the single sheet tester*, Journal of Magnetism and Magnetic Materials, Volumes 215-216, 2 June 2000, Pages 607-610.



# OS3: Magnetic Modeling

Session Chairman

**Carlo RAGUSA**

Politecnico Di Torino - Italy



## Keynote Lecture

*”Broadband magnetic losses in soft magnets: experimental and theoretical analysis”*



**Dr. Samuel Dobák**

*Institute of Physics, P.J. Safarik University, Kosice, Slovakia*

**Samuel Dobak** earned his PhD Degree in Condensed Matter Physics from the P.J. Safarik University in Kosice, Slovakia in 2018, where he continues to work as a Researcher. His scientific activity is mainly focused on the investigation of soft magnetic materials, e.g., amorphous and nanocrystalline alloys, ferrites, and powder compacted materials, from the view of their magnetization process and energy dissipation behavior up to very high frequencies. During his PhD studies, he completed an internship at the Nanoscience and Materials Division, Istituto Nazionale di Ricerca Metrologica, Torino, Italy. In 2014 he was awarded by the Slovak Magnetism Society for the best Master thesis in applied magnetism. He recently received the Rector’s prize for the Science & Research.

## Broadband magnetic losses in soft magnets: experimental and theoretical analysis

Samuel Dobák<sup>1</sup>, Cinzia Beatrice<sup>2</sup>, Fausto Fiorillo<sup>2</sup>, Carlo Ragusa<sup>3</sup>,  
Vasiliki Tsakaloudi<sup>4</sup>

<sup>1</sup>*Institute of Physics, Faculty of Science, P.J. Šafárik University, Košice, Slovakia*  
E-mail: samuel.dobak@upjs.sk

<sup>2</sup>*Istituto Nazionale di Ricerca Metrologica, Nanoscience and Materials Division,  
Torino, Italy*  
E-mail: c.beatrice@inrim.it; f.fiorillo@inrim.it

<sup>3</sup>*Politecnico di Torino, Energy Department, Torino, Italy*  
E-mail: carlo.ragusa@polito.it

<sup>4</sup>*Centre for Research and Technology-Hellas (CERTH), Themi-Thessaloniki, Greece*  
E-mail: vikaki@cperi.certh.gr

*Keywords:* Mn-Zn ferrites, alloys, magnetic losses.

The modern inducting, transforming, and absorbing devices dedicated for operation under increasingly wide range of frequencies call for magnetic cores with good wideband response. Smart nanocrystalline ribbons treated under specific magneto-thermal conditions can exhibit superior broadband magnetic behavior with respect to Mn-Zn ferrites, the materials of traditional industrial choice. Because of the very low ribbon thickness (10 – 20 micrometers), the eddy currents are significantly constrained and low energy dissipation up to very high frequencies is observed in these alloys, in spite of their metallic character. A narrow experimental window of material characterization is generally found in the literature. This limitation has so far precluded a thorough quantitative understanding of the involved microscopic magnetic phenomena and a comprehensive broadband comparison between ferrite and nanocrystalline properties.

In this communication we present an overview of the broadband magnetic permeability and loss behavior of sintered Mn-Zn ferrites and amorphous/nanocrystalline ribbons. To meet the challenging conditions envisaged for applications, we performed extensive fluxmetric measurements from DC regime up to 10 MHz, spanning a wide region of peak polarization  $J_p$  values, in combination with transmission line measurements, by which the GHz region could be approached. We report on recent progress made in understanding the complex phenomenology of loss and permeability behavior on such a broad range of frequencies range in all these materials. A comprehensive interpretative framework, relying on the statistical theory of losses and the related loss separation concept [1], has been worked out. It is aimed at the theoretical assessment of the involved magnetization process mechanisms (domain wall displacements and rotations) and the associated dissipation channels (eddy currents and spin damping).

The rotational process in ferrites and the related energy dissipation by spin damping are predicted through the Landau–Lifshitz–Gilbert (LLG) equation for spin dynamics under frequency-evolving distribution of the local anisotropy fields and the ensuing spectrum of resonance frequencies. Eddy-current losses have a classical character and can be predicted by numerical multiscale variational approach [2]. They can any case be experimentally separated from the spin-damping losses, because eddy current-free loss in Mn-Zn ferrites can be obtained in rings of reduced thickness (~ 1 mm).

The best broadband combination of low losses and high permeability is obtained with the amorphous/nanocrystalline ribbons endowed with transverse low-value magnetic anisotropy, as induced by conventional field annealing. These materials provide a highly interesting and analytically treatable case, because their magnetization process is dominated by rotations and the ensuing dynamic losses can correspondingly be calculated by recognizing a frequency-dependent magnetic constitutive equation, obtained as solution of the LLG equation, and applying to it the electromagnetic diffusion equation. Fig. 1 shows the wideband loss separation performed on a Mn-Zn ferrite (Fig. 1a) and a nanocrystalline transverse anisotropy Finemet ribbon (Fig. 1b). The rotational loss contribution  $W_{\text{rot,sd}}$  due to spin damping in ferrites is predicted using the Landau–Lifshitz constant  $\alpha_{\text{LL}} = 0.04$ , while the classical loss term  $W_{\text{rot}} = W_{\text{rot,sd}} + W_{\text{rot,eddy}}$  in transverse anisotropy tapewound ribbon is obtained for  $\alpha_{\text{LL}} \sim 0.06$  and the exchange stiffness constant  $A \sim 2 \times 10^{-11}$  J/m. The excess loss  $W_{\text{exc}}$ , calculated as  $W_{\text{exc}}(f) = W(f) - W_{\text{hyst}} - W_{\text{rot}}(f)$ , follows a law  $W_{\text{exc}}(f) \propto f^q$ , where  $0 < q \leq 1$  [3]. The theoretically predicted dynamic behavior of the domain walls, relaxing beyond a few hundred kHz, is experimentally supported by high-speed magneto-optical *in situ* observations of their domain structure [4].

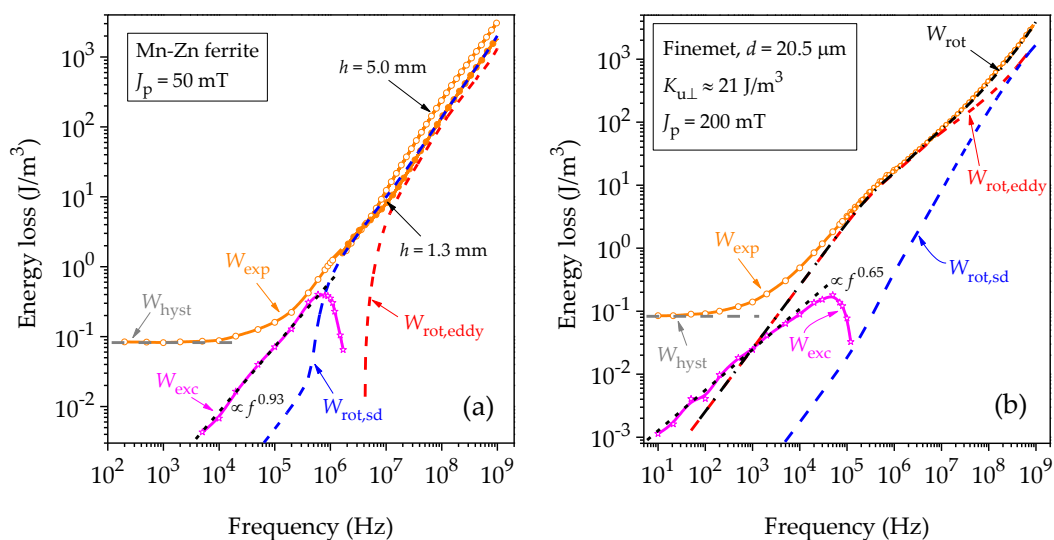


Figure 1: Broadband magnetic losses measured (a) in a Mn-Zn ferrite ring with two different values of thickness  $h$  and (b) in a 20.5  $\mu\text{m}$  thick tapewound nanocrystalline transverse anisotropy Finemet ribbon at a defined  $J_p$  level. The measured loss  $W_{\text{exp}}(f)$  is decomposed into the quasi-static hysteresis  $W_{\text{hyst}}$  component and the dynamic  $W_{\text{exc}}(f) + W_{\text{rot,eddy}}(f) + W_{\text{rot,sd}}(f)$  contribution.

### References

- [1] Bertotti, G., "Hysteresis in Magnetism", Academic Press, San Diego, CA (1998), 392.
- [2] Fiorillo, F., Beatrice, C., Bottauscio, O., Carmi, E., "Eddy-current losses in Mn-Zn ferrites", *IEEE Trans. Magn.*, **50** (2014), 6300109-1-9.
- [3] Ferrara, E., Fiorillo, F., Beatrice, C., Dobák, S., Ragusa, C., Magni, A., Appino, C., "Characterization and assessment of the wideband magnetic properties of nanocrystalline alloys and soft ferrites", *J. Mater. Res.*, **33** (2018), 2120-2137.
- [4] Magni, A., Beatrice, C., Bottauscio, O., Caprile, A., Ferrara, E., Fiorillo, F., "Magnetization process in thin laminations up to 1 GHz", *IEEE Trans. Magn.*, **48** (2012), 1363-1366.

# Testing the sheet thickness independence of a new dynamic magnetization property based on domains and walls within the diffusion-like equation for GO SiFe

O. Maloberti<sup>1,2</sup>, M. Nesser<sup>2</sup>, M L Ababsa<sup>1,4</sup>, E. Salloum<sup>2</sup>, J. Fortin<sup>2</sup>, S. Panier<sup>2</sup>, P. Dassonville<sup>1,3</sup>

<sup>1</sup>ESIEE Amiens, 14 quai de la Somme, 80080 Amiens, France.

E-mail: olivie.maloberti@gmail.com; maloberti@esiee-amiens.fr

<sup>2</sup>LTI Laboratory, IUT d'Amiens, Avenue des Facultés - Le Bailly 80 025 Amiens, France.

<sup>3</sup>MIS - UPJV, 14 quai de la Somme, 80080 Amiens, France.

<sup>4</sup>LSEE Laboratory, Technoparc Futura, 62400 Béthune, France.

*Keywords: Magnetization reversal processes, dynamic hysteresis, excess losses, diffusion equation.*

In the design of a magnetic component, the magnetic field calculation inside all materials and in every working condition is often a guarantee of quality. The most accurate methods are the numerical ones, such as the Finite Element Method. Software use a physical formulation based on the Maxwell equations in matter including the materials' electrical conductivity  $\sigma$  and magnetic permeability  $\mu$  [1]. It is thus possible to consider the impact of eddy currents losses in the field diffusion into account for any geometry. Several models are proposed with the aim to include either the static hysteresis [2, 3] and the dynamic one [4, 5]. These last require parameters hard to identify and interpret. They are also non-univocal and render the field computation less convergent and more time consuming. To improve the physical interpretation of identifications and try to ease and speed up the calculations, other authors derive a new energy formulation involving only univocal behavioral laws [6], while focusing on the dynamic losses and hysteresis [7]. These studies confirm that the dynamic hysteresis corresponds to excess iron losses, due to dynamic magnetization reversal processes within magnetic domains [8, 9] and especially to microscopic eddy currents around the magnetic walls in motion [10]. Whatever the magnetization mechanism (domain walls displacement, bowing, fusion, nucleation and multiplication), it is always possible to define a dynamic property  $\Lambda$  [11] involved in the magnetic field damping due to microscopical eddy currents ((1) & (2)):

$$H = \mu^{-1}B + \sigma\Lambda^2 \partial_t B \quad (1)$$

$$\Lambda = 1/\sqrt{2\sigma J_s n_w m_w S_w} \quad (2)$$

Usually, magnetization properties should be intrinsic to the materials, with its electrical resistivity  $\sigma^l=48 \mu\Omega cm$ , the saturation polarisation  $J_s=2.1 T$ , the walls mobility  $m_w$  only influenced by the magnetic walls density  $n_w$  and area  $S_w$  on one side; and by the grain boundaries and defects on the other side. Changes only occur due to experimental conditions (field magnitude  $B_{max}$ , frequency  $f$ ). Meanwhile, the geometry dependent macroscopic behaviour can be described by the field  $H_M = \mu^{-1}B$  diffusion-like equation (3), coming from the Maxwell theory.

$$\nabla \times \nabla \times \left( (1 + \sigma\Lambda^2\mu\partial_t)H_M \right) + \sigma\mu\partial_t H_M = 0 \quad (3)$$

The obtained formulation includes both the excess iron losses due to microscopic eddy currents and the geometry dependent macroscopic eddy currents. In this paper, we want to analyze the thickness  $\zeta$  dependence of the dynamic magnetization property  $\Lambda(\zeta)$ . To this extend, we suggest carrying out magnetic measurements on GO SiFe samples with the Epstein frame for four different thicknesses ( $\zeta = 0.23, 0.27, 0.30$  and  $0.35$  mm), at low induction magnitudes  $B_{max}$  (from 100 mT to

800 mT) and several frequencies  $f$  ( $f$  from 10 Hz to 800 Hz). For each thickness and experimental condition ( $B_{max}, f$ ),  $\mu$  and  $\Lambda$  are assumed constant and can be identified at once thanks to the 1D analytical calculation of two macroscopic observables: the apparent permeability ( $\mu_{app} = B_{max}/H_{max}$  [ $H.m^{-1}$ ]) and the mean power loss density per unit mass ( $P_f = f^*(\oint HdB)/\gamma$  [ $W.kg^{-1}$ ],  $\gamma$  is the mass density). It is then possible to compute the total hysteresis cycles *versus* the measurements.

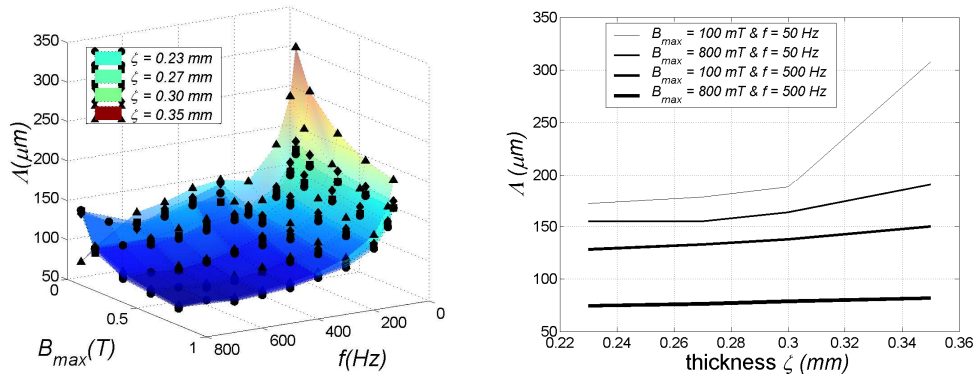


Figure 1: Identification  $\Lambda(B_{max}, f)$  with sinusoidal waveforms as a function of the thickness  $\zeta$ .

Expected results show in Fig. 1 that  $\Lambda$  is reduced while increasing both the frequency and the flux density magnitude (*i.e.* the product  $B_{max} * f$ ) thanks to domains walls bowing, multiplication and nucleation processes. The reduction of  $\Lambda$  while decreasing the thickness is more surprising but probably due to some surface anisotropy, demagnetizing or/and tension effects that naturally refine the domains structure. Having to change the properties with the thickness represents a serious limitation when using a simulation software supposed to handle different geometries. It leads us to investigate another physical formulation that takes the sensitivity of magnetic structures to the geometry and surface quality into account [12].

*Acknowledgements:* Samples with a stress relieving treatment were kindly given by TKES. Measurements were carried out by the LSEE. Part of the modeling and identification research was performed at the ESIEE Amiens and has received funding from the European Research Council under the European Union's H2020-IND-CE-2016-17/H2020-FOF-2017 Program (Grant Agreement No. 766437).

#### References

- [1] A. Bossavit, *Revue de Physique Appliquée*, vol. 23 (1988): pp. 1147-1159.
- [2] F. Preisach, "Über die magnetische Nachwirkung", *Zeitschrift für Physik*, 1935, Bd. 94.
- [3] D.C Jiles and D.L Atherton, *J. of Mag. and Mag. Mat.*, Vol. 61 (1986), pp. 48-60.
- [4] D. C. Jiles, *IEEE Transactions On Magnetics*, Vol.30. No.6 (1994).
- [5] M-A. Raulet et al., *IEEE Trans. on Magnetics*, vol. 42, n°2 (2004), pp. 872-875.
- [6] O. Maloberti et al., *IEEE Transactions on Magnetics*, vol. 42, n°4 (2006), pp. 895-898.
- [7] O. Maloberti et al., *IEEE Transactions on Magnetics*, vol. 44, no6 (2008), pp. 914-917.
- [8] P. Weiss, *J. Phys. Theor. Appl.*, 6 (1) (1907), pp.661-690.
- [9] F. Bitter, *Phys. Rev.*, Vol. 38 (1931), pp. 1903.
- [10] R.H. Pry, C.P. Bean, *J. Appl. Phys.*, vol. 29 (1958), 532-533.
- [11] O. Maloberti et al., *J. of Magnetism and Magnetic Materials*, vol. 304 (2006), pp. e507-e509.
- [12] O. Maloberti et al., "How to Formulate Soft Materials Heterogeneity?", *SMM'18* (2007).

Phenomenological modeling of hysteresis curves near transition temperature in La(Fe,Si)<sub>13</sub>-based alloysR. Gozdur<sup>1</sup>, P. Gębara<sup>2</sup>, K. Chwastek<sup>3</sup><sup>1</sup> Łódź University of Technology, Department of Semiconductor and Optoelectronics Devices, Wólczajska 211/215, 90-924 Łódź, Poland, e-mail: roman.gozdur@p.lodz.pl<sup>2</sup> Chair of Physics, Częstochowa University of Technology, Al. Armii Krajowej 19, 42-201 Częstochowa, Poland, e-mail: pgebara@wip.pcz.pl<sup>3</sup> Faculty of Electrical Engineering, Częstochowa University of Technology, Al. Armii Krajowej 17, 42-201 Częstochowa, Poland, e-mail: krzysztof.chwastek@gmail.com

The magnetocaloric effect (MCE) observed in the La(Fe,Si)<sub>13</sub>-based alloys in near-room temperature has been the subject of intensive research due to its potential applications in magnetic refrigeration [1-5]. Most of publications on the MCE focus on considerations on entropy changes near the Curie temperature and the possibility to tailor up the properties of different compounds by appropriate modifications of their chemical composition [2,3,6-10]. However, an interesting issue is also the examination of power losses [11] and magnetization curves in the vicinity of transition point.

Hysteresis in magnetocaloric materials has recently come into the spotlight of the engineering community [12]. Most often for modeling purposes the phenomenological Preisach-Mayergoyz model [13,14] and the description advanced by Jiles and Atherton are used [15,16]. In the present paper we suggest the use of the  $T(x)$  description [17] for modeling magnetization curves near the transition temperature, cf. Fig. 1.

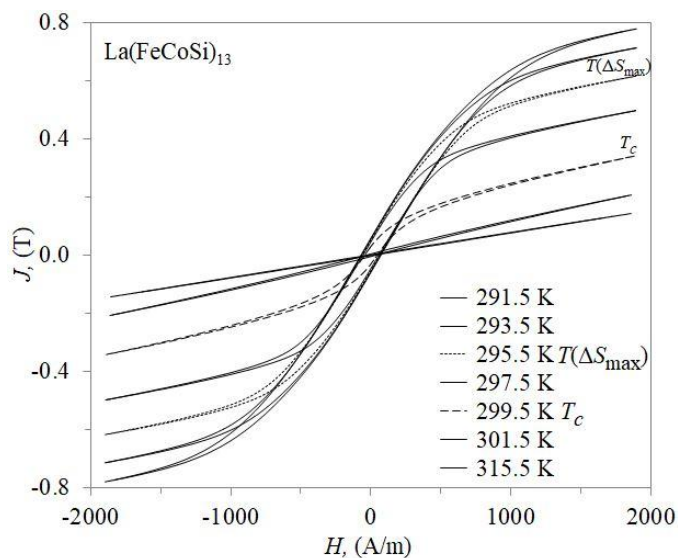


Fig. 1. Influence of temperature on the hysteresis loops near the transition point ( $T_c = 300\text{K}$ ).

The full text shall consider two versions of the  $T(x)$  description, namely the original one, described in the textbook [17] by model developer, and the more recent modification [18]. The correction introduced into the original model was aimed at a better representation of reversible magnetization processes. The structure of fundamental model equation was made similar to the one considered previously by Gy. Kádár in his product Preisach model [19,20]. The introduced magnetization

dependent function  $R(m) = 1 - m^2$ , which modulates total susceptibility in dependence on instant magnetization, has been considered by Basso and Bertotti as a direct measure of active domain wall area during magnetization [21]. An analogous modification introduced previously to the Jiles-Atherton model allowed one to obtain improved description of minor loops both symmetrical [22] and biased ones [23]. It is thus expected that promising results might also be obtained for the case of product- $T(x)$  model.

## References

- [1] A. M. Tishin, Y. I. Spichkin, The magnetocaloric effect and its application, Institute of Physics Publishing, London 2003.
- [2] J. Liu, J. D. Moore, K. P. Skokov, M. Krautz, K. Löwe, A. Barcza, M. Katter, O. Gutfleisch, Exploring La(Fe,Si)<sub>13</sub>-based magnetic refrigerants towards application, *Scripta Mat.*, vol. 67, pp. 584-9, 2012.
- [3] V. Franco, J. S. Blázquez, B. Ingale, A. Conde, The magnetocaloric effect and magnetic refrigeration near room temperature: materials and models, *Annu. Rev. Mater. Res.*, Vol. 42, 305-42, 2012.
- [4] M. Balli, S. Jandl, P. Fournier, A. Kedous-Lebouc, Advanced materials for magnetic cooling: fundamentals and practical aspects, *Appl. Phys. Rev.*, vol. 4, 021305 (27 pp.), 2017.
- [5] V. Basso, "Basics of the magnetocaloric effect", arXiv:1702.08347v1 [cond-mat.mtrl-sci] 27 Feb. 2017
- [6] V. Lollobrigida, V. Basso, F. Borgatti, P. Torelli, M. Kuepferling, M. Coisson, E. S. Olivetti, F. Celegado, L. Tortora, G. Stefani, G. Panaccione, F. Offi, Chemical, electronic, and magnetic structure of LaFeCoSi alloy: surface and bulk properties, *J. Appl. Phys.*, vol. 115, 203901 (9 pp.), 2014.
- [7] R. M'nassri, A. Cheikhrouhou, Magnetocaloric effect in LaFe<sub>10.7</sub>Co<sub>0.8</sub>Si<sub>1.5</sub> compound near room temperature, *J. Supercond. Nov. Mater.*, vol. 27, pp. 1059-64, 2014.
- [8] A. Fujita, S. Fujieda, K. Fukamichi, Relative cooling power of La(Fe<sub>x</sub>Si<sub>1-x</sub>)<sub>13</sub> after controlling the Curie temperature by hydrogenation and partial substitution of Ce, *J. Magn. Magn. Mat.*, vol. 310, pp. e1006-7, 2007.
- [9] P. Gębara, J. Kovac, Magnetocaloric effect of the LaFe<sub>11.2</sub>Co<sub>0.7</sub>Si<sub>1.1</sub> modified by partial substitution of La by Pr or Ho, *Mater. Des.*, vol. 129, 111-5, 2017.
- [10] P. Gębara, P. Pawlik, Broadening of temperature working range in magnetocaloric La(Fe,Co,Si)<sub>13</sub>-based multicomposite, *J. Magn. Magn. Mater.*, vol. 422, 145-51, 2017.
- [11] R. Gozdur, M. Lebioda, Ł. Bernacki, Power losses in LaFe<sub>x</sub>Co<sub>y</sub>Si<sub>1.1</sub> intermetallics near the magnetic phase transition, *Acta Phys. Pol. A*, Vol. 128, No. 1, pp. 98-103, 2015.
- [12] O. Gutfleisch, T. Gottschall, M. Fries, D. Benke, I. Radulov, K.P. Skokov, H. Wende, M. Gruner, M. Acet, P. Entel, M. Farle, Mastering hysteresis in magnetocaloric materials, *Philos. Trans. A Math. Phys. Eng. Sci.*, vol. 374, 2016, 20150308, doi: 10.1098/rsta.2015.0308.
- [13] I. D. Mayergoyz, Mathematical models of hysteresis and their applications, 2nd Ed., Academic Press, 2003.
- [14] V. Basso, M. Kuepferling, C. P. Sasso, M. LoBue, Modeling hysteresis of first-order magneto-structural phase transformations, *IEEE Trans. Magn.*, Vol. 44, pp. 3177-80, 2008.
- [15] D. C. Jiles, D. L. Atherton, Theory of ferromagnetic hysteresis, *J. Magn. Magn. Mater.*, vol. 61, pp. 48-60, 1986.
- [16] Y. Melikhov, R. L. Hadimani, A. Raghunathan, Phenomenological modelling of first order transitions in magnetic systems, *J. Appl. Phys.*, Vol. 115, 183902 (5 pp.), 2014.
- [17] J. Takács, Mathematics of hysteretic phenomena, Wiley-VCH, Weinheim 2003.
- [18] K. Chwastek, A. P. S. Baghel, B. Sai Ram, B. Borowik, L. Daniel, S. V. Kulkarni, On some approaches to model reversible magnetization processes, *J. Phys. D: Appl. Phys.*, vol. 51, 145003 (7 pp.), 2018.
- [19] Gy. Kádár, The bilinear product model of hysteresis phenomena, *Phys. Scr.*, vol. T25, pp. 161-4, 1989.
- [20] Gy. Kádár, On the product Preisach model of hysteresis, *Physica B*, vol. 275, pp. 40-4, 2000.
- [21] V. Basso, G. Bertotti, Hysteresis models for the description of domain wall motion, *IEEE Trans. Magn.*, vol. 32, pp. 4210-2, 1996.
- [22] K. Chwastek, J. Szczygłowski, W. Wilczyński, Modelling dynamic hysteresis loops in steel sheets, *COMPEL*, vol. 28, pp. 603-12, 2009.
- [23] K. Chwastek, Modelling offset hysteresis loops with the modified Jiles-Atherton description, *J. Physics D: Appl. Phys.*, vol. 42, 165002 (5 pp.), 2009.

# Phenomenologic model for incremental permeability micro-magnetic non destructive testing technique

Benjamin Ducharne<sup>1</sup>, Bhaawan Gupta<sup>2</sup>, Gael Sebald<sup>2</sup>, Tetsuya Uchimoto<sup>3</sup>

<sup>1</sup>*Laboratoire de Génie Electrique et Ferroélectricité, France*

*E-mail: benjamin.ducharne@insa-lyon.fr*

<sup>2</sup>*ElyTMax, Tohoku University, Japan*

<sup>3</sup>*Institute of fluid science IFS, Tohoku University, Japan*

*Keywords:* Magnetic incremental permeability, hysteresis model, mechanical stress

Residual stresses inevitably occur in metallic components due to industrial machining or heat treatment processes. These local micro-residual stresses affect real-life performance of industrial parts. Measurement and analysis of residual stresses is important for quality assurance and inspection, as stress affects bearable load and fatigue lifetime over specific failure mechanisms. The use of micro-magnetic techniques such as the Barkhausen noise evaluation or the incremental permeability has increased exponentially in the industrial field. The local magnetization processes are highly dependent on the distribution of the residual stresses and local micro-magnetic characterization are particularly effective sensing techniques to map the distribution of these residual stresses. The current industrial use of this micro-magnetic characterization techniques is very empirical; operators set thresholds of rejection using experimental results. Up to now, accurate models able to refine these thresholds and to improve the understanding of the phenomena are still missing. In this article, a model based on the time variations of both the local excitation field  $H$  and the local magnetic induction  $B$  is proposed to simulate the Magnetic Incremental Permeability (MIP) sensor. MIP is defined as the effective permeability for a small alternating field superimposed on a larger steady field. The MIP is calculated by measuring the minor loop magnetic flux density during the process of magnetization. Last investigations around ferromagnetic models such as the one we need for the incremental permeability simulation mainly focus on coupling Space Discretization Techniques (SDT), Finite Elements Method (FEM) or Finite Differences Method (FDM) extended with accurate scalar or vector, dynamic or static hysteresis material law [1][2]. For this magnetic material law, it seems that the best results come from the extension of the quasi-static hysteresis model (Preisach model [3], Jiles-Atherton model [4]) to dynamic behavior as a result of the separation losses techniques as proposed by Bertotti [5].

As in a classic MIP sensing technique controlled area is always lower than a few mm<sup>2</sup>, we can assume that in this area the material is spatially homogenous. The quasi-static DC excitation field amplitude is typically 1000 times higher than the AC one. For those two reasons, in the MIP simulator, the space discretization can be replaced by a lump phenomenological model where  $B$  and  $H$  are collinear and linked by a hysteretic material law.

For this material law, we have different options. Firstly, we consider the AC magnetic field amplitude sufficiently weak that even under high frequency level (50 kHz) the rate  $dH/dt$  is lower than the quasi-static DC field one. In this case, a scalar quasi-static hysteresis contribution is enough. For this quasi-static contribution again we have different options:

- \_ A modified Jiles-Atherton model, where the accommodation issue (i.e. it takes many cycles for a minor hysteresis loop to stabilize) is corrected by assuming the AC field amplitude sufficiently weak to ignore hysteresis during the minor loop situation. Minor cycles are then treated as a single slope as it has been done by Y. Gabi & al. in [6]. The Jiles-Atherton model is characterized by 5

parameters, according to the J-A's theory each parameter has a physical meaning. In [7] an extended version of the J-A's model has been proposed with temperature taken into account, in [8] another extension has been proposed for the behavior under mechanical stress excitation. These two extensions are useful for the MIP simulation under such external conditions. The modified J-A's model gives correct results for the MIP butterfly loop (variation of the permeability modulus versus excitation field) but the conservation of the slope forbids variations on the imaginary versus real part of the complex permeability.

\_ A modified "applied H dependent" type model, such as the Preisach model [3] or the dry friction model [9]. The essential limitation of such models is that they assume that the remanent magnetization depends only on the applied magnetic field. Hence, when a sample of magnetic material is cycled between two magnetic fields, the size and shape of the resulting minor remanence loop predicted by the Preisach model does not depend upon the magnetic state of the system. This phenomenon called the "congruency property" lead to a MIP butterfly loop limited to a single anhysteretic curve. Improvements can be done by correcting the model input as proposed:

$$H_{eff}(t) = H(t) + \alpha \cdot B(t) \quad (1)$$

Where  $H_{eff}$  is the effective field and  $\alpha$ , a constant of proportionality between the average field and the magnetization which depends on the shape and the angular dispersion of the particles in the media. The modified model gives correct simulations results but with these models the physical interpretations are limited.

Secondly, a dynamic contribution can be added to the quasi-static contribution described previously. When higher amplitude or frequency levels of the AC component are used, the quasi-static thresholds are reached and dynamic effects will influence the magnetization behavior. For this dynamic contribution and as the frequency of the AC component is constant, a simple viscous losses first order consideration is enough to correctly model this dynamic contribution. In the model the product of a constant  $\rho$  to the time derivation of the induction field dB/dt is considered as an equivalent excitation field H [10].

In the extended version of this article every solution will be detailed, comparisons simulations / measures will be compared and conclusions on the most appropriate simulation methods will be given.

### References

- [1] M. A. Raulet, B. Ducharme, J.P. Masson, and G. Bayada, "The magnetic field diffusion equation including dynamic hysteresis: a linear formulation of the problem", IEEE Trans. on Mag., vol. 40, n° 2, pp. 872 – 875, 2004.
- [2] B. Ducharme, G. Sebald, D. Guyomar, G. Litak, "Fractional model of magnetic field penetration into a toroidal soft ferromagnetic sample", Int. J. of Dyn. And Cont., pp. 1-8, 2017.
- [3] F. Preisach, "Über die magnetische Nachwirkung". Zeitschrift für Physik, 94: 277-302, 1935.
- [4] D. C. Jiles and D. L. Atherton, "Theory of ferromagnetic hysteresis", J. Magn. Magn. Mater., vol. 61, no. 1–2, pp. 48–60, Sep. 1986.
- [5] G. Bertotti, "General properties of power losses in soft ferromagnetic materials", IEEE Trans. on Mag., 24, pp. 621-630, 1988.
- [6] Y. Gabi, B. Wolter, A. Gerbershagen, M. Ewen, P. Braun, O. Martins, "FEM simulations of incremental permeability signals of a multi-layer steel with consideration of the hysteretic behavior of each layer", IEEE Trans. On Mag., vol. 50 n°14, 2014.
- [7] A. Raghunathan, Y. Melikhov, J.E. Snyder and D.C. Jiles, "Modeling the temperature dependence of hysteresis based on Jiles-Atherton theory", IEEE trans. on mag., vol. 45, pp. 3954-3957, 2009.
- [8] M.J. Sablik, D.C. Jiles, "Coupled magnetoelastic theory of magnetic and magnetostrictive hysteresis", IEEE Trans. on mag., vol. 29 n°3, 1993.
- [9] B. Ducharme, D. Guyomar, G. Sebald, "Low frequency modelling of hysteresis behaviour and dielectric permittivity in ferroelectric ceramics under electric field", Journal of Physics D: Applied Physics, vol. 40, iss. 2, pp. 551-555, 2007.
- [10] B. Gupta, B. Ducharme, G. Sebald, T. Uchimoto, "A space discretized ferromagnetic model for non-destructive eddy current evaluation", IEEE Trans. on. Mag, vol. 54 Iss. 3, 2018.

## Efficient and novel simulation method for the effective permeability of randomly ordered structures

Daniel Wöckinger<sup>1</sup>, Gerd Bramerdorfer<sup>1</sup>, Wolfgang Amrhein<sup>1</sup>  
Stefan Schuster<sup>2</sup>, Norbert Gstöettenbauer<sup>2</sup>, Johann Reisinger<sup>2</sup>

<sup>1</sup> Institute for electrical drives and power electronics, Johannes Kepler University, Austria  
E-mail: daniel.woeckinger@jku.at ; gerd.bramerdorfer@jku.at ; wolfgang.amrhein@jku.at

<sup>2</sup> voestalpine Stahl GmbH, Austria

E-mail: stefan.schuster2@voestalpine.com ; norbert.gstoettenbauer@voestalpine.com ;  
johann.reisinger@voestalpine.com

**Keywords:** effective permeability, numerical simulation, mixing models.

In many technical fields metal foams, ferrous powder mixtures, metallic granulates and sintered materials are used in various parts of production chains. Because of the complex and multi-phase nature of these products, their magnetic properties typically differ from the characteristics of the raw materials. If it is not required to describe the magnetic field in all randomly arranged particles and regions in microscopic detail, the concept of the effective permeability can be used. Generally, effective material parameters are described by mixing models. In [1] and [2] Sihvola et al. present mixing rules derived from electrostatic theory, which can be used for magnetic materials under certain conditions as well. These mixing formulas describe the effective magnetic properties depending on the volume fractions of the ingredients. However, a huge number of usually unknown parameters such as particle arrangement, particle size, inclusion shape and local packing density additionally affect the effective permeability. For example, Fig.1 shows that three different ordered two-phase mixtures differ in the resulting permeability  $\mu_{\text{eff}}$  even if they have the same volume proportions of the phases. Because of this, a variation in the magnetic behavior of randomly ordered structures must be expected. Its range and dependency on process parameters and ingredients is important for the design of magnetic devices and non-destructive magnetic testing methods.

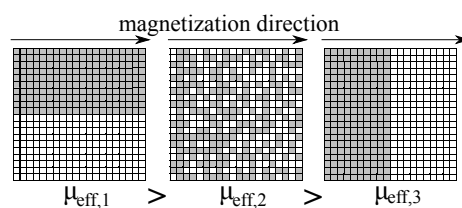


Figure 1: Two-phase structures with the same volume fraction of a magnetic inclusion phase (gray) in a non-magnetic background medium (white), but, evidently, different effective permeabilities.

In the present work the random assignment of the permeability is limited to a plane. Along the third dimension it is assumed that the magnetic properties are constant. A simplified example for this modeling approach is shown in Fig. 2a. To determine its effective permeability, the model is converted into an equivalent electrical network according to Fig.2b. Every particle of the structure

can be represented by an equivalent resistor network including the two resistors  $R_0 \propto \mu_0$  and  $R_1 \propto \mu_1$ . Of course, the resistors  $R_0$  and  $R_1$  can be nonlinear. The magnetization of the specimen is modeled by a voltage source  $V_{\text{mag}}$ , which generates a current  $I_{\text{mag}}$  depending on the resistor values and their arrangement. Finally, the effective permeability can be determined by using the relationship  $\frac{V_{\text{mag}}}{I_{\text{mag}}}$ . The extensive calculation of  $I_{\text{mag}}$  is done by the open source electronic circuit simulator SPICE [3]. For this reason, an algorithm was developed that generates the circuit netlist of a given model. Because of this very flexible method, the resulting permeability of any structure can be estimated. Figure 2c illustrates exemplary the results of thousand simulated randomly ordered mixtures with more than 5000 particles for various compoundings. The aim of the present work is both an introduction of the novel method to simulate the effective permeability and an evaluation of the simulated data with measurements of magnetic and non-magnetic powder mixtures. More details about the simulation algorithms, the experimental setup and a comparison of simulated and measured permeability of randomly ordered mixtures will be presented in the final paper.

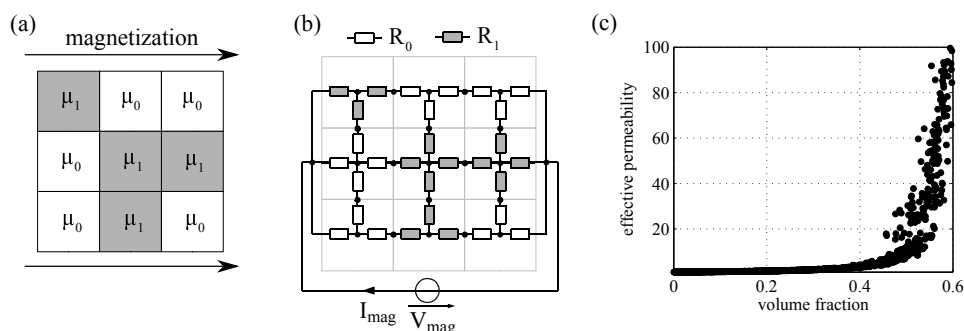


Figure 2: (a) Model of a randomly ordered two-phase powder mixture consisting of nine particles. (b) The equivalent electrical circuit of the model in Fig. 2a for the permeability analysis with SPICE. (c) Thousand simulated effective permeabilities of randomly ordered mixtures with a background medium  $\mu_0 = 1$  and randomly varied volume fractions of the inclusion phase  $\mu_1 = 1500$ .

#### Acknowledgements

The authors gratefully acknowledge the funding support of K1-MET GmbH, metallurgical competence center. For the numerical simulations it was necessary to fall back on simulation and optimization software developed by the LCM K2 Center for Symbiotic Mechatronics within the framework of the Austrian COMET-K2 program.

#### References

- [1] Sihvola, A. H., Lindell I. V., "Effective permeability of mixtures", *Prog Electromagn.*, **06** (1992) 153-180.
- [2] Sihvola, A. H., "Self-consistency aspects of dielectric mixing theories", *IEEE Transactions on Geoscience and Remote Sensing*, **17**, no. 4 (1989), 403-415.
- [3] M. S., Sandler, M., Steven, "SPICE Circuit Handbook", *McGraw-Hill, Inc.*, New York, (2006), ISBN 978-0-07-146857-2



# **OS1-B: 1D Measurement and Non-Conventional Characterization**

Session Chairman

**Kiyoshi WAJIMA**

Nippon Steel & Sumitomo Metal Corp. - Japan



## Keynote Lecture

*”Thermographic Measurement of Losses Due to Inter-laminar Contacts in Electrical Sheets”*



**Prof. Anouar Belhacen**

*Aalto University, Finland*

**Anouar Belhacen** received the M.Sc. (Tech.) and Doctor (Tech.) degrees from Helsinki University of Technology, Finland, in 1998, and 2004, respectively. He is now Professor of Energy and Power at Aalto University, Finland and Professor of electrical machines at Tallinn University of Technology, Estonia. His research interests are numerical modelling of electrical machines, magnetic materials, coupled magneto-mechanical problems, magnetic forces, magnetostriction, and fault diagnostics of electrical machines.

# Thermographic Measurement of Inter-Laminar Short Circuits and Related Losses

Anouar Belahcen<sup>1,2</sup>, Sahas Bikram Shah<sup>1</sup>, Osaruyi Osemwinyen<sup>1</sup>, Paavo Rasilo<sup>1,3</sup>, Antero Arkkio<sup>1</sup>

<sup>1</sup>*Aalto University, Dept. of Electrical Engineering and Automation, Finland*

*E-mail: anouar.belahcen@aalto.fi; sahas.shah@fi.abb.com, osaruyi.osemwinyen@aalto.fi; Antero.Arkkio@aalto.fi*

<sup>2</sup>*Tallinn University of Technology, Estonia*

*E-mail: anouar.belahcen@aalto.fi*

<sup>3</sup>*Tampere University of Technology, Lab. of Electrical Energy Engineering, Finland*

*E-mail: paavo.rasilo@tut.fi*

**Keywords:** Inter-laminar contacts, Iron losses, Thermal camera, Thermal measurements.

The magnetic core of electrical machines and transformers are constructed from electrical steel sheets, which are punched and stacked together. On one hand, the punching process deteriorates the magnetic properties of the electrical sheets, in terms of permeability and hysteresis losses [1], [2]. On the other hand, the punching burrs at the edges of the sheet might destroy the sheet insulation layer during the stacking process and produce short circuits between the sheets [3]. Both phenomena are harmful for the operation of the machines and are challenging to detect and quantify. In this paper, we present a thermal camera-based measurement method to detect the inter-laminar short circuits and measure the related power losses. Furthermore, we present a preliminary investigation on the possibility of measuring local iron losses with the same thermal camera methodology. The objective of this second part is to assess the detectability of the losses at the damaged, punched edges of the electrical sheet and their quantification.

For the first part, dealing with the inter-laminar short circuits, we artificially implemented short circuits between two iron sheets and measured the related losses with a thermal camera through the initial temperature rise method [4]. Some challenges related to this methodology are explained and several methods to tackle them are presented. The methodology has also been assessed through exhaustive numerical simulations [4]. A major challenge of this method consists of estimating the initial slope of the temperature rise under convective and conductive heat dissipation. We tackled this by either averaging the slope over some periods or by estimating the heat dissipation effect from the cooling behaviour of the measured area. The results of these methods can be used in coupled magnetic and thermal finite element simulations aiming at determining the depth of the lamination short circuit.

Figure 1 shows the temperature distribution around the inter-laminar short circuit at an instant of time and the temperature rise at the location of the short circuit. Figure 2 shows the temperature distribution at the surface of an iron sample when it is magnetized at 1.5 T and 50 Hz and the corresponding temperature rise averaged over a small area in the middle of the sample.

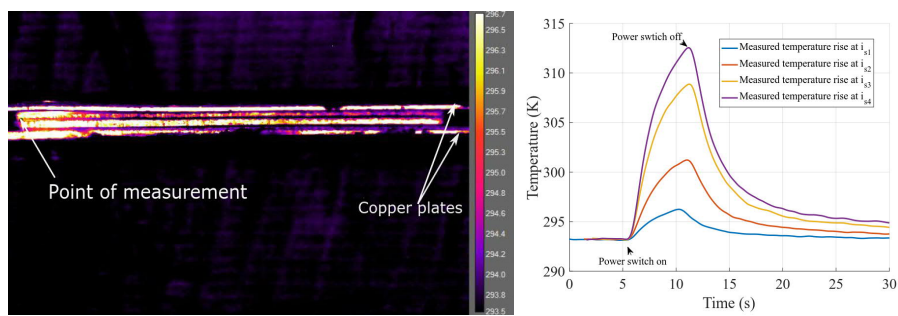


Figure 1: Temperature distribution (left) and filtered rise (right) at an artificial inter-laminar short circuit.

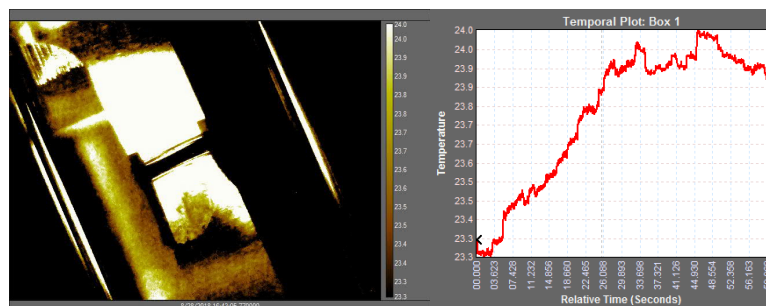


Figure 2: Temperature distribution (left) and rise (right) at the surface of a non-oriented iron sample under sinusoidal magnetization (1.5 T, 50 Hz)

### Acknowledgements

The research leading to these results has received funding from the European Research Council under the European Union's Seventh Framework Programme (FP/2007–2013)/ERC Grant Agreement No. 339380. This research has been also supported by the Estonian Research Council under grants PUT1260

### References

- [1] Kedous-Lebouc, A., Cornut, B., Perrier, J., Manf, P., Chevalier, T., "Punching influence on magnetic properties of the stator teeth of an induction motor," *J. Magn. Magn. Mat.*, **254255** (2003), 124 – 126.
- [2] Liu, C., Chang, B., Hung, K., Lin, S., "cutting and punching impacts on laminated electromagnetic steels to the designs and operations of synchronous reluctance motors," *IEEE Trans. Ind. App.*, **51**(2015), 3515-3520
- [3] Hamzeshbahmani, H., Anderson, P., Jenkins, K., Lindenmo, M., "Experimental study on inter-laminar short-circuit faults at random positions in laminated magnetic cores," *IET Elec. P. App.*, **10**(2016), 604-613.
- [4] Bikram Shah, S., Osemwinyen, O., Rasilo, P., Belahcen, A., Arkkio, A., "Thermographic measurement and simulation of power losses due to inter-laminar contacts in electrical sheets," *IEEE Trans. Instr. Meas.*, **xx**(2018),1-7 (Early Access)

# Universal modular high power wide frequency range controlled system for magnetic measurements

Roman Rygał<sup>1</sup>, Stanisław Żurek<sup>1</sup>, Wojciech Pluta<sup>2</sup>, Jacek Leszczyński<sup>3</sup>,  
Marian Soiński<sup>1</sup>, Jan Walak<sup>1</sup>, Jakub Rygał<sup>1</sup>

<sup>1</sup>*Magneto Sp. z o.o., ul. Odlewników 43, 42-202 Częstochowa, Poland*  
*E-mail: roman.rygal@magneto.pl*

<sup>2</sup>*Czestochowa University of Technology, Faculty of Electrical Engineering, Al. Armii  
Krajowej 17, 42-200 Częstochowa, Poland, e-mail: w.pluta@gmail.com*

<sup>3</sup>*AGH University of Science and Technology, Faculty of Energy and Fuels,  
Department of Hydrogen Energy, Al. Mickiewicza 30, 30-059 Kraków, Poland*  
*E-mail: jale@agh.edu.pl*

**Keywords:** magnetic properties, measurement system, Epstein frame, SST, toroidal sample.

There is continuing demand on improvement of performance and efficiency of energy conversion in high-frequency (HF) switch-mode power converters. Magnetic cores of HF transformers and chokes are exposed to ever more challenging operating conditions. Typical magnetic measurements standards [1]-[5] are either inadequate or insufficient for generating the required design information. As a consequence it is difficult to design magnetic cores operating under such conditions and even more difficult to verify the actual level of performance attained during industrial manufacturing. Cores designed to operate at 50 Hz can be powered directly from the mains network if certain safety conditions are met [6], but obviously this approach is very limited.

The **universal modular high power wide frequency range controlled measurement system** (Fig. 1a) represents a much more robust approach to magnetic testing. Large-size magnetic cores can be tested directly, rather than through the use of smaller-size samples.

**Universality** is provided because the system is capable of measurements in four different configurations of samples/cores under test: *toroidal*, *SST*, *Epstein frame* and *arbitrary core*. These options allow testing virtually all cores and samples relevant in the HF power industry.

**Modularity** of the system comes from the way it was designed and assembled. Various sub-modules can be swapped for different specification, which also aids the universality. There is an additional module comprising two-beam laser targeted system for precise temperature measurements of the core or the windings.

**High power** is provided by a low-DC offset precision linear power amplifier with rated maximum output power of 8 kW (22 kW pulse), and amplitude capabilities of 120 V and 210 A.

**Wide frequency range** is provided by such selection of all the components that magnetisation can be applied and measured from 1 Hz to 100 kHz (with reduced power) or 16 Hz to 50 kHz with full power.

**Control** is achieved by utilising state of the art approach for wave shaping of arbitrary waveforms [5]. The system is capable of controlling the shape of flux density  $B$ , polarisation  $J$  or magnetic field strength  $H$ . The waveforms can be controlled to be: sinusoidal, triangular, trapezoidal, arbitrarily assembled from harmonics, generated using 2-level or 3-level PWM, or an arbitrary waveform can be uploaded from an electronic file (Fig. 1b).

**Measurements** carried out by the system are automatically logged to an output file, ready for

access in any spreadsheet software. The measured data includes for each measured point: peak  $B$  or peak  $J$ , peak  $H$ , full waveform of  $B$  or  $J$ , full waveform of  $H$ , amplitude relative permeability, specific active power loss per unit mass, specific active power loss per unit volume, total active power loss, total apparent power loss, remanence  $B$ , coercive  $H$ , temperature of the sample, form factor error, THD error, peak amplitude error, RMS values of primary and secondary voltages and currents, and apparent power supplied by the power amplifier. Full configuration data for the sample is also stored with the output file.

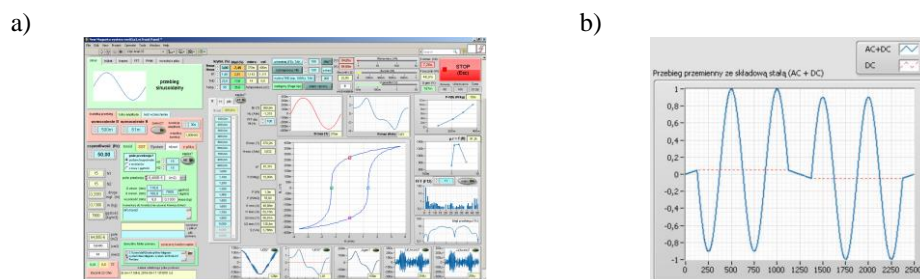


Figure 1: Control screen of the universal measurement system (a) and an example of a complex waveform which can be controlled by the system (b).

### Acknowledgements

This work has been carried out within the project grant "Industrial research a new type of magnetic cores made of amorphous and nanocrystalline strips, thin magnetic sheets and composite materials operating in higher frequencies", and was supported by the National Centre for Research and Development under European Regional Development Fund in the frame of European Smart Growth Funds, under contact No. POIR.01.01.01-00-0306/15-00. The support is gratefully acknowledged.

### References

- [1] IEC 60404-2, Methods of measurement of the magnetic properties of electrical steel strip and sheet by means of an Epstein frame.
- [2] IEC 60404-3, Methods of measurement of the magnetic properties of electrical steel strip and sheet by means of a single sheet tester.
- [3] ASTM A348/A348M, Standard test method for alternating current magnetic properties of materials using the wattmeter-ammeter-voltmeter method, 100 to 10 000 Hz and 25-cm Epstein frame.
- [4] IEC 60404-6, Methods of measurement of the magnetic properties of magnetically soft metallic and powder materials at frequencies in the range 20 Hz to 200 kHz by the use of ring specimens.
- [5] Zurek S., Practical implementation of universal digital feedback for characterisation of soft magnetic materials under controlled AC waveforms, *Electrical Review / Przegląd Elektrotechniczny*, R. 93 NR 7/2017, 2017, p. 16
- [6] Pluta W., Rygał R., Soiński M., Leszczyński J., Labview Based Testing System for the Aim of Construction of Energy Efficient Magnetic Cores. *E3S Web of Conferences*. ISSN 2267-1242 — 2017 vol. 14 No. 01039, pp. 1–10

# Novel model-based digital controller for facilitating soft magnetic material measurement under controlled magnetizing conditions

Anh-Tuan Vo, Marylin Fassenet, Afef Kedous-Lebouc, François Blache, Marie-Pierre Vaillant, Cédric Boudinet  
 Univ. Grenoble Alpes, CNRS, Grenoble INP, G2Elab, F-38000 Grenoble, France  
 Email: anh-tuan.vo@g2elab-grenoble-inp.fr

*Keywords*—model-based digital controller, magnetic measurement, waveform control

## Introduction

Dealing with requirements for modelling and simulating precisely performance of soft magnetic materials, magnetic measurement must be now conducted under different magnetizing conditions imposed by waveform, frequency and amplitude of flux density. The well-known nonlinearity of materials gives rise to a mandatory use of automatic controller in magnetic testing. Many studies about controllers were published. In [1], Zurek et al. reported an adaptive iterative feedback solution for 1D, 2D and even 3D measurement using any type of testers for diverse materials, wide range of frequency and high amplitude of flux density. In [2], the association of an analog circuit into a digital system helps to reduce 95% the convergence time comparing to results of [1], but the application range is narrow in terms of frequency (2 Hz to 100 Hz). We propose in this paper a novel digital controller which has two control loops, one for regulating amplitude and one for adjusting waveform of flux density based on equivalent circuit of magnetic testers such as Epstein frame and ring specimens. The adaptive ability and the high convergence speed of this controller are demonstrated by testing results with various families of materials (non-oriented SiFe, CoFe and amorphous alloys), diverse waveforms (sinusoidal, triangle, trapeze, user-defined periodic), wide range of frequency (up to 5 kHz) and high amplitude (up to 90% of the saturation) of flux density. Its principle and implementation in LabVIEW are also described.

## Methodology

For our study, a steady-state digital feedback measurement bench has been built consisting of a computer-based data acquisition system coupled with a voltage mode power amplifier. The system corrects iteratively the waveform voltage sent to the primary side of tester to yield the measured flux density  $B$  to its reference  $B_{ref}$ , within an acceptable error.

The tester circuit is mathematically modeled by the following equations:

$$\begin{cases} v_1 = N_1 S_{mat} \frac{dB}{dt} + R_{tot1} \frac{l}{N_1} H + N_1 S_{air} \mu_o \frac{dH}{dt} \\ v_2 = N_2 S_{mat} \frac{dB}{dt} + N_2 S_{air} \mu_o \frac{dH}{dt} \end{cases} \quad (1)$$

$v_1$ ,  $v_2$ ,  $N_1$ ,  $N_2$  are respectively primary and secondary winding voltage and number of turns;  $S_{mat}$ ,  $S_{air}$  are section of material and air part inside winding,  $R_{tot1}$  is total resistance of primary winding.

In steady-state, the relationship of the peak value of these quantities is approximated to be:

$$\bar{v}_1 = N_1 S_{mat} \cdot \frac{d\bar{B}}{dt} = N_1 S_{mat} K \bar{B} = G \cdot \bar{B} \quad (2)$$

Overbar represents the peak value of quantities,  $K$  is a proportional constant between  $\frac{dB}{dt}$  and  $\bar{B}$ . The constant  $G$  is determined by parameters of tester and waveform of  $B$ . A digital *PI* controller with a feedforward of the input voltage  $\bar{v}_1$  allows the system to reach the amplitude reference after two to three iterations. This *PI* controller is presented by the following formula:

$$\bar{v}_1(k+1) = \bar{v}_1(k) + K_I (\overline{B_{ref}} - \bar{B}(k)) \text{ with } \bar{v}_1(0) = G^{-1} \cdot \overline{B_{ref}} \quad (3)$$

$K_I$  must be chosen to be lower than  $G$  to eliminate the oscillation, in our study,  $K_I = 1 \cdot G$

At very low or high frequency and at high level of  $B$ , the waveform of  $v_1$  is corrected as follow:

$$v_1(k+1) = N_1 S_{mat} \frac{dB_{ref}}{dt} + R_{tot1} \frac{\bar{l}}{N_1} H(k) + N_1 S_{air} \mu_o \frac{dH(k)}{dt} \quad (4)$$

Most of parameters in (4) are required for any system of measurement for the determination of  $B$  and  $H$ , except  $R_{tot1}$ . Our model-based system provides an online estimation of  $R_{tot1}$  and thus is adaptive to many tester and material. In a real system, before applying the formula (4),  $B$  and  $B_{ref}$  are synchronized and  $H$  is filtered with a low pass filter. When the convergence conditions are satisfied at  $N$ th iteration, we must have  $v_1(N) \approx v_1(N-1)$  and  $H(N)$  converges to  $H_{ref}$ , the waveform of  $H$  corresponding to  $B_{ref}$ . The scheme of the controller is illustrated in Figure 1.

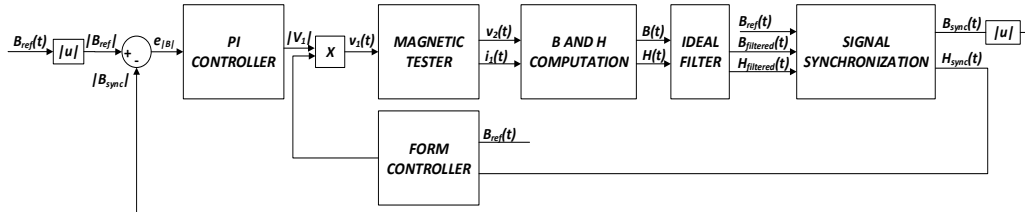


Figure 1 Block diagram of the control system

### Results

Figure 2 shows the solution for the measurement of a thin gauge non-oriented SiFe NO20 ring sample at diverse magnetizing conditions. The measured signal of  $B$  tracks closely its reference with form factor lower than 0.5% for three cases. The primary side voltage  $v_1$ , in other word the control signal, is corrected and highly distorted comparing to its initial waveform. More details about the implementation and the performance of the system will be presented in the full paper.

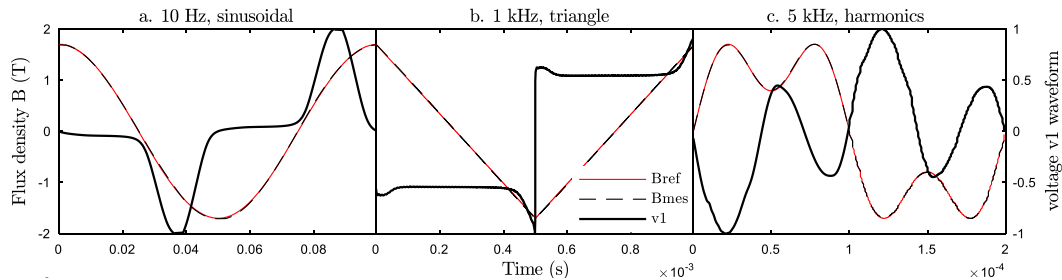


Figure 2 Measurement results for a NO20 ring sample at various waveform of  $B$  and frequency

### Conclusion

A novel measurement system for soft magnetic material has been described. Despite of its dependence on the equivalent circuit of tester, the system does not require more parameter than any published systems. Moreover, its volatility allows the testing of various soft magnetic materials under a wide-range of controlled magnetizing conditions without any change in control parameters.

### References

- [1] S. Zurek et al., "Use of novel adaptive digital feedback for magnetic measurements under controlled magnetizing conditions," *IEEE Trans. Magn.*, vol. 41, no. 11, pp. 4242–4249, 2005.
- [2] S. White et al., "A Multichannel Magnetic Flux Controller for Periodic Magnetizing Conditions," *IEEE Trans. Instrum. Meas.*, vol. 61, no. 7, pp. 1896–1907, Jul. 2012.

# Temperature dependence of magnetic losses in Co-doped Mn-Zn ferrites

Cinzia Beatrice<sup>1</sup>, Vasiliki Tsakaloudi<sup>2</sup>, Samuel Dobák<sup>3</sup>, Carlo Ragusa<sup>4</sup>,  
Luca Martino<sup>1</sup>, Fausto Fiorillo<sup>1</sup>,

<sup>1</sup> *Istituto Nazionale di Ricerca Metrologica - INRIM, Torino, Italy*

*c.beatrice@inrim.it; l.martino@inrim.it; f.fiorillo@inrim.it*

<sup>2</sup> *Laboratory of Inorganic Materials CERTH, Themi-Thessaloniki, Greece, vikaki@cperi.certh.gr*

<sup>3</sup> *Institute of Physics, P.J. Šafárik University, Košice, Slovakia,*

*samuel.dobak@student.upjs.sk*

<sup>4</sup> *Politecnico di Torino, Energy Department, Torino, Italy, carlo.ragusa@polito.it*

**Keywords:** Magnetic losses, Mn-Zn ferrites, Ferromagnetic resonance.

An expanding applicative area for soft magnetic cores in electronics calls for high permeability and low loss materials over a broad range of frequencies, from DC to several MHz. The high resistivity and low anisotropy of the Mn-Zn ferrites, in particular, favors good broadband magnetic behavior and, thanks to low costs and standardized preparation methods, ubiquitous applications in sensing and power electronics. Important modifications of the soft magnetic properties of the Mn-Zn ferrites can be induced by addition of oxides, which can act both on the material resistivity and the magnetocrystalline anisotropy [1]-[2]. It is therefore standard practice, for example, to introduce CaO and Nb<sub>2</sub>O<sub>5</sub> in order to modify the chemistry at the grain boundaries and increase the related resistivity. With additives like TiO<sub>2</sub>, SnO<sub>2</sub>, and CoO and the corresponding substitution of Fe<sup>3+</sup> cations with the foreign cations, the phenomenon of anisotropy compensation, where the negative anisotropy of the Fe<sup>3+</sup> ions in the octahedral sites is made to combine with the positive anisotropy of the extra-cations occupying the same sites, is expected to occur [3]. In this way, the overall magnetocrystalline anisotropy can be reduced, though in a temperature-dependent fashion. This can eventually lead to reduction of the loss and to increase of permeability.

In this work we investigated a set of Mn-Zn ferrite ring samples (outside diameter 14.15-14.44 mm, inside diameter 9.15 – 8.86 mm, thickness 4.55 – 5.02 mm), prepared following the conventional method of solid state reaction, starting from raw pure powders, sintered at 1325°C. In addition to the fixed doping scheme that included CaO and Nb<sub>2</sub>O<sub>5</sub>, Co-enrichment was made by addition of CoO, up to 6000 ppm (with 1000 ppm steps). The magnetic losses were measured from DC up to 1GHz, at different peak polarization values in the temperature range 0°C - 130°C. The magnetic characterization of the ring samples was performed using a calibrated hysteresisgraph-wattmeter in the range DC-10 MHz and a transmission line method in the range 100 kHz - 1 GHz using a Vector Network Analyzer (VNA) with a 50 Ω coaxial line and brass cell. The electrical impedance was measured, in the same temperature range, from 200 Hz up to about 10 MHz by the four-wire method. Fig. 1 shows an example of dependence of the real  $\rho'$  and imaginary  $\rho''$  resistivity components on frequency at different temperatures, measured on a 4000 ppm CoO-doped ring sample. This level of doping is the one leading, at room temperature, to the minimum loss figure upon the whole investigated frequency range [4]. Analysis of the  $\rho'(f)$  and  $\rho''(f)$  behaviors shows that their temperature dependence is mostly related to the corresponding behavior of the resistivity of the grain boundary layer, which decreases by more than an order of

magnitude on passing from

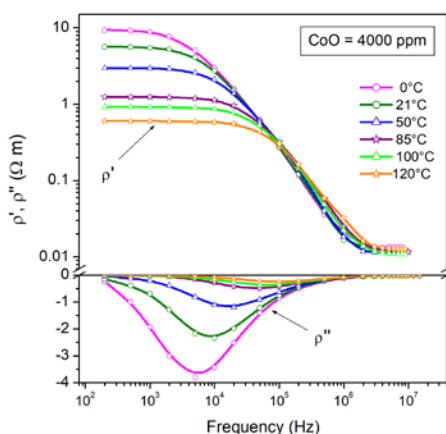


Fig. 1: Real  $\rho'(f)$  and imaginary  $\rho''(f)$  resistivity dependence on frequency in the 4000 ppm CoO-doped Mn-Zn ferrite ring between 0 °C and 120 °C. The shown behaviors chiefly relate to the evolution of the grain boundary resistivity with temperature.

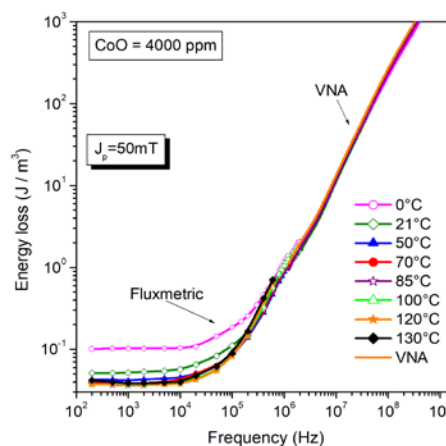


Fig. 2: Broadband energy loss behaviour at peak polarization  $J_p = 50$  mT and temperatures between 0 °C and 130 °C in the 4000 ppm CoO-doped Mn-Zn ferrite ring. The loss becomes quite independent of temperature beyond a few MHz.

0 °C to 120 °C. Little change is instead found for the intragrain resistivity. It has nevertheless been shown that eddy currents measurably contribute to the losses only beyond a few MHz in these and in typical Mn-Zn ferrite samples having similar size [5]. The temperature dependence of the energy loss  $W(f)$  versus frequency shown in the example provided in Fig. 2 is actually engendered by the corresponding evolution of the magnetic anisotropy. This is verified by estimating the average anisotropy constant  $K$  through the analysis of the permeability versus  $J_p$  and  $f$  and extracting the contribution provided by the rotational processes, which, for uniform angular distribution of the easy axes can be expressed as  $\mu_{DC,rot} = 1 + J_s^2/3\mu_0 K$ . It appears, in any case, that all the  $W(f)$  curves pertaining to different temperatures tend to coalesce beyond a few MHz. It is shown that at such high frequencies the domain wall processes have completely relaxed and only rotations survive. Once separated from a possible eddy current contribution, the associated energy dissipation can be calculated by resorting to the real and imaginary susceptibilities obtained as solutions of the Landau-Lifshitz equation for the damped motion of the precessing spins and lumping the effects of the internal effective anisotropy fields  $H_K$ , depending on anisotropy and internal demagnetizing fields, into a suitable distribution function. This implies that the spin motion resonates across a spectrum of frequencies, corresponding to the distribution of the local  $H_K$  values. It is found, in particular, by fitting the measured rotational loss, that the optimal CoO doping is associated with narrowest  $H_K$  distribution and lowest average effective anisotropy field.

#### References

- [1] Shokrollahi, H., Janghorban, K., *Mater. Sci. Eng. B* **141** (2007), 91–107.
- [2] Wang, S., Chiang Y., Hsu. Y., Chen C., *J. Magn. Magn. Mater.* **365**, (2014) 119-125.
- [3] Li, L., Lan, Z., Yu, Z., Sun, K., Xu, Z., *J. Alloys Comp.* **476** (2009), 755–759.
- [4] Beatrice, C., Dobák, S., Tsakaloudi, V., Ragusa, C., Fiorillo, F., Martino, L., Zaspalis, V., *AIP Advances*, **8** (2018) 047803.
- [5] Fiorillo, F., Beatrice, C., Bottauscio, O., Carmi, E., *IEEE Trans. Magn.* **50** (2014), 6300109.



# OS4: Multiphysics Coupling

Session Chairman

**Helmut PFUETZNER**

Tu Wien, Inst. of Electrodynamics, Microwave and Circuit Engineering -  
Austria



## Keynote Lecture

*”Relevance of multiscale approach for the modeling of various magneto-mechanical problems”*



**Prof. Olivier Hubert**

*LMT, ENS Paris-Saclay, France*

**O.Hubert** is mechanical engineer from University of Technology of Compiègne France. He received his Master Degree in Applied acoustics and materials in 1994 and PhD on relation between plastic deformation and magnetics in 1998. He has been successively associate professor in University Pierre et Marie Curie (UPMC Paris) and full professor in Ecole Normale Supérieure de Paris Saclay since 2009. The main theme of his research activities is the development of constitutive models for phase-change media, either thermo-mechano-chemically induced, like for shape memory alloys, or electro-magneto- mechanically induced as for ferro / ferri-magnetic and / or ferroelectric materials. On the one hand, it involves the establishment of experimental methods for the identification and validation of mechanisms (measurement of deformations, magnetic measurements, phase change monitoring by XRD) under thermal and / or multiaxial mechanical loading, and on the other hand the development of modeling tools essentially based on scaling methods (homogenization, finite elements).

# Relevance of multiscale approach for the modeling of various magneto-mechanical problems

Olivier Hubert

*LMT (ENS-Paris-Saclay, CNRS, Université Paris-Saclay), 61 avenue du Président Wilson, F-94235 Cachan, cedex, France*

*E-mail: hubert@lmt.ens-cachan.fr*

*Keywords:* magneto-mechanics, multiscale coupled constitutive laws, morphic effect, plasticity

Our time is characterized by an increasingly intensive use of actuators in extremely large fields of applications, from the largest to the smallest scales. The miniaturization of these systems adds new design constraints and requires the development of materials with controlled properties and robust models. One of the solutions being considered is the use of material exhibiting at least one strong multiphysic coupling (one of the physic being mechanics). This includes magnetostrictive materials [1], classical (SMA) or magnetic shape memory alloys (MSMA) [2], piezoelectric materials, multi-ferroic composite media, etc. One of the modeling challenges is to better describe the complex interactions observed experimentally (nonlinearity, non-monotony, irreversibly, dynamic and multiaxial effects etc ...), and to derive constitutive models with sufficient accuracy and validity range for the considered applications without requiring full field approach (micromagnetism, phase field) that still remain highly time-consuming. In this communication, the modeling of materials exhibiting magneto-elastic behavior in a reversible framework is addressed.

Showing the relevancy of scale change requires first going back to the initial foundation of Gibbs free energy density at the local scale  $\alpha$  ( $\text{J/m}^3$ ) involving mechanical and magnetic terms. The variation of Gibbs free energy  $dg_\alpha$  is function of stress  $\bar{\sigma}_\alpha$  and magnetic field  $\bar{H}_\alpha$  variations as control variables (1) ( $\bar{\epsilon}_\alpha$  is the total strain and  $\bar{B}_\alpha$  the magnetic induction).

$$dg_\alpha = -\bar{\epsilon}_\alpha : d\bar{\sigma}_\alpha - \bar{B}_\alpha \cdot d\bar{H}_\alpha \quad (1)$$

Small perturbation hypothesis allows the total deformation  $\bar{\epsilon}_\alpha$  to be considered as a sum of different contributions, highlighting some specific couplings between mechanics and another physic to be defined. In the case of the target materials, classical elastic  $\bar{\epsilon}_\alpha^e$  and free deformation  $\bar{\epsilon}_\alpha^M$  associated with magnetostriction are considered leading to:

$$\bar{\epsilon}_\alpha = \bar{\epsilon}_\alpha^e + \bar{\epsilon}_\alpha^M = \mathbf{C}_\alpha^{-1} : \bar{\sigma}_\alpha + \bar{\epsilon}_\alpha^M \quad (2)$$

$\mathbf{C}_\alpha$  is the 4<sup>th</sup> order local stiffness tensor. Derivation of the mechanical Gibbs free energy function involves consequently an integration of magnetostriction over the stress path making its expression complicated without any other assumption<sup>1</sup> (3). The magnetic part of Gibbs free energy is obtained after a Legendre transformation of the Helmholtz free energy density usually expressed as function of magnetization instead of induction (even function of magnetization) (4) [3].

$$g_\alpha^M = -\frac{1}{2} \bar{\sigma}_\alpha : \mathbf{C}_\alpha^{-1} : \bar{\sigma}_\alpha - \int_0^{\bar{\sigma}_\alpha} \bar{\epsilon}_\alpha^M : d\bar{\sigma}_\alpha \quad (3)$$

---

<sup>1</sup> Numerous authors simplify this expression by removing the pure mechanical part and forgetting to integrate the second part.

$$g_{\alpha}^{\mu} = \bar{M}_{\alpha} \cdot \bar{P}_{\alpha}^0 \cdot \bar{M}_{\alpha} + \bar{M}_{\alpha} \bar{M}_{\alpha} : \mathbf{P}_{\alpha}^1 : \bar{M}_{\alpha} \bar{M}_{\alpha} + \bar{M}_{\alpha} \cdot \bar{M}_{\alpha} \bar{M}_{\alpha} : \bar{P}_{\alpha}^2 : \bar{M}_{\alpha} \bar{M}_{\alpha} \cdot \bar{M}_{\alpha} - \mu_0 \bar{H}_{\alpha} \cdot \bar{M}_{\alpha} \quad (4)$$

This expression is using a second order  $\bar{P}_{\alpha}^0$ , 4<sup>th</sup> order  $\mathbf{P}_{\alpha}^1$  and 6<sup>th</sup> order  $\bar{P}_{\alpha}^2$  tensors as material dependent whose expressions are strongly correlated to material symmetries and requires assumptions for simplification. The scaling is relevant for that.

The multiscale model of a representative volume element (RVE) that is proposed involves domain and grain as subscales (figure 1). Indeed magnetization at the domain scale has a constant norm equal to the saturation magnetization  $M_s$ . At this scale the magnetostriction can be considered on the other hand as stress independent, allowing a simplification of the magneto-elastic coupling energy term  $g_{\alpha}^{M\mu}$  as linearly dependent to stress and as a quadratic function of magnetization (5) [4].

$$g_{\alpha}^{M\mu} = -\bar{R} : \bar{E}_{\alpha} : \bar{\sigma}_{\alpha} = -\int_0^{\bar{\sigma}_{\alpha}} \bar{\varepsilon}_{\alpha}^{\mu} : d\bar{\sigma}_{\alpha} = -\bar{\varepsilon}_{\alpha}^{\mu} : \bar{\sigma}_{\alpha} \quad (5)$$

$\bar{R}$  is the second order orientation tensor and  $\bar{E}_{\alpha}$  is the piezomagnetic 4<sup>th</sup> order tensor defined by 3 constants in the cubic crystallographic framework and reduced to 2 constants considering incompressibility. The constitutive behavior is assumed to follow a Boltzmann distribution allowing a statistical calculation of the domain families' volume fraction [5]. Localization and homogenization procedures, homogeneous stress and magnetic field conditions at the grain scale do complete the scheme. Some examples of applications and relevancy of stress dependent magnetostriction consideration (*morphic effect*) [3,6] will be detailed in the full paper.

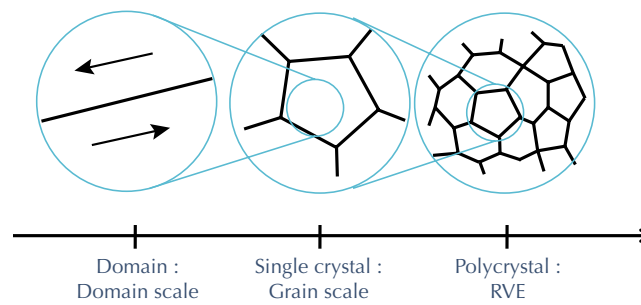


Figure 1: Detail of scales involved in the modeling approach

### References

- [1] M.J. Dapino, "On magnetostrictive materials and their use in adaptive structures," *Str. Eng. and Mechanics*, 17 (3-4), (2004) 303-330.
- [2] C. LExcellent, "Shape-Memory Alloys Handbook", ed. Wiley, 2013.
- [3] W.P. Mason, "A phenomenological derivation of the first- and second-order magnetostriction and morphic effects for a nickel crystal", *Phys. Rev.*, 82 (5) (1951) 715-723.
- [4] E. Du Tremolet de Lacheisserie, "Magnetostriction: theory and applications of magnetoelasticity", CRC Press, Boca Raton 1993.
- [5] L. Daniel, O. Hubert, N. Buiron, R. Billardon, "Reversible magneto-elastic behavior: A multiscale approach", *J. of the Mech. and Phys. of Solids*, 56 (2008), 1018-1042
- [6] O. Hubert, "Multiscale magneto-elastic modeling of magnetic materials including second order stress effect", *J. Magn. Magn. Mater.*, *submitted*.

# On the correlation of crystallographic macro texture and magnetic magnetization anisotropy in non-oriented electrical steel

Nora Leuning, Benedikt Schauerte, Simon Steentjes, Kay Hameyer

*Institute of Electrical Machines (IEM), RWTH Aachen University, D-52062 Aachen, Germany*

**Keywords:** Non-oriented electrical steel, crystallographic texture, magnetic anisotropy.

Non-oriented electrical steels are used to guide and increase the magnetic flux in rotating electrical machines. Even though the name suggests isotropic magnetic properties due to the random grain orientation, non-oriented steel grades do have a magnetic anisotropy [1,2]. This anisotropy is affected by various factors, e.g., anisotropic grain size, residual stress from the manufacturing process and the crystallographic texture [2]. The dependence of the magnetization behavior on the crystallographic texture is related to the magnetocrystalline anisotropy of the body-centered-cubic iron single crystals which require different magnetic fields along the cube edges (easy axes) and the space diagonal (hard axes) to be magnetized [3].

When general magnetization related topics are discussed or the magnetization curves are preprocessed for magnetic machines simulations the results are generally based on measurements in rolling (RD) and transverse direction (TD). For the commonly applied machine simulations anisotropy is not modeled and the material behavior is only included with curves averaged in RD and TD. However, as Fig. 1 highlights, the mean value between RD and TD does not include all magnetization curves and therefore, is insufficient to be used for averaging and a general description of magnetization behavior in the entire lamination sheet plane. In saturation, the curves converge because the saturation polarization is determined by the chemical composition of the material. But

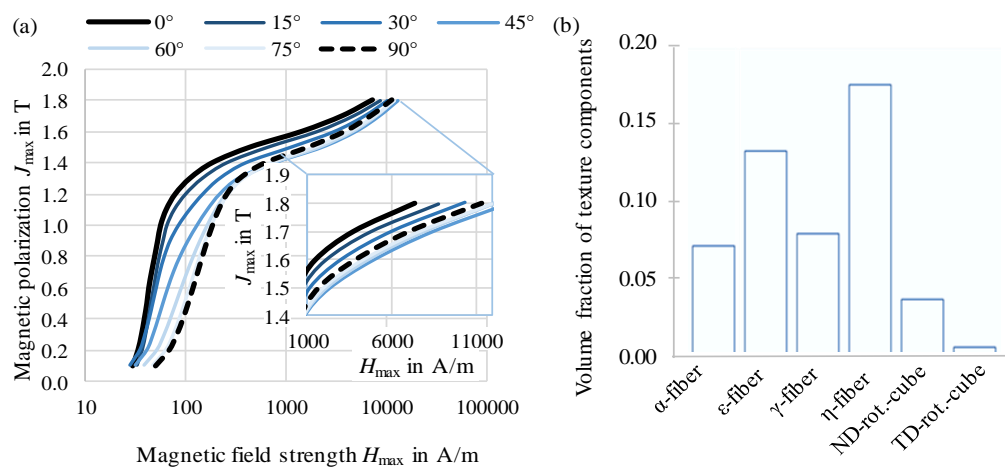


Figure 1: Magnetic and crystallographic anisotropy of a non-oriented M270-50A (a) Magnetization curves at 50 Hz and (b) volume fraction of texture components.

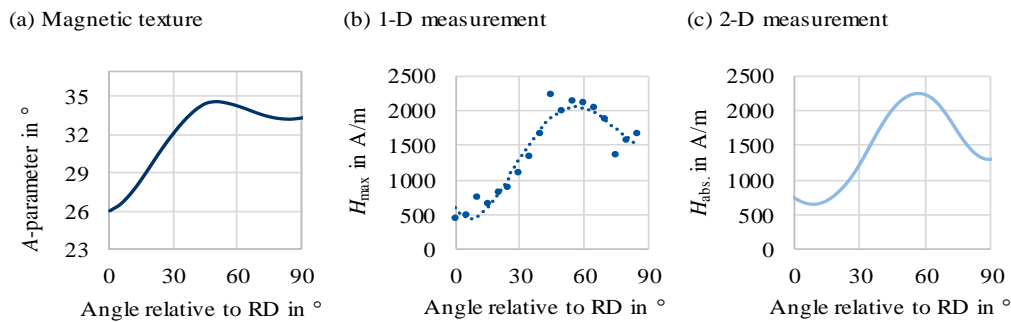


Figure 1: (a)  $A$ -parameter calculated from the ODF according to [4] and magnetic measurements at 50 Hz and 1.5 T (b) unidirectional SST, (c) rotating magnetic field on a rotational SST.

at high polarizations, here between 1.3 to 1.8 T, the influence of crystallographic texture is dominant, and therefore, the curves of intermediate orientations have to be considered for descriptions of the magnetization behavior.

In this paper, different approaches to measure and estimate the magnetic anisotropy of three non-oriented materials (M270-50A, M300-35A, 280-30AP) are compared with respect to the crystallographic texture of the materials. In Fig. 2, 1-D and 2-D magnetic measurements are compared to the  $A$ -parameter, which can be calculated solely from the orientation distribution function (ODF) obtained by x-ray goniometry [4]. The magnetic measurements on the unidirectional single-sheet-tester are performed on 18 samples cut in  $5^\circ$  angles relative to RD, whereas the 2-D measurements are performed on a rotational single-sheet-tester under a rotating magnetic field. In the full paper the magnetization at higher flux densities and the magnetic loss will be evaluated. Both approaches show a good accordance with the crystallographic texture and therefore are a promising approach to minimize the measurement effort. A substitution of ODF measurements with magnetic measurements or vice versa is thereby conceivable [5].

#### Acknowledgements

This work is funded by the Deutsche Forschungsgemeinschaft (DFG, German Research Foundation) – 255713208, 218259799, 1487/31-1 and carried out in the research group project – “FOR 1897 – Low-Loss Electrical Steel for Energy-Efficient Electrical Drives” and in the priority program – “SPP 2013 – Focused Local Stress Imprint in Electrical Steel as Means of Improving the Energy Efficiency”.

#### References

- [1] E. Gomes, et al. ‘Correlation Between Microstructure, Texture, and Magnetic Induction in Nonoriented Electrical Steels’, IEEE Trans. on Magn., vol. 46, no. 2, pp. 310–313, Feb. 2010.
- [2] F. J. G. Landgraf, et al. ‘Modelling the angular dependence of magnetic properties of a fully processed non-oriented electrical steel’, JMMM, vol. 254–255, pp. 328–330, Jan. 2003.
- [3] R. M. Bozorth, Ferromagnetism. Van Nostrand, 1951.
- [4] L. Kestens and S. Jacobs, ‘Texture Control During the Manufacturing of Nonoriented Electrical Steels’, Texture, Stress, and Microstructure, vol. 2008, pp. 1–9, 2008.
- [5] E. Cardelli, et al. “Magnetic modelling for the texture analysis of Fe-Si alloys,” 2016 IEEE Conference on Electromagnetic Field Computation (CEFC), Miami, FL, 2016

# Influence of Laminating Process on Magnetic Property of Permendur for High Power Density of Motors

Yuya Ako<sup>1</sup>, Yasuhito Takahashi<sup>1</sup>, Koji Fujiwara<sup>1</sup>,  
and Takehiro Jikumaru<sup>2</sup>

<sup>1</sup> Doshisha University, Kyoto, Japan

E-mail: {ctwb0301@mail4; ytakahashi@mail; koji.fujiwara@mail}.doshisha.ac.jp

<sup>2</sup> IHI Corporation, Kanagawa, Japan

E-mail: takehiro\_jikumaru@ihi.co.jp

**Keywords:** Permendur, laminated specimen, mechanical stress, SPMSM, more electric Aircraft

The use of a permendur is one of the hopeful approaches to realize further downsizing and weight reduction of motors. A permendur has an advantage of the higher saturation magnetic flux density compared with ordinary electrical steel sheets. However, there are only a few cases where a permendur is applied to motors as iron core, and the influence of manufacturing process on its magnetic properties has not sufficiently discussed. In this paper, the change of magnetic properties due to laminating processing was evaluated by measuring laminated and single sheet specimens of the permendur [1].

Table 1 shows specifications of specimen and measurement conditions. The stress applied to the single sheet specimen is  $\pm 20$  MPa,  $\pm 10$  MPa,  $\pm 7.5$  MPa,  $\pm 0.5$  MPa, 0 MPa, where the signs of + and - mean tensile and compressive stress, respectively.

Table. 1 Specifications of specimen and measurement conditions.

Specimen	Length [mm]	Width [mm]	Thickness [mm]	H detection method	frequency [Hz]
Single sheet (stress application)	360	60	0.2	2 Hcoil method	50, 100
Laminated	90	16	16	Hcoil method	

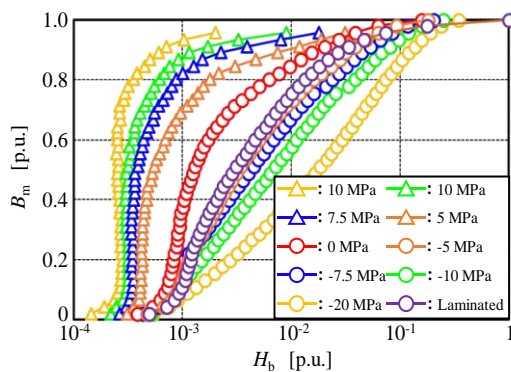


Fig. 1. Magnetization property.

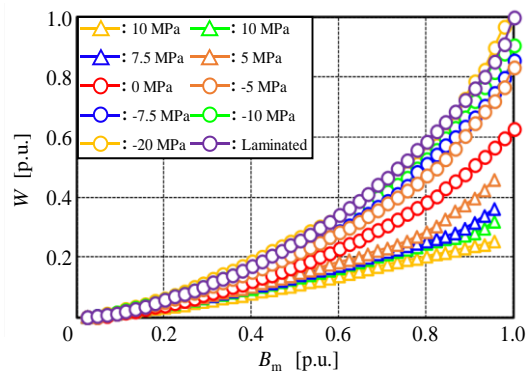


Fig. 2. Iron loss property.

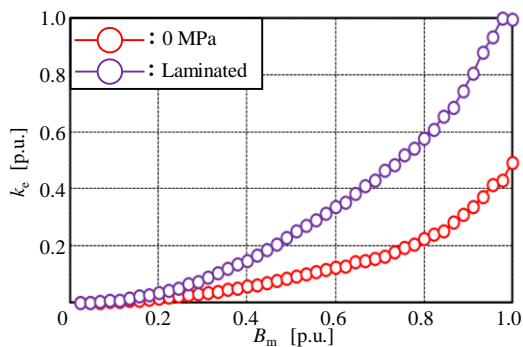


Fig. 3. Eddy current loss coefficient.

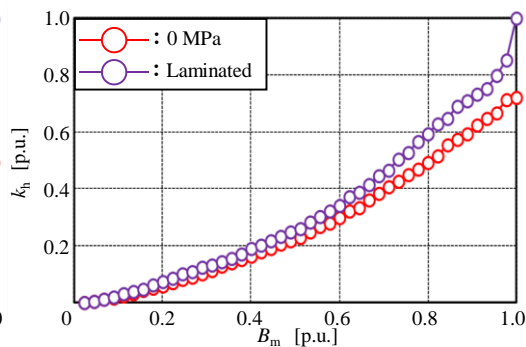


Fig. 4. Hysteresis loss coefficient.

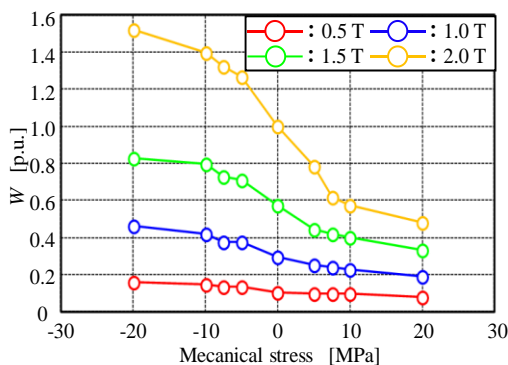


Fig. 5. Stress dependence of iron loss at 50 Hz.

The space factor of the laminated specimen is about 96 %. Figs. 1 and 2 show the magnetization properties and iron loss properties of the laminated and the single sheet specimen under the stress application at 50 Hz. Figs. 3 and 4 show hysteresis loss and eddy current loss coefficients of the single sheet specimen (0 MPa) and the laminated specimen. These coefficients are calculated by using iron losses measured at 50 Hz and 100 Hz. Fig. 5 shows the stress dependence of iron loss at the maximum flux density  $B_m = 0.5, 1.0, 1.5$  and  $2.0$  T

From Fig. 1, a stress from  $-5$  to  $0$  MPa may be applied to the laminated specimen. However, from Fig. 2, the iron loss of the laminated specimen is larger than any other stress application conditions. Although the hysteresis loss coefficient of the single sheet specimen without stress application is almost the same as that of the laminated specimen, the eddy current loss coefficient of the laminated specimen is significantly larger. The cause may be the short-circuit of the surfaces of laminated specimen due to wire-cut electrical discharge machining after lamination. We performed 3-D analysis of Surface Permanent Magnet Synchronous Motor (SPMSM) using the measurement results for laminated specimen. In motors having a wide gap, deterioration of magnetization properties does not significantly affect power density of motors. From Fig. 5, the iron loss increases as the compressive stress increases and it decreases as the tensile stress increases. The effect of stress application on operating characteristic of SPMSM will be reported in the full paper. The above mentioned results were obtained by collaborative research with IHI on More Electric Aircraft.

#### Reference

- [1] Y. Ako, Y. Takahashi, K. Fujiwara, and T. Jikumaru “Improvement of Power Density of Surface Permanent Magnet Synchronous Motor by Applying Permendur to Stator Core,” *The Papers of Joint Technical Meeting on Static Apparatus and Rotating Machinery, IEE Japan*, SA-16-31, RM-16-31, pp. 87-92 (2018) (in Japanese).

## The effet of punching on electrical machine

Mohamad EL YOUSSEF<sup>1</sup>, AbdelKader BENABOU<sup>2</sup>, Adrien VAN GORP<sup>1</sup>, Stéphane CLENET<sup>2</sup>, Pierre FAVEROLLE<sup>3</sup>, Jean-Claude MIPO<sup>3</sup>, Yannick LAVALLEY<sup>4</sup>, Thomas LECUPPE<sup>4</sup>.

<sup>1</sup>Arts & Metiers ParisTech; Mechanics, Surfaces and Materials Processing (MSMP); 8, boulevard Louis XIV 59046 Lille.

<sup>2</sup>Univ. Lille, Arts et Metiers ParisTech, Centrale Lille, HEI, EA 2697 - L2EP - Laboratoire d'Electrotechnique et d'Electronique de Puissance, F-59000 Lille, France

<sup>3</sup>Valeo-2 Rue André Charles Boulle, 94000 Créteil, France

<sup>4</sup>R.Bourgeois-25, Rue de Trépillot BP 1077 25002 Besançon, France.

**Keywords:** Punching, Magnetic characterization, Stator.

The punching process is based on a shearing phenomenon with a precisely shaped tool. Due to its cutting speed, it represents the widespread lamination cutting method. However, as any manufacturing process, it affects the material properties and leads to magnetic behavior degradation [1]-[2]. Globally, it leads to the decrease of the magnetic permeability and increase of the iron losses. Several studies have tried to define the impacted zone with different methods. Results show that punching could impact the material, depending on the cutting parameters, up to 10mm from the cut edge [3]-[4]-[5].

In the case of electrical machines, the width of the stator teeth can be of the same order of degraded zone by the punching process. Existing studies address the impact of punching on the magnetic behavior considering normalized characterization devices and the extrapolation of the results to real application is not necessarily straightforward because the effect of punching depends highly on the parameters of the process. In this communication, we propose an approach to characterize the effect of punching on samples collected from the manufacturing line of slinky stators, which enables to highlight the effect of the process on this specific geometry.

Two types of punched samples are obtained: the first type represents a closed magnetic path (without airgap), the second one is made from two parts, which represent the upper and the lower parts of the first sample type. In fact, the slinky stator yoke fabrication is performed in several steps that allow to extract these two types of samples. Measurements are performed directly on the samples (Figure 1).

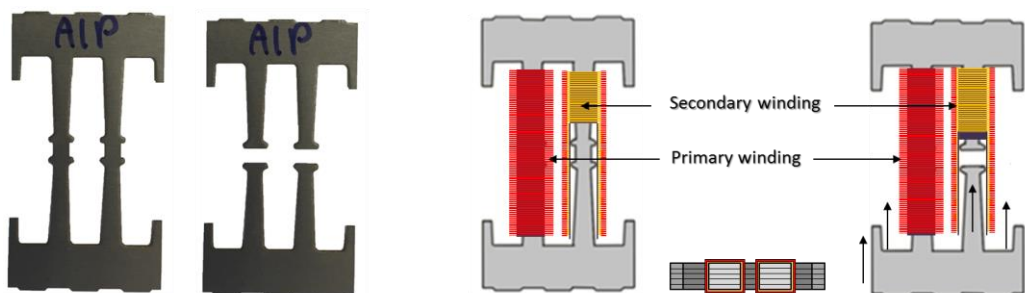


Figure 1: Punched test Samples and the schematic of the teeth magnetic characterization.

The considered samples can be arranged to form a closed magnetic path but with a non-constant cross-section. Thus the estimation of the magnetic flux density is not straightforward as it will not

be homogeneous. Therefore, it is chosen to consider the evolution of the magnetic flux and the imposed Ampere-turns (NI) in order to evaluate the impact of the process. To estimate the punching impact, samples with the same geometry and extracted from the same lamination sheet are obtained using the wire electrical discharge machining (WEDM). This process is known to have a limited impact on the magnetic behavior and these samples will be considered as a reference.

In Figure 1, we present the hysteresis loops  $\Phi(N\cdot I)$  corresponding to the single core samples at 50Hz: Punch\_C for punched samples and WEDM\_C for wire cut samples. It is clear that punching has a drastic effect on the magnetic properties, a significant degradation of the permeability is observed. Furthermore, we present in Figure 3 the hysteresis loops at 50Hz corresponding to the open magnetic circuit (with air gap) samples: Punch\_O for punched samples and WEDM\_O for wire cut samples. As expected, the air gap affects significantly the global magnetic behavior. Nevertheless, the impact of punching is clearly emphasized when compared with the wire-cut sample. Thus it is important to quantify the global impact of punching and its evolution in the presence of air gap.

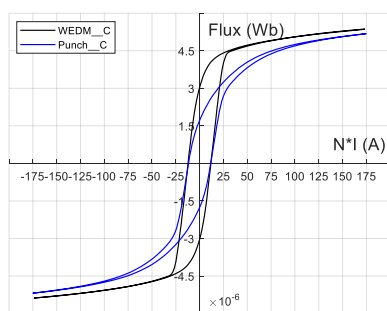


Figure 2: Comparison between single core WEDM and punched samples hysteresis loops at 50Hz.

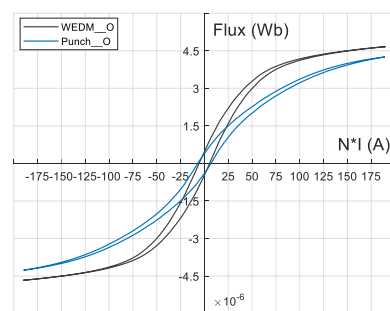


Figure 3: Comparison between WEDM and punched Samples in two parts hysteresis loops at 50Hz.

### References

- [1] S. Jana et N. S. Ong, « Effect of punch clearance in the high-speed blanking of thick metals using an accelerator designed for a mechanical press », *J. Mech. Work. Technol.*, vol. 19, n° 1, p. 55–72, 1989.
- [2] P. Baudouin, M. De Wulf, L. Kestens, et Y. Houbaert, « The effect of the guillotine clearance on the magnetic properties of electrical steels », *J. Magn. Magn. Mater.*, vol. 256, n° 1, p. 32–40, 2003.
- [3] M. Z. Salih, B. Weidenfeller, N. Al-hamdany, H.-G. Brokmeier, et W. M. Gan, « Magnetic properties and crystallographic textures of Fe 2.6% Si after 90% cold rolling plus different annealing », *J. Magn. Magn. Mater.*, vol. 354, p. 105–111, mars 2014.
- [4] Z. Gmyrek et A. Cavagnino, « Analytical method for determining the damaged area width in magnetic materials due to punching process », in *IECON 2011-37th Annual Conference on IEEE Industrial Electronics Society*, 2011, p. 1764–1769.
- [5] F. Ossart, E. Hug, O. Hubert, C. Buvat, et R. Billardon, « Effect of punching on electrical steels: Experimental and numerical coupled analysis », *IEEE Trans. Magn.*, vol. 36, n° 5, p. 3137–3140, sept. 2000.

# Frequency dependence and vector magnetic properties of non-oriented electrical steel sheet under arbitrary stress conditions

Yuichiro Kai<sup>1</sup>, Masato Enokizono<sup>2</sup>

<sup>1</sup>Graduate School of Science and Engineering, Kagoshima University, Japan  
E-mail: ykai@eee.kagoshima-u.ac.jp

<sup>2</sup> Vector Magnetic Characteristic Technical Laboratory, Japan  
E-mail: enoki@eee.oita-u.ac.jp

*Keywords:* frequency, stress, vector magnetic property.

Development of electrical motors, which have high efficiency and low loss, are required in the industrial field and electrical car field. In general, induction machine motors are operating at high speed rotation. However, core loss in the core of the induction motor increase due to the increment of the frequency. Therefore, it is important to clarify the factor of the increment of the loss and develop the new technique to decrease the loss.

Previously, we have been reported the residual stress in the motor core and vector magnetic properties in non-oriented electrical steel sheets under stress. From these results, it was clear that not only tensile and compressive stress but also the shear stress in the motor core occur by measuring the residual stress [1]. In addition, we reported measurement results for vector magnetic properties under tensile, compressive, and shear stresses. It was clear that the magnetic field strength and magnetic power loss decrease when tensile, compression, and shear stresses are applied [2]. From these results, we suggested that the motors with high efficiency and low loss can be developed by controlling the vector magnetic properties of a non-oriented electrical steel sheet. In this paper, the effect of frequency on the vector magnetic properties of a non-oriented electrical steel sheet are investigated under stress.

Fig. 1 shows the loci of the  $\mathbf{B}$ ,  $\mathbf{H}$  and  $\mathbf{H}^\sigma$  vectors depending on the stress angle  $\theta_\sigma$  under alternating magnetic flux conditions with  $|\mathbf{B}|_{\max} = 0.1$  T and  $\theta_B = 45^\circ$ . The uniaxial stress condition is  $\sigma = +30$ ,  $-30$  MPa and  $\theta_\sigma = 0^\circ, 45^\circ, 90^\circ, 135^\circ$ . The locus of the  $\mathbf{H}$  means the measured magnetic field strength vector under the non-stress condition. The magnitude and inclination angle of the  $\mathbf{H}^\sigma$  vector varied with the stress angle  $\theta_\sigma$ . When the excitation direction becomes parallel to the applied stress direction, the special phase difference of the  $\mathbf{B}$  and  $\mathbf{H}^\sigma$  vector becomes small. In addition, the area of locus of the  $\mathbf{H}^\sigma$  vector became large because the eddy current increases.

Fig. 2 shows the magnetic power loss  $W_m$  depending on the frequency. The magnetic power loss increase due to the increment of the frequency. In particular, the magnetic power loss at  $\sigma = 30$  MPa and  $\theta_\sigma = 45^\circ$  decrease in comparison with that of the non-stress. When the excitation direction becomes parallel to the applied tensile stress direction, the magnetic power loss decrease. On the other hand, the change of the magnetic power loss at  $\sigma = -30$  MPa and  $\theta_\sigma = 135^\circ$  become small in comparison with that of the non-stress.

From these results, it was clear that not only the magnitude and inclination angle of the locus of the  $\mathbf{H}^\sigma$  vector but also the spatial phase difference changed by applying the stress. In addition it is possible to decrease the magnetic power loss under the high-frequency conditions by applying the

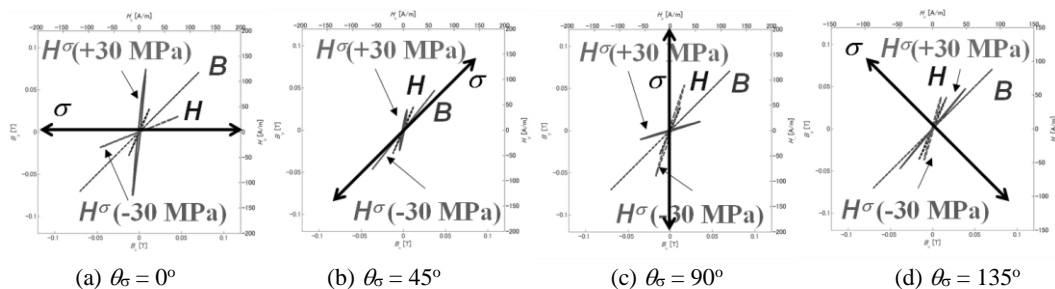


Figure 1: Domain and wall images from a (100)-oriented silicon-iron crystal [2].

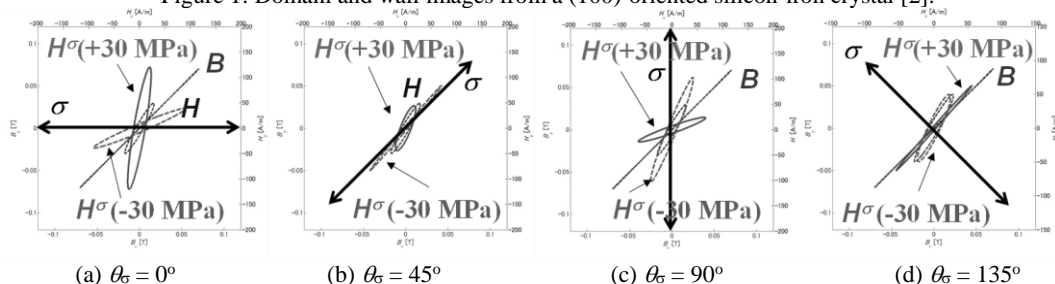


Figure 1: Loci of  $B$  and  $H$  vector by changing the stress angle  $\theta_\sigma$ .

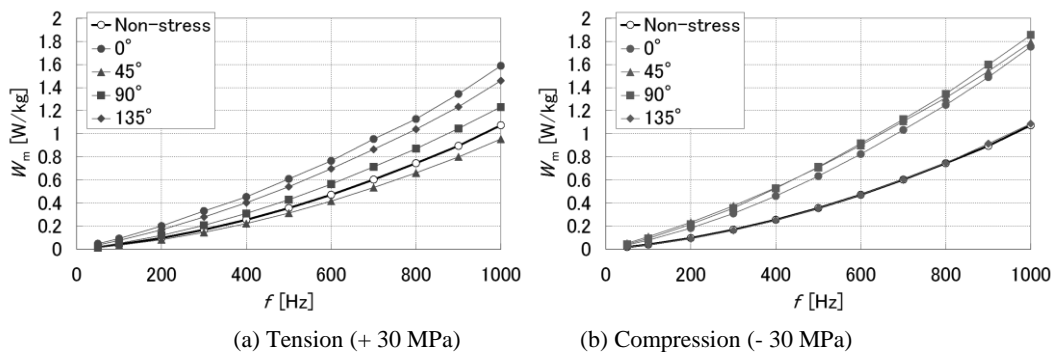


Figure 2: Magnetic power loss depending on frequency.

parallel tensile stress along the excitation direction.

References

[1] Yuichiro Kai, Yuji Tsuchida, Takashi Todaka and Masato Enokizono, "Evaluation of Local Residual Stress Distribution of Stator Core in a Rotating Machine", Electrical Engineering in Japan, Vol. 181, No.3 (2012), 1-8.  
 [2] Yuichiro Kai, Masato Enokizono and Yukihito Kido, "Influence of shear stress on vector magnetic properties on non-oriented electrical steel sheets," International Journal of Applied Electromagnetics and Mechanics, Vol.44, No.3,4 (2014), 371-378.



# **PS2: Poster Session**

Session Chairs

**Fausto FIORILLO**

Inrim National Institute Of Metrological Research - Italy

**Georgi SHILYASHKI**

Tu Wien, Inst. of Electrodynamics, Microwave and Circuit Engineering -  
Austria



# A measuring system for the magnetic properties of amorphous strip under high-frequency PWM excitation

Xiwei Zhang<sup>1</sup>, and Lin Li<sup>1</sup>

<sup>1</sup>State Key Laboratory of Alternate Electrical Power System with Renewable Energy Sources, North China Electric Power University, P. R. China.

E-mail: [m15200892878\\_1@163.com](mailto:m15200892878_1@163.com); [lilin@ncepu.edu.cn](mailto:lilin@ncepu.edu.cn)

**Keywords:** High-frequency, amorphous strip, PWM.

The single-sheet tester is always used to test the silicon steel <sup>[1]</sup>. In order to improve the accuracy, the compensated coil used in [2] is capable of deciding the length of magnetic circuit more precisely. Meanwhile, the H-coil is gradually applied in the magnetic measurement widely for avoiding the influence of air-gap <sup>[3]</sup>. In contrast to traditional silicon steel, the amorphous with better magnetic characteristics become more and more popular. However, the amorphous strip is so thin that the accuracy of the measuring device withstands stricter requirement. Considering that power electronics components, e.g. transformers, inductance, are excited mostly by PWM, it is valuable to accurately measure the magnetic characteristic of the amorphous under PWM excitation. In this paper, we proposed a measurement system for the amorphous strip under high-frequency PWM excitation.

Two closed magnetic circuits are built in the measurement system shown in figure1, which are composed of a double-C amorphous yoke, and the tested 25  $\mu\text{m}$  thick amorphous strip. Closed to the surface of the tested strip, a 1000 turns H-coil is placed so as to measure the magnetic field strength of the strip. The 100 turns exciting coil, which is connected to the excitation module, is wound on the secondary outer layer. The induction coil with 300 turns is wounded on the outermost layer to offer the induction voltage. The frequency of the excitation is controlled by Digital Signal Processor (DSP). In this work, DC-source is used to supply power to the half-bridge module that provides the alternative voltage for the exciting coil. By regulating the output of DC-source, we can obtain different voltages of the induction coil that actually reflect the magnetic flux density of the tested sample based on the Faraday's induction's Law. In addition, two ways are used to acquire the magnetic field strength, the magnetic circuit method and the H-coil method. Through two methods mentioned above, the influence of air-gap on magnetic field strength could be detected <sup>[4]-[5]</sup>.

The hysteresis loops under different frequencies and magnetic flux densities are shown in figure2. By comparing the thickness of the sample with the skin depth under different frequencies, weather the inhomogeneous distribution of magnetic density should be considered or not can be decided. Based on the loss separation method, the static hysteresis loss, dynamic loss, and excess loss are calculated respectively, and the sum of these three kinds of losses are compared with experimental results. The calculated and measured results will be compared in the full paper, and the results verify the validity of the measurement system.

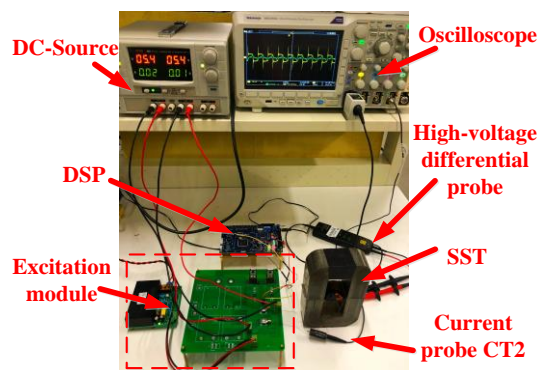


Figure1: The diagram of measurement system

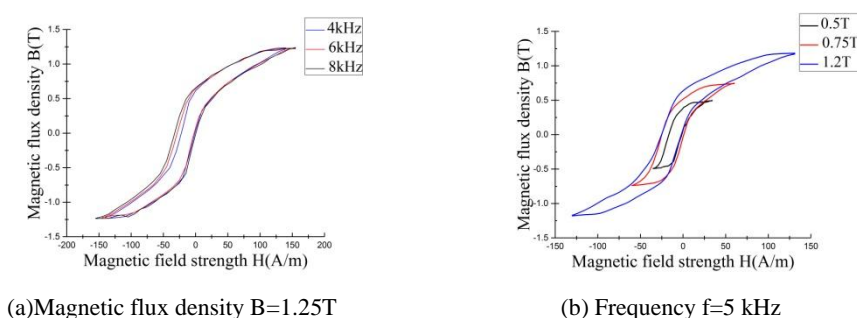
(a) Magnetic flux density  $B=1.25\text{T}$ (b) Frequency  $f=5\text{ kHz}$ 

Figure2: The hysteresis loops under different conditions

### Acknowledgements

This work was supported by the National Key R&D Program of China under Grant 2017YFB0903902 and National Natural Science Foundation of China under Grant 51677064.

### References

- [1] Antonio S Q, Pompei M. Dynamic hysteresis modelling of soft magnetic materials for automotive applications[C]// IEEE, International Forum on Research and Technologies for Society and Industry. IEEE, 2017:1-6.
  - [2] Barri ère O D L, Ragusa C, Khan M, et al. A Simple Compensation Method for the Accurate Measurement of Magnetic Losses With a Single Strip Tester[J]. *IEEE Transactions on Magnetics*, 2016, 52(5):1-4.
  - [3] Nakata T, Ishihara Y, Nakaji M, et al. Comparison between the H-coil method and the magnetizing current method for the single sheet tester[J]. *Journal of Magnetism & Magnetic Materials*, 2000, s 215–216(1):607-610.
  - [4] Gmyrek Z, Cavagnino A. Modified single sheet tester system for engineering measurements[C]// Xxii International Conference on Electrical Machines. IEEE, 2016.
  - [5] Gmyrek Z. Single Sheet Tester With Variable Dimensions[J]. *IEEE Transactions on Instrumentation & Measurement*, 2016, 65(7):1661-1668.
- Nakata T, Ishihara Y, Nakaji M, et al. Comparison between the H-coil method and the magnetizing current method for the single sheet tester[J]. *Journal of Magnetism & Magnetic Materials*, 2000, s 215–216(1):607-610.

# A Multiphysics-dependent Hysteresis Model with Experiment Validation

Weijie Xu<sup>1</sup>, Nana Duan<sup>2</sup>, Yongjian Li<sup>3</sup>, Shuhong Wang<sup>2</sup>, Jianguo Zhu<sup>4</sup>

<sup>1</sup> State Grid Shaanxi Electric Power Company Economic Research Institute, China  
E-mail: xuweijie@outlook.com

<sup>2</sup> School of Electrical Engineering, Xi'an Jiaotong University, Xi'an 710049, China  
E-mail: duannana@xjtu.edu.cn; shwang@xjtu.edu.cn

<sup>3</sup> Hebei University of Technology, Tianjin, 300130, China  
E-mail: liyongjian@hebut.edu.cn

<sup>4</sup> University of Technology Sydney, Sydney, NSW 2007, Australia  
E-mail: Jianguo.Zhu@uts.edu.au

**Keywords:** Hysteresis model, experiment validation, elemental operator.

The design and performance analysis of the electrical equipment usually involve the coupling of electrical, magnetic, thermal, mechanical and other physical fields. With the development of numerical calculation technology of electromagnetic field and the improvement of computer performance, the electromagnetic field numerical simulation software has been widely used to analyze the coupling problem of electromagnetic field, thermal field and mechanical field. The magnetic properties of magnetic material under work conditions will be influenced by some non-magnetic factors, such as temperature and stress. However, these characteristics are difficult to be simulated by the traditional hysteresis models [1].

In this paper, based on the microscopic magnetization mechanisms of magnetic materials, a hysteresis elemental operator, which contains two easy axes and two hard axes, as shown in Figure 1(a), has been presented [2]. Besides, with the help of the energy minimum principle, as illustrated in Figure 1(b), the octagonal law which can determine the orientation of the magnetization has been introduced.

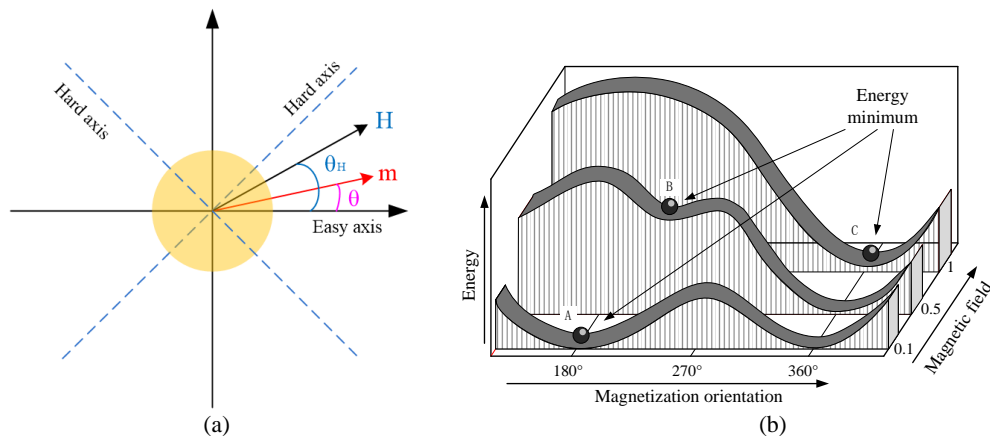


Figure 1: (a) Elemental operator under the magnetic field, and (b) the stable orientation of the magnetization and the corresponding energy minimum of the elemental operator.

By taking into account the differences between the laboratory conditions and the practical engineering manufacturing and operation, the temperature-depended saturation magnetization, temperature-depended anisotropy, and stress-depended distribution function are introduced to the hysteresis elemental operator [3].

$$K(T) = K(T_0)[1 + \alpha_K(T - T_0)] \quad (1)$$

$$P(h_i, h_k) = N \frac{1}{2\pi\sigma_i\sigma_k} \exp\left(-\frac{h_i^2}{2\sigma_i^2} - \frac{(K - \mu_k)^2}{2\sigma_k^2}\right) \quad (2)$$

With the employment of the Gaussian-Gaussian distribution function and the interaction field, a temperature and stress dependent hysteresis model is proposed to simulate the magnetic properties under different temperature and stress conditions.

$$M(H, T, \sigma) = \iiint m(H, T, \theta) P(h_i(\sigma), h_k(\sigma)) \cos \theta dh_i dh_k d\theta \quad (3)$$

Finally, by comparing the simulation results with the experimental measurement results, as shown in Figure 2, the effectiveness and viability of this proposed hysteresis model have been confirmed.

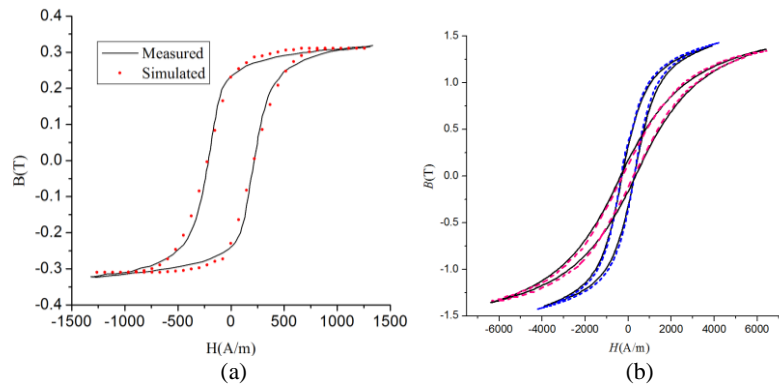


Figure 2: Comparisons of measured and simulated results of (a) the Siemens 4C65 under 90°C and (b) the SOMALOY™ 500 under 800Mpa.

#### Acknowledgements

The research leading to these results has received funding from the National Natural Science Foundation of China under Grant 51707142 and in part by the China Postdoctoral Science Foundation under Grant 2016M602818.

#### References

- [1] E Cardelli, "A general hysteresis operator for the modeling of vector fields", *IEEE Trans. Magn.*, 47(2011), 2056-2067.
- [2] C. Appino, "Representation of memory in particle assembly hysteresis models", *IEEE Trans. Magn.*, 45(2009), 5184-5187.
- [3] P. Andrei, et al. "Temperature, stress, and rate dependent numerical implementation of magnetization processes in phenomenological models", *J. Optoelectron. Adv. Mater.*, 9(2007), 1137-1139.

# Advanced iron-loss estimation for arbitrary magnetization loci in non-oriented electrical steel considering anisotropic effects

Benedikt Schauerte, Andreas Thul, Simon Steentjes, Kay Hameyer  
Institute of electrical machines (IEM), RWTH Aachen University, D-52062 Aachen, Germany

E-mail: [benedikt.schauerte@iem.rwth-aachen.de](mailto:benedikt.schauerte@iem.rwth-aachen.de)

*Keywords:* rotational magnetization, iron-loss estimation, magnetic anisotropy.

The design of electrical machines requires accurate models for the estimation of locally occurring iron losses. The Bertotti formulation is the most common approach for the calculation of the resulting iron-losses with respect to the magnetization frequency  $f$  and peak value of the flux density  $\hat{B}$  [1]. This approach yields results with good accuracy in the range 50 Hz and 1.3 T magnetization. Due to increasing frequency for the operation of high speed electrical machines, Bertottis' approach was adjusted continuously to assure acceptable accuracy over the entire range of magnetizing frequency and magnetization. One of these models is the IEM 5-parameter formula proposed in [2]. If rotational magnetizations are applied, the measured iron-losses differ significantly from the losses that can be calculated by the aforementioned unidirectional approaches. These approaches only consider the resulting iron losses for unidirectional magnetizations and have to be adjusted to allow the consideration of rotational spatial pathways on the resulting iron-losses. The spatial field-curves of rotational magnetizations are defined by the peak value  $\hat{B}_{abs}$ , axis ratio  $f_{Ax}$  and the displacement angle of the ellipses main-axis  $\theta$  as depicted in Fig. 1.

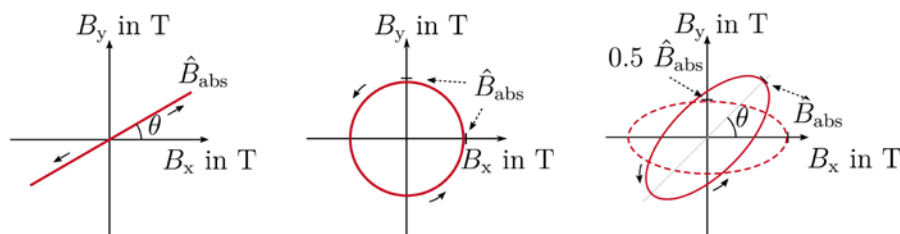


Figure 1: Representation of different magnetic flux-loci that can be applied to the specimen by the utilized measurement system.

The occurring iron losses at different applied flux loci are obtained by measurements performed on a rotational single sheet tester (RSST) introduced in [3], and reveal clear deviations from the typical unidirectional measured behavior. Particularly the decline of losses at high saturations as depicted in Fig.2 and the increased losses at lower magnetizations can not be recreated by the unidirectional descriptions. This specific loss behavior at rotational magnetization is caused by the changed domain wall motions for rotating magnetizations, and depends in its influence on the global loss behavior on the axis ratio of the respective magnetization and the actual displacement angle of the ellipse  $\theta$ .

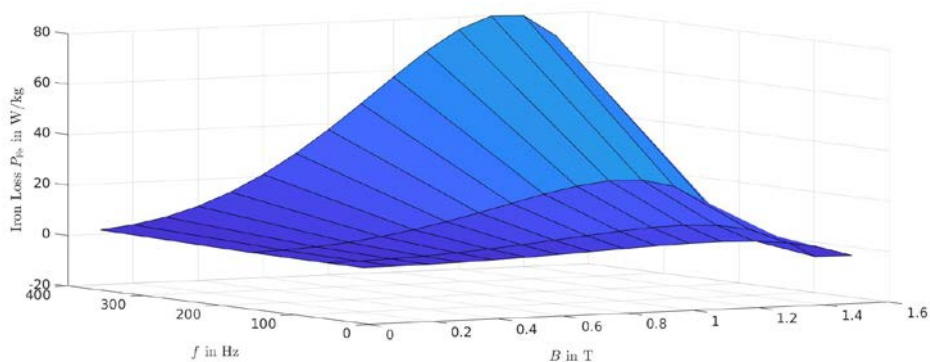


Figure 2: Measured rotational iron losses with  $f_{Ax} = 1$ .

Measurements at different displacement angles  $\theta$  and different axis ratios of the magnetizations and thus the magnetic anisotropy and its influence on the measured resulting iron losses are examined, as the transition from uniaxial to rotational loss-behavior.

The prediction of the iron losses under the consideration of these influences will be performed by the adjustment of the iron loss prediction formula for rotational magnetization as described in [4]:

$$P_{Fe} = k_{hyst} \left( 1 + f_{Ax} (r_{hyst} - 1) \right) \hat{B}^\alpha f + k_{cl} \hat{B}^2 f^2 + k_{cl} (r_{exc} - 1) \hat{B}^{1.5} f^{1.5} \quad (2)$$

This mathematical formulation of the loss-model will be examined in its suitability to recreate the measured behavior with respect to the different axis ratios of the rotating magnetizations and their respective displacement angle  $\theta$ . Further adjustments on the model and its parameters will be performed, in order to achieve better accordance with the measurements and an increased scope of loss-prediction considering the magnetic anisotropy.

#### *Acknowledgements*

The work of the authors is performed in the research project group project "SP-2013 – The utilization of residual stresses induced by metal forming" funded by the Deutsche Forschungsgesellschaft (DFG) HA 4395/22-1 as DFG 255713208 and carried out in the research group project FOR 1897 Low-Loss Electrical Steel for Energy-Efficient Electrical Drives.

#### *References*

- [1] Bertotti, G. (1998), "Hysteresis in magnetism: for physicists, materials scientists, and engineers", Academic press.
- [2] Eggers, D., Steentjes, S., and Hameyer, K. (2012), "Advanced iron-loss estimation for nonlinear material behavior", IEEE Transactions on Magnetics, 48(11), 3021-3024.
- [3] Thul, A., Steentjes, S., Schauerte, B., Klimczyk, P., Denke, P., & Hameyer, K. (2018). "Rotating magnetizations in electrical machines: Measurements and modeling", AIP Advances, 8(5), 056815.
- [4] Steentjes, S., Leßmann, M., & Hameyer, K. (2012), "Advanced iron-loss calculation as a basis for efficiency improvement of electrical machines in automotive application." In Electrical Systems for Aircraft, Railway and Ship Propulsion (ESARS), 2012 (pp. 1-6). IEEE.

# Application of orientation distribution functions' theory in the case of grain-oriented steels cut through non-conventional technologies

Veronica Manescu (Paltanea)<sup>1</sup>, Gheorghe Paltanea<sup>1</sup>, Horia Gavrilă<sup>1</sup>,  
Iosif Vasile Nemoianu<sup>1</sup>, Paul Cristian Andrei<sup>1</sup>, Radu Ciuceanu<sup>1</sup>

<sup>1</sup>University Politehnica of Bucharest, Romania

E-mail: paltanea03@yahoo.com; gheorghe.paltanea@upb.ro

**Keywords:** grain-oriented electrical steel, orientation distribution function, magnetic properties, water-jet cutting, electro-erosion cutting.

Today, electrical devices that have a magnetic core are analyzed and classified, by considering their energy efficiency, which depends on the grain-oriented alloy quality and cutting technology. Due to the metallurgical process, to develop the Goss texture, the magnetocrystalline anisotropy is induced and it appears in all types of electrical steels. The Goss texture in grain-oriented electrical steels determines, that an increased number of grains have their [001] easy magnetization axis oriented parallel to the rolling direction (RD). The hard magnetization axis is placed perpendicular to the RD, in the case of low magnetic fields and it switches to 55° for the medium and high values of the magnetic field strength [1].

The magnetic cores of the electrical transformers are cut as sheets, through mechanical punching technology, which induces usually mechanical stresses and generates a plastic deformation of the cut edge in the form of a burr [2]. Thus the cutting non-conventional methods are preferred by the transformer manufacturers in the prototyping production and they lead to lower energy losses than those in the case of punching. In the paper, grain-oriented MOH samples, cut through water-jet and travelling wire electro-erosion, are characterized, using a standardized unidirectional Single Strip Tester. The samples, with an area of 280 mm × 30 mm, were cut at different angles, from 0° to 90° with a step of 15°. The water-jetting technology is based on high-pressure water flow that is usually combined with air injected abrasive particles. The cut is made through erosion, micro-machining effects or dislocating flanks from the material. It results a high quality of the cut edge on the upper side and burs on the lower side. The cutting speed could be adjusted, although the process is slow. In the case of travelling wire electrical discharge machining (WEDM) it is involved a vertical moving electrode, made of different electrically conductive materials with increased hardness, having a diameter of maximum 0.3 mm. The wire is tensioned, using a mechanical tensioning device and the possibility of cutting errors is reduced in that way. The steel is eroded, due the wire movements, and because there is no contact between the sample and the travelling wire (TW) the induced mechanical stresses are minimized.

Seven angle-oriented samples were magnetically characterized at the industrial frequency of 50 Hz. The normal magnetization curves and the energy losses were determined at imposed values of the magnetic field strength  $H$  ranging from 50 A/m to 10000 A/m, in the case of each angle  $\varphi$  and both cutting technologies. It is well known that grain-oriented silicon iron steels have orthorhombic symmetry of body centered cubic crystals and the Goss texture (110)[001] samples could be analyzed with the orientation distribution functions' (ODF) theory. In [3, 4] it is put in evidence that any magnetic properties  $A$  could be described with a series of ODF parameters as:

$A = A_0 + \sum_{i=1}^{n-1} A_i \cos(2i\theta)$ , where  $n$  can be associated with the number of characterized samples. The coefficients  $A_0$  and  $A_i$  are determined from the experimental data, which are the normal magnetization curves  $J(H)$  or energy loss variations  $W(H)$ , measured for the samples cut between  $0^\circ$  and  $90^\circ$  with a given step. From previous studies [3]-[6] it is observed that, if the first three coefficients, experimentally determined from data obtained for  $\theta$  of  $0^\circ$ ,  $45^\circ$  and  $90^\circ$ , are used, the low magnetic field strength region, below 100 A/m, cannot be correctly investigated and modelled.

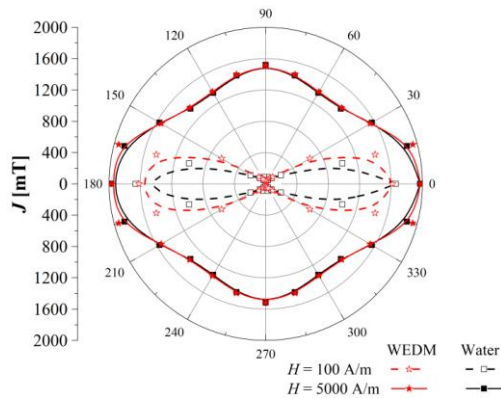


Figure 1: Polar diagrams  $J(\phi)$  at two values of the magnetic field strength for both methods.

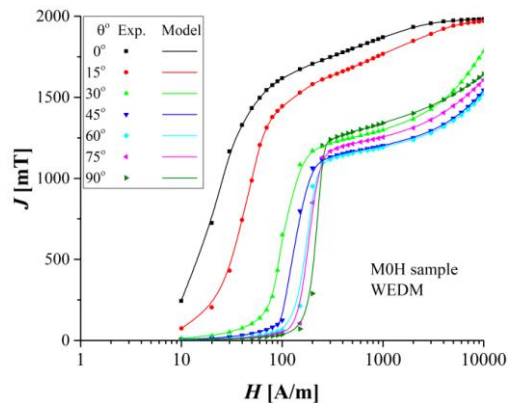


Figure 2: Computed and experimental normal magnetization curves in case of WEDM.

### Acknowledgements

The work of V. Manescu (Paltanea), G. Paltanea and P.C. Andrei has been funded by U.P.B., through "Excellence Research Grants" Program, UPB-GEX 2017. Identifier: UPB-GEX2017, Ctr. No. 04/25.09.2017 (OPTIM-IE4), Ctr. No. 02/25.09.2017 (ANIZ-GO) and Ctr. No. 06/25.09.2017 (STATIC-BH). The work of H. Gavrilă has been funded by a grant of CNCS/CCCDI – UEFISCDI, Project Number 10PTE/2016, within PNCDDI III "Brushless servo-motors series utilizing soft magnetic composite materials".

### References

- [1] M. Soinski, "The anisotropy of coercive force in cold-rolled Goss texture electrical sheets", *IEEE Trans. Magn.*, **23** (1987), 3878- 3881.
- [2] Th. Waeckerle, L-L. Rouve, C. Talowski, "A study of anisotropic B-H models for transformer cores", *IEEE Trans. Magn.*, **31** (1995), 6, 3991-3993.
- [3] H.-J. Bunge, "Texture analysis in materials science – mathematical methods", ed. London, Butterworths (1982).
- [4] H. J. Bunge, "Advances and applications of quantitative texture analysis", ed. Clausthal, FRG (1989), Oberursel, 3-18.
- [5] M. F. de Campos, "Anisotropy of steel sheets and consequence for Epstein test: I theory," *Proc. 28<sup>th</sup> IMEKO World Congr.* (2006), 1–6.
- [6] H. Pfützner, E. Mulasalihovic, H. Yamaguchi, D. Sabic, G. Shilyashki, F. Hofbauer, "Rotational magnetization in transformer cores—A review", *IEEE Trans. Magn.*, **47** (2011), 4523–4533.

# Assessment of Static B-H Relationship for Soft Magnetic Alloys Using a Novel Equipment

Veronica Manescu (Paltanea)<sup>1</sup>, Gheorghe Paltanea<sup>1</sup>, Paul Cristian Andrei<sup>1</sup>, Florea Ioan Hantila<sup>1</sup>, Catalin Ionut Grumeza<sup>1</sup>, Victor Bucata<sup>1</sup>

<sup>1</sup>Department of Electrical Engineering, University Politehnica of Bucharest, Romania  
E-mail: veronica.paltanea@upb.ro; gheorghe.paltanea@upb.ro; paul.andrei@upb.ro; hantila@elth.pub.ro; catalin\_ionut\_82@yahoo.com; victor.bucata@upb.ro

**Keywords:** B-H relationship, Green function method, Inverse magnetic field problem

The classical standard devices used to determine the  $B$ - $H$  relationship are Epstein, Single Sheet Tester (SST) and hysteresis graph set-ups that are based on AC magnetizing current method [1], presenting the following disadvantages: specific sample shape, uniform magnetic field, time variable excitation current leading to eddy currents presence. These facts are not found in the case of DC measurements.

In this paper, a novel laboratory device set-up and a measuring procedure are used, in order to determine the  $B$ - $H$  relationship in magneto-static conditions. The proposed device (Fig. 1) consists of an "8" shaped magnetic circuit, in which the columns and the horizontal yokes are made from an isotropic material with negligible remanence (1). The currents feeding the two DC coils (5, 6) can be adjusted in such a way that the magnetic flux  $\varphi_0$  in the median yoke (2) may be cancelled. The air-gap (3) on the upper yoke contributes to the procedure stability. On the lower yoke the analyzed sample (4) can be inserted. The method to determine the static  $B$ - $H$  relationship is as follows: a given DC current value  $i_1$  is supplied through the coil (6) and the current  $i_2$  in the coil (5) is searched until the flux  $\varphi_0$  is null. This operation is repeated, by increasing the value of  $i_1$ . Finally, a set of currents ( $i_1, i_2$ ) are obtained and are used as input data in an inverse magnetic field problem.

Using the polarization fixed point method (PFPM) [2], the nonlinear relationship  $\mathbf{H} = \mathbf{F}(\mathbf{B})$  is replaced by:

$$\mathbf{B} = \mu\mathbf{H} + \mathbf{I} \quad (1)$$

and the magnetic polarization  $\mathbf{I}$  has a nonlinear dependence:

$$\mathbf{I} = \mathbf{B} - \mu\mathbf{F}(\mathbf{B}) \equiv \mathbf{G}(\mathbf{B}). \quad (2)$$

For each  $m$  iteration, the magnetic field is computed, through the following relations:

$$\nabla \times \mathbf{H}^{(m)} = \mathbf{J}; \nabla \cdot \mathbf{B}^{(m)} = 0; \mathbf{B}^{(m)} = \mu\mathbf{H}^{(m)} + \mathbf{I}^{(m-1)}, \quad (3)$$

where  $\mathbf{J}$  is the value of the current density and  $\mathbf{I}^{(0)}$  is arbitrary chosen. The Green function method (GFM) [3] is applied, to solve (3), if the magnetic permeability is considered equal to  $\mu_0$ .

After the measuring procedure, a set of currents ( $i_1^{(n)}, i_2^{(n)}$ ) is obtained. The searched  $I$ - $B$  (then  $H$ - $B$ ) relationship is considered to be a linear piecewise dependence and the slope  $v^{(n)}$  of each segment  $n$  is computed, considering that the magnetic flux  $\varphi_0$  through the median yoke is null. The following equation must be solved:

$$\varphi_0 = \Phi\left(v^{(n+1)}; i_1^{(n+1)}, i_2^{(n+1)}, B^{(n)}\right) = 0, \quad (4)$$

with respect to  $v^{(n+1)}$ , considering that  $i_1^{(n+1)}, i_2^{(n+1)}, B^{(n)}$  are input parameters.

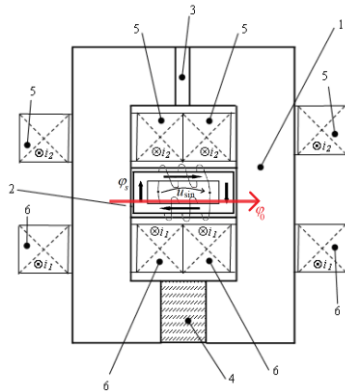


Figure 1: Measuring set-up description: 1 - magnetic circuit; 2 - median yoke; 3 - auxiliary air-gap; 4 - sample; 5, 6 - DC coils.

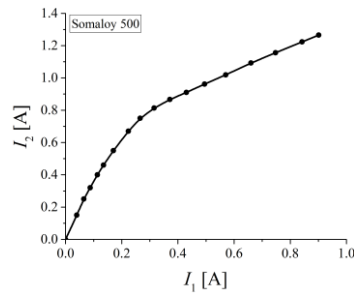


Figure 2: Dependence of currents  $I_2(I_1)$  measured with the proposed device for Somaloy 500 cubic sample.

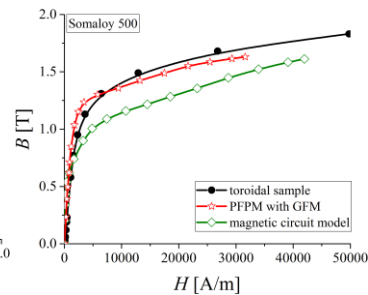


Figure 3:  $B-H$  relationship obtained for toroidal and cubic samples

In Fig. 2 are presented the  $(i_1, i_2)$  pairs of currents, in the case of a soft magnetic composite (Somaloy 500), measured with the developed device. Fig. 3 shows three  $B-H$  relationships: one is obtained after solving the inverse magnetic field problem (red line), another one is obtained on a toroidal sample using a hysteresisgraph wattmeter (black line) and the third one is obtained adopting an equivalent magnetic circuit model of the device, which admits uniform magnetic field distribution (green line). The magnetization curve obtained with the proposed set-up and by solving the inverse magnetic field problem is in a good approximation with the one obtained on the toroidal sample, considered as reference.

#### Acknowledgements

The work of V. Manescu (Paltanea), G. Paltanea, P. Andrei and V. Bucata has been funded by University Politehnica of Bucharest, through “Excellence Research Grants” Program. Identifier: UPB-GEX2017, Ctr. No. 04/25.09.2017 (OPTIM-IE4), Ctr. No. 02/25.09.2017 (ANIZ-GO), Ctr. No. 06/25.09.2017 (STATIC-BH). The work of C. Grumeza and F. Hantila was supported by a grant of the CNCS/CCCDI – UEFISCDI, Project Number 10PTE/2016, within PNCDI III “Brushless servo-motors series utilizing soft magnetic composite materials”.

#### References

- [1] C. Appino, E. Ferrara, F. Fiorillo, L. Rocchino, C. Ragusa, J. Sievert, et. al., “International comparison on SST and Epstein measurements in grain-oriented Fe-Si sheet steel,” *Int. J. Appl. Electrom.*, vol. 48, pp. 123-133, 2015.
- [2] F. Hantila, G. Preda, M. Vasiliu, “Polarization method for static fields,” *IEEE Trans. Magn.*, vol. 36, 4, pp. 672-675, 2000.
- [3] F. Hantila, G. Grama, “An overrelaxation method for the computation of the fixed point of a contractive mapping,” *Rev. Roum. Sci. Techn. – Electrotechn. Et. Energ.*, vol. 27, 4, pp. 395-398, 1982.

# Development of Measurement Method for Magnetostriction of Electrical Steel Sheets Using an Open-type Single Sheet Tester.

Ryo Matsubara, Yasuhito Takahashi, and Koji Fujiwara

*Doshisha University, Kyoto, Japan*

*E-mail: {ctwb0328@mail4; ytakahashi@mail; koji.fujiwara@mail}.doshisha.ac.jp*

**Keywords:** Magnetostriction, electrical steel sheets, laser Doppler vibrometer, single sheet tester.

The magnetostriction of electrical steel sheets is a main cause of acoustic noise of electrical machines. In order to measure the magnetostriction, a single sheet tester (SST) with a strain gauge has been used [1]. A strain gauge should be directly pasted on a specimen and it leads to low reproducibility of measured magnetostriction. A SST with yokes (closed magnetic path) is widely used for the magnetostriction measurement [2]. However, the influence of electromagnetic force between the yoke and specimen could become a problem when using the closed-type SST. The purpose of this study is to develop the measurement method for magnetostriction by means of an open-type SST and a laser Doppler vibrometer (LDV) as a non-contact and highly accurate method [2].

Fig. 1 shows the dimensions of the coil unit of SST and the schematic diagram of a test apparatus. Two LDVs individually measure the velocities of two reflecting mirrors placed at different positions (distance between them: 100 mm) on the surface of the specimen simultaneously. The magnetostriction is calculated as the difference of displacements obtained by numerical integration of the velocities. This measurement method does not require clamping of the specimen. The magnetostriction is evaluated by its amplitude  $\lambda_{p-p}$  along the direction of applied AC magnetic field. Rectangular specimens of M90-23P5 (GO) and M250-50A5 (NO) are measured, in which the rolling direction is parallel to a longitudinal direction of the specimen. The dimensions of the specimens are 60 mm  $\times$  360 mm. The flux density is detected by a B-coil, and its amplitude  $B_m$  is controlled from 0.5 T to 1.7 T at intervals of 0.1 T under the sinusoidal flux condition. Exciting frequency is 50 Hz. Fig. 2 shows the effect of the average number of times on the amplitude of magnetostriction  $\lambda_{noise}$  corresponding to the environmental noise. The more the average number of times increases, the more  $\lambda_{noise}$  decreases. The average number of times is set to be 500 from the standpoint of measurement time.  $\lambda_{noise}$  is  $9.74 \times 10^{-9}$ .

Fig. 3 shows the butterfly loops of GO and NO. In order to examine the influence of each harmonic component on  $\lambda_{p-p}$ , the harmonic components of the measured magnetostriction waveforms were calculated by using FFT. Fig. 4 shows the relative standard deviation of  $\lambda_{p-p}$  of amplitude  $\lambda_n$  of the each harmonic component. The odd harmonic components tend to have a larger relative standard deviation than the even harmonic components. Fig. 5 shows the ratio of  $\lambda_n$  with respect to  $\lambda_{p-p}$ . Their values are less than  $0.05 \times 10^{-2}$  on the 11th and higher harmonic components.

The proposed method for measuring the magnetostriction of electrical steel sheets can be applied to the measurement of relatively small magnetostriction. The magnetostriction waveform does not have the odd harmonic components theoretically, and the reproducibility of those

components is low. Therefore, the odd harmonic components should be eliminated as noise. The influence of the 11th and higher harmonic components of the magnetostriction waveform on  $\lambda_{p-p}$  is negligibly small.

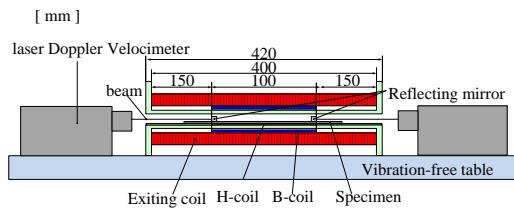


Fig. 1. Dimensions of the coil unit of the SST and schematic diagram of a test apparatus.

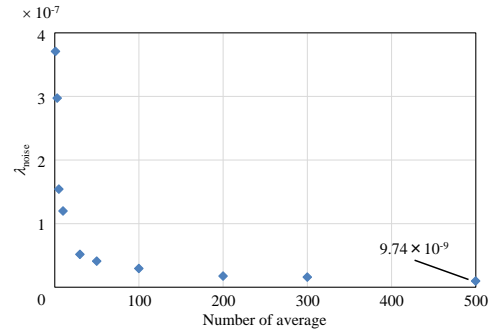


Fig. 2. Effect of the number of averages.

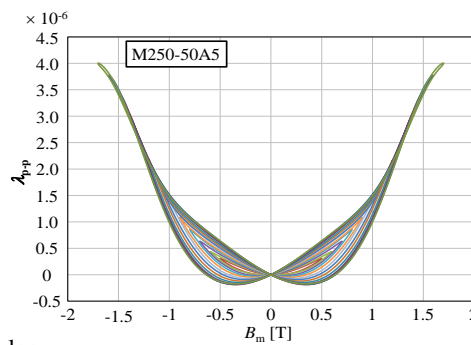
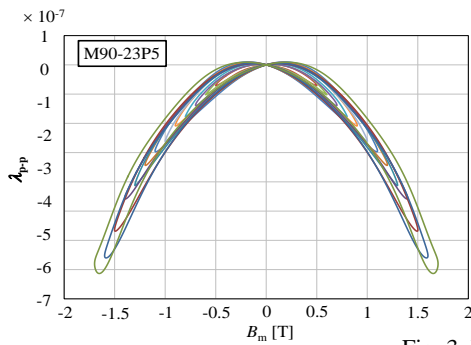


Fig. 3. Butterfly loop.

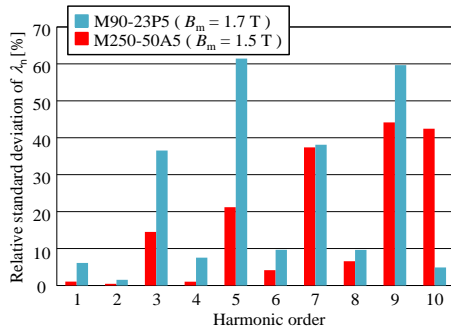


Fig. 4. Relative standard deviation of the  $\lambda_{p-p}$  of the each harmonic order amplitude  $\lambda_n$ .

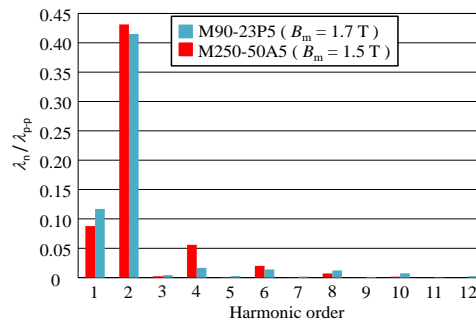


Fig. 5. Ratio of  $\lambda_n$  with respect to  $\lambda_{p-p}$ .

### References

- [1] IEC, "Electrical steel – Methods of Measurement of the Magnetostriction Characteristics by Means of Single Sheet and Epstein Test Specimens," TR 62581 (2010).
- [2] T. Nakase, M. Nakano, K. Fujiwara, and N. Takahashi, "Measuring System for Magnetostriction of Silicon Steel Sheet under AC Excitation Using Optical Methods," *IEEE Trans. Magn.*, vol. 34, no. 4, pp. 2072-2074 (1998).

# Eddy-Current Loss Measurement of Permanent Magnetic Material at different frequency

Yongjian Li<sup>1</sup>, Baolin Jiang<sup>1</sup>, Changgeng Zhang<sup>1</sup>, Yang Liu<sup>2</sup>, Xuehai Gong<sup>2</sup>

<sup>1</sup>State Key Lab. of Reliability and Intelligence of Electric Equipment, Hebei University of Technology, Tianjin, CHINA

E-mail: [liyongjiang@hebut.edu.cn](mailto:liyongjiang@hebut.edu.cn)

<sup>2</sup>Global Energy Interconnection Research Institute, China

**Keywords**—Permanent Magnet, hysteresis loop, eddy current

## I INTRODUCTION

Permanent magnetic materials have been widely used in rotating electrical machines. The eddy current loss induced by the fundamental air-gap field is usually neglected, since it rotates in synchronism with the rotor [1]. To improve torque density and decrease torque ripple, novel PM machines are emerging in which stator coils are wound around consecutive or alternate teeth with a fraction number of tooth per pole [2]. However, the large number of harmonics caused by slot ripple, inverter [3] will lead to significant eddy current loss in the magnets, which makes the temperature increase and may cause the thermal demagnetization [4]. As a result, it is necessary and important to study the eddy current loss in the permanent magnets. Many analytical models were developed to predict induced eddy current loss, but few has been verified by experiments until now.

In this paper, the eddy current loss of NeFeB sintered magnetic material is measured by using a newly developed closed-circuit testing equipment, meanwhile the same size simulation model is established by Ansoft to compare with the experimental results. The behavior of the eddy current loss is investigated at different frequency.

## II Measurement System Setup

### (A) The Excitation Structure

Fig.1 shows the novel dynamic hysteresis loop tester of permanent magnet material with the frequency up to 1 kHz. The alternating flux density inside the magnet material is up to 0.2 T, which is large enough for the rotor of various AC machines.

The closed-loop magnetic circuit is composed of the double C-shaped core, flexible excitation windings and the permanent sample. The excitation C-shaped cores are made of ultra-thin 0.1mm silicon steel, which can work up to 5 kHz. The permanent samples are made into the cylinder-shaped, which is located in the air-gap between the double C-shaped cores. And the air-gap between the magnetic poles can be adjusted according to the length of the sample, for the C-shapes is placed on the slide rail.

The four multi-layer excitation windings are separately wound on the C-shaped cores. And the windings are twisted by 12-turns Litz wire, which can work up to 10 kHz. The power amplifier for the excitation windings is PA500 made by Brockhause Company with the frequency from DC to 20 kHz.

### (B) The Sensing Structure

The magnetic flux density sensing coil is directly wounded on the sample, in which number of turns is 6 and area size is the same as the cross-section of the sample.

As shown in the Fig.2, there are two samples between one air-gap. The area between the two samples is close enough so that it creates a relatively uniform magnetic field strength area which is measured by the Hall-probe of Bell Gaussmeter 8030. In the full paper, the electro-magnetism finite element analysis illustrates the distribution of magnetic field strength and flux density and validates the rationality of our magnetic circuit structure.

## III Measurement Results and Discussion

In the measurement system, the eddy current loss and its dynamic hysteresis loop of the permanent magnets can be directly measured.

### (A) Measurement of static magnetic properties

The four permanent magnetic material samples and the magnetic yokes compose a closed circuit. Based on the static hysteresis loop of permanent magnet, the static working point can be measured and calculated.

### (B) Measurement of dynamic magnetic hysteresis loop

Under the alternating current by the flexible excitation winding, the magnetic field inside the permanent magnet is alternatively changing at the static working point of static demagnetization curve. Fig.3 shows the dynamic hysteresis loop of the permanent magnet at 50 Hz. The area of hysteresis loop is the sum of the hysteresis loss and the eddy current loss

according to the Poynting vector theorem. A series of  $\sigma$ -loss characteristics of permanent magnetic material will present in the full paper.

#### IV Conclusion

In this paper, a novel dynamic hysteresis loop and eddy current loss tester of permanent magnetic material was designed. For the NdFeB material, neglecting the hysteresis loss, the area of hysteresis loop represents eddy current loss. The measurement results provide the basis for the eddy-current modeling of permanent magnetic materials at different frequency.

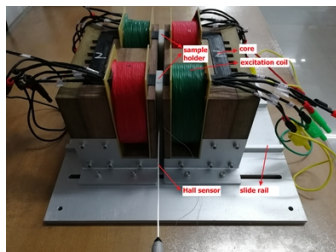


Fig.1 The setup of measurement system.

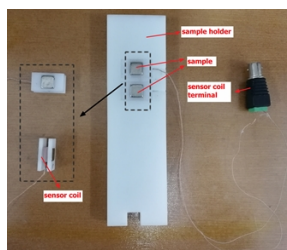


Fig.2 The structure of NdFeB sample of NdFeB sample and the  $B$  sensing coils.

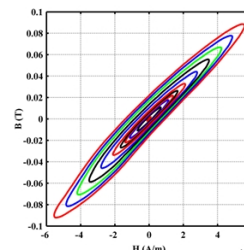


Fig.3 Dynamic hysteresis loops of permanent magnet under the biased static magnetic field.

#### Acknowledgment

This work was supported in part by the National Natural Science Foundation of China, (No. 51777055), the National Key R & D Program of China (2017YFB0903904), and the National Key Basic Research Program of China (973 Project) under Grant 2015CB251000.

#### References

- [1] K. Atallah, D. Howe, P. H. Mellor, D. A. Stone, "Rotor loss in permanent magnet brushless ac machines", *IEEE Trans Industry Application*, vol.36, no.6, pp.1612-1618, 2000.
- [2] J. Wang, K. Atallah, R. Chin, W. M. Arshad, H. Lendenmann, "Rotor eddy-current loss in permanent magnet brushless ac machines", *IEEE Trans Industry Application*, vol.46, no.7, pp.2701-2707, 2010.
- [3] K. Itoh, Y. Hashiba, K. Sakai, and T. Yagisawa, "The A.C. losses of the rare-earth permanent magnets", *Trans. IEE Jpn.*, vol. 118-A, no. 2, pp.182-187, 1998.
- [4] A. Fukuma, S. Kanazawa, D. Miyagi, and N. Takahashi, "Investigation of AC loss of permanent magnet of SPM motor considering hysteresis and eddy-current losses", *IEEE Transactions on Magnetics*, vol. 41, no. 5, pp. 1964-1967, May 2005.

# Galvanically separated voltage sensor used in industrial magnetic core measurements

Roman Rygał<sup>1</sup>, Wojciech Pluta<sup>2</sup>, Stanisław Żurek<sup>1</sup>, Jacek Leszczyński<sup>3</sup>,  
Marian Soiński<sup>1</sup>, Jan Walak<sup>1</sup>, Jakub Rygał<sup>1</sup>

<sup>1</sup>*Magneto Sp. z o.o., ul. Odlewników 43, 42-202 Częstochowa, Poland*  
*E-mail: roman.rygal@magneto.pl*

<sup>2</sup>*Czestochowa University of Technology, Faculty of Electrical Engineering, Al. Armii  
Krajowej 17, 42-200 Częstochowa, Poland, e-mail: w.pluta@gmail.com*

<sup>3</sup>*AGH University of Science and Technology, Faculty of Energy and Fuels,  
Department of Hydrogen Energy, Al. Mickiewicza 30, 30-059 Kraków, Poland*  
*E-mail: jale@agh.edu.pl*

**Keywords:** voltage transducers, magnetic core testing

In laboratories, there is a need to measure shape of voltage waveforms of the electrical network. Most often this is realized by using special instrumental voltage transformers but it has the disadvantage of working only within limited range of nominal voltage and at nominal frequency. For voltage that varies in a wide range, it is required in testing or teaching laboratories that resistive or capacitive voltage dividers are used; alas they do not provide galvanic separation. At present measurements are realized by oscilloscopes or more often using DAQ cards connected to computer. Both work with grounded zero connector and direct connections of the measuring equipment can expose it to damage, as well as it can be dangerous for people operating such equipment. Improvement of safety can be reached by connecting through an insulating transformer. In this paper we demonstrate experimentally that the proposed sensor measures voltage ranging from 10 V up to 240 V provides galvanic separation of testing equipment from electrical network. Experimental results are also presented.

## ***Proposed voltage sensor***

At individual stages of production of electrical devices magnetic material is tested first in Epstein frame or Single Sheet Tester, next in a form of magnetic core and finally in a complete device. The middle stage is performed only in a case of small cores. Large cores are usually not tested due to their mass and required large excitation power, although in special applications this can be done [1]. To overcome such problem the test system can be powered directly from low voltage mains network. Measurement of voltage in such case is more difficult due to safety implications and hence there is necessity for galvanic separation.

For the above mentioned reasons voltage transducer was designed. It consists of a low power current transformer and current limiting resistors [2], (Fig. 1a). The main advantage of the proposed voltage sensor, in relation to others sensors, is the inherent galvanic separation and passive operation not requiring any additional power supply. The proposed sensor is characterized by high repeatability and high accuracy. The peak voltage error does not exceed  $\pm 1.5\%$  and if required it can be calibrated to a much tighter tolerance. The angle error is about  $\pm 20$  min at small voltages and  $\pm 10$  min for voltage range from 5% to 120%, (Fig. 1b). The voltage sensor was successfully employed for testing large industrial cores [3]. Cores designed to operate at frequency

higher than 50 Hz can be tested another test system [1], but obviously this approach is limited by the power of amplifier.

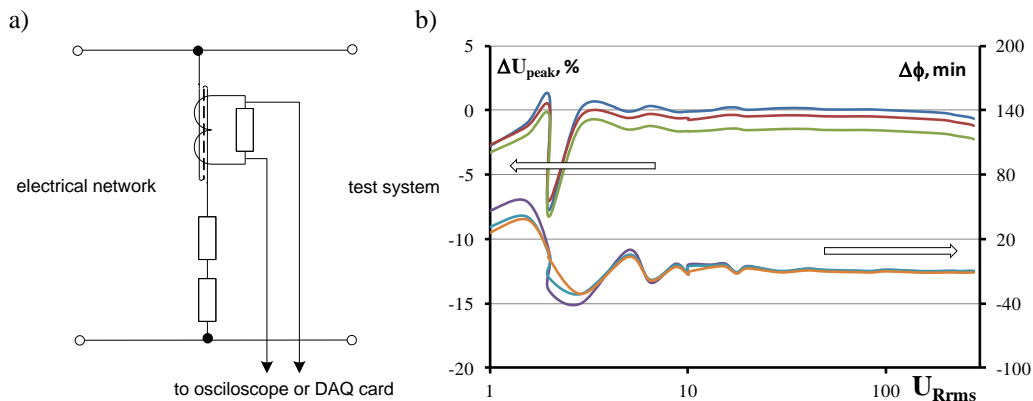


Fig. 1. Schematic diagram of voltage sensor (a) and its amplitude and angle error (b)

### Acknowledgements

This work has been carried out within the project grant "Industrial research a new type of magnetic cores made of amorphous and nanocrystalline strips, thin magnetic sheets and composite materials operating in higher frequencies", and was supported by the National Centre for Research and Development under European Regional Development Fund in the frame of European Smart Growth Funds, under contact No. POIR.01.01.01-00-0306/15-00. The support is gratefully acknowledged.

### References

- [1] Rygał R., Żurek S., Pluta W., Leszczyński J., Soiński M., Walak J., Rygał J., Universal modular high power wide frequency range controlled system for magnetic measurements, to be presented at 15th 1&2DM, Grenoble, France, 2018
- [2] Pluta W., Rygał R., Zurek S., Apparatus for measuring AC voltage with galvanic separation (in Polish: Układ do pomiaru napięcia przemiennego z separacją galwaniczną), Patent Application PL420750, 2017
- [3] Pluta W., Rygał R., Soiński M., Leszczyński J., Labview Based Testing System for the Aim of Construction of Energy Efficient Magnetic Cores. E3S Web of Conferences. ISSN 2267-1242 — 2017 vol. 14 No. 01039, pp. 1–10

# Improved High-Frequency Rotating Magnetic Properties Tester for Ultra-thin Silicon Steel Material Considering Stress Effects

Changgeng Zhang<sup>1</sup> Member, IEEE, Angxuan Li<sup>1</sup>, Yongjian Li<sup>1</sup>, Member, IEEE, Qingxin Yang<sup>2</sup>

<sup>1</sup> State Key Laboratory of Reliability and Intelligence of Electrical Equipment, Hebei University of Technology, Tianjin, 300130, China

<sup>2</sup> Tianjin Key Laboratory of AEEET, Tianjin Polytechnic University, Tianjin, 300387, China

In this paper, a novel high-frequency rotating magnetic properties tester is designed and modeled to comprehensively measure and analyze the bi-axial magneto-mechanical characteristics of ultra-thin silicon steel material. The shape of the cores and the specimen in the tester are concentrated and optimized, which can generate relatively uniform and strong magnetic field in the center of the specimen. A feedback control algorithm and a harmonics compensation are established to obtain the desired magnetization loci and improve the measurement precision. Meanwhile, a flexible method of the rotating magnetic properties measurement under bi-axial stress is proposed, which is verified by mechanical finite element simulation.

**Index Terms**— 2-D magnetization properties, the bi-axial magneto-mechanical characteristics, feedback control, Ultra-thin silicon steel Material.

## I. INTRODUCTION

Ultra-thin silicon steel Material with high saturation flux density and low losses under high-frequency is widely applied in aerospace and power electronic device to fabricate cores of high-frequency power transformers and electrical machines. In multi-phase power transformers and rotating electrical machines, the rotating magnetic flux may cause the increase of core losses, leading to local overheating and damage of the equipment. In early 2-D magnetic properties tester, excitation structure is complex and the fabrication of magnetic core is difficult. The test result is easy to be affected by the assembly precision of the magnetic core. The working frequency of the excitation structure made by silicon steel is low because of the limitation of the high frequency core losses [1] [2]

In the actual operation of the power transformer and motor, the stress applied on the material sheet will affect the magnetic domain arrangement, which means changing the magnetic properties of the cores [4]. However, bi-axial magneto-mechanical characteristics can give a deeper insight into the magneto-elastic coupling, which was rarely reported in literature.

In this paper, a novel 2-D magnetic properties tester is designed to measure the bi-axial magneto-mechanical characteristics. The excitation structure is optimized by changing the shape of cores and specimen, which can generate the high frequency rotating magnetic field. Both feedback control algorithm and harmonics compensation are established.

## II. IMPROVED DESIGN OF 2D TESTER

### A. Design of excitation structure

The new magnetization structure in this paper is shown in Fig.1 (a), two U type cores are made of high performance ultra-thin silicon steel, which limits the losses and the heating in cores with the increased of frequency. Each core and specimen constitutes a magnetic circuit separately without affecting each other. The physical diagram of the novel magnetization structure is shown in Fig.1 (b).

The simulation of magnetic field distribution in novel magnetic circuit structure and in specimen are shown in Fig.1(c) (d). It can be seen that the magnetic flux distributed uniformly in two cores. Each core and the specimen

constitute an independent magnetic circuit and then establish a standard rotating magnetic field in the center of specimen, which verifying the rationality of this magnetization structure.

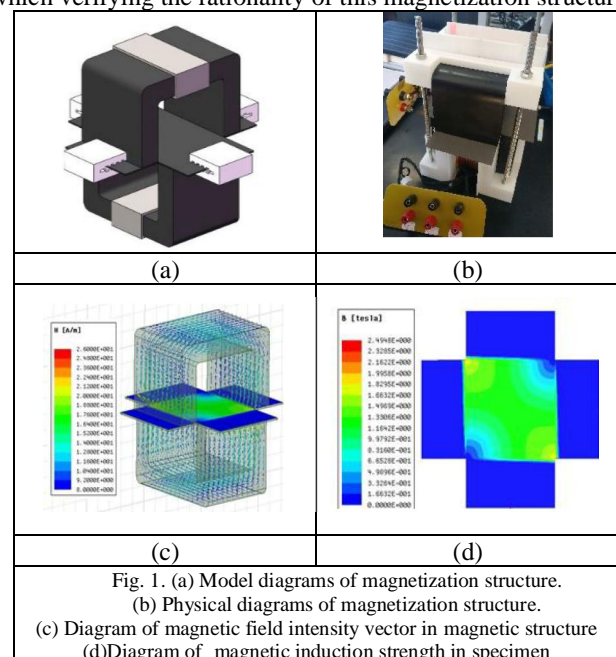


Fig. 1. (a) Model diagrams of magnetization structure.

(b) Physical diagrams of magnetization structure.

(c) Diagram of magnetic field intensity vector in magnetic structure

(d) Diagram of magnetic induction strength in specimen

### B. The compression-testing system

The model of stress applied devices as shown in Fig.1 (a), which can apply the stress to the sample. The forces in two orthogonal directions are combined in the center of the specimen by controlling the magnitude of the stress of four devices. The stress tensor on the specimen can be calculated by:

$$\sigma = [K] \cdot F$$

where  $\sigma$  is the local stress tensor,  $F$  is the two direction force,  $K$  is the interacting matrix. The  $K$  matrix has non-diagonal terms, which is calculated by mechanical finite element analysis.

## III. FEEDBACK CONTROL AND HARMONICS COMPENSATION

A feedback control algorithm for rotating magnetic field are proposed, as shown in Fig. 2. More detailed introductions for

harmonics compensation method will be presented in the full paper. The efficiency and feasibility have been strongly validated through the waveform control in a 3-D magnetic properties testing system [5].

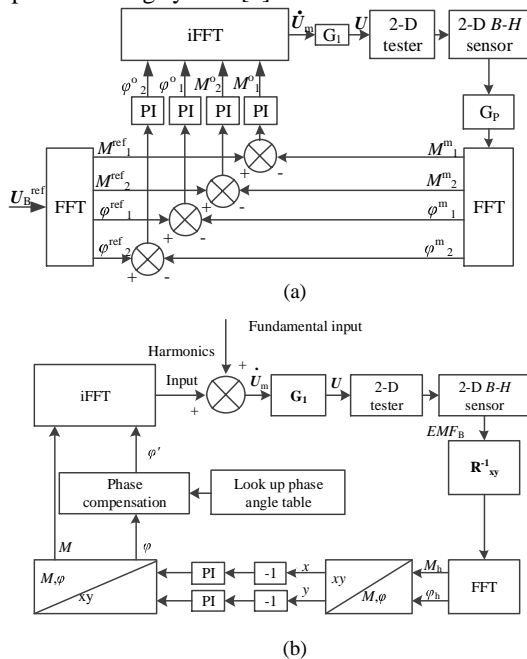


Fig. 2. Control flowchart: (a) feedback control algorithm; (b) harmonics compensation method.

#### IV. CONCLUSION

A novel high frequency rotational excitation structure was designed to measure the magnetic properties under bi-axial stress and bi-axial magnetization in this paper. The optimized magnetic circuit structure was verified by finite element analysis, which reduces the difficulty of processing and assembling the cores and improve the accuracy of the testing system. By optimizing the excitation structure, the bi-axial stress applied device was designed in coordination with the high frequency rotational magnetic tester. A feedback control algorithm and a harmonics compensation are established to achieve accurately simulation of rotating magnetic field. The uniformity of the stress and the characteristic matrix of loading were verified by the mechanical FEA, which is the foundation of measuring and modeling 2D magneto-mechanical properties of nanocrystalline material in high frequency.

#### V. ACKNOWLEDGMENT

This work was supported in part by the National Natural Science Foundation of China, (No. 51777055), the National Key R & D Program of China (2017YFB0903904), and the National Key Basic Research Program of China (973 Project) under Grant 2015CB251000.

#### VI. REFERENCES

[1] Yanli Zhang, Young Hwan Eum, Dexin Xie, Chang Seop koh. "An improved engineering model of vector magnetic properties of grain-oriented electrical steels," et al. IEEE Trans Magn. 2008

[2] [2] S. Higuchi, T. Nakao, Y. Takahashi, T. Tokumasu, K. Fujiwara and Y. Ishihara, "Modeling of Two-Dimensional Magnetic Properties Based on One-Dimensional Magnetic Measurements," IEEE Trans. Magn., vol. 48, no. 11, pp. 3486-3489, Nov. 2012.

[3] Rongge Yan, Xu Gao, Lihua, Zhu, Qingxin Yang. "Research on Three-Dimensional Stress Distribution of Reactor Core" IEEE Transactions on Applied Superconductivity, vol. 26, no. 4, pp. 1-4, June 2016.

[4] C. G. Zhang, Y. J. Li, J. S. Li, Q. X. Yang, and J. G. Zhu, "Measurement of Three Dimensional Magnetic Properties with Feedback Control and Harmonic Compensation," IEEE Trans. Ind. Electron., vol. 64, no. 3, pp.2476-2485, Mar. 2017.

# Improved nondestructive testing of condenser tubes using a cylinder-type integrated hall sensor array

Sejin Kim<sup>1</sup>, Hoyong Lee<sup>2</sup>, Jungmin Kim<sup>1</sup>, Heejong Lee<sup>1</sup>, and Jinyi Lee<sup>1</sup>

<sup>1</sup>Research Center for IT-based Real Time NDT for Nano-Damage Tolerance, Chosun University, Gwangju, 61452, Korea

E-mail: sejinkim1989@gmail.com, 79.jmkim@gmail.com, happybell221@naver.com, jinylee@chosun.ac.kr

<sup>2</sup>Department of Defense Science and Technology, Gwangju University, Gwangju, 61743, Korea

E-mail: hylee@gwangju.ac.kr

**Keywords:** CIHaS, ghost signal, titanium.

The condenser of a nuclear power plant has two major functions. One is that it condenses and recovers the steam which passes through the turbine and the other is that it maintains vacuum to optimize the efficiency. One of the major components of condenser is condenser tubes that consist of thousands of small tubes, made of titanium, stainless steel, or copper. Condenser tubes that use seawater as a medium of heat transfer are mainly made of titanium due to their high corrosion resistance. However, wear may occur between tubes and tube support plates (TSP) due to tube vibration during long term operations. Thus, for old nuclear power plants, periodic inspections of the condenser tubes are required.

Since a large number of condenser tubes must be inspected at a limited time, eddy current tests (ECT) have been applied due to their high speed characteristic. Among various ECT methods, the nondestructive testing method using cylinder-type integrated hall sensor (CIHaS) array is particularly suitable for inspecting condenser tubes due to its high reliability and agility [1]. However, this technique has a disadvantage in that a ghost signal, that is, a false signal is generated during the test. In previous ECT technique, a line of hall sensors among CIHaS are selected to measure the magnetic flux leakage. In this case, before the sensors pass the flawed position, the coil's impedance change is measured due to the large width of the coil, so a ghost signal is detected.

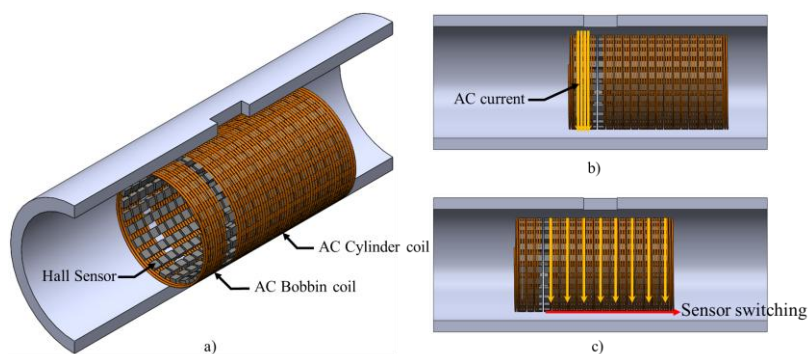


Figure 1: Configuration of improved CIHaS system

In this paper, the improved nondestructive testing method using a CIHaS array is introduced. One coil is separated into a bobbin coil and a cylinder coil as seen in fig. 1: a). By operating and measuring these two coils separately, a ghost signal generated by an unnecessary large area of the coil can be eliminated. When AC current is applied to the bobbin coil, the sensors can measure the magnetic flux leakage of the area and detect the defect's information and location (fig. 1: b)). Next, applying AC current to the cylinder coil, moving the coil to the detected location, and switching sensors (fig. 1: c)). Through these procedures, it is possible to visualize the defect locations in real time without any ghost signals.

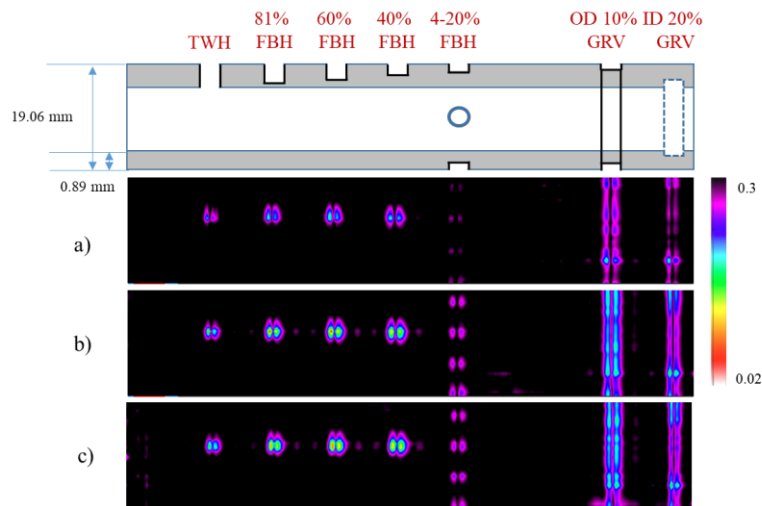


Figure 2: Experimental results of artificial flaws by improved CIHaS; a) 6khz b) 15khz c) 30khz

Fig. 2 shows the test specimen and the experimental results. A titanium condenser tube which has 19.06mm OD, 17.28mm ID, and 0.89mm W.T was used. 25x25 hall sensors were arranged in the circumferential direction and the axial direction. The current of the coil was fixed to 200mA and the signals are measure by increasing the frequency to 6, 15, and 30khz. A clear signal measurement could be obtained in case of high frequency, and all the artificial flaws of the condenser tube shown in fig. 2. were detected.

#### Acknowledgements

This research was funded by the Korea Institute of Energy Technology Evaluation and Planning (KETEP 20171520101610). We are grateful for the support.

#### References

- [1] M. Le, J. Kim, J. Kim, H. Do, and J. Lee. "Electromagnetic testing of moisture separator reheater tubes using a bobbin-type integrated Hall Sensor Array", *International Journal of Applied Electromagnetics and Mechanics*, 55 (2017), 203-209.

# Influences of Machining and Acid Etching on Magnetic Properties of Soft Magnetic Composites

Yuto Higashigawa<sup>1</sup>, Yasuhito Takahashi<sup>1</sup>, Koji Fujiwara<sup>1</sup>  
Masahiro Aoyama<sup>2</sup>, and Ryosuke Akaki<sup>3</sup>

<sup>1</sup> *Doshisha University, Japan*

*E-mail: {ctwc0313@mail4; ytakahashi@mail; koji.fujiwara@mail}.doshisha.ac.jp*

<sup>2</sup> *Shizuoka University, Japan*

*E-mail: aoyama.masahiro@shizuoka.ac.jp*

<sup>3</sup> *Suzuki Motor Corporation, Japan*

*E-mail: ryosukeakaki@hhq.suzuki.co.jp*

**Keywords:** Soft magnetic composites (SMC), acid etching, magnetic properties.

A soft magnetic composites (SMC) core is produced by compressing iron powders. Each powder has insulation coating. SMC core has the features of excellent shape freedom and possibility of reduction of eddy-current loss. When SMC is applied to motor cores, the machining process is required after the compression molding to adjust shape and size. However, it is well-known that the magnetic properties deteriorate due to the machining process [1]. This is because the insulation on the surface of the core is destroyed by machining. Therefore, in this paper, we examined the degree of improvement of magnetic properties by applying acid etching treatment to a SMC core after machining.

The SMC core investigated in this paper is Somaloy 700 3P manufactured by Höganäs AB, which is molded to a density of about 7.43 g/cm<sup>3</sup> with 600 ton press machine and is subjected to steam treatment. All the faces of core are cut by machining under the conditions of cut amount: 0.1 mm per face, diameter of radius end mill: 4 mm, rotational speed: 10,000 min<sup>-1</sup>, and feed speed: 1,000 min<sup>-1</sup>. We try to remove the surface layer of core by applying acid etching treatment (85 % phosphoric acid H<sub>3</sub>PO<sub>4</sub> diluted by 25 %). We performed acid etching treatment with immersion time of 9, 45, 54, 63, 72, 81 min to the specimen after machining. Then the resistivity  $\rho$  and iron loss  $W$  are measured. We prepare ring specimens in consideration of the final form of use.

Fig. 1 shows the effect of acid etching treatment time on resistivity. It is normalized by the value of the resistivity of the core without machining. Since the surface layer due to the machining process is removed by the acid etching treatment, the resistivity increases with the immersion time. However, in the case where the immersion is continued more than necessary, the normal insulation coating is broken and the resistivity gets lower.

Fig. 2 shows the comparison of iron loss  $W$  property measured at 1 kHz. A digitally-controlled measuring system [2] is used. The iron losses are normalized by the maximum value of  $W$  of the specimen with no processing. It is confirmed that the iron loss property is almost the same as those before machining regardless of the immersion time in acid etching.

Fig. 3 shows the results of iron loss separation. The hysteresis loss coefficient  $k_h$  and the eddy current loss coefficient  $k_e$  are obtained by linearly approximating the measured results of  $W$  at 50, 100, 500, 1000 Hz. Both coefficients are normalized with the value of  $k_h$  of the specimen with no processing at  $B_m = 1.8$  T. Although  $k_h$  slightly decreases as the immersion time for acid etching

treatment increases, its change is sufficiently small. On the other hand, it is confirmed that  $k_e$  is improved drastically by acid etching treatment after machining and its effect is not significantly dependent on the immersion time. Therefore, it is possible to remove the deteriorated surface layer with a relatively short immersion time.

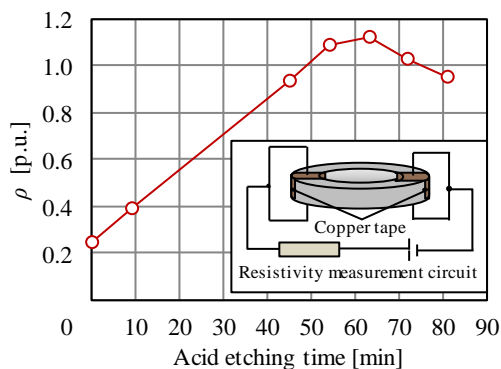


Fig. 1. Effect of acid etching time on resistivity.

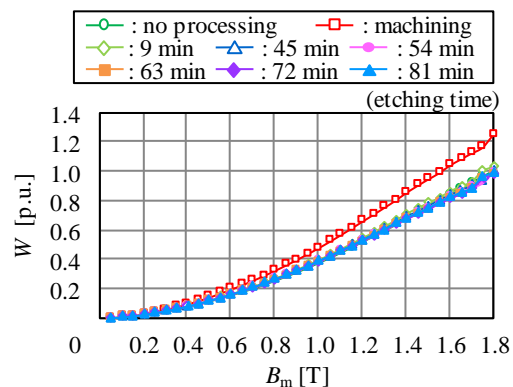
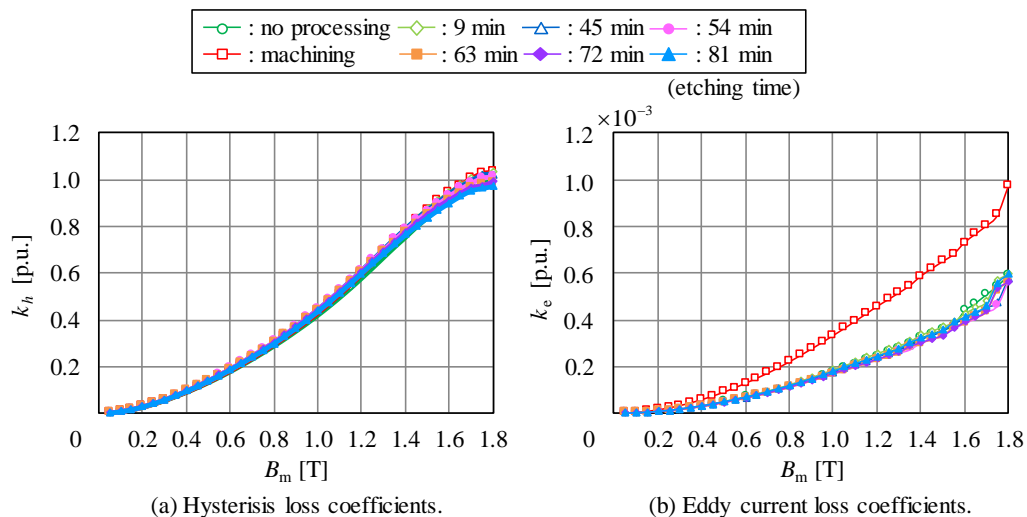


Fig. 2. Iron loss properties.



(a) Hysteresis loss coefficients.

(b) Eddy current loss coefficients.

Fig. 3. Core loss separation.

From the above results, there is a possibility that the eddy current loss coefficient of the SMC core can be reduced by acid etching treatment within 9 minutes. We plan to investigate the optimum immersion time to improve the magnetic properties of the SMC core.

#### References

- [1] K. Aiso and K. Akatsu, "Design of Axial Type Switched Reluctance Motor Considering Magnetic Characteristics of Soft Magnetic Composite Material," *IEEJ Trans. Industrial Applications*, vol. 136-D, no. 9, pp. 664-665 (2016).
- [2] Y. Kimura et al., "Measurement of Magnetic Properties of Non-oriented Electrical Steel Sheets Up to High Flux Density for Magnetic Field Analysis of Generator," *International Colloquium of CIGRE Study Committee A1 (Rotating Electrical Machines)*, pp. 1-10 (2017).

# Iron Loss Estimation Method of PWM Inverter-Fed AC Filter Reactor

Toshihiro Kubo<sup>1, 2</sup>, Nobuyuki Momochi<sup>1</sup>, Yoshio Matsubara<sup>2</sup>, Yasuhito Takahashi<sup>1</sup>, Koji Fujiwara<sup>1</sup>, and Naoto Nagaoka<sup>1</sup>

<sup>1</sup>*Doshisha University, Kyoto, Japan*

*E-mail: euo1303@mail4.doshisha.ac.jp; nobu9021@gmail.com; ytakahashi@mail.doshisha.ac.jp; koji.fujiwara@mail.doshisha.ac.jp; nnagaoka@mail.doshisha.ac.jp*

<sup>2</sup>*Nissin Electric Co., Ltd., Kyoto, Japan*

*E-mail: kubo\_toshihiro@nissin.co.jp; matsubara\_yoshio@nissin.co.jp*

*Keywords:* DC-biased magnetization, minor loops, non-sinusoidal current.

## 1. Introduction

High frequency switching operation enables to downsize reactors in a PWM inverter. However, the operation increases loss and temperature of the reactors. In order to design an efficient inverter with high power density, the reactor loss has to be accurately estimated.

In the PWM inverter, the reactor for AC-filter is excited by a non-sinusoidal voltage, and the magnetization trajectory on  $BH$ -plane has many minor loops. Since the iron loss has been estimated based on a measured magnetic characteristic under a sinusoidal excitation, the accuracy of the predicted loss is unsatisfactory for the PWM inverter.

This paper proposes an iron-loss estimation method of the filter reactor for a single-phase PWM voltage source inverter. In order to improve the accuracy of the loss estimation, the effects of the flux bias, eddy-current loss coefficients and waveform distortion are investigated. The estimated result is compared with a measured iron loss of a filter reactor.

## 2. Iron loss estimation method for iron core under PWM excitation

The iron loss for a distorted exciting voltage has been estimated by the sum of hysteresis and eddy current losses at each frequency, i.e., the effect of the flux bias has been neglected. A method extracting the minor loop loss from the iron loss under the case in which a single harmonic is superposed on a fundamental frequency (Figure 1) has been originally proposed [1] and one of the authors investigated in detail to apply the method to magnetic field simulation [2]. In this paper, the method is improved for a PWM-excited iron core taking into account the triangle waveform of the flux density, which includes several harmonics.

As shown in Figure 2, the minor loop is divided into two sections whose durations are  $T_{A-B}$  and  $T_{B-C}$ , respectively. The inverses of those are apparent frequencies, and the loss of each section is estimated by a half of the loss obtained by a single sheet test at the apparent frequency with a flux bias whose value is the average flux of the minor loop. The loss of the outline loop is estimated by the single sheet test applying a sinusoidal excitation voltage without a flux bias at the frequency of the loop, which is higher than the fundamental frequency of the original hysteresis loop.

Figure 3 shows the test results using a single sheet circuit excited by PW-modulated voltage. This results shows that the proposed method has a satisfactory accuracy compared with the conventional method.

## 3. Conclusions

This paper investigates an iron-loss estimation method of a filter reactor for a single-phase PWM voltage inverter. The loss of the minor loop is divided into incline and decline parts and

respective losses are determined by a single sheet test at the harmonic frequency with a flux bias. The proposed method improves the estimated error from 12 % of the conventional method to 3 %.

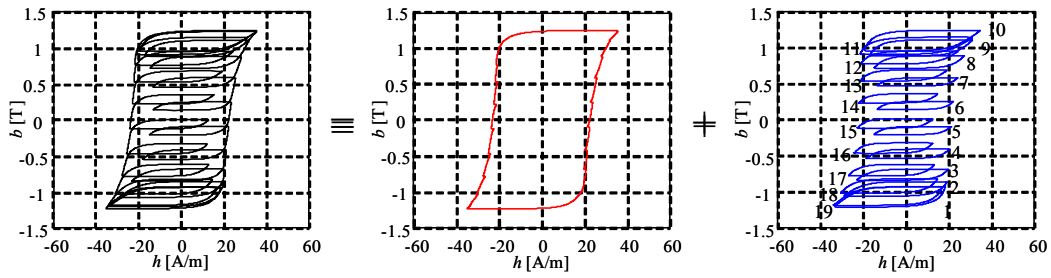


Figure 1: Dividing  $BH$ -loop into an outline loop and minor loops.

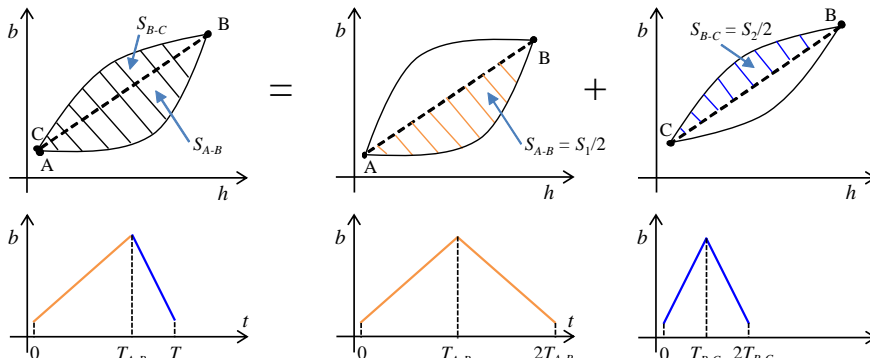
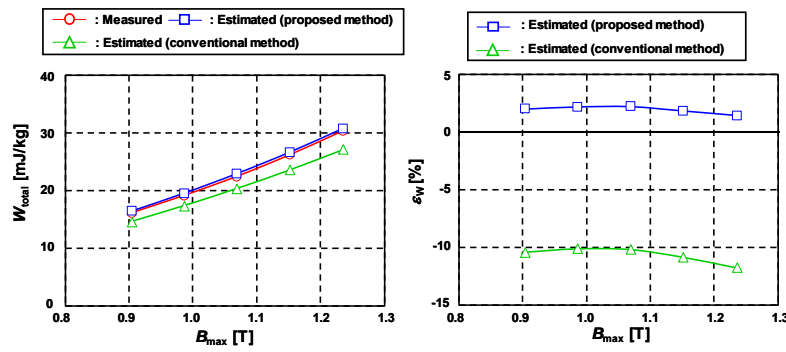


Figure 2: PWM-excited flux density waveforms and two sections of a minor loop.



(a) Iron loss.

(b) Error against measured results.

Figure 3: Measurement and estimated iron losses under PWM excitation.

References

- [1] S. Yanase, H. Kimata, Y. Okazaki, and S. Hashi, “A Simple Predicting Method for Magnetic Losses of Electrical Steel Sheets under Arbitrary Induction Waveform”, *IEEE Trans. Magn.*, vol. 41, no. 11, pp. 4365–4367, (2005).
- [2] T. Taitoda, Y. Takahashi and K. Fujiwara, “Iron Loss Estimation Method for General Hysteresis Loop with Minor Loops”, *ibid*, vol. 51, no. 11, 8112304 (2015).

# Loss model for transformer core under non-sinusoidal excitation

Zhigang Zhao, Ying Guo, Jia Liu, Saining Yin, Kai Yang

State Key Laboratory of Reliability and Intelligence of Electrical Equipment, Hebei

University of Technology, Tianjin 300132, china

E-mail: zhaozhigang@hebut.edu.cn; 2427519546@qq.com

**Keywords:** transformer, distorted magnetic flux, loss separation, loss model.

The loss calculation methods for magnetic materials can basically be divided into three categories: hysteresis model method, Steinmetz equation (SE) method and core loss separation method. These methods have matured on core loss calculation under the sinusoidal excitation. Due to the development of HVDC transmission system, as one of the most important equipment, converter transformers increase a large number of high harmonics on load current during normal operation, which results in harmonic pollution and serious threat to power system. Aiming at the calculation of high harmonic magnetic flux distortion on the total core losses in the transformer, an engineering approach was introduced in this paper. It's of great practical signification to study the calculation of core losses under non-sinusoidal excitation.

The Epstein magnetic characteristic test system can only measure the core losses<sup>[1]</sup>. The proportion of the hysteresis loss and the eddy current loss can't be distinguished. A simplified Bertotti model as equation (1) was used to obtain separation data on the material of grain-oriented electrical steel<sup>[2]-[3]</sup>.

$$W_T = hfB_m^x + ef^2B_m^y \quad (1)$$

Accordingly, the energy of core loss can be determined by

$$W_T / f = hB_m^x + efB_m^y \quad (2)$$

By extracting the core losses of 25~400Hz,  $B_m = 1.0T$ , computing  $W_T/f$ , and diagram the frequency, the linear regression line can be obtained as shown in Figure 1. According to the above method, the core loss can be separated by measuring the core loss values under different magnetic densities as shown in figure 2. Therefore, the model parameters can be obtained by linear fitting.

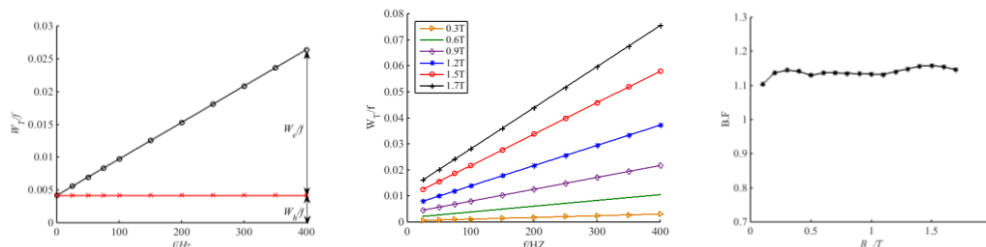


Figure 1 The core energy Figure 2 Different flux density energy Figure 3 The change of process coefficient

Note that, the construction about power transformer and the Epstein are different, in order to realize transformer core loss separation, the core process coefficient of equation (3) is introduced. The variation of the process coefficient with magnetic flux density is shown in Figure 3.

$$B.F = \frac{W_T}{P_s \times m_{\text{weight}}} \quad (3)$$

By using the loss separation model, hysteresis loss and eddy current loss of transformer under the

power frequency (50 Hz) are determined, as shown in Figure 4

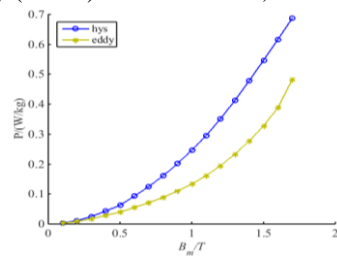


Figure 4 The separation diagram of iron loss

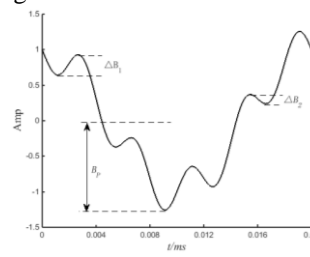


Figure 5 Flux density distortion waveform

With harmonic phase, harmonic content and harmonic order changes, the magnetic waveform dynamically changes, which affects core loss. Considering the impact of these factors, a correction factor for hysteresis loss and eddy current loss as equation (4) is proposed in this paper.

$$\left. \begin{aligned} \Delta B_T &= \frac{1}{B_p} \sum_{i=1}^N \Delta B_i, \\ f(hys) &= 1 + k\Delta B_T, \\ f(eddy) &= \left( \frac{B_l}{B_p} \right)^2 \sum_n \left( \frac{nB_n}{B_l} \right)^2 \end{aligned} \right\} \quad (4)$$

Therefore, loss mode of transformer under non-sinusoidal excitation can be expressed as (5):

$$W_T(B_p) = f(hys) \times W_{hys(\sin)}(B_p) + f(eddy) \times W_{eddy(\sin)}(B_p) \quad (5)$$

Table 1 gives the measured data of respectively superposing the content of 30% fifth harmonic with the phases of  $0^\circ$ ,  $90^\circ$  and  $180^\circ$ , and there is a comparative analysis between measurement and calculation data. It can be seen that the error is less than 10%, which meets the accuracy requirements, so the correctness of loss model is verified. The results can provide reference for core loss prediction.

Table 1 The core loss of 5th harmonic with 30%

$B_1(T)$	Phase $0^\circ$		Phase $90^\circ$		Phase $180^\circ$	
	Measured loss (W/kg)	Calculated loss (W/kg)	Measured loss (W/kg)	Calculated loss (W/kg)	Measured loss (W/kg)	Calculated loss (W/kg)
1.0	0.911	0.895	0.890	0.890	0.891	0.848
1.1	1.126	1.099	1.120	1.116	1.096	1.056
1.2	1.368	1.338	1.368	1.352	1.330	1.248

#### Acknowledgements

The research leading to these results has received funding from National Natural Science Foundation of China under Grant 51107026, 51677052, 51237005.

#### References

- [1] GB/T 12325-2008, "Method of measurement of the magnetic properties of electrical steel sheet and strip by means of an Epstein frame" [S].
- [2] Du, Y., et al. "Modeling for multi-directional magnetic property of anisotropic grain-oriented silicon steel." *High Voltage Engineering* 35.12(2009):3022-3026.
- [3] Marin-Hurtado, Ana Julieth, S. Rave-Restrepo, et al "Calculation of core losses in magnetic materials under nonsinusoidal excitation." *International Conference on Power Electronics IEEE*, 2016:87-91.

# Magnetic Properties Measurement of Nanocrystalline Under DC Bias

Yongjian Li<sup>1</sup>, He Sun<sup>1</sup>, Qingxin Yang<sup>1,2</sup>, Changgeng Zhang<sup>1</sup> and Shuaichao Yue<sup>1</sup>

<sup>1</sup> State Key Laboratory of Reliability and Intelligence of Electrical Equipment Hebei University of Technology, 300130, Tianjin, China

<sup>2</sup> Tianjin Key Laboratory of ATEEE, Tianjin Polytechnic University, Tianjin, 300387, China  
(liyongjian@hebut.edu.cn)

*Keywords*—DC bias, nanocrystalline, magnetic properties, core loss.

## 1. Introduction

Miniaturization and high frequency have become the development trend of electrical equipment. Because of fine magnetic properties, nanocrystalline is replacing the silicon steel gradually and make electrical equipment develop towards energy saving and efficiency [1,2]. In this paper, the comprehensive magnetic properties of nanocrystalline under DC bias are tested. The DC magnetization curve of nanocrystalline is calculated based on the experimental data of induction voltage and excitation current. Based on the measured data and the calculation results of DC magnetization curve, the hysteresis loop of nanocrystalline is determined under DC bias. The influence of the DC bias on these curves is analyzed. Combined with core loss models under sine wave excitation, the influences of DC bias on core loss are studied. The rules of these influence are found from the experimental results.

## 2. Methods and Results

The test system consist of a signal generator, an am amplifier, an oscilloscope, and a PC for interfacing and calculation. The calculation have been done in MATLAB. As shown in Fig.1. Due to DC flux can not be obtained directly in the experiment, the  $B_m-H_b$  curve is used to approximate the DC magnetization curve of nanocrystalline under standard sine excitation ( $B_m$  means the maximum of average AC flux density in nanocrystalline.  $H_b$  refers to the value of  $H$ , when  $B$  reaches to  $B_m$ ). When flux density  $B$  reaches the maximum time,  $dB/dt \approx 0$ , the eddy current loss of the material is almost zero [3], so it is considered to be reasonable to use this hypothesis under the standard sinusoidal excitation. Through the following calculation principle, as shown in Fig.2, the DC flux  $\Delta\phi$  of nanocrystalline is calculated under the same DC bias but different AC operating point. The specific method is as follows: through the formula (1), the measured voltage  $U_2$  is integrated. Then the alternating magnetization curve is obtained which  $\Delta\phi$  is not included.  $\phi_m-i_b$  is obtained ( $i_b$  means that the excitation current when the magnetic flux reaches the maximum  $\phi_m$ ). When excitation current reaches  $i_b$ , corresponding  $\phi_M$  is obtained by interpolating DC magnetization curve. Moreover, through formula (2), the flux density  $\Delta B$  is obtained under DC bias. Finally, the hysteresis loop of nanocrystalline under different DC bias conditions is obtained, as shown in Fig.3 and Fig.4. More data analysis will be displayed in the full text.

The loss curve of magnetic materials is essential for calculating the model loss by electromagnetic field numerical method. In this paper, the loss curves of nanocrystalline under different DC bias are obtained through experiment and calculation, as shown in Fig.7. Loss curve of nanocrystalline changes when DC bias magnetic field changes, and with the increase of DC bias magnetic field, the loss of nanocrystals has also increased, compared with no DC bias. When  $H_{dc}=15A/m$ ,  $B_m=1T$ , the core loss of nanocrystalline increase about 45%, compared with no DC bias; when  $H_{dc}=15A/m$ ,  $B_m=0.5T$ , the core loss of nanocrystalline increase about 60%, compared with no DC bias. Therefore, the calculation and analysis of core loss of nanocrystalline under DC bias is of great significance. The influence of the DC bias on these curves and the core loss calculation model of the nanocrystalline will be discussed in the full text.

$$\phi(t_i) = \phi(0) + \frac{1}{N} \int_0^{t_i} e(t) dt \quad (1)$$

$$\Delta B = \frac{\Delta\phi}{S} \quad (2)$$

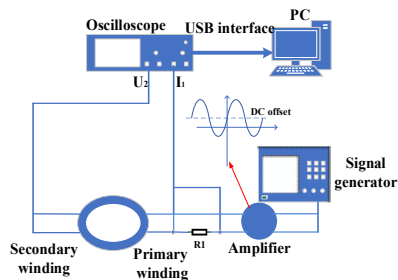


Fig.1. Schematic diagram of the test setup.

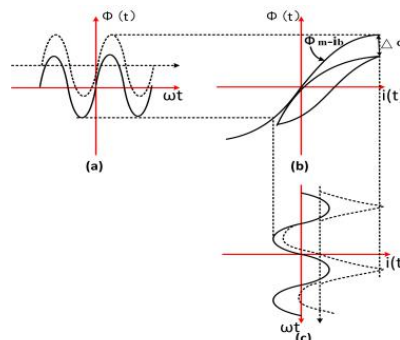
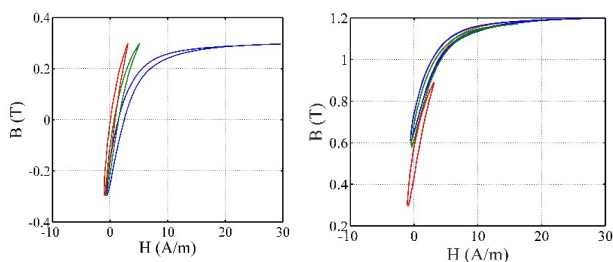
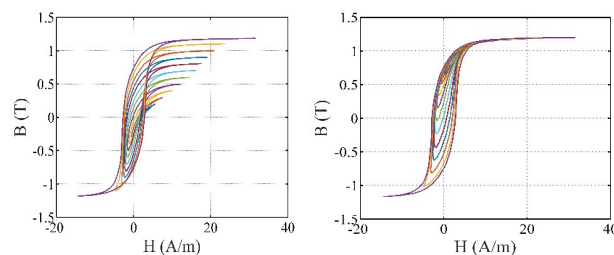
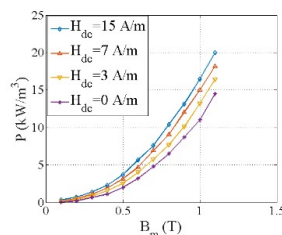


Fig.2. Calculation principle of DC bias flux

Fig. 3 (a) Hysteresis loops of nanocrystalline at  $B_m=0.3\text{T}$ ,  $f=2\text{kHz}$  ( $\Delta B$  not included). (b) Hysteresis loops of nanocrystalline at  $B_m=0.3\text{T}$ ,  $f=2\text{kHz}$  (included  $\Delta B$ ).Fig. 4 (a) Hysteresis loops of nanocrystalline at  $H_{dc}=3\text{A/m}$ ,  $f=2\text{kHz}$  ( $\Delta B$  not included). (b) Hysteresis loops of nanocrystalline at  $H_{dc}=3\text{A/m}$ ,  $f=2\text{kHz}$  (included  $\Delta B$ ).Fig. 7.  $P$ - $B_m$  curve of nanocrystalline under different DC bias magnetization.

### 3. Conclusions

The measurement of magnetic properties of electrical materials is the key to improve the accuracy of electromagnetic numerical simulation. In this paper, The hysteresis loop and the loss curve of nanocrystalline under the different DC bias are studied. The influence of the DC bias on these curves is analyzed and the core loss models are proposed.

### References

- [1] S. Iyasu, T. Shimizu, and K. Ishii, "A novel iron loss calculation method on power converters based on dynamic minor loop," in Proc. Eur. Conf. Power Electron. Appl., 2005, pp. 2016–2022.
- [2] T. Shimizu and K. Ishii, "An iron loss calculating method for AC filter inductors used on PWM inverters," in Proc. 37th IEEE Power Electron. Spec. Conf., 2006, pp. 1–7.
- [3] K. Terashima, K. Wada, T. Shimizu, T. Nakazawa, K. Ishii, and Y. Hayashi, "Evaluation of the iron loss of an inductor based on dynamic minor characteristics," in Proc. Eur. Conf. Power Electron. Appl., 2007, pp. 1–8.
- [4] G. Niedermeier and M. Esguerra, "Measurement of power losses with DC-bias—The displacement factor," in Proc. PCIM., 2000, pp. 169–174.
- [5] J. Mühlethaler, J. Biela, J. W. Kolar, and A. Ecklebe, "Core losses under the dc bias condition based on Steinmetz parameters," in IEEE Trans. Power Electron., vol. 27, no. 2, pp. 953–963, Feb. 2012.
- [6] S. Zhu, M. Cheng, J. Dong, and J. Du, "Core loss analysis and calculation of stator permanent-magnet machine considering DC-biased magnetic induction," in IEEE Trans. Ind. Electron., vol. 61, no. 10, pp. 5203–5212, Oct. 2014.

# Measurement and Loss Estimation of Nanocrystalline Cores With Nonsinusoidal Excitations

Yongjian Li<sup>1</sup>, Shuaichao Yue<sup>1</sup>, Qingxin Yang<sup>2</sup>, and Xinran Yu<sup>1</sup>

<sup>1</sup>*State Key Lab of Reliability and Intelligence of Electric Equipment, Hebei University of Technology, Tianjin, CHINA, E-mail: liyongjian@hebut.edu.cn*

<sup>2</sup>*Tianjin Key Laboratory of AEEET, Tianjin Polytechnic University, Tianjin, CHINA E-mail: qxyang@tjpu.edu.cn*

*Keywords:* Core loss, nanocrystalline, nonsinusoidal excitations, duty cycle.

## 1. Introduction

Magnetic components, including inverters, high frequency transformers and inductors, perform the function of energy conversion, galvanic isolation and harmonic filtering in power converters. The power converters usually work at high frequency (kHz level) in order to reduce volume, which means that the core loss will be remarkable [1]. Thus, achieving an optimal design of power converters is based on a good measurement and estimation of core loss. Traditional, three approaches, including hysteresis models, core loss separation method and Steinmetz equation (SE) method, are usually adopted to calculate core loss for sinusoidal excitations, among which the SE is most widely used for its simplicity and practicality. However, note that the magnetic components in power converters often suffer from nonsinusoidal excitations, such as high frequency square and rectangular waveforms with variable duty cycle  $D$ . Extensive experimental results have shown that there is quite a difference of core loss between sinusoidal and nonsinusoidal excitations [2], that is to say, the aforementioned core loss calculation methods are no longer applicable. Recent years, although many other calculation methods based on SE have been developed for non-sinusoidal excitations, the accuracy and applicability of these methods have not been well analyzed and discussed.

In this paper, the core loss calculation formulas for square and rectangular excitations are derived based on the existing methods, of which the accuracy and applicability are discussed theoretically and verified experimentally. The results can provide reference for core loss prediction under nonsinusoidal excitations.

## 2. Methods and Results

A full-bridge inverter, controlled by DSP, is established to generate square and rectangular excitations with variable  $D$ . The excitations then removes the possible DC component through a blocking capacitor, thereby exciting the core under test (CUT). The  $B-H$  loop measurement method is selected to estimate core loss for the copper loss is excluded [3].

The core loss of Finemet nanocrystalline FT-3KS under both square and rectangular excitations, with  $D$  (from 0.05 to 0.95) are measured and compared with the prediction results from above methods. It is found that the waveform coefficient Steinmetz equation (WcSE) is more applicable for the case of relatively small harmonics content of  $H$  (normal duty cycle region), while the improved generalized Steinmetz equation (IGSE) has better precision where the harmonics count (extreme duty cycle region). In addition, the IGSE can better follow the changing trend of core loss with  $D$  and have better frequency applicability than WcSE. The WcSE is proved to be not valid in low frequency (where the static hysteresis loss dominates). The research results can provide

reference for core loss prediction under nonsinusoidal excitations.

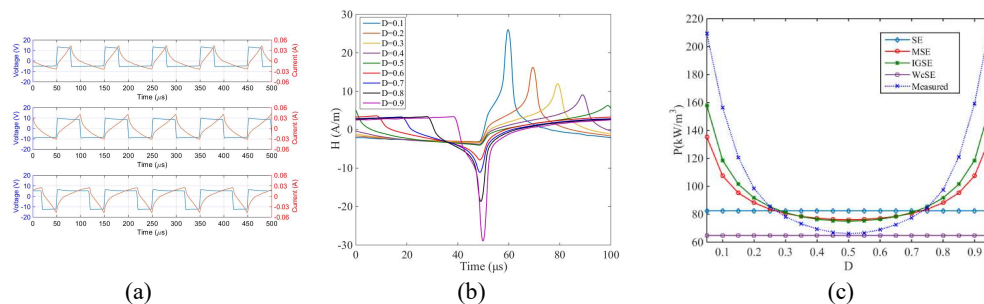


Fig. 1 (a) Voltage and current waveforms for square excitations at 10 kHz, when  $D$  is 0.3 (up), 0.5 (middle) and 0.7 (bottom). (b)  $H$  waveforms for square excitations with variable  $D$  [0.1-0.9], at 10 kHz and 0.8T. (c) Core loss comparison of measurement and estimation under square excitations with  $D$  [0.05-0.95], at 10 kHz and 0.8T.

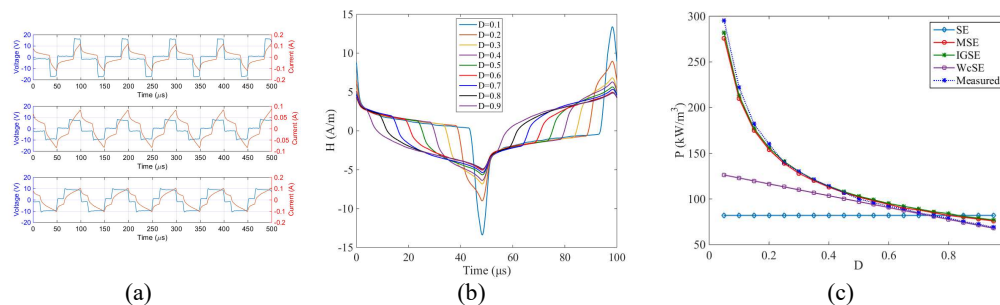


Fig. 2 (a) Voltage and current waveforms for rectangular excitations at 10 kHz, when  $D$  is 0.3 (up), 0.5 (middle) and 0.7 (bottom). (b)  $H$  waveforms for rectangular excitations with variable  $D$  [0.1-0.9], at 10 kHz and 0.8T. (c) Core loss comparison of measurement and estimation under rectangular excitations with  $D$  [0.05-0.95], at 10 kHz and 0.8T.

#### Acknowledgements

This work was supported in part by the National Natural Science Foundation of China, (No. 51777055, 51690181), the National Key R & D Program of China (2017YFB0903904), and the National Key Basic Research Program of China (973 Project) under Grant 2015CB251000.

#### References

- [1] W. Shen, F. Wang, D. Boroyevich, and C.W. Tipton, "Loss Characterization and Calculation of Nanocrystalline Cores for High-Frequency Magnetics Applications," *IEEE Trans. Power. Electron.*, vol. 23, no. 1, pp. 475-484, 2008.
- [2] J. Muhlethaler, J. Biela, J. W. Kolar, and A. Ecklebe, "Improved Core-Loss Calculation for Magnetic Components Employed in Power Electronic Systems," *IEEE Trans. Power. Electron.*, vol. 27, no. 2, pp. 964-973, 2012.
- [3] Barg S, Ammous K, Hanen M, et al. "An Improved Empirical Formulation for Magnetic Core Losses Estimation Under Non-Sinusoidal Induction," *IEEE Trans. Power. Electron.*, PP(99):1-1, 2016.
- [4] Roshen W A. "A Practical, Accurate and Very General Core Loss Model for Nonsinusoidal Waveforms," *IEEE Trans. Power. Electron.*, 2007, 22(1):30-40.

# Methods of improving magnetic properties for powder cores made of nanocrystalline flakes

Dominik Grybos<sup>1</sup>, Cezary Swieboda<sup>2</sup>, Jacek Leszczynski<sup>1</sup>, Marian Soinski<sup>2</sup>

<sup>1</sup>AGH University of Science and Technology, Faculty of Energy and Fuels, al. Mickiewicza 30, 30-059 Krakow, Poland

E-mail: dgrybos@agh.edu.pl; jale@agh.edu.pl

<sup>2</sup>Magneto Sp. z o.o., Odlewnikow 43, 42-202 Czestochowa, Poland

E-mail: Cezary.Swieboda@magneto.pl; Marian.Soinski@magneto.pl

**Keywords:** Soft Magnetic Powder Core, Particle Size Distribution, Compaction, Nanocrystalline Particles.

The paper focuses on improving magnetic properties, such as magnetic induction characteristic  $B(H)$  and relative permeability  $\mu_r$ , in magnetic powder cores (MPC) made of nanocrystalline flakes. Three main attributes of MPC, which have significant influence on magnetic properties, were itemized. These are: mass ratio of coarse to fine flakes  $\epsilon$  [1], size of nanocrystalline flakes  $d$  [2] and value of compaction stress  $\sigma$ , which is related to core density [3].

Magnetic powder cores (MPC) contain magnetic granular material, such as ferrite, iron, amorphous and nanocrystalline material, mixed with binder material, such as polymer, resin or mineral material [4]. A mixture of magnetic powder and binder is integrated by sintering or compaction method [5]. Characteristic attribute of MPC is a distributed-air-gap, achieved by filling free spaces between magnetic particles with binding material. This feature defines the magnetic characteristics of magnetic powder cores, such as magnetic induction  $B$  and relative permeability  $\mu_r$ .

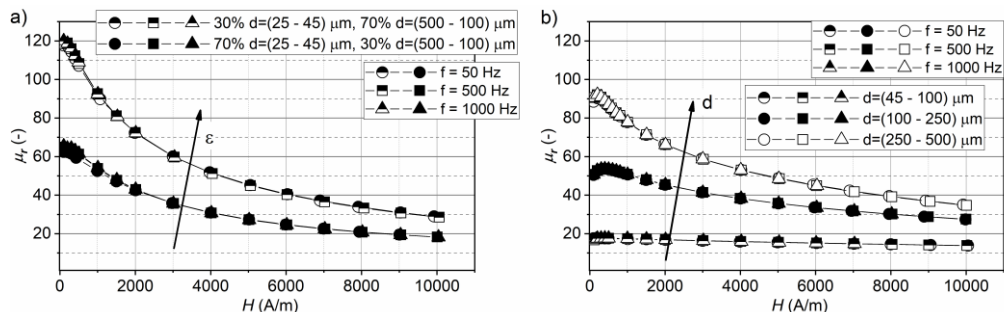


Figure 1: Relative permeability  $\mu_r$  characteristic of MPC with different mass ratio of fine and coarse (a) and size of nanocrystalline flakes (b)

Figure 1 shows relative permeability  $\mu_r$  characteristic of MPC with different mass ratio of coarse to fine nanocrystalline flakes  $\epsilon$  (a) and size of nanocrystalline flakes  $d$  (b) with magnetic field  $H$ . This magnetic parameter is growth with increase of coarse to fine flakes mass ratio  $\epsilon$  and

size of nanocrystalline flakes  $d$ . However, smaller sizes of flakes  $d$  cause more stable relative permeability  $\mu_r$  characteristic with magnetic field  $H$ .

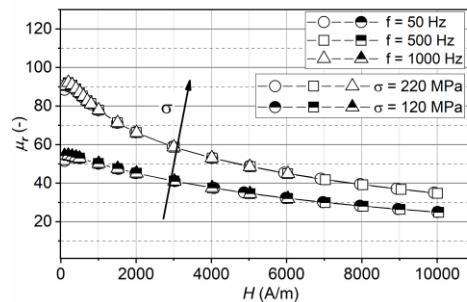


Figure 2: Relative permeability  $\mu_r$  characteristic of MPC with different tension  $\sigma$  value of press.

Figure 2 shows relative permeability  $\mu_r$  characteristic of MPC with magnetic field  $H$  for different values of stress  $\sigma$  of hydraulic press. Increasing value of stress  $\sigma$  of core compaction causes higher value of relative permeability  $\mu_r$  for all range of magnetic fields  $H$ . This feature is strictly related to density of MPC and with higher compaction stress, the mass of core is growing with unchanged volume.

#### *Acknowledgements*

This work has been carried out within the project grant "Industrial research a new type of magnetic cores made of amorphous and nanocrystalline strips, thin magnetic sheets and composite materials operating in higher frequencies" and was supported by the National Centre for Research and Development under European Regional Development Fund in the frame of European Smart Growth Funds, under contact No. POIR.01.01.01-00- 0306/15-00. The support is gratefully acknowledged.

#### *References*

- [1] J. Leszczynski, M Soinsk, R Rygal, et al., "Manufacturing method for magnetic powder cores made from nanocrystalline magnetic materials," patent pending No. P.420752, Polish Pending Patent Office, Warsaw, Poland, 2017.
- [2] F. Mazaleyrat, V. Leger, R. Lebourgeois and R. Barrue, "Permeability of Soft Magnetic Composites From Flakes of Nanocrystalline Ribbon," IEEE Transaction on Magnetics, vol. 38, no. 5, pp. 3132-3134, 2002.
- [3] A. W. Kelley and P. F. Symonds, "Plastic-Iron-Powder Distributed-Air-Gap Magnetic Material," in Power Electronics Specialists Conference, 1990.
- [4] Y. Liu, Y. Yi, W. Shao, Y. Shao, "Microstructure and magnetic properties of soft magnetic powder cores of amorphous and nanocrystalline alloys," Journal of Magnetism and Magnetic Materials, vol. 330, pp. 119-133, 2013.
- [5] R. Nowosielski, J. Wyslocki, I. Wnuk, P. Gramatyka, "Nanocrystalline soft magnetic composite cores," Journal of Materials Processing Technology, vol. 175, No. 1-3, pp. 324-329, 2006.

## Modeling of DC-biased hysteresis loops with the GRUCAD description

R. Jastrzębski, A. Jakubas, K. Chwastek

Faculty of Electrical Engineering, Częstochowa University of Technology

Excitation signals in real-life conditions may differ significantly from those prescribed in appropriate standards e.g. IEC-60404. Prediction of power losses and hysteresis curves under distorted induction waveforms has thus become an important subject of study for engineers [1,2]. Accurate prediction of distorted magnetization patterns is important e.g. in geophysical research for characterization of natural samples [3] or in the analysis of the effects of geo-magnetically induced currents on the working point of large power transformers [4].

The similarity of magnetization curves has been noticed and described for the first time by E. Madelung [5]. His concepts have been transformed into a number of useful engineering approaches to model first and higher order reversal curves [6,7]. It should be remarked that some of the aforementioned methods rely extensively on the hysteresis model used in the analysis.

Among different hysteresis models the Preisach-Mayergoyz description [8] and the formalism advanced by Jiles and Atherton [9] have attracted a lot of attention. Despite some attractive features of the latter model (low dimensionality, ease of numerical implementation), the scientific community has become aware that it required a number of refinements and updates of the values of model parameters in order to model DC-biased minor loops accurately [10,11].

In order to avoid some problems encountered during previous research we have turned our attention to another macroscopic hysteresis model, advanced by the Brazilian team GRUCAD [12,13]. Some properties of the GRUCAD model have been described in detail in the papers [14,15]. In the GRUCAD description the reversible and irreversible processes are decoupled. The irreversibility is implemented by offsetting the loop branches along the  $H$ -axis from the anhysteretic (truly reversible in thermodynamic sense) curve, given with Langevin function. There is no need to introduce additional conditions, which are aimed at the modification of model equations after a field reversal. This description is similar in spirit to some models consistent with the laws of irreversible thermodynamics, to mention [16, 17]. The model equations are as follows:

$$H_{an} = B / \mu_0 - M_s (\coth \lambda - 1 / \lambda) \quad (1)$$

$$\lambda = \frac{1}{a} \left[ (1 - \alpha) H_{an} + \alpha \frac{B}{\mu_0} \right] \quad (2)$$

$$\frac{dH_h}{dB} = \frac{H_{HS} (\coth \lambda_H - 1 / \lambda_H) + H_h}{\gamma \delta} \quad (3)$$

$$\lambda_H = \frac{H_h + \delta H_{HS}}{a} \quad (4)$$

$$H = H_{an} + H_h \quad (5)$$

Herein  $\delta = \text{sign}(dB/dt) = \pm 1$ , whereas  $\alpha, a, \gamma, H_{HS}$  and  $M_s$  are model parameters. Two first equations refer to the reversible, whereas the third and the fourth one – to the irreversible magnetization processes.

In the present paper we focus on the description of DC-biased loops for self-developed soft magnetic composite (SMC) cores with the GRUCAD model at low excitation frequency.

We have produced a number of SMC cores from iron powder and suspense polyvinyl chloride at different proportions of constituent components and for different processing conditions [18]. We have carried out measurements of their magnetic properties with the use of a computer-aided setup with an additional winding for introducing DC offset. During modelling we have kept the values of model parameters constant. Modelling results of a representative DC-biased loop are depicted in Figure 1. The sample under study was made of SMC with iron grain size from the range  $(100;150) \mu\text{m}$

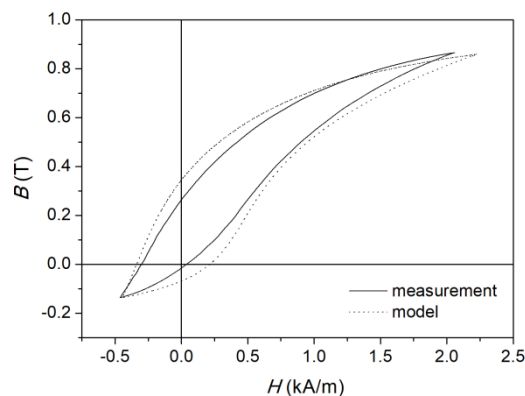


Figure 1. An exemplary DC-biased hysteresis loop

## References

- [1] E. Barbisio, F. Fiorillo, C. Ragusa, Predicting loss in magnetic steels under arbitrary induction waveform and with minor hysteresis loops, *IEEE Trans. Magn.* 40 (4) (2004) 1810-1819
- [2] S. Yanase, H. Kitama, Y. Okazaki, S. Hashi, A simple predicting method for magnetic losses of electrical steel sheets under arbitrary induction waveform, *IEEE Trans. Magn.* 41 (11) (2005) 4365-4367
- [3] X. Zhao, A. P. Roberts, D. Heslop, G. A. Paterson, Y. Li, J. Li, Magnetic domain state diagnosis using hysteresis reversal curves, *J. Geophys. Res. Solid Earth* 122 (2017) 4767-4769
- [4] S. A. Moussavi, Electromagnetic modelling of power transformers with DC magnetization, Thesis, Royal Institute of Technology (KTH), Stockholm, Sweden 2001
- [5] E. Madelung, Über Magnetisierung durch schnellverlaufende Ströme und die Wirkungsweise des Rutheford-Marconischen Magnetdetektors, *Ann. Phys.* 322 (10) (1905) 861-890
- [6] S. N. Talukdar, J. R. Bailey, Hysteresis models for system studies, *IEEE Trans. Power App. Syst.* 95 (4) (1976) 1429-1434
- [7] J. Takács, Mathematics of hysteretic phenomena, Wiley-VCH, Weinheim 2003.
- [8] I. D. Mayergoyz, Mathematical models of hysteresis, Springer 1991
- [9] D. C. Jiles, D. L. Atherton, Theory of ferromagnetic hysteresis, *J. Magn. Magn. Mater.* 61 (1986) 48-60
- [10] A. Benabou, J. V. Leite, S. Clénet, C. Simao, N. Sadowski, Minor loops modelling with a modified Jiles-Atherton model and comparison with the Preisach model, *J. Magn. Magn. Mater.* 320 (2008) e1034-e1038
- [11] K. Chwastek, Modelling offset hysteresis loops with the modified Jiles-Atherton description, *J. Phys. D: Appl. Phys.* 42 (2009) 165002 (5 pp.)
- [12] P.I. Koltermann, L.A. Righi, J.P.A. Bastos, R. Carlson, N. Sadowski, N.J. Batistela, A modified Jiles method for hysteresis computation, *Physica B* 275 (2000) 233-237
- [13] L. A. Righi, N. Sadowski, R. Carlson, J. P. A. Bastos, N. J. Batistela, A new approach for iron losses calculation in voltage fed time stepping Finite Elements, *IEEE Trans. Magn.* 37 (5) (2001) 3353-3356
- [14] S. Steentjes, K. Chwastek, M. Petrun, D. Dolinar, K. Hameyer, "Sensitivity analysis and modeling of symmetric minor hysteresis loops using the GRUCAD description," *IEEE Trans. Magn.* 50 (11) 2014, <http://dx.doi.org/10.1109/TMAG.2014.2323250>
- [15] R. Jastrzębski, K. Chwastek, A comparison of macroscopic descriptions of magnetization curves, *ITM Web of Conferences* 15 (2017) 03003, doi:10.1051/itmconf/20171503003
- [16] A. Bergqvist, Magnetic vector hysteresis model with dry friction-like pinning, *Physica B* 233 (1997) 342-347
- [17] V. François-Lavet, F. Henrotte, L. Stainer, L. Noels, C. Geuzaine, An energy-based variational model of ferromagnetic hysteresis for finite element computations, *J. Comp. Appl. Math.* 246 (2013) 243-250
- [18] A. Jakubas, P. Gębara, S. Seme, A. Gnatowski, K. Chwastek, Magnetic properties of SMC cores produced at a low compacting temperature, *Acta Phys. Pol. A* 131 (2017) 1289-1293

# Modeling of magnetic component behaviors under distorted excitations based on an integrated magnetic measure-bench

Tao Liu<sup>a</sup>, Lanrong Liu<sup>a</sup>, Fulai Che<sup>a</sup>, Zhenbin Du<sup>a</sup>,  
Behzad Forghani<sup>b</sup>, Yongjian Li<sup>c</sup>, Yang Liu<sup>d</sup>, Xiaojun Zhao<sup>e</sup>, and Zhiguang Cheng<sup>a,\*</sup>

<sup>a</sup>Institute of Power Transmission and Transformation Technology, Baoding, CHINA, E-mail: [emlab@btw.cn](mailto:emlab@btw.cn)

<sup>b</sup>Mentor Infolytica a Siemens Business, Place du Parc, Montreal, CANADA, E-mail: [forghani@infolytica.com](mailto:forghani@infolytica.com)

<sup>c</sup>State Key Lab. of Reliability and Intelligence of Electric Equipment, Hebei University of Technology, Tianjin, CHINA, E-mail: [liyongjian@hebut.edu.cn](mailto:liyongjian@hebut.edu.cn)

<sup>d</sup>State Key Lab. of Advanced Transmission Technology, Global Energy Interconnection Research Institute, Beijing, CHINA, E-mail: [liuyang\\_white@hotmail.com](mailto:liuyang_white@hotmail.com)

<sup>e</sup>Department of Electrical Engineering, North China Electric Power University, CHINA, E-mail: [zxjnccpu@ncepu.edu.cn](mailto:zxjnccpu@ncepu.edu.cn)

**Keywords:** Electrical steel, magnetic components, magnetic property, magnetic measure-bench, extreme excitation, modeling and simulation.

## 1. Background and motivation

The standard magnetic property data of electrical steel measured by the standard means under standard condition cannot meet the strict requirements of analysis and design of very large electrical equipments, usually working under non-sinusoidal, even extreme conditions. In addition, there has been a consensus among the industrial and scientific communities that the magnetic material properties are always different from those of assembled magnetic components. Accordingly the accurate measurement and prediction of the working properties of magnetic materials and components under the actual operating conditions are in great demand [1]-[2].

This paper aims to establish a smart magnetic measure-bench, including integrated measurement system and well-designed component-level models, to investigate the magnetic component behavior under distorted excitations, examine the effect of variation of excitation condition on magnetic property, and compare the core-based properties with those measured by Epstein frame[3].

## 2. Integrated magnetic measure-bench and component behavior modeling

The magnetic measure-bench includes multi-function generator of arbitrary waveforms (35MHz), 3 sets of power amplifiers (4520A) and boosters (4521A), power analyzer (WT3000E), and a specially designed DC power supply (SM33P), as shown in Fig.1. Two laminated core models (C70 and C50) are configured, having the same step-lap joints as the actual transformer core, and fastened by wooden frame to keep fasten force like to transformer core. Moreover, the two models have the same construction design except for different length of the limb, i.e., 70cm for Model C70 and 50cm for Model C50. It is shown that the double core model scheme enables us to reasonably determine and predict the magnetic properties inside the laminated core [4]-[5].

The harmonic flux density  $B$  inside core model can be expressed by (1),

$$B = \sum_{n=1}^J B_n \sin(n\omega t + \phi_n) \quad (1)$$

where  $\omega$ , fundamental angle frequency,  $n$ , harmonic order,  $B_n$  and  $\phi_n$ , amplitude and phase angle of  $n^{\text{th}}$  harmonic components respectively,  $J$ , maximum harmonic order.

In measurement the harmonic magnetic flux density inside laminated core can be controlled. Based on the Faraday's law, by means of some simple deduction, the resulting harmonic flux density in the core and the induced voltage  $E(t)$  in the measuring coil meet the following relationship, as shown in (2),

$$E(t) = -NS\omega B_1 \sum_{n=1}^J nk_n \cos(n\omega t + \phi_n) \quad (2)$$

Where  $N$ , number of turns of measurement coil,  $B_1$ , fundamental amplitude,  $S$ , cross-sectional area of laminated core,  $K_n = B_n/B_1$ , corresponds to the  $n^{\text{th}}$  harmonic content(%).

A number of magnetic measurement results, including specific loss, exciting power, and B-H loop, have been obtained under distorted magnetic excitations. Meanwhile, the effect of the excitation parameters (e.g., harmonic content, order, and phase angle) on non-standard magnetic properties (e.g., specific loss and exciting power) are also experimentally investigated. See Fig.2.

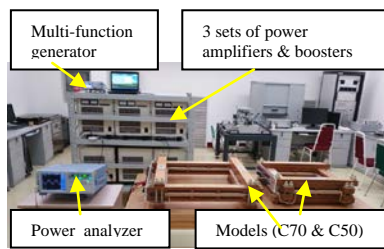
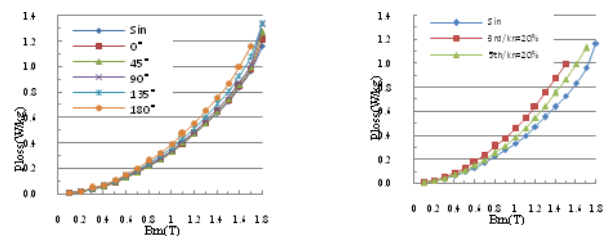


Fig.1 Measuring system and core models



(a) Fundamental only or includes 3rd harmonic ( $K_3=10\%$ , different phase) (b) Fundamental only or includes 3rd or 5th harmonic ( $k_3=k_5=20\%$ , 0 phase angle)

Fig.2. Effect of harmonic parameters on specific loss

### 3. Remarks

The further model-based magnetic properties under harmonic and/or DC-bias excitations, regarding the non-uniformity of both specific total loss and exciting power, the distortion of B-H loop, and the evaluation of building factor [7], will be presented in the full paper.

#### Acknowledgements

The research project was funded by the National Key Research and Development Program of China (no.2016YFB0300300 and no.2017YFB0902703).

#### References

- [1] A.J.Moses, Relevance of microstructure and texture to the accuracy and interpretation of 1 and 2 directional characterisation and testing of grain-oriented electrical steels, *International Journal of Applied Electromagnetics and Mechanics*, **55**(2017), 3-13.
- [2] E.Barbisio, F.Fiorillo, and C.Ragusa, Predicting loss in magnetic steels under arbitrary induction waveform and with minor hysteresis loops, *IEEE Trans Magn* **40**(2004), 1810–1819.
- [3] IEC 60404-2 AMD 1-2008: Magnetic Materials - Part 2: Methods of measurement of the magnetic properties of electrical steel sheet and strip by means of an Epstein frame; Amendment 1.
- [4] Z. Cheng, N. Takahashi, B. Forghani, A. J. Moses, P. Anderson, Y. Fan, T. Liu, X. Wang, Z. Zhao, and L. Liu, Modeling of magnetic properties of GO electrical steel based on Epstein combination and loss data weighted processing, *IEEE Trans Magn* **50** (2014), 6300209.
- [5] Z.Cheng, B.Forghani, X.Wang, L.Liu, T.Liu, Y.Fan, J. Zhang, X.Zhao, and Y. Liu, Engineering-oriented investigation of magnetic property modeling and application, *International Journal of Applied Electromagnetics and Mechanics*, **55**(2017), 147-158.
- [6] J.Sievert, Private communication, Oct. 2017.

# Novel H-coil design with improved off-axis immunity

Stan Zurek

*Megger Instruments Ltd, Archcliffe Road, Dover, CT17 9EN, Kent, United Kingdom*

*E-mail: stan.zurek@ieee.org*

**Keywords:** H-coil, magnetic field strength, rotational power loss.

Wire-wound H-coils are not completely immune to off-axis vector components of  $H$ . The unwanted sensitivity arises because a wire-wound H-coil has some effective active area in various directions, as shown in Fig. 1 and analysed in full detail in [1].

In particular, some of the clockwise-anticlockwise differences in rotational power loss typically encountered with low to medium amplitudes of rotational magnetisation can be caused by this unwanted off-axis sensitivity [2]. It can be shown that the combined area of such partial active areas does not depend on the number of turns, but just on the dimensions and wire positioning [1].

This paper proposes a novel concept of an H-coil design with significantly improved immunity to the off-axis  $H$  components. Measurement accuracy in the fieldmetric method [3] with sensors manufactured in this new proposed way should be significantly improved [4], as far as the off-axis components are concerned.

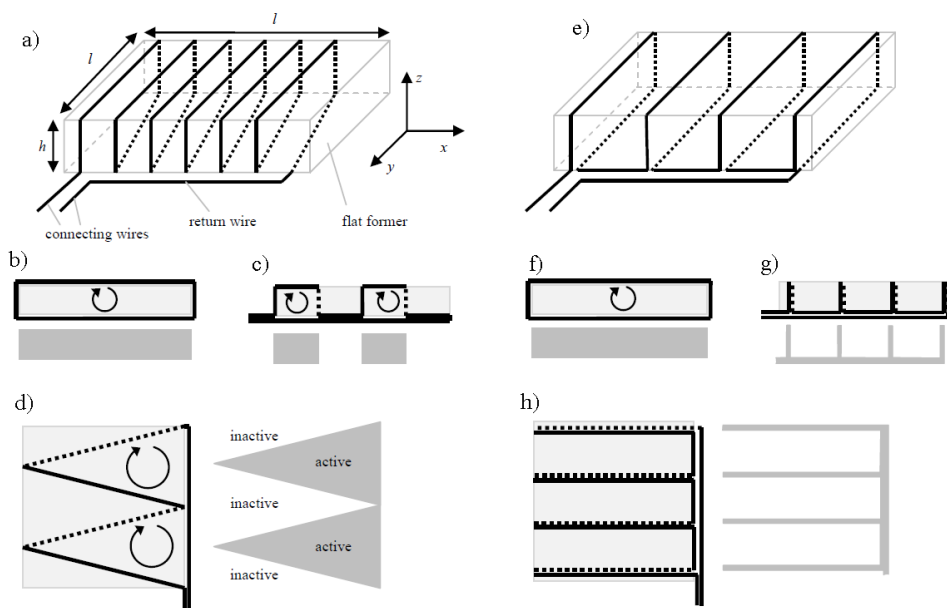


Figure 1: Conventional wire-wound H-coil: a) overview of conventional H-coil with definitions of directions, b) projection along the  $x$  axis and the active cross-sectional area, c) projection along the  $y$  direction, d) projection along the  $z$  direction; and the proposed novel "ideal" H-coil: e) overview, f) projection along the  $x$  direction, g) projection along the  $y$  direction, h) projection along the  $z$  direction

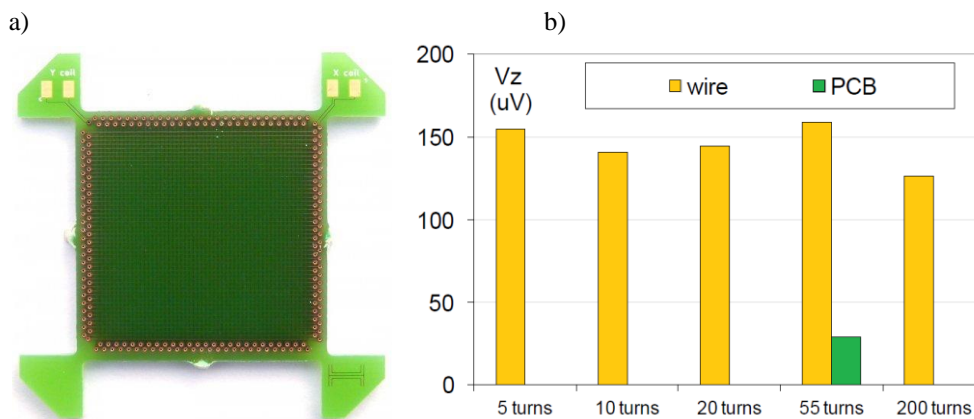


Figure 2: Novel H-coil made on a PCB (a) and the comparison of sensitivities of various H-coils detected the induced voltage by applying  $H$  in the  $z$  direction (b)

The novel concept of H-coils presented in this paper offers several exciting performance parameters:

- significant improvement of immunity to off-axis components of  $H$
- easily implementable extrapolation of  $H$  towards the sample surface
- excellent repeatability of parameters between various coils made in the same series ("magnetic angle" vs. "mechanical angle")
  - large H-coils (>200 mm) can be easily made
  - grooves for multiple B-coil wires can be also provided within the same structure
  - needle probes for measurement of  $B$  can be also accommodated within the same PCB as the H-coil
  - signal amplification can be integrated on the same PCB

#### *Acknowledgements*

The author would like to thank Dr Piotr Klimczyk of Brockhaus Measurements for supporting the costs and providing a prototype of the "ideal" H-coil used in this study.

The photographs of the prototypes were kindly provided by Mrs Joanna Kaczmarzyk.

#### *References*

- [1] Zurek S., "Sensitivity to off-axis vector components of typical wire wound flat H-coil configurations", *IEEE Sensors Journal*, Vol. **17** (13), 2017, p. 4021.
- [2] Zurek S., "Effect of off-axis H-coil sensitivity on clockwise-anticlockwise differences of rotational power loss in isotropic samples", *IET Science, Measurement & Technology*, accepted for publication, 2018.
- [3] Zurek S., "Characterisation of Soft Magnetic Materials Under Rotational Magnetisation", CRC / Taylor & Francis, 2017, ISBN 978-1-138-30436-9
- [4] Zurek S., "Optimum magnetising apparatus for standardised measurements of rotational power loss", to be published at 1&2DM Workshop, Grenoble, France, Sep 2018

# Research of the influence of DC component to stray-field loss under AC-DC hybrid excitation

Zhigang Zhao<sup>1</sup>, F.Liu<sup>1</sup>, Z.Cheng<sup>2</sup>, X.Zhao<sup>3</sup>, Ying Guo<sup>1</sup>

<sup>1</sup>State Key Laboratory of Reliability and Intelligence of Electrical Equipment, Hebei University of Technology, Tianjin 300130, China

E-mail: zhaozhigang@hebut.edu.cn; liufg@hebut.edu.cn

<sup>2</sup>R & D Center, Baoding Tianwei Group Co., LTD, Baoding, China

E-mail: emlabbzcheng@yahoo.com

<sup>3</sup>North China Electric Power University, Baoding, China

E-mail: 158748295@163.com

**Keywords:** Benchmarking, hybrid excitation, leakage flux, stray-field loss.

Recently, various kinds of extreme exciting conditions, such as the ac-dc hybrid excitation, are applied to power transformers, reactors etc, with the development of the HVDC system. The modeling and estimation of stray-field losses are of increasingly importance in the electromagnetic design of such devices, and it is challenging to measurement and numerical analysis<sup>[1]</sup>.

The major difficulties of the stray-field loss modeling under ac-dc hybrid condition are: 1) coming from loss measurements: it is impossible to directly measure the losses in each component; 2) coming from loss analysis: the material's magnetic property data under the ac-dc hybrid working conditions are not sufficient for the electromagnetic computation<sup>[2]</sup>. The purpose of this paper is to investigate the efficient methods to exactly determine the stray-field losses.

In the measurement of the stray-field loss, the obtained total stray-field loss  $P_{total}$  usually includes two parts, as shown in (1).

$$P_{total} = P_{components} + P_{excitation} \quad (1)$$

Note that, the  $P_{excitation}$  contains the induced eddy current loss due to the leakage flux linked with coils, as well as the resistive loss, as shown in (2).

$$P_{excitation} = P_r + P_{eddy} \quad (2)$$

Accordingly, the stray-field loss in the components can be indirectly determined by

$$P_{components} = P_{total} - P_{excitation} \quad (3)$$

The leakage flux of the exciting coils changes when the magnetic components are removed from the assembly shield models<sup>[3]</sup>. To keep the leakage magnetic field of the exciting coils almost no changing under two modes of operation, two complementary coils (called the C-coils) are utilized, which have completely the same specification as the generator coils (E-coils), and are movable in parallel rails, as shown in Figure 1.

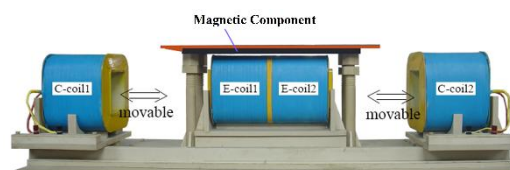


Figure 1 Loss measurement with upgraded E-coil and moveable C-coils.

Therefore, the value of  $P_{excitation}$  can be expressed as (4).

$$P_{excitation} = \frac{P_{E-coils} + P_{C-coils}}{2} \quad (4)$$

In this paper, the eddy current loss analysis based on the solved 3-D transient electromagnetic field have been validated based on the extended benchmark models under different excitations.

The measured loss and calculated loss on exciting coil under DC, AC and hybrid excitation is given in this paper. It has a good agreement between the calculated and measured results can be seen in Table 1.

To indirectly determine the iron loss in magnetic shielding, the first step is to exactly measure the total loss of the whole test model, and then calculated the eddy current loss of the exciting coil based on the transient eddy current field solution, as the second step. According to the results obtained at the first and second steps and relation (3), the stray-field losses generated in the magnetic shielding can be determined, as the third step.

The measured total loss of the test model and the calculated results of the loss caused in exciting coil under different hybrid current excitations, have been obtained, as shown in Table 2.

Accordingly, the contribution of dc component to stray-field loss inside components, referred to as  $\Delta P$ , under hybrid excitation is confidently estimated, see Table 3.

Table 1 Loss in air core exciting coil

Exciting currents (A)		Calculated loss (W)	Measured loss (W)
AC (50Hz, rms)	DC		
0	15	117.82	116.03
20	0	141.21	141.35
20	15	365.48	366.43

Table 2 Test model and experiment

AC (A)	DC (A)	Measured total loss (W)	Calculated coil loss (W)	Loss in component (W)
20	0	255.90	255.47	0.43
20	10	308.40	307.00	1.40
20	15	375.60	372.91	2.69

Table 3 Contribution of DC stray field loss

Exciting currents (A)		$P_{components\_ac+d}$ (W)	$P_{components\_ac}$ (W)	$\Delta P$ (W)
AC	DC			
20	10	1.40	0.43	0.97
20	15	2.69		2.26

It is obvious that when the AC component of the applied exciting current at the same value, the stray-field loss generated in the magnetic components with hybrid excitation is greater than that with only AC current, and the contribution of DC to stray-field loss is enhanced along with the increase of the DC current value.

#### Acknowledgements

The research leading to these results has received funding from National Natural Science Foundation of China under Grant 51107026, 51677052, 51237005.

#### References

- [1] Flórez G. A. D., Mombello E. E., Voss S., "Novel technique for the calculation of eddy current losses and Lorentz forces in foil winding transformers", *International Journal of Applied Electromagnetics & Mechanics*, 2017, 55(1,2):1-14.
- [2] Ma G., Cheng L., Lu L., et al, "Effects of DC bias on magnetic performance of high grades grain-oriented silicon steels", *Journal of Magnetism & Magnetic Materials*, 2017, 426.
- [3] Xiao L., Li M., Cheng W., et al, "Magnetic properties and eddy current losses in Fe-based soft magnetic composites", *International Journal of Applied Electromagnetics & Mechanics*, 2016, 52(3-4):1433-1441.

# Research on the improved loss model of electrical steel sheets under non-sinusoidal excitation

Zhigang Zhao, Jia Liu, Ying Guo, Saining Yin, Kai Yang

State Key Laboratory of Reliability and Intelligence of Electrical Equipment, Hebei University of Technology, Tianjin 300130, China

E-mail: zhaozhigang@hebut.edu.cn; 702352870@qq.com; 2427519546@qq.com; 287397097@qq.com; 1427369427@qq.com

**Keywords:** loss model, non-sinusoidal multivariate conditions, Non-Linear Least Square Method

Recently, the distorted magnetic flux is widely distributed in the large-scale electrical equipment, leading to local overheating and damage of equipment [1]. Numerous loss models of magnetic materials have been presented [2]. Based on the Bertotti loss model [3], an improved loss model is proposed in this paper, taking the implications of non-sinusoidal multivariate conditions on iron loss. And the loss data of oriented electrical steels under different excitation, which is measured by Epstein frame, can be fitted by using the Non-Linear Least Squares Method. The results show a remarkably good agreement between the calculated results and experimental data points. The conclusions are of significant theoretical value for further exploring the magnetic properties of soft magnetic materials under complex excitation environments.

The total loss of magnetic materials under sinusoidal excitation environment is expressed by

$$P_{\text{sin}} = P_h + P_c + P_{\text{exc}} = k_h f_m B_m^\alpha + k_c f_m^2 B_m^2 + k_{\text{exc}} f_m^{3/2} B_m^{3/2} \quad (1)$$

Respectively, the correction factors of loss components are given by (2)-(4), where  $k=0.65$ ,  $\Delta B_T = \sum_m \Delta B_i / B_p$ , as is shown in Figure 1.

$$F_h = 1 + k \Delta B_T \quad (2)$$

$$F_c = \left(\frac{B_1}{B_p}\right)^2 \sum_n \left(\frac{n B_n}{B_1}\right)^2 \quad (3)$$

$$F_{\text{exc}} = \left(\frac{B_1}{B_p}\right)^{3/2} \sum_n \left(\frac{n B_n}{B_1}\right)^{3/2} \quad (4)$$

Consequently, the total loss of magnetic materials under distorted magnetic flux is provided by (5), where  $K_h = k_h F_h$ ,  $K_c = k_c F_c$ ,  $K_{\text{exc}} = k_{\text{exc}} F_{\text{exc}}$  are the modified loss coefficients.

$$P = P_h + P_c + P_{\text{exc}} = K_h f B^{\alpha+1} + K_c f^2 B^2 + K_{\text{exc}} f^{3/2} B^{3/2} \quad (5)$$

Especially, the study on simultaneous corrections of three components of the total loss under distorted magnetic field has been infrequently reported in the previous literature.

According to [4], there are grain-oriented silicon steel sheets as specimens (B30P105). The original measuring platform is adjusted under the non-sinusoidal multivariate conditions, as is shown in Figure 2.

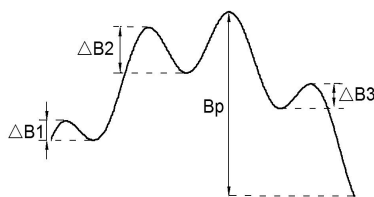


Figure 1 Typical waveform contained flux reversals

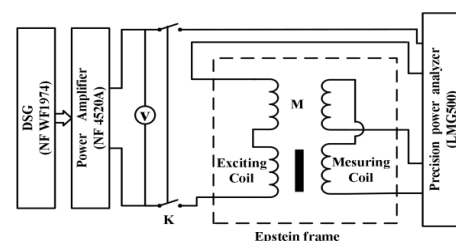


Figure 2 Schematic under multivariate conditions

The *Gauss-Newton* algorithm (*G-N*) and *Levenberg-Marquardt* algorithm (*L-M*) are employed respectively to determine the uncertain coefficients in (1) and its error, as is shown in Table 1-Table 2. However, fitting under non-sinusoidal multivariate condition is merely realized with *lsqcurvefit* function based on *L-M* algorithm, as is shown in Table 3.

Table 1 Fitting coefficients of Bertotti loss model

Schemes	$k_h \times e3$	$\alpha$	$k_c \times e5$	$k_{exc} \times e6$
<i>G-N</i>	6.868	1.42	4.579	1.141
<i>L-M</i>	6.867	1.42	4.577	1.140

Table 2 Error analysis of two fitting schemes

Schemes	<i>SSE</i>	<i>RMSE</i>	<i>R-Square</i>
<i>G-N</i>	0.6459	0.0898	0.9988
<i>L-M</i>	0.6457	0.0872	0.9988

Table 3 Fitting coefficients and error of the improved loss model

Scheme	$K_h$	$\alpha_1$	$K_c$	$K_{exc}$
<i>L-M</i>	0.0063	1.7349	$3.8455e-5$	$3.6186e-7$
	<i>SSE</i>	<i>RMSE</i>	<i>R-Square</i>	—
	2.2849	0.0864	0.9989	—

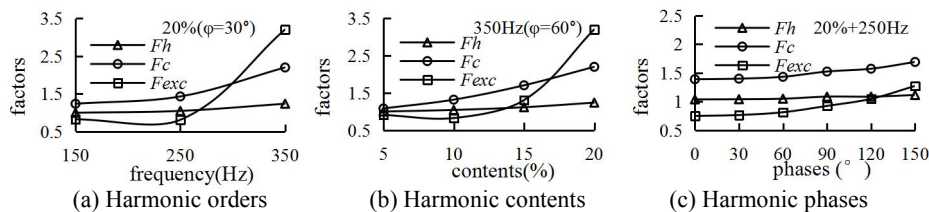


Figure 3 Correction factors under multivariate conditions

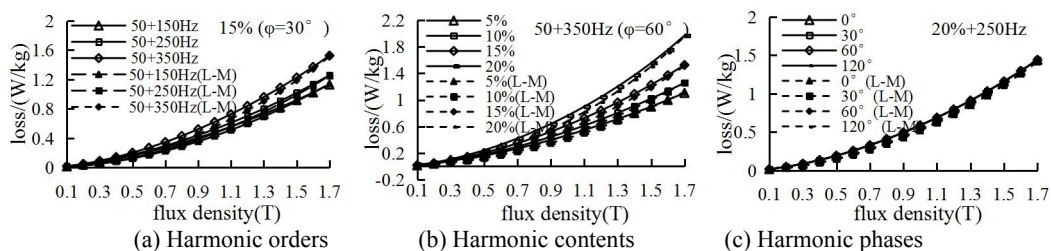


Figure 4 The calculated and measured iron loss behaviors under non-sinusoidal excitation

Especially, the derivation process of the improved loss model and the analysis of loss separation under different environments are elaborated in the full manuscript.

#### Acknowledgements

The research leading to these results has received funding from National Natural Science Foundation of China (NSFC) under Grant 51107026, 51677052, 51237005.

#### References

- [1] Kapeller H., Plaßnegger B., Gragger J. V., "Iron-loss modeling based on a loss separation approach in modelica", *IEEE Trans. Magn.*, 2017, PP(99):1-4.
- [2] Fiorillo F., Novikov A., "An improved approach to power losses in magnetic laminations under non-sinusoidal induction waveform", *IEEE Trans. Magn.*, 1990, 26(5):2904-2910.
- [3] Bertotti G., "Physical interpretation of eddy current losses in ferromagnetic materials. I.Theoretical considerations", *Journal of Applied Physics*, 1985, 57(6):2110-2117.
- [4] The State Bureau of Quality and Technical Supervision, "GB/T 3655-2008, method for measuring magnetic properties of electrical steel sheets (belt) by Epstein Frame", *Standards Press of China, Beijing*, 2000.

# **OS5: Applications, Sensors, NDT**

Session Chairman

**Marian SOINSKI**

Magneto Sp. Z O.o. - Poland



## Keynote Lecture

*”Inline integration of electromagnetic NDT methods using 3MA”*



**Dr Yasmine Gabi & Dr Bernd Wolter**

*Fraunhofer-Institute for Nondestructive Testing - IZFP, Saarbrücken, Germany*

**Yasmine Gabi** studied magnetic systems engineering at Joseph Fourier University, in France. In 2012, she received a doctoral degree in electrical engineering, automatic and signal processing at Grenoble INP. She has experience in magnetic characterization and modelling at multiscale behavior. Since May 2012 she joined Fraunhofer IZFP as expert in characterization and simulation for ferromagnetic material. Her main focus is the integration of electromagnetic NDT technique inline production. She was involved in different project: DPS-MODD, EU SYMPOSIUM, and MAGNUS (Fraunhofer-Carnot).

**Bernd Wolter** Studied material science at Saarland University, partly as guest researcher at Southwest Research Institute, San Antonio. Since 1995 he is working at the Fraunhofer ZFP. In 2001 he received his PhD regarding to the application of Nuclear Magnetic Resonance in Non-Destructive Testing. In the same year he was awarded for his research work with the “Bertholdpreis“ of the German Society for Non-Destructive Testing (DGZfP). Dr. Wolter is certified quality manager of the European Organization for Quality (EOQ). Currently, he is the head of department “Production Integrated NDT” of the IZFP. His current research activities include the application and integration of NDT techniques in production in order to monitor, control and optimize production processes.

## Inline integration of electromagnetic NDT methods using 3MA

Yasmine Gabi<sup>1</sup>, Bernd Wolter<sup>1</sup>, Andreas Haas<sup>1</sup>, Thorsten Müller<sup>1</sup>, Benjamin Straß<sup>1</sup>, Christian Conrad<sup>1</sup>

<sup>1</sup>Fraunhofer Institute for Nondestructive Testing IZFP, Saarbrücken, Germany  
Yasmine.Gabi@fraunhofer.izfp.de,

*Keywords:* NDT electromagnetic methods, mechanical properties, inline environment.

In the late 70-ties, Fraunhofer IZFP started research on electromagnetic methods (EM), in order to develop microstructure sensitive NDT techniques for German reactor safety applications [1]. Fraunhofer IZFP has investigated different classical electromagnetic techniques such as Barkhausen noise, eddy current and more exotic ones such as incremental permeability and analysis of upper harmonics in tangential magnetic field.

Later, these first investigations led to a combination of 4 different testing methods with focus on the development and design of robust sensors. This merging offers a multi-parametric characterization (output of 41 magnetic measuring quantities) and allows studying the tested material in different depths. This approach avoids calibration problems linked to measuring disturbances.

Meanwhile a broad range of applications on different parts and components has been reported. Several equipment variants and a wide range of sensors like MicroMach, 3MA-II [2], 3MA-X8 [3], Magnus, Magnetic Flux Leakage, EMAT, etc. were successfully developed and used to determine quantitative or qualitative technological parameters and to characterize defects [3-4].

The application of EM NDT technology is linked to the inspection situation and to the targets to be determined. The target quantities can be local or global values as well as microscopic or meso-macroscopic information. The use of such EM NDT devices is not only dedicated to the laboratory inspection, furthermore they can also be adapted into the production environment.

The challenge of EM inline integration is two-fold; material characterization but furthermore process monitoring and control. The design and the signal processing of these sensors have to fulfill a series of requirements, defined by the inline environment and the machining process data. Generally, electronic devices and especially probe heads have to be designed in a robust way, to be applicable in an industrial manner. In contrast to laboratory conditions, in production facilities disturbances are always present and have to be identified, described quantitatively and compensated regarding their influences on the NDT measuring techniques. The sensors have to be able to withstand conditions in harsh environment like for example in steel plants: elevated temperature, lift off, vibrations, roller stress (see figure 1).



Figure 1: 3MA NDT probe head integrated in line production

In order to anticipate to these environmental behaviors, laboratory tests are processed. To guarantee stable characterization and calibration, the variation of 3MA outputs and signals are assessed. In this work, a complete inline protocol investigation will be described in detail.

#### *References*

- [1] W.A. Theiner; K. Goebels; P. Höller. „Zerstörungsfreier Nachweis von Eigenspannungen mittels Ultraschall-Doppelbrechung und Magnetostriktion“ Staatliche Materialprüfungsanstalt Universität Stuttgart: MPA-Seminar (5), Stuttgart, 1979..
- [2] P. Höller. “Nondestructive analysis of structure and stresses by ultrasonic and micromagnetic methods”, Nondestructive Characterization of Materials II, Plenum Press, New York London, p 211-225, 1987.
- [3] W. A. Theiner; I. Altpeter, “Hardness and residual stress measurements on components using micro-magnetic NDT quantities ”in: 7th international Conference on NDE in the Nuclear Industry”, Grenoble, France 1985. 1985.
- [4] C. Conrad; B. Wolter; B.; R. Kern; T. Wicke; J. Tonne. “Industrial demands and Non-Destructive Testing (NDT) Solutions for Process Monitoring and Quality control in Hot and cold Formed Steel Production. International conference on advances in Metallurgy of long and forged products, 12-15 July 2015.
- [5] B. Wolter; C. Boller; C. Conrad; H.G. Herrmann; R. Kern; H. Kopp. “In Process Non-destructive Inspection of Press Hardened Car body Parts Based on Electromagnetic Techniques”, Future trends in steel development, processing technologies and applications: bringing the automotive, supplier and steel industries together. Düsseldorf, p 698-705, 2014.

# A Novel Family of Magnetic Detector Bands of Minimum Effective Thickness

Helmut Pfützner, Georgi Shilyashki

*Inst. EMCE-Electrodynamics, TU Wien; Vienna Magnetics Group (Austria)*

*E-mail: pfutzner@tuwien.ac.at; shilyashki@tuwien.ac.at*

*Keywords:* sensors, flux distributions, losses, magnetostriction.

*Abstract* - The paper describes novel detector bands for magnetic analyses in laminated machine cores. About 100  $\mu\text{m}$  thick sensors register local distributions of 3D induction components, magnetostriction, losses, temperature and vibrations. By “handles”, a band can be positioned in different core regions, or it can be placed permanently during assembling.

## 1. Introduction

Referring to a magnetic sensor of minimum effective thickness may yield associations with a so-called nano-sensor. But according to definition (e.g. [1]), the latter is a sensor that *includes* nano-sized components as the active element that may register nano-sized particles. The resulting sensor element may be mounted on a solid-state substrate or chip, of rather high thickness – typically being of the order of millimetre.

In contrast to the above sensors, this project aims on sensors of absolute flatness, including also the electric components for contacts to measurement electronics. Comparing the corresponding literature, the about 100  $\mu\text{m}$  thick “detector bands” (DBs) may represent the thinnest existing sensor type. In magnetism, such sensors are of interest if physical quantities should be measured in extremely small air gaps, or if sensor-caused gaps should be avoided. Such a case is given for interior analyses of laminated machine cores, e.g. of transformers, reactors or generators.

The present paper describes the basic strategy of measurements by means of DBs. Also it summarizes concepts of sensors for different induction components, losses, temperature variations, strain (from magnetostriction or forces), and vibration.

## 2. Concept of Detector Bands

For a summary of novel concept, let us start out from the example of an analysis of local distributions of in-plane induction  $B_{IP}$  in the interior of a transformer core. Usually (e.g. [2]), smallest holes are drilled through selected core laminations, and search coils of thinnest wires are arranged. Then, the laminations are arranged in the core with high effort, carefully preventing breaks of wires and connections to electronics. As further drawbacks, the procedure is not non-destructive and both-side inter-laminar air gaps arise, even with thinnest components.

Fig.1 depicts the basis of novel concept. It is based on a DB of typically 4 cm width and 25 cm length (up to 1 m for large cores). The DB consists of five sections, including two “handles” at the ends. By means of a novel 2D/3D assembler [3] that combines different print techniques, different sensors can be arranged at the bands “sensor section” (SS). The following long “interconnection section” (IS) mediates printed electric connections to the “clamping section” (CS) that connects to and from the sensors. As an important feature, the CS remains outside the core which means that inter-laminar gaps are restricted to less than 100  $\mu\text{m}$  height in clamped state.

In core production, bands can be arranged during stacking without handles and remain in the core. However, the main advantage of design concerns tests in finished model cores, or small distribution cores where flexible re-positioning represents a problem. Here the SS can be positioned in

successive ways at different locations of the core interior. For insertion to a given layer, the core is de-clamped, a local gap of about 10 mm height is opened by the end of a long plastic knife - with a stiff “pull-through wire” (Fig.1) - the SS-side handle is pulled through the core. The two handles are used for exact positioning (supported by an xy-raster on the DB), and the core is re-clamped for measurements. In fact, no alternative suggests itself for this – seemingly trivial – procedure.

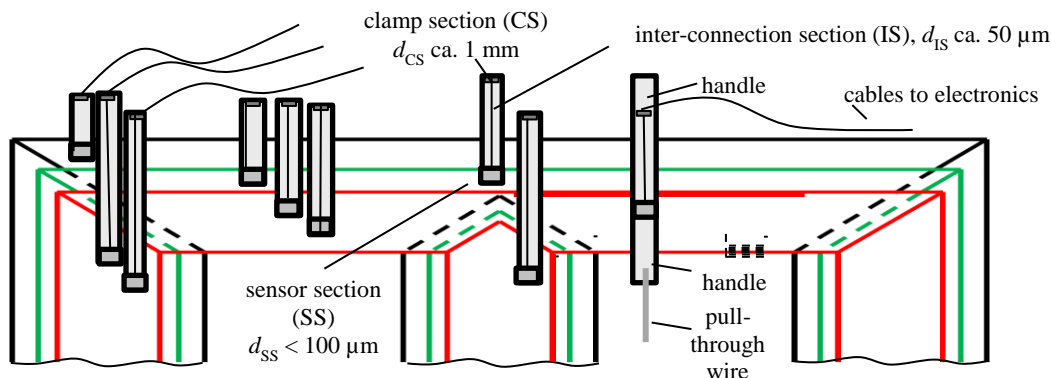


Figure 1: Schematic outline of detector band (DB) arrangements in the interior of a transformer core that consists of three packages. Notice: One DB is depicted with “handles” for insert.

### 3. Design of Sensors

The 2D/3D-assembler with up to four print nozzles for conducting or non-conducting print materials was already applied for the following so far established sensor types:

- Sensors for in-plane induction  $B_{IP}(t)$ , that represent the most complicated sensor type. Following the novel concept of a tangential induction sensor,  $B_{IP}(t)$  is derived from the corresponding induction  $B_{NR}(t)$  of an incorporated  $18 \mu\text{m}$  thick nano-crystalline ribbon with print-on windings. Though hysteresis complicates exact waveform determination, tests are highly effective [3].
- Sensors for off-plane components  $B_{OP}(t)$  of induction - They resemble multi-turn frame coils. Calibration is complicated, since the effective thickness depends on clamping that also affects the to-be measured term  $B_{OP}$ . But comparison tests prove to be highly effective [4, 5].
- Thermal sensors for analyses of local losses  $P$  or temperature increases  $\Theta(t)$  – They consist of two layers of conductive suspension, e.g. containing particles of Cu and Ni, as thermo-couples. So far, the sensitivity is restricted, but sufficient for effective interior analyses.
- Sensors for strains  $\varepsilon(t)$  from magnetostriction or magneto-static forces – They exhibit a 30 mm sized longitudinal meander structure on a  $20 \mu\text{m}$  thick elastic substrate for take-up of local strain. Problems are calibration and linearity, since effectiveness needs strong core clamping, as being typical for industrial machines. The sensitivity proves to be unexpectedly high.

As a conclusion, for the first time, quite rapid, non-destructive measurements of induction, losses and strain in the inner of machine cores are offered by a novel family of detector bands with as little as about  $100 \mu\text{m}$  effective thickness.

*Acknowledgement* – We thank for support from the Austrian Science Fund FWF (P28481-N30).

- J.J.Liou (Ed.). Nano Devices and Sensors. De Gruyter (2016).
- F.Marketos, D.Marnay, T.Ngnegueu. *IEEE Trans.Mag.*48, 1677-1680 (2012).
- H.Pfützner, G.Shilyashki, A.Windischhofer. *Int.J.Appl.Elmagn.Mech.* 56, 585-593 (2018).
- G.Shilyashki, H.Pfützner, C.Huber. *IEEE Trans.Magn.*53, 8400706, 1-6 (2017).
- G.Shilyashki, H.Pfützner, M.Palkovits, A.Windischhofer, M.Giefing. *Sensors* 17/12, 2953, (2017).

# Nondestructive testing and evaluation of high pressure feed water heat exchanger tubes using differential-type bobbin probes and solid-state integrated GMR sensor arrays

Sunbo Sim<sup>1</sup>, Hoyong Lee<sup>2</sup>, Heejong Lee<sup>1</sup>, and Jinyi Lee<sup>1</sup>

<sup>1</sup>Research Center for IT-based Real Time NDT for Nano-Damage Tolerance, Chosun University, Gwangju, 61452, Korea

E-mail: [ssb3842@gmail.com](mailto:ssb3842@gmail.com); [happybell221@naver.com](mailto:happybell221@naver.com); [jinyilee@chosun.ac.kr](mailto:jinyilee@chosun.ac.kr)

<sup>2</sup>Department of Defense Science and Technology, Gwangju University, Gwangju, 61743, Korea

E-mail: [hylee@gwangju.ac.kr](mailto:hylee@gwangju.ac.kr)

**Keywords:** HPFW heat exchanger tube, differential-type bobbin probe, solid-state integrated GMR sensor.

High pressure feed water (HPFW) heat exchanger is one of the balance of plant (BOP) installed in a nuclear power plant, which increases the thermal efficiency by preheating the water from the turbine condenser. The tubes in the heat exchanger are operated in extremely harsh environment such as high temperature, high pressure, and highly corrosive condition, which makes the frequent tube failures such as corrosion, erosion, crack, and etc. [1], [2]. Therefore nondestructive inspections are performed periodically using bobbin probes and rotating pancake coils. The inspection using bobbin probe is fast and has the capability of easy detection of various type of defects but it cannot characterize the type and size of the defects. On the other hand, rotating pancake coil enables the defect characterization but it is slow and low durability.

This paper presents the development and evaluation of non-destructive testing method of high pressure feed water exchanger tubes using differential type bobbin probes and solid-state integrated GMR sensor arrays. Defects of the tubes are detected by measuring the impedance and phase of differential-type bobbin coils and the shape and the size of the defects are measured and visualized by solid-state integrated GMR sensor arrays. In addition, the quantitative evaluation of defects is performed through the analysis of Lissajous curves and alternating magnetic field distributions.

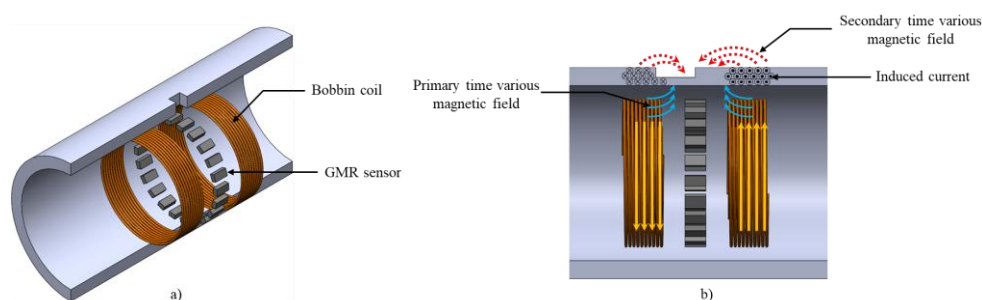


Figure 1: Configuration of probes using: a) GMR sensor array, a bobbin coil, b) Current and Magnetic field direction

Fig. 1 shows the proposed sensor probe system. The sensor probe consisted of two bobbin coils and 22 GMR sensor arrays between the coils. The bobbin coils that were powered by an AC current, induced an eddy current in the circumferential direction of the heat exchanger tube. The eddy current, which was distorted by the flaw of the tube, produced a secondary alternating magnetic field around the flaw and the radial component of the magnetic field was measured by the GMR sensor arrays.

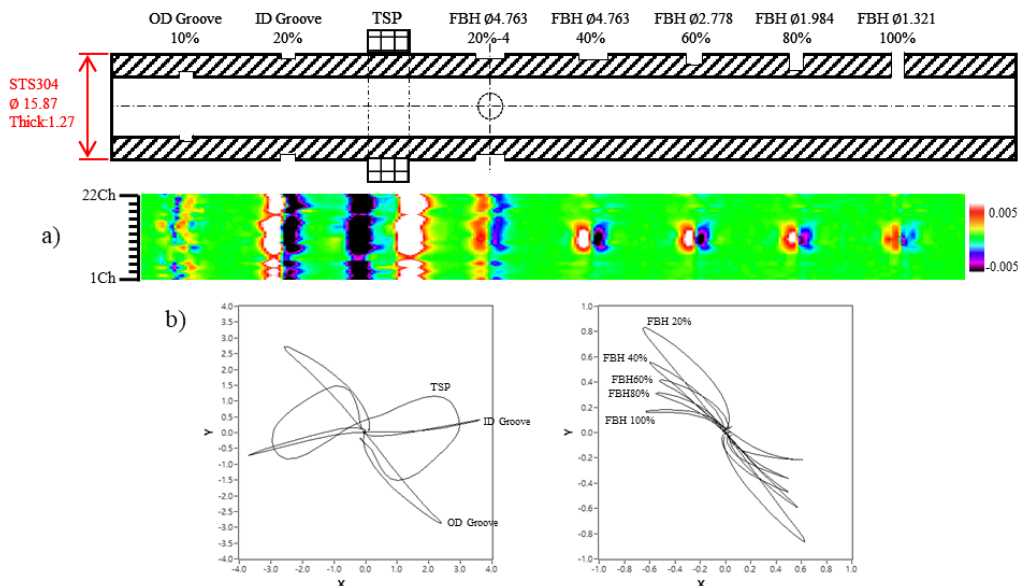


Fig.2. Experimental results of defects on the HPFW tube by: a) GMR sensor, b) bobbin coils

Fig. 2 shows the one of experimental results of the proposed method. The outer diameter (OD) and the wall thickness (W.T) of the HPFW tube for tests are 15.87mm and 1.27mm each. In this case, the artificial flaws with holes of 20~100% of W.T and grooves of 10~20% of WT are examined. The shapes of flaws were detected through GMR sensors and the depth were figured by the phase change of the bobbin coil signal.

#### Acknowledgements

The research leading to these results has received funding from the Korea Hydro & Nuclear Power Co. (KHNP L16S055000) and Korea Institute of Energy Technology Evaluation and Planning (KETEP 20171520101610). We are grateful for the supports.

#### References

- [1] EPRI, "Feedwater Heater Maintenance Guide," Final Report, EPRI 1003470 (2002).
- [2] ASME, 1998b, "ASME Section 5. Article 26: Eddy Current Standards," The American Society for Mechanical Engineering, New York, NY.



# Author Index

**A**  
Ababsa Mohamed Lamine . . . . . 64, 65, 78, 79  
Akaki Ryosuke . . . . . 135, 136  
Ako Yuya . . . . . 13, 14, 106, 107  
Amrhein Wolfgang . . . . . 11, 12, 84, 85  
Anderson Philip . . . . . 15, 16, 57, 58  
Andrei Paul Cristian . . . . . 121–124  
Aoyama Masahiro . . . . . 135, 136  
Appino Carlo . . . . . 26, 27  
Arbenz Laure . . . . . 37, 38

**B**  
Beatrice Cinzia . . . . . 76, 77, 96, 97  
Belhacen Anouar . . . . . 89–91  
Benabou Abdelkader . . . . . 37, 38, 108, 109  
Birat Jean-Pierre . . . . . 47, 48  
Blache François . . . . . 94, 95  
Boudinet Cédric . . . . . 94, 95  
Bramerdorfer Gerd . . . . . 11, 12, 84, 85  
Bucata Victor . . . . . 123, 124

**C**  
Camacho Nicolas . . . . . 57, 58  
Caruso Matteo . . . . . 47, 48  
Che Fulai . . . . . 149, 150  
Cheng Zhiguang . . . . . 149, 150, 153, 154  
Chwastek Krzysztof . . . . . 80, 81, 147, 148  
Ciuceanu Radu . . . . . 121, 122  
Clénet Stéphane . . . . . 37, 38, 108, 109  
Conrad Christian . . . . . 160, 161  
Cossale Marco . . . . . 11, 12

**D**  
Dassonville Pascal . . . . . 35, 36, 47, 48, 78, 79  
Davies Ryan . . . . . 57, 58  
De La Barriere Olivier . . . . . 26, 27  
Denke Patrick . . . . . 68, 69  
Dobák Samuel . . . . . 75–77, 96, 97  
Dou Yu . . . . . 31, 32  
Du Zhenbin . . . . . 149, 150  
Duan Nana . . . . . 51, 52, 117, 118  
Ducharme Benjamin . . . . . 41, 42, 82, 83  
Dupuis Julien . . . . . 47, 48  
Dyer Christopher . . . . . 15, 16

**E**  
Eaton Mark . . . . . 15, 16  
El Youssef Mohamad . . . . . 108, 109  
Enokizono Masato . . . . . 24, 25, 110, 111

**F**  
Fassenet Marylin . . . . . 94, 95  
Faverolle Pierre . . . . . 108, 109  
Ferrara Enzo . . . . . 26, 27  
Fiorillo Fausto . . . . . 6, 7, 26, 27, 76, 77, 96, 97  
Forghani Behzad . . . . . 149, 150  
Fortin Jérôme . . . . . 47, 48, 78, 79  
Fujiwara Koji . . . . . 13, 14, 45, 46, 49, 50, 106, 107, 125, 126, 135–138

**G**  
Gabi Yasmine . . . . . 159–161  
Gavrila Horia . . . . . 121, 122  
Gebara Piotr . . . . . 80, 81  
Gkaliou Kyriaki . . . . . 15, 16  
Gong Xuehai . . . . . 127, 128  
Gozdur Roman . . . . . 80, 81  
Grumeza Catalin Ionut . . . . . 123, 124  
Grybos Dominik . . . . . 145, 146  
Gstoettenbauer Norbert . . . . . 84, 85  
Guo Ying . . . . . 139, 140, 153, 154  
Gupta Bhaawan . . . . . 82, 83

**H**  
Haas Andreas . . . . . 160, 161  
Hall Jeremy . . . . . 15, 16  
Hameyer Kay . . . . . 68, 69, 104, 105, 119, 120  
Hantila Florea Ioan . . . . . 123, 124  
Harrison Christopher . . . . . 15, 16  
Hernandez Yves . . . . . 47, 48  
Higashigawa Yuto . . . . . 135, 136  
Hubert Olivier . . . . . 101–103

**I**  
Inoue Shinichi . . . . . 43, 44

**J**  
Jakubas Adam . . . . . 147, 148  
Jamil Meryeme . . . . . 37, 38  
Jastrzebski Radoslaw . . . . . 147, 148  
Jha Amit . . . . . 33, 34

Jia Liu ..... 155, 156  
Jiang Baolin ..... 127, 128  
Jikumaru Takehiro ..... 106, 107

## K

Kai Yang ..... 155, 156  
Kai Yuichiro ..... 110, 111  
Kawaguchi Kohei ..... 49, 50  
Kedous-Lebouc Afef ..... 33, 34  
Kim Jungmin ..... 55, 56, 133, 134  
Kim Sejin ..... 133, 134  
Kitao Junji ..... 13, 14  
Kitzberger Martin ..... 11, 12  
Klimczyk Piotr ..... 35, 36, 68, 69  
Kubo Toshihiro ..... 137, 138

## L

Lavalley Yannick ..... 108, 109  
Lebouc Afef ..... 94, 95  
Lecuppe Thomas ..... 108, 109  
Lee Heejong ..... 133, 134, 164, 165  
Lee Hoyong ..... 133, 134, 164, 165  
Lee Hoyoung ..... 55, 56  
Lee Jinyi ..... 55, 56, 133, 134, 164, 165  
Leszczyński Jacek 92, 93, 129, 130, 145, 146  
Leuning Nora ..... 104, 105  
Li Angxuan ..... 31, 32, 131, 132  
Li Lin ..... 115, 116  
Li Yongjian ... 22, 23, 31, 32, 51, 52, 62, 63,  
117, 118, 127, 128, 131, 132,  
141–144, 149, 150  
Liu Fugui ..... 153, 154  
Liu Jia ..... 139, 140  
Liu Lanrong ..... 149, 150  
Liu Tao ..... 149, 150  
Liu Yang ..... 127, 128, 149, 150  
Luening Kai ..... 59–61

## M

Müller Thorsten ..... 160, 161  
Maloberti Olivier . 35, 36, 47, 48, 64, 65, 78,  
79  
Mandil Faustin ..... 33, 34  
Manescu Paltanea Veronica ..... 121–124  
Martino Luca ..... 96, 97  
Masato Enokizono ..... 43, 44  
Matsubara Ryo ..... 125, 126  
Matsubara Yoshio ..... 137, 138  
Matsusita Makoto ..... 49, 50  
Mipo Jean-Claude ..... 37, 38, 108, 109  
Mitani Ryo ..... 49, 50  
Momochi Nobuyuki ..... 137, 138

## N

Nagaoka Naoto ..... 137, 138  
Nemoianu Iosif ..... 121, 122

Nesser Manar ..... 47, 48, 78, 79  
Ninet Olivier ..... 64, 65  
Nojima Yoichi ..... 43, 44

## O

Osemwinyen Osaruyi ..... 90, 91  
Owzareck Michael ..... 59–61

## P

Paltanea Gheorghe ..... 121–124  
Panier Stéphane ..... 35, 36, 78, 79  
Park Juhyeon ..... 55, 56  
Parspour Nejila ..... 59–61  
Pfützner Helmut ... 53, 54, 66, 67, 162, 163  
Pineau Camille ..... 47, 48  
Pluta Wojciech ..... 39, 40, 92, 93, 129, 130

## R

Ragusa Carlo ..... 26, 27, 76, 77, 96, 97  
Rasilo Paavo ..... 90, 91  
Reisinger Johann ..... 84, 85  
Rivoirard Sophie ..... 33, 34  
Robinson Fiona ..... 57, 58  
Rygał Jakub ..... 92, 93, 129, 130  
Rygał Roman ..... 92, 93, 129, 130

## S

Saining Yin ..... 155, 156  
Salloum Elias ..... 35, 36, 78, 79  
Schauerte Benedikt ... 68, 69, 104, 105, 119,  
120  
Schmöllebeck Fritz ..... 53, 54  
Schuster Stefan ..... 84, 85  
Sebald Gael ..... 82, 83  
Shah Sahas ..... 90, 91  
Shibatani Takuya ..... 45, 46  
Shilyashki Georgi ... 53, 54, 66, 67, 162, 163  
Shutta Yusaku ..... 13, 14  
Sim Sunbo ..... 164, 165  
Soinński Marian ... 92, 93, 129, 130, 145, 146  
Stahlschmidt Jochen ..... 35, 36  
Steentjes Simon ..... 104, 105, 119, 120  
Strass Benjamin ..... 160, 161  
Sun He ..... 141, 142  
Swoboda Cezary ..... 145, 146

## T

Takahashi Yasuhito .. 13, 14, 45, 46, 49, 50,  
106, 107, 125, 126, 135–138  
Thul Andreas ..... 68, 69, 119, 120  
Tokumasu Tadashi ..... 49, 50  
Tsakaloudi Vasiliki ..... 76, 77, 96, 97  
Tsuchida Yuji ..... 43, 44

## U

Uchimoto Tetsuya ..... 82, 83  
Ueno Shohei ..... 43, 44

**V**  
 Vaillant Marie-Pierre ..... 94, 95  
 Van Gorp Adrien..... 108, 109  
 Vo Anh Tuan..... 94, 95

**W**  
 Wakabayashi Daisuke ..... 24, 25  
 Walak Jan ..... 92, 93, 129, 130  
 Wang Shuhong..... 51, 52, 117, 118  
 Woeckinger Daniel..... 84, 85  
 Wolter Bernd..... 159–161

**X**  
 Xu Weijie..... 51, 52, 117, 118

**Y**  
 Yamada Masaki ..... 13, 14  
 Yang Kai ..... 139, 140  
 Yang Qingxin..... 62, 63, 131, 132, 141–144

Yasumuro Kei ..... 49, 50  
 Yin Saining ..... 139, 140  
 Ying Guo ..... 155, 156  
 Yu Xinran ..... 62, 63, 143, 144  
 Yue Shuaichao..... 22, 23, 62, 63, 141–144

**Z**  
 Zhang Changgeng .... 22, 23, 31, 32, 62, 63,  
 127, 128, 131, 132, 141, 142  
 Zhang Kai ..... 22, 23  
 Zhang Xiwei ..... 115, 116  
 Zhao Xiaojun..... 149, 150, 153, 154  
 Zhao Zhigang..... 139, 140, 153, 154  
 Zhigang Zhao ..... 155, 156  
 Zhou Xing ..... 70, 71  
 Zhu Jianguo..... 31, 32, 51, 52, 117, 118  
 Zurek Stan..... 19–21, 151, 152  
 Zurek Stanisław..... 92, 93, 129, 130

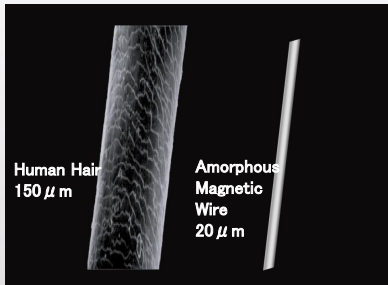


# Amorphous MI Sensor

## 1. Development of the MI Sensor

### Amorphous Wire

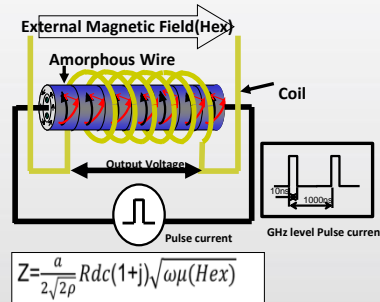
Amorphous magnetic metal wire is a 20um diameter FeCoSiB alloy wire in an amorphous state without crystalline structure due to its unique production method. Amorphous wire exhibits ideal soft magnetic properties and is an optimal material for high sensitivity magnetic sensors.



1. Amorphous Magnetic Wire

### MI Effect

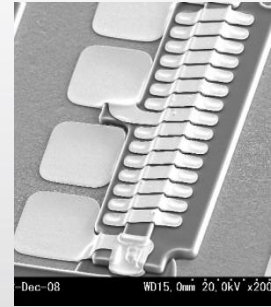
The MI Sensor is a practical application of the MI effect. The MI effect is when a pulse electric current is passed through an amorphous metal wire and the wire impedance changes significantly in response to the strength of the external magnetic field.



2. MI (Magnetic Impedance Effect)

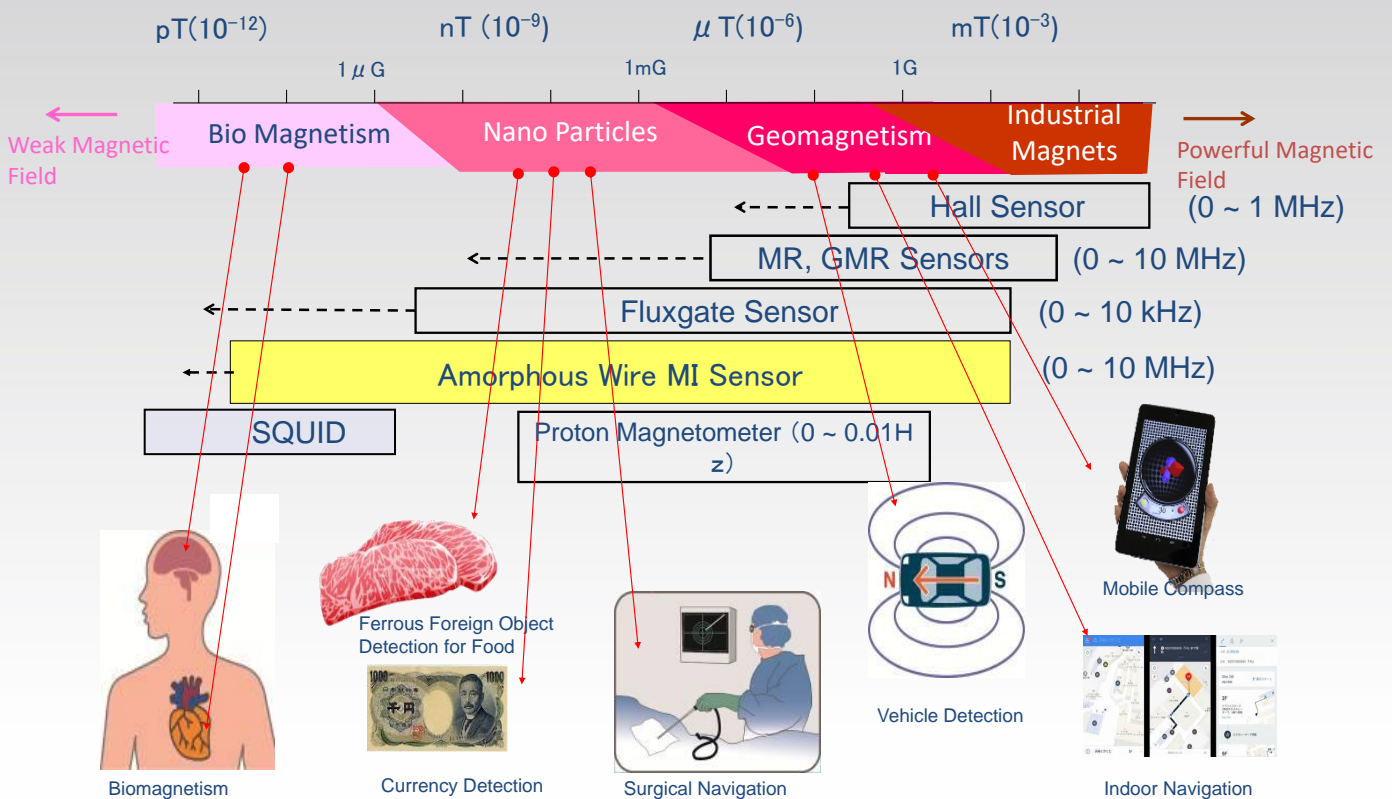
### Ultra Small MI Element

In 2002, Aichi Steel Corporation developed a micro sized MI element, utilizing the MEMS process.



3. Ultra-Small MI Sensor

## 2. Position and Application of the MI Sensor





All you need for magnetics



# MAGNET-PHYSIK

Dr. Steingrover GmbH

Magnetizing and Magnetic Measuring Technology  
Integrated Working Solutions  
Accredited Calibration Laboratory

Permagraph® C



Automated Solutions



Impulse Magnetizer up to  
300000 W's



Coils



Gaussmeter



Remagraph® C



Tabletop Magnetizer



Fluxmeter



Technology and Quality made in Cologne, Germany

[www.magnet-physik.de](http://www.magnet-physik.de)



# De facto Standard Tester to specify

## HIGHLIGHTS

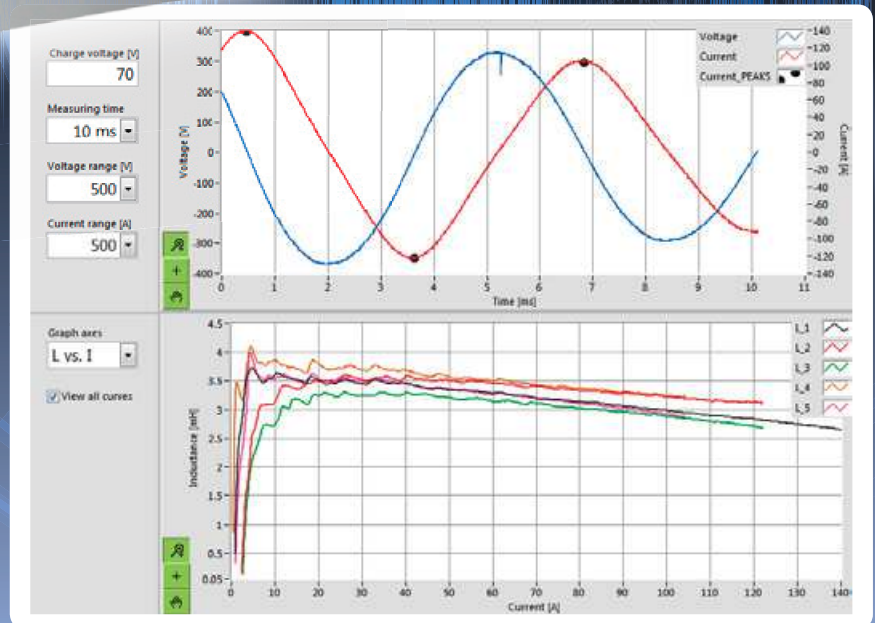
- power magnetic component
- low permeable soft magnetic material
- like powdered core, gapped ferrite core or stress annealed nanocrystalline tape wound core

Supported by  
DIN-Connect



Bs&T

Pulse



Bs&T Thyristor Pulse Technology provide the highest discharge current among same power class to excite the magnetic component under test bipolar into saturation the most accurate inductance value for didt method. Magnetic component, like solide state transformer, harmonic and sinus filter for DC

grid of mid voltage till 1000 V, can be finally specified. ■

**i More info**

[www.powerlosstester.de](http://www.powerlosstester.de)



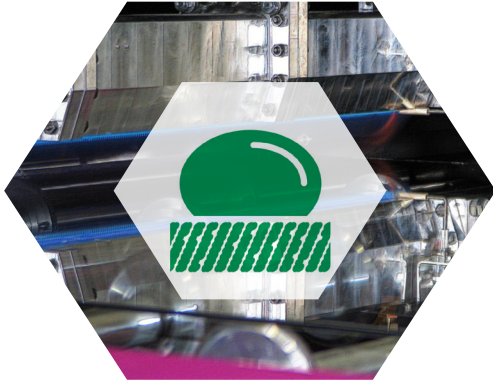
# INNOVENT e.V.

## Technology Development



INNOVENT is a private non-profit research institute for applied research and development in the high tech region Jena/Germany. Applications encompass surface engineering of glass, metals and plastics, medical engineering, optics as well as microsystems technology including product and technology development. The institute with over 140 employees is initiator and coordinator of networks and alliances, member in numerous expert panels and organiser of several successful conferences and user forums.

### Services of our divisions:



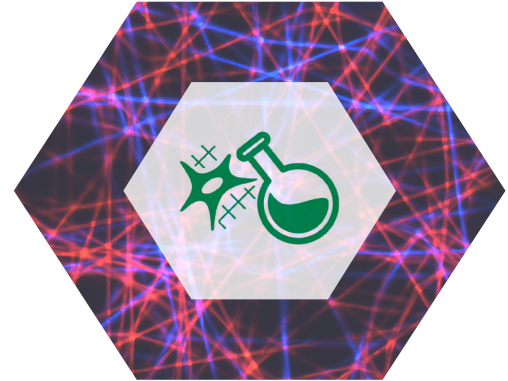
#### Surface Engineering

- Plasma processes
- Flame coating
- Electrochemical processes
- Sol-Gel-coating
- Fluorination
- Parylene coatings
- Process combinations



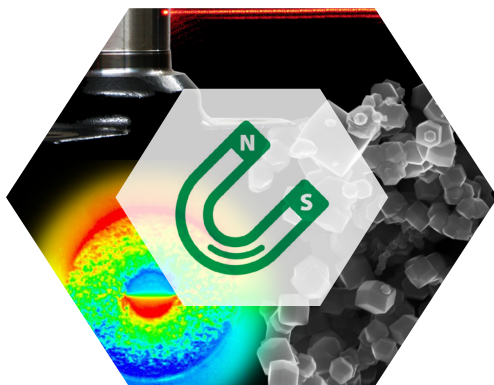
#### Primer and chemical surface treatment

- Bonding agents
- Composite materials
- Adhesive bonding, vernishing, encapsulating
- UVC (VUV) activation
- Corrosion protection



#### Biomaterials

- Biomaterial synthesis
- Biological testing
- Resorbable polymers
- Bioactive coatings
- Bone substitutes
- Electrospinning
- Functional nanoparticles



#### Magnetic and optical systems

- Simulations
- Characterization of magnetic materials
- Magn. Nanoparticles
- Magnetization
- Single crystals / epitaxial films
- Magneto-optical sensor



#### Analytics and material testing

- Analysis of elements
- Surface analysis
- Dissolution test
- Separation technology
- Special metrology
- Failure analysis
- Processing, ageing



#### Contact

INNOVENT e.V. Technology Development  
Pruessingstrasse 27 b | D-07745 Jena | Managing Directors: Dr. Bernd Gruenler, Dr. Arnd Schimanski  
Phone: +49 36 41 2825-10 | Telefax: +49 36 41 2825-30 | [innovent@innovent-jena.de](mailto:innovent@innovent-jena.de) | [www.innovent-jena.de](http://www.innovent-jena.de)





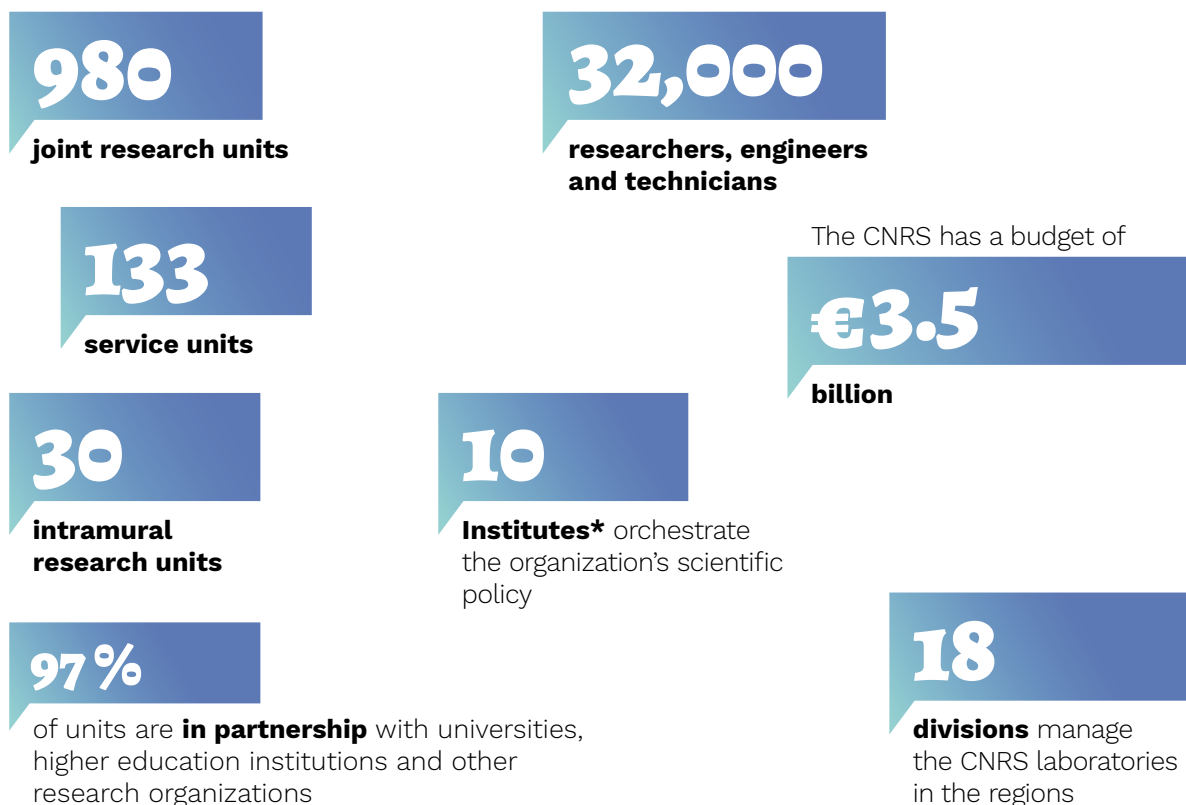
# The CNRS in brief

France's **National Center for Scientific Research** is a public research institution under the responsibility of the French Ministry of Higher Education, Research and Innovation.

**A pluridisciplinary organization**, it covers all scientific disciplines, including the humanities and social sciences, biological sciences, nuclear and particle physics, information sciences, engineering and systems, physics, mathematical sciences, chemistry, Earth sciences and astronomy, ecology and the environment.

**An interdisciplinary body**, it promotes research at the interface between disciplines.

Each year, the CNRS awards its **Gold Medal**, the highest scientific distinction in France. Since 2011, the CNRS **Medal of Innovation** has been rewarding outstanding research in the technological, therapeutic, economic and social fields.



\* **INSB** Institute of Biological Sciences, **INC** Institute of Chemistry, **INEE** Institute of Ecology and Environment, **INSHS** Institute for Humanities and Social Sciences, **INS2I** Institute for Information Sciences and Technologies, **INSIS** Institute for Engineering and Systems Sciences, **INSMI** National Institute for Mathematical Sciences, **INP** Institute of Physics, **IN2P3** National Institute of Nuclear and Particle Physics, **INSU** National Institute for Earth Sciences and Astronomy



Grenoble



# Grenoble INP

Établissement public d'enseignement supérieur et de recherche

Institut d'ingénierie  
Institute of engineering  
Univ. Grenoble Alpes



**FORMATION** EDUCATION



**RECHERCHE** RESEARCH



**ENTREPRISES** BUSINESS

Membre du **Groupe INP**